UNIVERSIDADE FEDERAL DO RIO GRANDE DO SUL
INSTITUTO DE CIÊNCIAS BÁSICAS DA SAÚDE
PROGRAMA DE PÓS-GRADUAÇÃO EM CIÊNCIAS BIOLÓGICAS:
BIOQUÍMICA

Marcelo Rigon Zimmer

The role of Agrp neurons in nonfood-related behaviors and their functional ontogeny in mice

O papel dos neurônios Agrp em comportamentos não relacionados à ingestão alimentar e sua ontogenia funcional em camundongos

Porto Alegre
2019

Marcelo Rigon Zimmer

The role of Agrp neurons in nonfood-related behaviors and their functional ontogeny in mice

O papel dos neurônios Agrp em comportamentos não relacionados à ingestão alimentar e sua ontogenia funcional em camundongos

Thesis submitted to the Graduate Program in Biological Sciences: Biochemistry, in partial fulfillment of the requirements for the degree of Doctor of Philosophy in Biological Sciences: Biochemistry.

Tese apresentada ao Programa de Pós-graduação em Ciências Biológicas: Bioquímica como requisito parcial para obtenção de título de Doutor em Ciências Biológicas: Bioquímica.

Advisor (Orientador) : Prof. Dr. Marcelo de Oliveira Dietrich (Universidade de Yale, New Haven, Estados Unidos)

Co-advisor (Co-orientador): Prof. Dr. Diogo Onofre Gomes de Souza (Universidade Federal do Rio Grande do Sul, Porto Alegre, Brasil)

Porto Alegre

2019

"If monkeys have taught us anything it's that you've got to learn how to love before you learn how to live".
Harry F. Harlow, 1961

“Aos meus pais, Nelson e Arlete, meus irmãos, Aline, Karine e Eduardo, e aos meus mestres Diogo Souza e Marcelo Dietrich que fizeram que meus sonhos tornassem realidade”.

PREAMBLE

Presentation

This thesis (written in English) is organized in three parts, in accordance with local rules of the *Graduate Program in Biological Sciences: Biochemistry* (UFRGS):

Part I: Introduction and Aims.

Part II: Results presented as scientific articles. Each article corresponds to one chapter.

Part III: Discussion, conclusion and references. References correspond to citation in Parts I and III. References in Part II are within each chapter.

Scientific contributions in the form of co-authored research articles that are not part of the main body of this thesis can be found in Annexes.

The experiments described in this thesis were performed in the Department of Comparative Medicine - Yale School of Medicine (New Haven, CT, USA) under the supervision of Dr. Marcelo de Oliveira Dietrich as part of an initiative in collaboration with Dr. Diogo O. Souza from the Department of Biochemistry – UFRGS (Porto Alegre, RS, Brazil) to foster collaboration between UFRGS and Yale University.

PREÂMBULO

Apresentação

Esta tese (escrita em inglês) será organizada em três capítulos, cada uma sendo constituída dos seguintes itens:

Parte I: Introdução e Objetivos.

Parte II: Resultados que serão apresentados na forma de artigos científicos. Cada artigo científico representa um capítulo.

Parte III: Discussão, Conclusão e Referências Bibliográficas citadas na Introdução e Discussão.

Em anexos constarão artigos científicos publicados durante a tese e que não fazem parte do corpo principal da tese.

Os trabalhos realizados durante esta tese foram desenvolvimentos no Departamento de Medicina Comparativa da Universidade de Yale (New Haven, CT, EUA), sob a orientação do Prof. Dr. Marcelo de Oliveira Dietrich como parte de uma iniciativa de colaboração com o Prof. Dr. Diogo O. Souza do Departamento de Bioquímica – UFRGS (Porto Alegre, RS, Brasil) e entre a UFRGS e a Universidade de Yale.

Abstract

Obesity and eating disorders result from altered energy balance. In addition to weight gain or loss, these conditions are associated with other symptoms. For example, obese people commonly exhibit impulsive behavior for food consumption, and patients with Anorexia Nervosa exhibit high physical activity levels and compulsive behaviors. To better understand these medical conditions, it is important to study the function of neuronal mechanisms involved in the control of energy balance. In the mammalian brain, including humans, hypothalamic Agrp neurons release AgRP, NPY, and GABA and are considered critical for the regulation of energy balance. These neurons when active promote robust food intake as demonstrated in mice. Interestingly, Agrp neurons have delayed arborization, and the maturation of their projections to other brain areas occurs only around the third week of life. Here, I studied the function of these hunger-promoting neurons in three different studies. In the chapters 1 and 2, we assessed whether Agrp neurons were involved in behaviors not directly associated to food intake in adult mice using an animal model in which Agrp neurons were specifically activated. In the chapter 3, we evaluated the functional ontogeny of this neuronal population during the postnatal developmental period in neonatal mice. In the first study, we found that specific activation of Agrp neurons induced obsessive-compulsive behaviors in the absence of food. The presence of food suppressed these behaviors. Also, we found that these stereotypic behaviors were mediated via Y_5 receptor signaling. Activation of Agrp neurons also led to reduced anxiety levels and elevated exploration of naturally aversive environments in mice. In the second study, we found that Agrp neurons play an important role in cognitive processes. Activation of Agrp neurons led to diminished performance in a working memory test that was mediated via Y_5 receptor signaling. In the last study, we found that Agrp neurons are involved in aspects of the mother-infant interaction in postnatal mice. In neonates, Agrp neurons were responsive to maternal separation regardless of the level of milk ingestion, but the activation of these neurons was mediated by the lack of thermal stimulation. Moreover, we found that specifically activating Agrp neurons in neonates increased the emission of ultrasonic vocalizations to attract the mother. Overall, our results demonstrate new perceptions about the importance of Agrp neurons in modulating behaviors and cognitive processes that are not directly related to feeding, suggesting a broader role for these neurons in brain function. These results may provide new approaches to eating disorders and psychiatric conditions where energy balance is disrupted and stereotyped behaviors are seen. Our subsequent results investigating the functional development of Agrp neurons may contribute to better understand the infant-mother bonding, that is considered the basis for the development of social relationships in adult life.

Keywords: Agrp, hypothalamus, stereotypic behaviors, cognitive processes, neonatal behaviors, functional ontogeny.

Resumo

Disfunções no balanço energético resultam em incidência de obesidade e distúrbios alimentares. Além de mudanças no peso corporal (ganho ou perda) a desregulação energética está associada com outros sintomas. Por exemplo, pessoas obesas geralmente apresentam comportamento impulsivo por alimentos e pacientes com Anorexia Nervosa demonstram um aumento de atividade física e comportamentos associados à compulsão. Para o melhor entendimento dessas condições médicas, é importante estudar os mecanismos neuronais envolvidos no controle do balanço energético. Em cérebros de mamíferos, incluindo humanos, neurônios hipotalâmicos Agrp liberam AgRP, NPY e GABA e são considerados críticos para a regulação do balanço energético. Esses neurônios quando ativados promovem aumento da ingestão alimentar como demonstrando em estudos em camundongos. Interessantemente, neurônios Agrp possuem maturação tardia de suas projeções, ou seja, as projeções para outras áreas cerebrais completam-se apenas após a terceira semana de vida. Nessa tese, foi avaliada a função dos neurônios Agrp em três diferentes estudos. Nos capítulos 1 e 2 avaliamos se os neurônios Agrp estavam envolvidos em comportamentos não associados a ingestão alimentar em camundongos adultos utilizando um modelo animal no qual os neurônios Agrp foram especificadamente ativados. No capítulo 3 investigamos a ontogenia funcional desse grupo de neurônios durante o período de desenvolvimento em camundongos neonatos. No primeiro estudo, nós encontramos que a ativação específica dos neurônios Agrp induz comportamentos obsessivos-compulsivos na ausência de comida. Esses comportamentos foram silenciados mediante a presença de alimento. Também, encontramos que ativação dos neurônios Agrp induziu esses comportamentos estereotipados via sinalização de receptor Y_5 do NPY. Ademais, a ativação dos neurônios Agrp levou a uma redução dos níveis de ansiedade resultando em maior exploração de ambientes naturalmente aversivos aos camundongos. No segundo estudo encontramos que neurônios Agrp possuem um papel importante em processos cognitivos. A ativação específica resultou em uma diminuição da performance na memória de trabalho mediante sinalização de receptor Y_5 do NPY. No último estudo, encontramos que neurônios Agrp estão envolvidos na interação mãe-filhote em camundongos pós-natais. Em neonatos, neurônios Agrp foram responsivos a separação materna independente de ingestão de leite, porém a ativação desses neurônios foi induzida pela falta de estímulo térmico. Além disso, encontramos que a ativação específica desse grupo neuronal em camundongos neonatos levou a aumento de vocalizações ultrassônicas para atrair a mãe. Em conclusão, nossos resultados demonstram novas percepções sobre a importância dos neurônios Agrp mediando comportamentos estereotipados e processos cognitivos não relacionados diretamente a alimentação, sugerindo que esses neurônios possuem um papel mais amplo na função cerebral. Esses resultados fornecem novas abordagens em distúrbios alimentares e doenças psiquiátricas que apresentam desregulação do balanço energético associado com comportamento estereotipados. Os resultados do último estudo investigando a função dos neurônios Agrp durante o desenvolvimento podem contribuir para o melhor entendimento da interação mãe-filhote que é considerada a base para desenvolvimento de relações sociais na vida adulta.

Palavras-chave: Agrp, hipotálamo, comportamentos estereotipados, processos cognitivos, comportamentos neonatais, ontogenia funcional.

List of abbreviations

CNS	Central nervous system
ARC	Arcuate nucleus of the hypothalamus
Agrp	Agouti-related protein
NPY	Neuropeptide Y
POMC	Pro-opiomelanocortin
GABA	Gamma-Aminobutyric acid
VMH	Ventromedial hypothalamic nucleus
LH	Lateral hypothalamus
MC3R	Melanocortin receptor 3
MC4R	Melanocortin receptor 4

Table of contents (Sumário)

PART I

Here will be described the abstract, introduction, and the aims of this thesis.

Introduction

The incidence of obesity has risen in the last decades at alarming rates (Finkelstein et al., 2009; Hill et al., 2013). In the past, obesity affected mainly adults but the in the last decades incidences of obesity are growing in children and adolescents as well (Gungor, 2014; Raj and Kumar, 2010). Obesity is the leading preventable cause of death worldwide, and it is implicated in various diseases, such as diabetes, cancer and cardiovascular disease (Al-Goblan et al., 2014; Barnes, 2011; Goldstone, 2006). On the other side of the spectrum, anorexia nervosa is an eating disorder manifested by extremely low levels of food consumption and pronounced reduction in body weight (Matsunaga et al., 1999; Treasure et al., 2015). Anorexia nervosa results from a combination of genetic, behavioral, psychological, and social factors (Brockmeyer et al., 2018; Treasure et al., 2015). In addition to reduced food consumption, people with anorexia nervosa also exhibit high physical activity and increased obsessive-compulsive behavior (Coëffier et al., 2016; Gummer et al., 2015; Halmi et al., 2003; Serpell et al., 2002; Thiel et al., 1995). Obesity and anorexia nervosa are suggested to be primarily a consequence of the dysregulation of energy homeostasis (Goldstone, 2006; Treasure et al., 2015). The imbalance between calorie intake and energy expenditure results in the development of obesity and anorexia nervosa. Energy intake and expenditure are interdependent and regulated at several levels. Here, I will briefly review key neuronal circuits involved in energy intake and expenditure regulation.

The brain viewed as the central regulator of energy intake

The first evidence of brain areas involved in the regulation of energy intake was described over 100 years ago by Morh (Mohr, 1840) and Frohlich (Frohlich, 1901) and suggested the hypothalamus, a brain area located below the thalamus (**Figure 1A**), as a critical region implicated in controlling feeding. Later, in the 1940s, studies identified specific areas in the hypothalamus involved in feeding by using systematic lesions to various hypothalamus

nuclei in rats (Anand and Brobeck, 1951a; Hetherington and Ranson, 1940, 1942). Lesions in the hypothalamic ventromedial (VMH), paraventricular (PVH) and dorsomedial (DMH) nuclei induced obesity and hyperphagia (Brobeck, 1946; Hetherington and Ranson, 1940; Marshall et al., 1955; Mayer and Marshall, 1956), whereas lesions in the lateral hypothalamus (LH) led to the suppression of feeding (Anand and Brobeck, 1951b). Based on these results, it was proposed that the hypothalamus contain a "dual center model" in which the VMH acts as the satiety center and the LH acts as the hunger center (Anand and Brobeck, 1951b; Hetherington and Ranson, 1940) (**Figure 1B**). Later, the arcuate nucleus of the hypothalamus (ARC) was also identified to be critical in the regulation of energy intake (Brecher and Waxler, 1949; Marshall et al., 1955; Olney, 1969; Olney et al., 1971). Rodents injected with monosodium glutamate, a compound that produced cellular death in the ARC but not in the VMH, led to obesity development (**Figure 2**). These finds were an entry point to the discovery of the Melanocortin System, one of the most important neuronal signaling pathways to control energy balance.

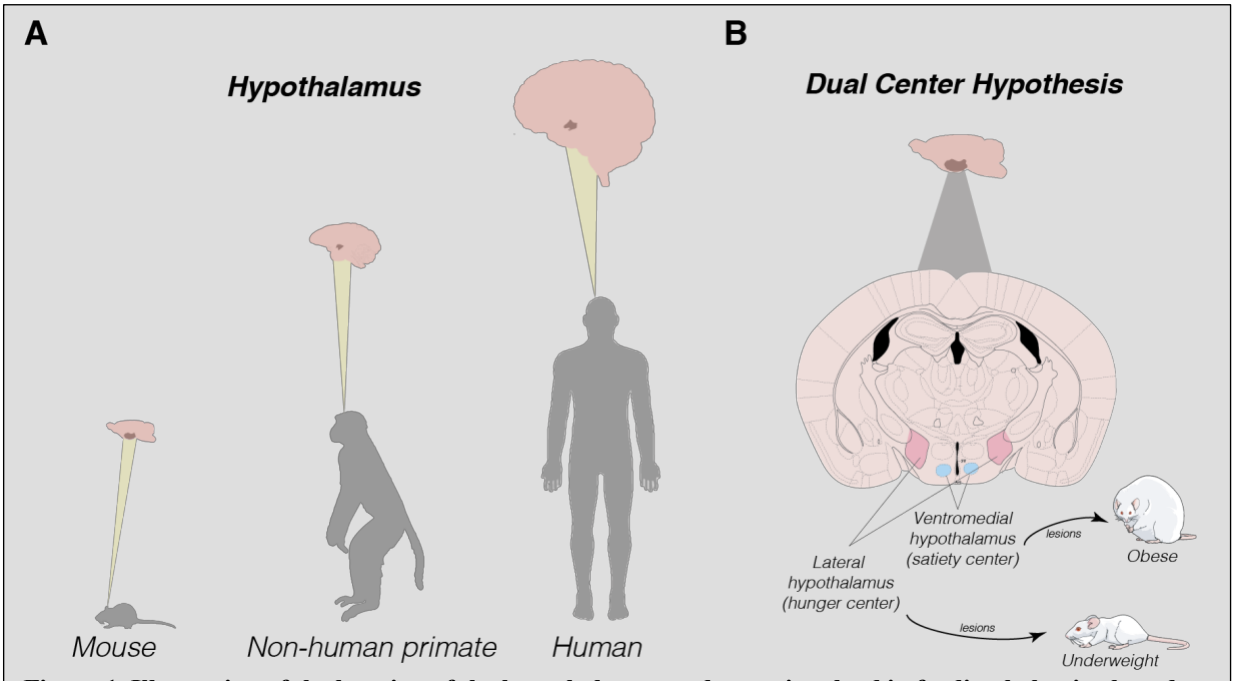

Figure 1. Illustration of the location of the hypothalamus and areas involved in feeding behavior based on the Dual Center Hypothesis. (A) Location of the hypothalamus in mouse, non-primate humans and humans. **(B)** Representative mouse brain in coronal plane demonstrating the "hunger" and "satiety" centers. Lesions in the VMH induced to obesity whereas lesions in the LH led to aphagia (lack of eating).

The central melanocortin system

The ARC is positioned at the bottom of the third ventricle close to a circumventricular organ called median eminence, and neurons located in this region have direct contact with metabolic and hormonal signals from the periphery (Cansell et al., 2012; Sternson and Atasoy, 2014) **(Figure 2)**. Two main sets of neurons, with opposing effects on energy homeostasis, have been described in the ARC as core components of the melanocortin system (Cone, 2005; Cone, 2006). Pro-opiomelanocortin neurons (POMC) are anorexigenic[1], whereas Agouti-related protein neurons (Agrp) are orexigenic[2]. Melanocortin peptides released by POMC neurons include α-, and β-melanocyte stimulating hormones (α- and β-MSH) that bind to melanocortin receptors and initiate the central anorexic signaling pathway that results in

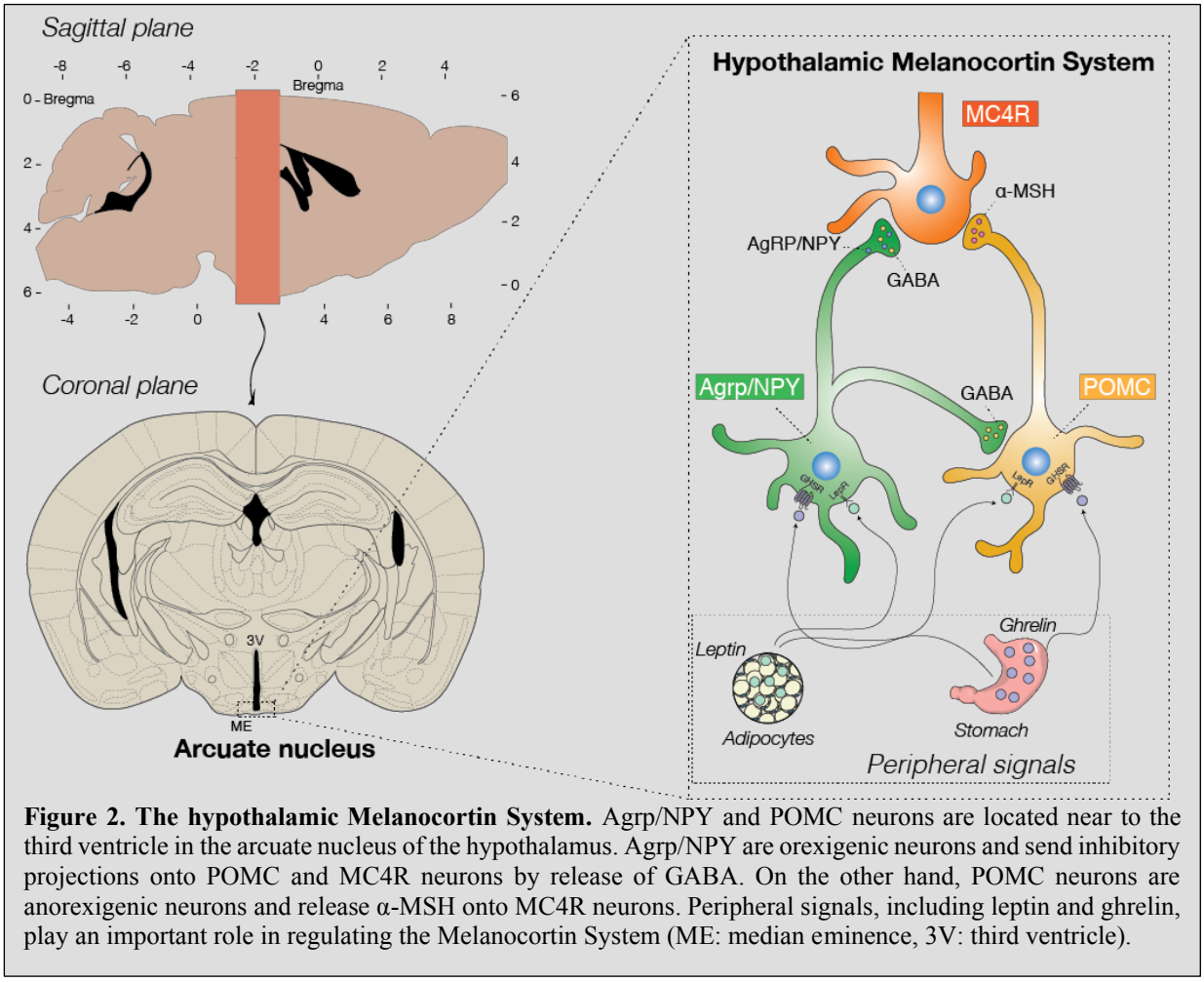

Figure 2. The hypothalamic Melanocortin System. Agrp/NPY and POMC neurons are located near to the third ventricle in the arcuate nucleus of the hypothalamus. Agrp/NPY are orexigenic neurons and send inhibitory projections onto POMC and MC4R neurons by release of GABA. On the other hand, POMC neurons are anorexigenic neurons and release α-MSH onto MC4R neurons. Peripheral signals, including leptin and ghrelin, play an important role in regulating the Melanocortin System (ME: median eminence, 3V: third ventricle).

[1] Anorexigenic neurons are neurons that when active promote suppression of appetite for food.
[2] Orexigenic neurons are neurons that when active promote increased appetite.

decreased food consumption and increased energy expenditure (Adan et al., 2006; Cone, 2006; Ellacott and Cone, 2006; Mori, 2001). Melanocortin receptors are a family of G-coupled protein melanocortin receptors (MC1R to MC4R) distributed throughout the body, and not only in the brain (Cone, 2005; Cone, 2006; Gantz et al., 1993a; Gantz et al., 1993b; Gantz et al., 1994; Griffon et al., 1994; Mountjoy et al., 1994; Mountjoy et al., 1992). Among these receptors, MC3R and MC4R are expressed mainly in the brain (Mountjoy et al., 1994; Roselli-Rehfuss et al., 1993).

POMC neurons are composed of heterogeneous subpopulations (Lam et al., 2017; Sohn and Williams, 2012; Williams et al., 2010) that can release either GABA or glutamate as classic neurotransmitters (Dicken et al., 2012; Hentges et al., 2004; Hentges et al., 2009). On the other hand, Agrp neurons release the peptide AGRP that acts as a natural antagonist of MC3R and MC4R preventing the binding of α- and β-MSH to these receptors (Cone, 2005; Cone, 2006; Haskell-Luevano and Monck, 2001; Lu et al., 1994; Oosterom et al., 2001; Roselli-Rehfuss et al., 1993). Agrp neurons also produce and release neuropeptide Y (NPY) and GABA (Hahn et al., 1998; Horvath et al., 1997). An interesting functional property of these neurons is that Agrp neurons send inhibitory projections onto POMC neurons, thus inhibiting POMC neuronal activity in conditions of food deprivation that favors increased appetite (Cowley et al., 2001; Horvath et al., 1992; Pinto et al., 2004; Rau and Hentges, 2017). The hypothalamic Agrp neurons (see **Box 1** for extended review) will be the focus of my studies in this thesis.

The development of genetic mouse models provided valuable platforms to understand the role of Agrp neurons by manipulating the neuronal activity of these neurons. Activation of the Agrp neurons using optogenetic[3] or chemogenetic[4] tools leads to acute and robust feeding behavior (Aponte et al., 2011; Dietrich et al., 2015; Krashes et al., 2011; Ollmann et al., 1997;

3 Optogenetics: Technique by which light-responsive proteins selectively modulate neuronal activity.

4 Chemogenetic: An approach used to modulate neuronal activity utilizing genetically engineered receptors that selectively interact with previously unrecognized small molecules.

Rossi et al., 1998). Conversely, inhibition of the Agrp neurons results in appetite suppression (Atasoy et al., 2012; Krashes et al., 2011). Furthermore, ablation of Agrp neurons leads to starvation and subsequently death in adult mice (Bewick et al., 2005; Gropp et al., 2005; Luquet et al., 2005), demonstrating that these neurons are important for feeding behavior. In vivo recordings of the activity of Agrp neurons using electrophysiology and calcium imaging[5] studies have revealed the dynamics of Agrp neuronal response to food. Food ingestion or even the sensory detection of food rapidly suppresses the neuronal activity of Agrp neurons (Betley et al., 2015; Chen et al., 2015; Mandelblat-Cerf et al., 2015).

The Agrp neural circuits governing food intake comprise projections onto the paraventricular nucleus of the hypothalamus (PVH), the anterior portion of the bed nucleus of the stria terminalis (aBNST), the paraventricular thalamic nucleus (PVT), and the lateral hypothalamus (LH) (Atasoy et al., 2012; Betley et al., 2013; Broberger et al., 1998; Wu et al., 2009). Altogether, the neurocircuitry of Agrp neurons in mediating food intake is well documented, but neural circuits governing energy balance are substantially connected with various systems, and recent studies have attempted to understand if these neurons were involved in behaviors not related to feeding.

The involvement of Agrp neurons in nonfood-related behaviors

Studies aimed at determining the role of Agrp neurons in behavioral responses not directly associated with food intake were performed based on the anatomical and functional organization of Agrp neuron circuitry within the brain. Agrp neurons send inhibitory projections to approximately 15 brain regions including mesolimbic, midbrain, and subcortical areas (Bouret et al., 2004; Broberger et al., 1998; Cone, 2005; Sternson and Atasoy, 2014; Wu

5 Calcium imaging: Optical approach to record the physiological activity of cells using calcium-sensitive fluorescence proteins.

et al., 2009). Thus, it was intuitive to postulate that Agrp neurons could modulate a broad range of behaviors by using multiple intertwined neuronal circuits. Our group identified that Agrp neurons regulate the development of dopamine neurons by defining the set point of the reward circuitry and associate behaviors (Dietrich et al., 2012).

Box 1 | A historical perspective on the hypothalamic Agrp neurons

Agouti protein was primarily linked to skin pigmentation by acting via MC1R to suppress α-melanocyte stimulating hormone-induced eumelanin (black pigment) deposition and favoring pheomelanin (yellow pigment) production and yellow hair color (Lamoreux and Mayer, 1975; Silvers, 1958; Silvers, 1979). An analogous effect of this protein was found in the brain. Agouti protein signaling on the brain MC3R and MC4R led to obesity in mice (Lu et al., 1994; Ollmann et al., 1997). However, there was no agouti protein produced in the brain, raising the question of whether there was any natural antagonist of these receptors in the nervous system.

A few years later, a gene producing a peptide similar to the agouti protein was cloned (Bultman et al., 1992; Miller et al., 1993). This peptide - and the corresponding gene - were then named Agouti-related protein (AGRP) (Ollmann et al., 1997; Shutter et al., 1997). AGRP has 25% of homology to the agouti protein, and it is found only in the hypothalamus of mice (Shutter et al., 1997) . The hypothalamic neurons that produce AGRP were activated under food deprivation and co-expressed neuropeptide Y (NPY) (Hahn et al., 1998). The Agrp/NPY neurons are located close to the third ventricle in the arcuate nucleus of the hypothalamus and release the neurotransmitter gamma-aminobutyric acid (GABA) (Horvath et al., 1997).

The role of Agrp neurons on food intake was first suggested by the strong appetite-promoting effects of brain injections of NPY (Clark et al., 1985; Morley et al., 1987a; Morley et al., 1987b; Stanley et al., 1985; Stanley and Leibowitz, 1985). Subsequently, intracerebroventricular injections of AGRP were also found to increase food intake (Hagan et al., 2000; Rossi et al., 1998). Later metabolic studies evaluating the role of peripheral nutrients signals on food intake revealed that Agrp neurons are activated by circulating hormones released during energy deficit (e.g., ghrelin) (Chen et al., 2004; Cowley et al., 2003; Howard et al., 2004; van den Top et al., 2004; Wang et al., 2002), and hormone signals of energy surfeit inhibit these neurons (e.g., leptin) (Baquero et al., 2014; Pinto et al., 2004; Spanswick et al., 1997; van den Top et al., 2004). These findings led to Agrp neurons be referred to as “first order neurons” (Cansell et al., 2012) since they respond to peripheral circulating signals of hunger and satiety.

Dopamine is well known to be involved in motivational behaviors (Arias-Carrion and Poppel, 2007; Cools, 2008), and dysregulation of this neurotransmitter lead to neuropsychiatric conditions including Obsessive-compulsive disorder (OCD) (Abramowitz and Jacoby, 2015; Brambilla et al., 2000; Pauls et al., 2014). Mouse models and human patients with OCD exhibited high levels of anxiety, repetitive and compulsive behaviors (Alonso et al., 2015; Benito and Storch, 2011; Heyman et al., 2006; Leonard et al., 1994). Repetitive and compulsive behaviors are also displayed in eating disorders such as Anorexia nervosa (Thiel et al., 1995; Treasure et al., 2015) and Prader-Willi Syndrome (Cassidy and Driscoll, 2009; Clarke et al., 2002; Dykens, 2004). These findings reinforce the connection between metabolism and neuropsychiatric conditions. Based on these previous observations, in the first part of this thesis, I probed the capacity of Agrp neurons to alter behaviors not immediately related to food intake in adult mice (See Chapter I: "Hypothalamic Agrp neurons Drive Stereotypic Behaviors beyond Feeding"). In the second part of this thesis, I probed the capacity of Agrp neurons to modulate cognitive performance in adult mice (See Chapter II: "Activation of hypothalamic Agrp neurons impairs cognitive processes in mice").

The functional ontogeny of Agrp Neurons

Previous research identified some principles of the functional organization of Agrp neurons during development. Circuit mapping studies revealed that projections of the Agrp neurons to other sites in the brain are still under development after birth in mice and rats (Bouret et al., 2004; Grove et al., 2003; Grove and Smith, 2003; Nilsson et al., 2005). For instance, axonal projections of Agrp neurons to the LH are not fully developed until the third postnatal week (Bouret et al., 2004; Nilsson et al., 2005). Moreover, ablation of Agrp neurons in neonates did not lead to aphagia (Luquet et al., 2005), suggesting these neurons were not involved in nutrient ingestion early in mouse development. Despite these previous studies, there is a lack

of data on the functional development of hypothalamic Agrp neurons. This is important as all mammals transition from breastfeeding to ingestion of solid food sources independently of their mothers. Before delving into the experimental part of this thesis, I will briefly review key findings in the ontogeny of nutrient intake. I experimental investigated the ontogeny of Agrp neurons in the third part of this thesis (See Chapter III: "Functional ontogeny of hypothalamic Agrp neurons in neonatal mouse behaviors").

The development of nutrient intake in rodents: The transition from suckling to independent feeding

Shortly after birth, the newborn mouse – as well as all other mammals - must initiate milk intake to survive. Milk is obtained by suckling behavior (Blass and Teicher, 1980; Blass, 1979; Hall et al., 1975). Suckling provides all nutrients and fluids for the infant as well as transfers the necessary signals for growth and the development of the immune system (Nowak, 2006).

Studies using laboratory mice and rats have demonstrated that suckling can be divided in three distinct phases (Blass and Teicher, 1980; Fox, 1966). The first phase, which happens after birth until the 11th day of life, comprises the period in which the neonates are fully dependent on the mother. In this period, neonates spend the majority of the time in the nest, and are almost continuously attached to the dam's nipples. Milk release occurs in intermittent intervals upon stimulation of the nipple, triggering the release of oxytocin and milk ejection (Lincoln et al., 1973; Lincoln and Paisley, 1982). Thus, suckling varies in episodes of nutritive, when milk letdown occurs, and non-nutritive suckling behavior (see **Box 2** for extended review). During this phase, nipple attachment is primarily guided by olfactory cues (Al Ain et al., 2013; Logan et al., 2012; Teicher and Blass, 1977). For instance, disruption of olfactory function severely disrupts nipple attachment in infant rats (Singh and Tobach, 1975; Singh et

al., 1976). Furthermore, nipple attachment in newborn mice occurred through learning of signature odors released by the mother (Logan et al., 2012).

The second phase occurs approximately between the 12th and 15th days after birth. During this period, the infants have better motor skills and starts to explore the environment, spending time away from the nest in laboratory conditions (Blass and Teicher, 1980; Lehrman, 1963). At this stage of postnatal development, the auditory system is functional with ears opening around postnatal day 12 (Alford and Ruben, 1963; Castelhano-Carlos et al., 2010). Additionally, the visual system is also fully functional with eyes opening around postnatal day 14 (Blass and Teicher, 1980; Castelhano-Carlos et al., 2010; Hall, 1985). By the end of this period, after eyes open, infants begin to gradually consume solid food sources.

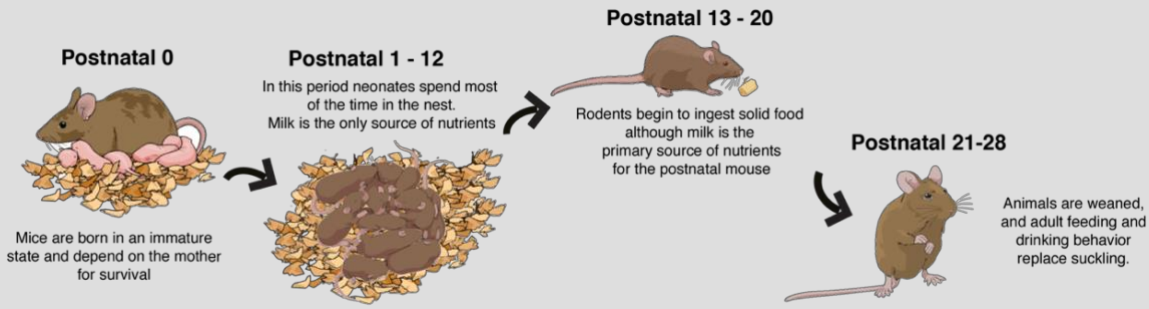

Figure 3. Diagram of postnatal development period in laboratory mice. The postnatal development in laboratory mice lasts 21 days. During this period the neonates undergo profound behavioral and metabolic changes. Until 12 days of age, neonates are entirely dependent on the mother and milk is the sole source of nutrients. Later, postnatal mice start to consume solid food. Food intake gradually increases and fully replace milk around three weeks of age where animals are separated from the mother (weaning).

The third phase befalls from the 16th day of life and continues until the 21st day of life, a period during which suckling and consumption of solid food co-exist in infants (Blass, 1979; Hall et al., 1977). Thereafter, when laboratory rodents reach 21 days of age, they are ready to live independently from the dam. Weaning in laboratory rodents occurs approximately 21 days after birth (Cramer et al., 1990; Thiels and Alberts, 1991) (**Figure 3**).

Box 2 | The behavioral pattern of suckling behavior during development in rodents

Suckling is the defining mammalian behavior performed by infant mammals to obtain milk (Blass, 1990; Bondar, 2018; Nowak, 2006). Suckling plays a vital role in providing the only source of nutrients for the neonates in the first days of life (Bondar, 2018; Nowak, 2006), although the time in which infants spend attached to the mother's nipple exceed the episodes of milk release (Blass, 1990; Blass and Teicher, 1980; Blass, 1979; Brake et al., 1979). These lines of evidence led scientists to divide suckling into two different categories: nutritive and non-nutritive suckling (Brake et al., 1979; German and Crompton, 2000; Wolff, 1968).

Milk release occurs at random intervals (Lincoln et al., 1973), and nutritive suckling occurs when infants are attached to the mother's nipples while ingesting milk (Blass, 1990; German and Crompton, 2000). By contrast, non-nutritive suckling occurs during attachment of the infant to the mother's nipples in the absence of milk release (Brake et al., 1979; Wolff, 1968).

Among scientists, non-nutritive suckling is thought to occur due to the lack of nutrient sensing at early postnatal development in the neonate rodents (e.g., prolonged periods of milk deprivation do not affect milk intake and nipple attachment in neonate rodents until the second week of life) and its role has divided opinions (Blass, 1990; Blass and Teicher, 1980).

For example, non-nutritive suckling can be seen as a strategy used by the neonates to avoid losing the opportunity of milk ingestion since they spend a substantial amount of time performing non-nutritive suckling (Hall, 1985). Thus, early in life, neonates are attached to the mother's nipple to ensure ingestion of milk and consequently to increase the chances of survival.

However, non-nutritive suckling can be viewed from a different perspective. Episodes of non-nutritive suckling are high during the first week of life, and this period coincides with the development of thermoregulation of the neonates (prior one week of life the neonates have limited thermoregulation) (Kleitman and Satinoff, 1982; Leon, 1986). Thus, since a significant part of the thermal exchange in rodents occurs through contact behavior (i.e., huddling) (Alberts, 1978), it can be implied that neonates are attached and in contact with the mother to prevent heat losses.

The episodes of non-nutritive suckling decrease around postnatal day 13 (it ceases around weaning). This period coincides with the time in which neonates develop independence from the mother and start to ingest solid food (Blass, 1990; Blass and Teicher, 1980; Hall et al., 1977). Also, it coincides with the development of nutrient sensing to deprivation in rodents (Blass, 1990; Blass and Teicher, 1980; Hall et al., 1975; Kenny et al., 1979), but whether non-nutritive suckling performed by neonates represents a strategy of contact behavior or a strategy to ensure milk ingestion is a question that remains to be addressed.

Aims

Evaluate the role of Agrp neurons in mediating complex behaviors not proximally associated to food intake (chapter I and II).

Evaluate the functional role of neonatal Agrp neurons during the early postnatal development of mice (chapter III).

PART II

Here, the results in each chapter are presented as scientific articles. The objectives of each chapter are described in the introduction of each scientific article.

Chapter I. Hypothalamic Agrp neurons drive stereotypic behaviors beyond feeding

Scientific article published on *Cell*.

Article

Cell

Hypothalamic Agrp Neurons Drive Stereotypic Behaviors beyond Feeding

Graphical Abstract

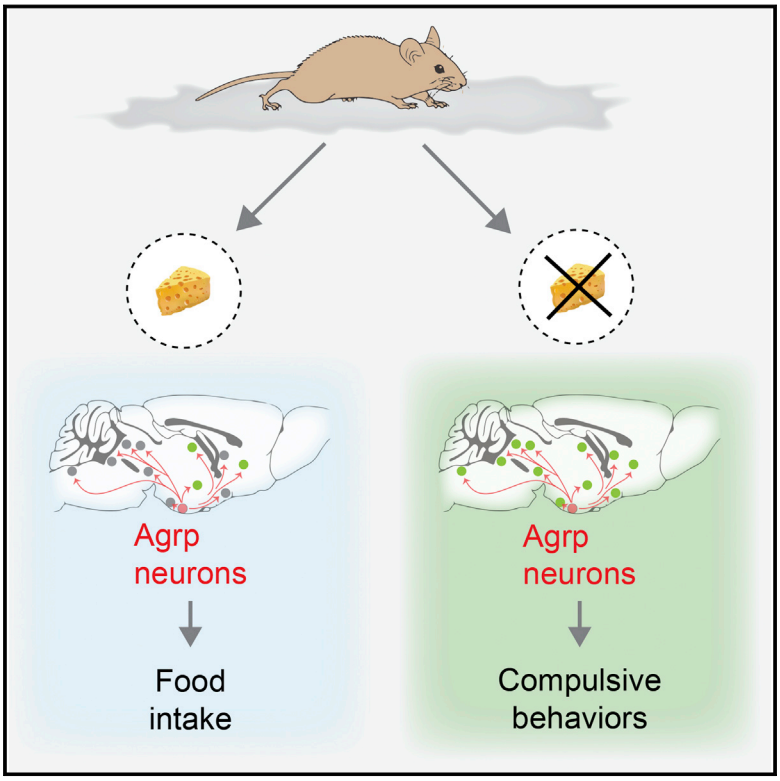

Authors

Marcelo O. Dietrich, Marcelo R. Zimmer, Jeremy Bober, Tamas L. Horvath

Correspondence

marcelo.dietrich@yale.edu

In Brief

Activity of Agrp neurons in the hypothalamus is known to stimulate feeding behavior, but activating them in the absence of food reveals that they also promote a set of stereotyped compulsive behaviors in mice.

Highlights

- Agrp neuron activation leads to foraging and displacement behaviors
- Agrp neurons promote stereotypic behavioral responses
- Activation of Agrp neurons decreases anxiety levels
- Y_5R signaling is necessary for Agrp neuron-mediated stereotypic behaviors

Dietrich et al., 2015, Cell *160*, 1222–1232
March 12, 2015
http://dx.doi.org/10.1016/j.cell.2015.02.024

Cell

Article

Hypothalamic Agrp Neurons Drive Stereotypic Behaviors beyond Feeding

Marcelo O. Dietrich,[1,2,3,*] Marcelo R. Zimmer,[1,3] Jeremy Bober,[1] and Tamas L. Horvath[1,2,4]

[1]Program in Integrative Cell Signaling and Neurobiology of Metabolism, Section of Comparative Medicine, Yale University School of Medicine, New Haven, CT 06520, USA

[2]Department of Neurobiology, Yale University School of Medicine, New Haven, CT 06520, USA

[3]Graduate Program in Biochemistry, Universidade Federal do Rio Grande do Sul, Porto Alegre, RS 90035, Brazil

[4]Kavli Institute for Neuroscience at Yale University, New Haven, CT 06520, USA

*Correspondence: marcelo.dietrich@yale.edu

http://dx.doi.org/10.1016/j.cell.2015.02.024

SUMMARY

The nervous system evolved to coordinate flexible goal-directed behaviors by integrating interoceptive and sensory information. Hypothalamic Agrp neurons are known to be crucial for feeding behavior. Here, however, we show that these neurons also orchestrate other complex behaviors in adult mice. Activation of Agrp neurons in the absence of food triggers foraging and repetitive behaviors, which are reverted by food consumption. These stereotypic behaviors that are triggered by Agrp neurons are coupled with decreased anxiety. NPY_5 receptor signaling is necessary to mediate the repetitive behaviors after Agrp neuron activation while having minor effects on feeding. Thus, we have unmasked a functional role for Agrp neurons in controlling repetitive behaviors mediated, at least in part, by neuropeptidergic signaling. The findings reveal a new set of behaviors coupled to the energy homeostasis circuit and suggest potential therapeutic avenues for diseases with stereotypic behaviors.

INTRODUCTION

Neural circuits are responsible for organizing and regulating flexible goal-oriented behaviors by integrating sensory and interoceptive information. The observation that mice can perform complex dynamic computations similar to humans (Kheifets and Gallistel, 2012) supports the view that brain mechanisms involved in complex goal-oriented behaviors rely on phylogenetically primitive neural circuits.

Homeostatic functions—for example, food intake—are adaptive responses that allow successful survival of the individual in the environment. The hypothalamus is an ancient brain region present in all vertebrates that is critical for the regulation of homeostatic functions, including energy balance, sexual behavior, sleep, and thirst. For more than 20 years, hypothalamic neurons that produce NPY, Agrp, and GABA have been thought to be involved in the promotion of hunger (Hahn et al., 1998; Horvath et al., 1992; Horvath et al., 1997). Neuropeptide injections in the brain elicit robust increases in food intake (Clark et al., 1984; Ollmann et al., 1997; Rossi et al., 1998; Stanley et al., 1986), and food deprivation increases the activity of these neurons (Hahn et al., 1998; Liu et al., 2012; Takahashi and Cone, 2005; Yang et al., 2011). Acute (Gropp et al., 2005; Luquet et al., 2005), but not chronic (Xu et al., 2005), ablation of Agrp neurons leads to cessation of feeding and, ultimately, death (Luquet et al., 2005). Conversely, acute activation of these neurons induces robust feeding (Aponte et al., 2011; Krashes et al., 2011). The neural circuits involved in the regulation of hunger by Agrp neurons seem to involve several brain nuclei (Atasoy et al., 2012; Betley et al., 2013; Wu et al., 2012). Agrp neurons have a broad projection field (Broberger et al., 1998) with important developmental characteristics as well (Dietrich et al., 2012; Grove et al., 2001). It is, therefore, intuitive to postulate that Agrp neurons orchestrate complex behavioral and physiological changes that encompass hunger rather than just food intake. This hypothesis gains momentum when neuropsychiatric conditions with strong homeostatic components are considered (e.g., anorexia nervosa). For instance, anorexia nervosa is a state of severe negative energy balance, in which brain circuits controlling feeding may be involved in the development of cognitive impairments of this disorder.

Here, we tested these assumptions by performing analysis of mouse behavior under conditions of Agrp neuron activation. Our results uncover a fundamental role for Agrp neuron activation in promoting repetitive/stereotypic behaviors in mice, unmasking a previously unsuspected role for these hypothalamic neurons.

RESULTS

Hunger-Related Behaviors

We first determined the effects of food deprivation, a physiological state of elevated Agrp neuronal activity (Hahn et al., 1998; Takahashi and Cone, 2005), on behavior. We used software-assisted characterization of mouse home-cage behaviors (Adamah-Biassi et al., 2013; Jhuang et al., 2010; Kyzar et al., 2012) to assess different aspects of the behavioral repertoire that occurs during hunger (Figure 1A). We studied fed, food deprived (FD), and food-deprived mice that were re-fed (RF). We divided our analysis into three large groups of behaviors: (1) consummatory responses represented by eating-related behaviors (e.g., time spent in the eating zone and chewing); (2) appetitive

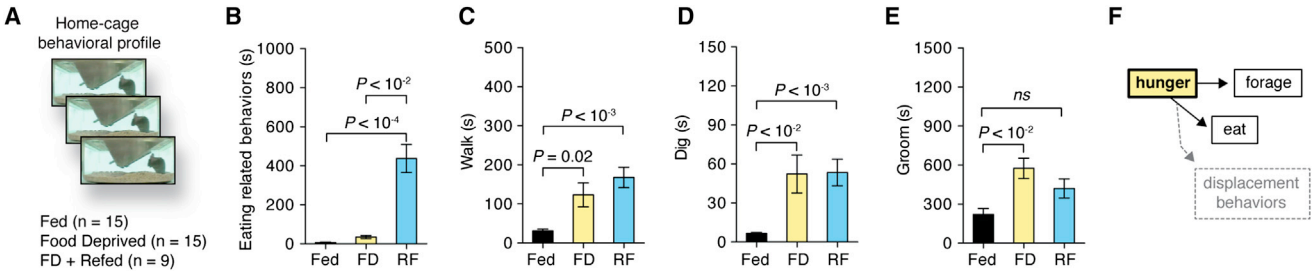

Figure 1. Home-Cage Behaviors in Food-Deprived and Re-Fed Mice

(A) Mouse behaviors in the home cage of fed (black bars), food-deprived (yellow bars), and re-fed (blue bars) mice.

(B–E) Time spent in (B) eating-related behaviors, (C) walking, (D) digging, and (E) grooming.

(F) Behaviors elicited by hunger states.

Error bars represent mean ± SEM. p values represent Holm-Sidak's multiple comparisons test.

behaviors (forage-related behaviors, e.g., digging and walking); and (3) displacement behaviors (e.g., grooming). As expected, fed and FD animals did not engage in eating-related behaviors when food was not presented in the home cage, an effect promptly reverted in re-fed animals (Figure 1B). Food deprivation stimulated forage-related behaviors, an effect that persisted in the re-fed group (Figures 1C and 1D). Because our analyses lasted for 1 hr after the introduction of food to mice, our data indicate that the mechanisms involved in foraging behaviors during food deprivation are slowly switched off by satiety and not acutely by immediate presentation of food. Food deprivation also exacerbated grooming behavior (Figure 1E). In such conditions, grooming has been considered a displacement behavior (Barnett, 1956), a substitute of consummatory eating. Refeeding acutely attenuated grooming (Figure 1E), reinforcing that displacement behaviors, such as grooming, manifest when animals lack the consummatory response. Thus, hunger promotes foraging (appetitive), eating (consummatory), and grooming (displacement) behaviors in mice (Figure 1F). Because the activation of Agrp neurons promotes hunger in sated mice (Aponte et al., 2011; Krashes et al., 2009; Krashes et al., 2011), we next asked what aspects of the behavior repertoire promoted by food deprivation may be induced by acute activation of the Agrp neurons.

Acute Agrp Neuronal Activation

Agrp neurons have a broad projection field (Broberger et al., 1998), which extends to a wide range of subcortical areas (Figure 2A). This complex connectivity indicates that Agrp neurons have the capability to modulate a broad range of behaviors using multiple parallel circuits. In a previous study, we showed that Agrp neurons influence motivational states not related to feeding—for example, responses to cocaine (Dietrich et al., 2012). As an underlying mechanism, our data indicated that Agrp neurons have a developmental effect on dopamine cell function. These data reinforce the notion that animal models with altered Agrp neuronal activity during development are not suitable for the study of their acute role in the adult (Dietrich et al., 2012). Here, to examine the acute effects of Agrp neurons on adult animal behavior, we utilized animal models that allowed activation of Agrp neurons in a rapid, reliable, and reproducible manner.

Several techniques have been developed to acutely manipulate neuronal function in vivo. Optogenetics (Aponte et al., 2011) and chemical genetics using designer receptors exclusively activated by designer drugs (DREADDs) (Krashes et al., 2011) have been used to study the effects of Agrp neuron activity on the feeding behavior of adult mice. Optogenetics provide good time resolution with early onset of feeding behavior (Aponte et al., 2011); however, it requires the insertion of a light source deep into the brain, which adds a bias when analyzing complex behaviors. On the other hand, DREADD can be used to activate Agrp neurons by peripherally injecting receptor-ligand with robust induction of food intake (Krashes et al., 2011) but with more coarse kinetics (Rogan and Roth, 2011). We used transgenic mice that conditionally express Trpv1 in Cre-expressing cells (Arenkiel et al., 2008; Güler et al., 2012) (*R26-LSL-Trpv1*; Figure 2B) to selectively introduce Trpv1 in Agrp neurons. By backcrossing these mice (*R26-LSL-Trpv1*) to a Trpv1 knockout background and then to *Agrp-Cre* mice, we generated animals that express Trpv1 exclusively in the Agrp neurons (hereafter, Agrp-Trpv1 mice; Figures 2B and S1). We performed a series of control experiments to confirm that expression of Trpv1 was restricted to Agrp neurons in the arcuate nucleus and not in off-target cells (Figure S1 and Experimental Procedures). Trpv1 is a cation channel that is activated by the exogenous agonist capsaicin (Caterina et al., 1997) in a rapid and reversible manner (Güler et al., 2012). Slice whole-cell recordings showed that capsaicin increased the firing rate of Agrp neurons (Figure 2C). The analysis of c-*fos* expression in Agrp neurons after capsaicin injection (i.p.) in Agrp-Trpv1 mice revealed that most Agrp neurons throughout the arcuate nucleus were activated in these transgenic mice (Figure 2C). Capsaicin injection of Agrp-Trpv1 mice led to increased food intake in both female (Figure 2D) and male mice (Figure 2E and Movie S1). Notably, the amount of food consumed by the activation of Agrp neurons in our studies was of similar magnitude as that observed when these cells were activated by optogenetics or DREADDs (Aponte et al., 2011; Krashes et al., 2011). The latency to eat in Agrp-Trvp1 mice was faster (mean = 110.1 s [95% CI = 95.5–124.6], n = 15 mice) compared to these other techniques (Aponte et al., 2011; Krashes et al., 2011) (Figures 2F and 2G). Thus, this animal model enabled us to rapidly and reliably activate Agrp neurons by peripheral injection of capsaicin and explore their role on behaviors.

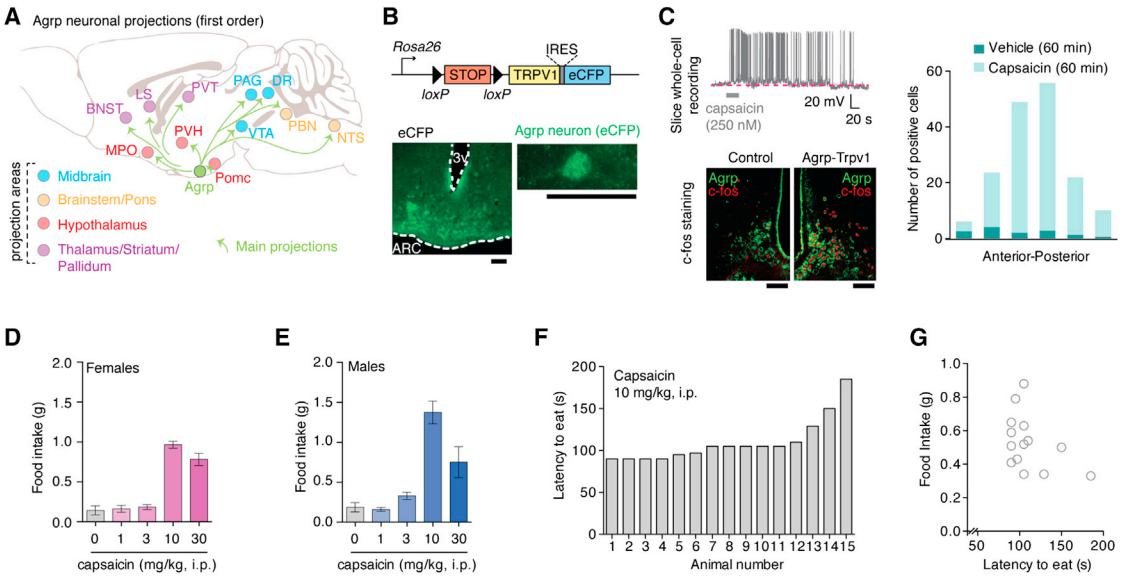

Figure 2. Trpv1 Channels in Agrp Neurons Allow Acute Control of Neuronal Activity

(A) Main projection from Agrp neurons.

(B) Reporter Trpv1 mice and CFP staining in the arcuate nucleus of Agrp-Trvp1 mice.

(C) Whole-cell recording of an Agrp-Trpv1 neuron and c-*fos* staining in Agrp-Trpv1-HA reporter mice 60 min after capsaicin injection (10 mg.kg, i.p.).

(D and E) Food intake in (D) female Agrp-Trpv1 and in (E) male mice.

(F) Latency to eat in female Agrp-Trpv1 mice.

(G) Correlation between latency and food intake.

Error bars represent mean ± SEM. Scale bars, 50 μm. See also Figure S1 and Movie S1.

Repertoire of Home-Cage Behaviors

To screen for broad changes in behavior after Agrp neuron activation, we investigated changes in home-cage behaviors in the presence or absence of food in sated mice (Figure 3). In the presence of food, activation of Agrp neurons did not statistically change ambulatory activity (Figure 3A), while it evoked feeding in all Agrp-Trvp1 mice tested. Conversely, when food was removed, Agrp neuron activation increased activity levels (Figure 3B). To dissect these behavioral changes, we characterized mouse behaviors in their home cages upon activation of the Agrp neurons, similarly to what we did in FD mice (Figure 1). These experiments were performed in sated mice provided with food or with an empty food container. In all Agrp-Trpv1 mice tested in this paradigm, when food was present in their home cage, injection of capsaicin evoked robust food intake (data not shown). As expected, consummatory aspects of feeding, as measured by eating-related behaviors, were greatly enhanced by Agrp neuron activation (Figure 3C). Interestingly, activation of Agrp neurons in sated mice in the absence of food also led to increases in eating-related behaviors (e.g., interaction with the empty food container and chew bedding material; Figure 3C). The persistence of these behaviors indicates a degree of repetitiveness and stereotypy in the behavior repertoire of Agrp neuron activated animals in the absence of food.

Forage-related behaviors were increased in Agrp-neuron-activated mice in the absence of food, an effect that was almost completely reverted in the presence of food (Figures 3D and 3E). Grooming also increased after treatment of Agrp-Trpv1 mice with capsaicin in the absence of food but decreased when animals were provided food (Figure 3F). Grooming is considered a displacement behavior to attenuate the appetitive response (forage) in the absence of the stimulus (food). When manifested in excess, grooming has also been related to obsessive-compulsive behaviors in mice (Ahmari et al., 2013; Burguière et al., 2013), similar to digging (Karvat and Kimchi, 2012). Thus, our findings indicate that, in addition to appetitive and consummatory aspects of hunger, the activation of Agrp neurons in Agrp-Trpv1 mice is sufficient to drive repetitive/stereotypic behaviors, an unsuspected role for these hypothalamic neurons. To corroborate these findings, we expressed hM3Dq in Agrp neurons by injecting *Agrp-Cre* mice with a recombinant AAV vector carrying a cre-dependent coding sequence (rAAV-FLEX- hM3Dq-mCherry). The activation of Agrp neurons by peripheral injection of the receptor ligand, clozapine-N-oxide (CNO, 0.3 mg/kg, i.p), led to similar results as observed in Agrp-Trpv1 mice injected with capsaicin (Figure S2) but with a delayed response, consistent with the slow effect of hM3Dq in stimulating neuronal activity (Krashes et al., 2011; Rogan and Roth, 2011). Altogether, we conclude that activation of the Agrp neurons resembles many, but not all, aspects of food deprivation. Our findings place interoceptive regions of the mammalian brain, such as the arcuate nucleus of the hypothalamus, as crucial mediators of repetitive and stereotypic behaviors (Figures 3C and 3F). Thus, we set out to investigate these behavioral responses in greater detail.

Agrp Neurons Trigger Repetitive Behaviors

To further evaluate the extent to which the activation of Agrp neurons can engage mice in repetitive behaviors, we tested

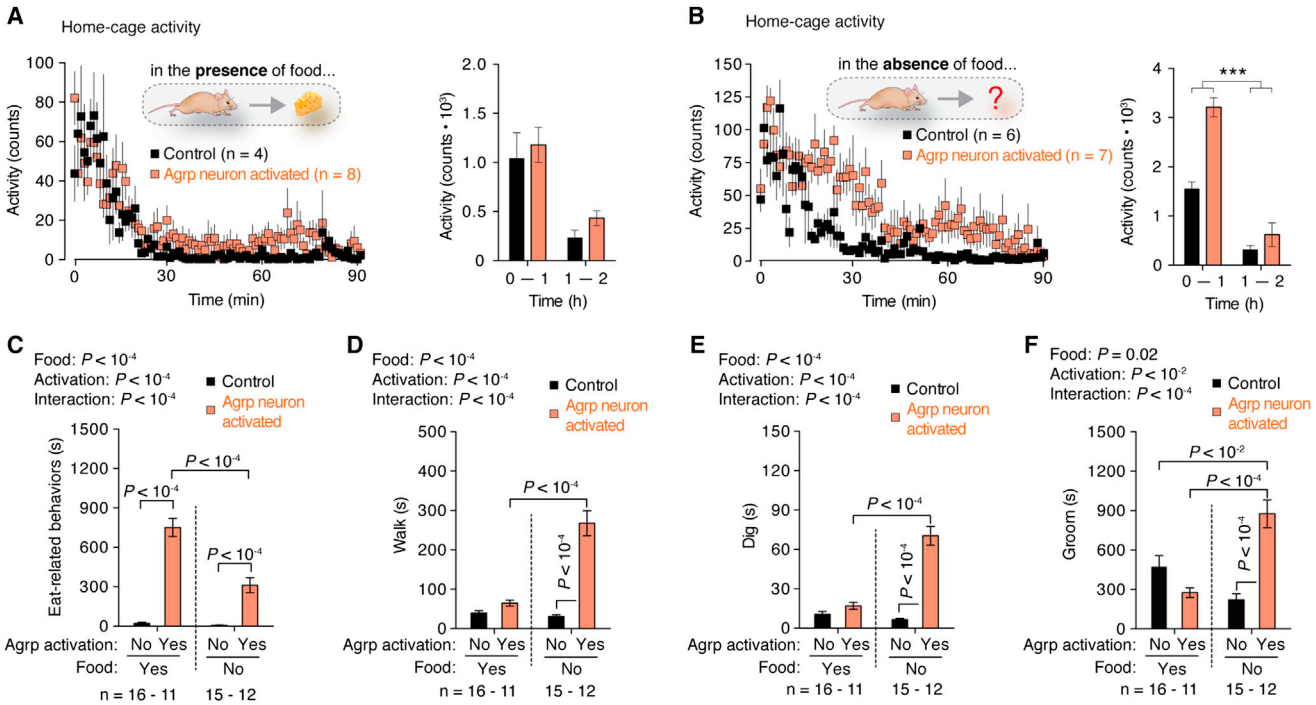

Figure 3. Home-Cage Behavior Analysis of Agrp Neuronal Activated Mice

(A) Activity in the home cage with food provided.

(B) Activity with no food provided.

(C) Eat-related behaviors.

(D) Time walking.

(E) Time digging.

(F) Time grooming.

Symbols and bars represent mean ± SEM. Statistical data derived from two-way ANOVA and Holm-Sidak's multiple comparisons test. See also Figure S2.

Agrp-Trpv1 mice in the marble-burying test (Deacon, 2006; Gyertyán, 1995; Witkin, 2008). The activation of Agrp neurons led to a robust increase in the number of marbles buried by males (Figure 4A and Movies S2 and S3) and females (data not shown), an effect that was, at least, in the same order of magnitude as mouse models of obsessive-compulsive disorders (Amodeo et al., 2012). Because food deprivation increases digging and grooming in the absence of food (Figure 1), which can also be considered repetitive behaviors (Ahmari et al., 2013; Burguière et al., 2013; Karvat and Kimchi, 2012), we tested food-deprived mice in parallel to Agrp-neuron-activated mice in the marble-burying test. We did not find statistical differences in the number of marbles buried after food deprivation (Figure 4B). To further test whether the increase in marble-burying behavior was due to repetitiveness, we performed a modified marble-burying test. We assessed mice in a larger cage with 40 marbles, which decreases the overall number of marbles buried and increases exploratory behavior. We found similar data in this modified version of the marble-burying test, with activation of Agrp neurons increasing the number of marbles buried (Figure 4C) while decreasing total activity during the test (control = 42.96 ± 3.12 m [n = 14], Agrp-Trpv1 = 32.27 ± 2.05 m [n = 20, mean ± SEM]; p = 0.004, two-tailed Mann-Whitney test), likely due to the extended time that mice spent burying marbles rather than exploring the arena. To test whether chronic negative energy balance impacts Agrp neuron activation responses, we placed animals on a 20% calorie-restricted regimen for 4 weeks and then tested them. Similar to the ad libitum fed animals (Figure 4), the activation of Agrp neurons by capsaicin increased marble-burying behavior in calorie-restricted mice (Figure S3). These results, together with the data gained in sated mice, argue for the importance of Agrp neuronal activity rather than metabolic state per se as a controller of stereotypic behaviors.

To further investigate whether the increase in marble burying was due to a goal-oriented repetitive behavior (to bury marbles) (Gyertyán, 1995; Londei et al., 1998; Thomas et al., 2009), we performed a place preference test (Figure 4D). Marbles were distributed on only one side of the cage, and bedding was present on both sides. Agrp-Trvp1 mice that received capsaicin buried a much larger number of marbles (Figure 4D) and spent ~16% more time on the marble side of the chamber (Figure 4E) than control mice. Notably, even with only half of the cage covered with marbles (Figure 4D), the number of marbles buried did not differ from the previous experiment (Figure 4C) in Agrp-Trpv1 mice injected with capsaicin)full cage = 41.25% ± 4.55% [n = 20]; half cage = 33.00% ± 5.45% [n = 20, mean ± SEM]; p = 0.183, two-tailed Mann-Whitney test) but decreased in the control group (full cage = 20.89% ± 5.25% [n = 14]; half

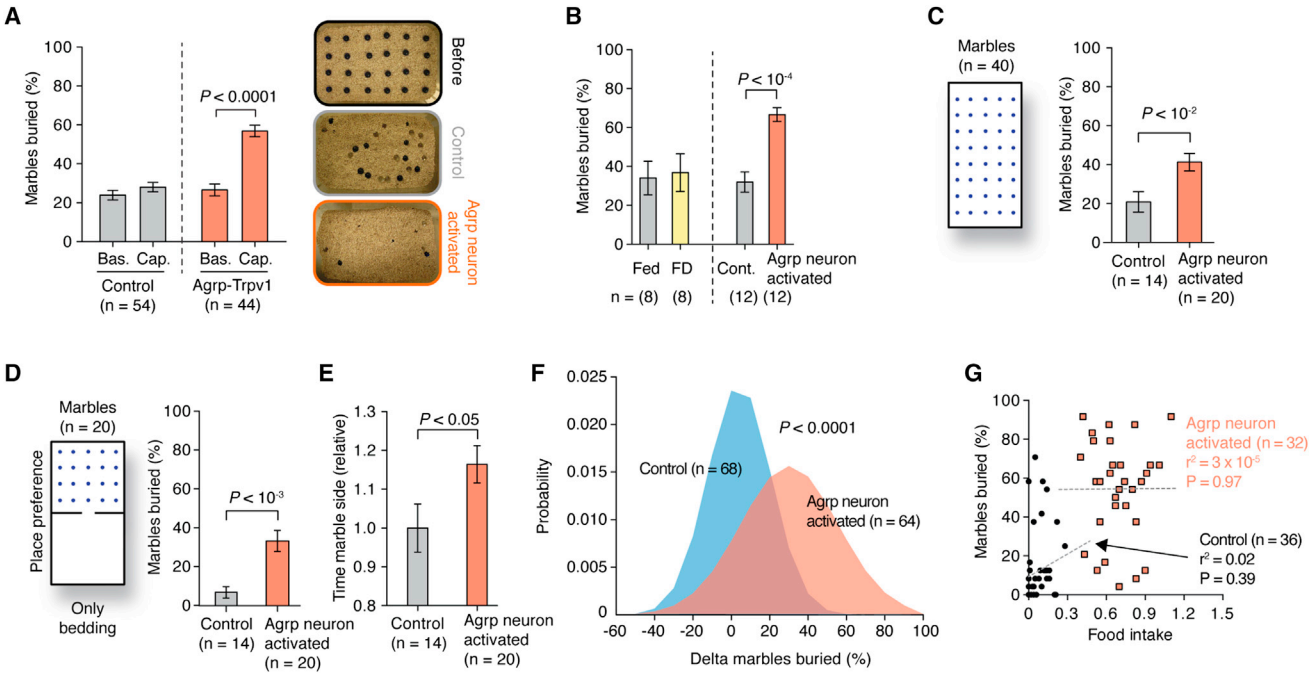

Figure 4. Repetitive Behaviors after Agrp Neuron Activation

(A) Marbles buried after Agrp neuron activation.

(B) Marble buried in fed, food-deprived (FD), control, and Agrp-neuron-activated mice.

(C) Marble buried in the modified marble-burying test.

(D) Marble buried in the modified place-preference test.

(E) Time animals spent in the marble side relative to control animals.

(F) Normal distribution fitted to pooled experimental data (delta marbles buried [capsaicin injection – baseline]). p value was calculated using unpaired t test with Welch's correction.

(G) Linear regression analysis correlating marble-burying behavior and food intake. Each data point represents one mouse. Female mice were used in this study. Error bars represent mean ± SEM, and p values were calculated using t test. See also Figure S3 and Movies S2 and S3.

cage = 6.78% ± 2.80% [n = 14, mean ± SEM]; p = 0.01, two-tailed Mann-Whitney test], indicating that the activation of Agrp neurons directs the animal's behavior toward repetitive, stereotypic responses when food is not available.

We hypothesized that, if Agrp neuron-mediated feeding and repetitive behaviors are a result of the same brain circuit, then these two behaviors should be correlated. We took advantage of the marble-burying behavior to test repetitive responses in mice. Frequency distribution histograms show a shift to the right in the number of marbles buried in Agrp-neuron-activated mice (Figure 4F), highlighting the idea that these behavioral changes are variable and affect differently subpopulations of mice. Linear regression analysis of individual responses did not show a correlation between marble-burying and feeding behaviors (Figure 4G), suggesting that the brain circuits that drive these behaviors by Agrp neurons are distinct and not completely overlapping.

Agrp Neuron Activation Decreases Anxiety

It is possible that changes in repetitive and stereotypic behaviors observed after Agrp neuron activation are due to increased anxiety. It is expected that treatments that increase anxiety levels will also increase repetitive/stereotypic responses in mice. Hunger is an unpleasant physiological state. Thus, it is possible that the promotion of hunger by activation of Agrp neurons generates an anxiogenic state in mice that leads to repetitive behaviors, as described above. To test anxiety-related behaviors, we performed a series of tests. First, we placed mice in a novel open-field exploratory test following activation of Agrp neurons by capsaicin. We did not find significant changes in total activity (Figure 5A) or time that animals explored the center of the arena (data not shown). We then put mice in a two-stage open-field test, in which a novel object is added to the center of the arena to induce novelty exploration and anxiety (Dietrich et al., 2012). In this test, activation of Agrp neurons increased the time that animals spent exploring the object (Figures 5B and 5D), but not total activity (Figure 5C). This indicates a decrease in anxiety levels compared to control mice. Next, we assessed mice in the zero- and plus-maze apparatuses, in which anxiety-related behaviors inversely correlate with the time that animals spend in the open arms. In both tests, we did not observe significant changes in activity levels between groups (Figures 5E and S4 and Movies S4 and S5), but we found that the activation of Agrp neurons increased the time in the open arms (Figures 5F and S4). Intriguingly, Agrp-neuron-activated mice accelerated once in the open arms (Figures 5G-H), perhaps due to changes in risk assessment. This hypothesis needs further investigation. Overall, the data show that activation of Agrp neurons in mice leads to repetitive behaviors that are not due to increases in anxiety levels.

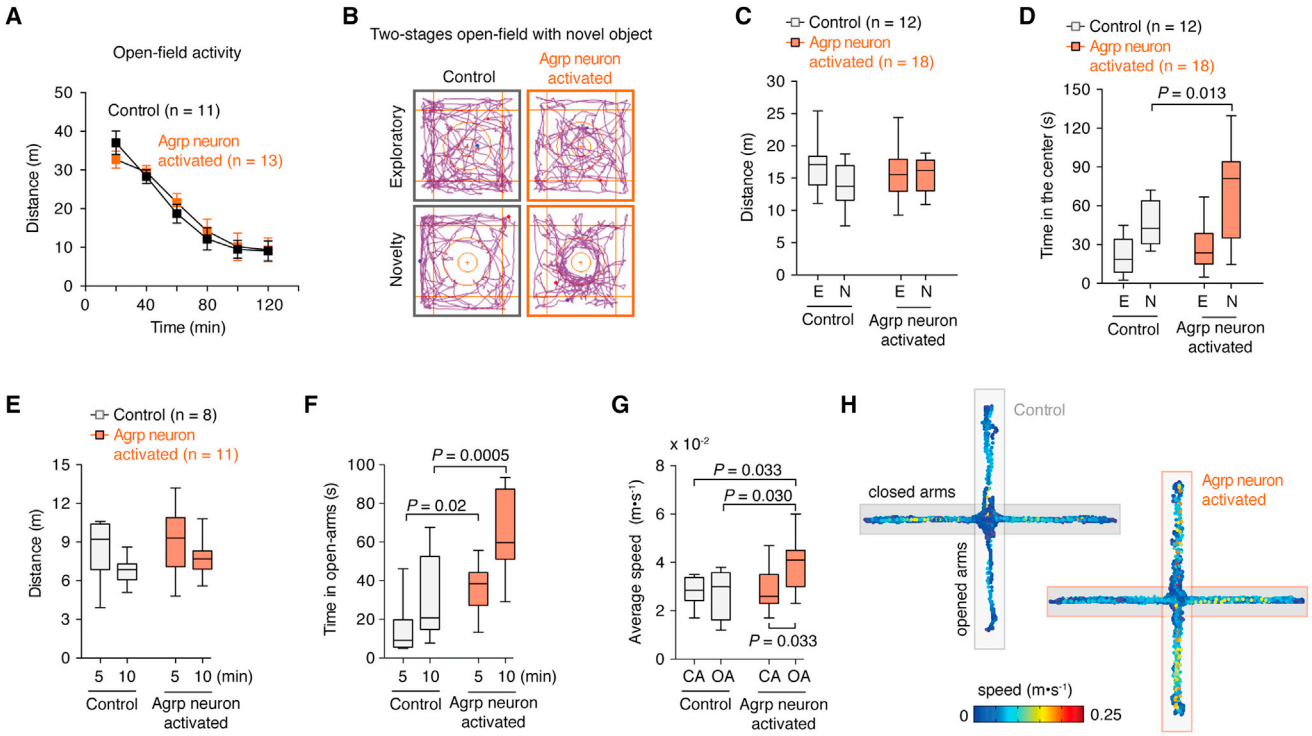

Figure 5. Activation of Agrp Neurons Decreases Anxiety-Related Behaviors

(A) Activity in the open field. Data points represent mean ± SEM.

(B) Two-stage open-field test.

(C) Total distance traveled in the two-stage open-field test.

(D) Time spent in the center of the open field.

(E) Distance traveled by mice in the plus-maze test.

(F) Time animals spent in the open arms.

(G) Average speed of mice in the close arms (CA) and open arms (OA) of the apparatus.

(H) Representative tracking data.

See also Figure S4 and Movies S4 and S5. Box and whiskers represent median ± min/max values. p values were calculated using two-way ANOVA with repeated-measures followed by Holm-Sidak's multiple comparisons test.

Conversely, the activation of Agrp neurons is anxiolytic in several behavior tests.

Alleviation of Behaviors by Y5 Receptor Antagonist

Agrp neurons have been shown to induce voracious food intake after acute activation due to NPY and GABA release (Aponte et al., 2011; Krashes et al., 2013). Because animal models in which GABA and/or NPY signaling is removed from Agrp neurons have developmental consequences (Atasoy et al., 2012; Dietrich et al., 2012), we examined whether pharmacological blockage of these signaling pathways would prevent repetitive behaviors after Agrp neuron activation. Systemic injection of a $GABA_A$ receptor antagonist was unable to reverse the induction of marble-burying behavior (Figure 6A) and food intake (Figure 6B) in Agrp-Trpv1 mice injected with capsaicin. NPY from the arcuate nucleus seems to signal mostly through NPY_1 and NPY_5 receptors, with overlapping expression and function (Atasoy et al., 2012; Gerald et al., 1996; Kanatani et al., 2000; Pedrazzini et al., 1998; Wolak et al., 2003). We have shown an anatomical link between the lateral hypothalamic orexin/hypocretin neurons and the arcuate nucleus NPY/Agrp cells (Horvath et al., 1999). Neuropeptides released by orexin/hypocretin neurons promote feeding, an effect that we showed to be diminished by administration of a NPY_5 receptor antagonist (Dube et al., 2000). These previous observations together with the translatability of NPY_5 receptor antagonists (Erondu et al., 2006) led us to interrogate the role of NPY_5 receptor signaling in behavioral changes mediated by Agrp neuron activation. Systemic injection of a NPY_5 receptor antagonist before activation of Agrp neurons was sufficient to block the increase in marble-burying behavior (Figure 6D) while slightly decreasing food intake (Figure 6E). Neither $GABA_A$ receptor nor NPY_5 receptor antagonists altered locomotor activity in an open field at the maximum dose used in this study (Figures 6C and 6F). These results indicate that NPY_5 receptor signaling is necessary for the repetitive behaviors induced by the activation of Agrp neurons. To further evaluate the participation of NPY_5 receptor signaling in the behavior repertoire of mice after Agrp neuronal activation, we scrutinized mouse behavior in the home cage. We treated mice with the NPY_5 receptor blocker before activating Agrp neurons by capsaicin in Agrp-Trpv1 mice (Figure 7A). While activation of Agrp neurons increased eating-related (Figure 7B) and foraging-related

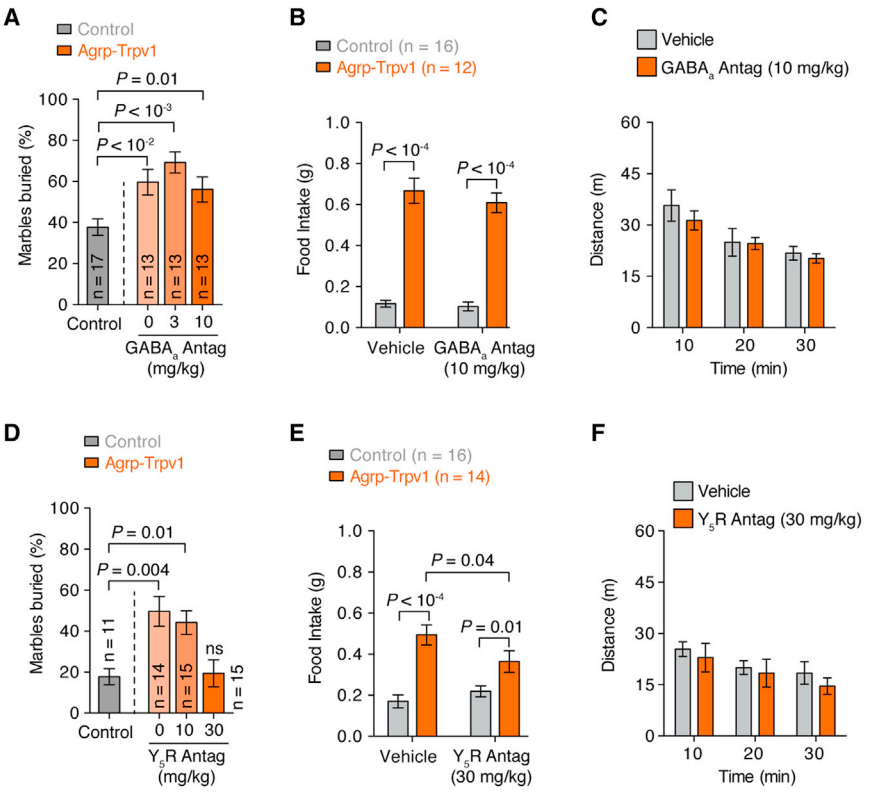

Figure 6. Effects of $GABA_A$ or NPY_5 Receptors Blockade in Agrp-Neuron-Activated Mice

(A) Effect of the $GABA_A$ receptor blocker, bicuculline, in the marble-burying test after activation of Agrp neurons.
(B) Effect of bicuculline on food intake.
(C) Effect of bicuculline on locomotor activity.
(D) Similar to A but using the NPY_5 receptor antagonist (CGP71683 hydrochloride).
(E) Similar to B using CGP71683.
(F) Similar to C using CGP71683.
Error bars represent mean ± SEM. p values were calculated using one-way ANOVA in A and D and two-way ANOVA with repeated-measures in B, C, E, and F followed by Holm-Sidak's multiple comparisons test.

behaviors (Figures 7C–7E), blockage of NPY_5 receptor signaling attenuated all of these behavioral responses with no effects in control mice (Figures 7B–7E). Remarkably, the effects of Agrp neuron activation on grooming were completely reverted by systemic injection of NPY_5 receptor blocker (Figures 7F–7H), similar to the effects reported in the marble-burying experiment (Figure 6D). Thus, we found that activation of Agrp neurons leads to repetitive behaviors, a behavioral phenotype that is completely reverted by NPY_5 receptor blockade. Notably, treatment of control mice with a NPY_5 receptor antagonist did not significantly alter baseline behaviors, but only behaviors driven by Agrp neuron activation. Because feeding response is not fully reverted by blocking NPY_5 receptor signaling (Figure 6E) and because repetitive and feeding responses are not correlated behaviors (Figure 4G), our data provide further support for the idea that different Agrp neuronal subpopulations promote food intake versus repetitive/stereotypic behaviors (Figure S5).

DISCUSSION

The hypothalamus integrates hormonal and ascending neural inputs that bring information from the periphery (Chaudhri et al., 2006; Coll et al., 2007; Dietrich and Horvath, 2009; Lam et al., 2005). Our findings highlight the importance of Agrp neurons in mediating the effect of the peripheral environment on complex brain functions and behaviors. Our results identified the hypothalamic Agrp neurons as initiators of stereotypic behaviors in mice. These behaviors were triggered when the vast majority of Agrp neurons were simultaneously activated. Some aspects of the stereotypic behaviors induced by chemical genetic activation of Agrp neurons were not seen in food-deprived animals or calorie-restricted mice. These observations suggest that different subpopulations of Agrp neurons subserve different functions, and it is likely that their activity patterns are not synchronized and are under differential input control. The fact that some behavioral shifts induced by Agrp neuronal activation can while others cannot be suppressed by a NPY_5 receptor blocker further argue for the segregation of function of different subpopulations of Agrp cells. Thus, it is anticipated that an intricate and highly complex input organization and efferent connectivity of various subpopulations of Agrp neurons exists to support predictable and dynamic behavioral and autonomic adaptations to the changing environment (Figure S5).

Our results unmasked a previously unsuspected role for the hypothalamic hunger-promoting neurons in controlling repetitive, stereotypic behaviors in mice. Also, we showed that the activation of Agrp neurons decreases anxiety levels in several tests in mice. Because the hypothalamus is an evolutionarily conserved brain region, it is likely that these results are relevant to higher-order organisms, including humans. A recent report reinforces this view by providing evidence that mice are capable of estimating probabilities and calculating risks to make behavioral adjustments in dynamic environments analogous to humans (Kheifets and Gallistel, 2012). This supports the argument that brain mechanisms involved in complex behaviors are phylogenetically preserved. It is relevant to note, however, that our behavior tests were performed in animals in isolation, and not in a social context. It will be important to study whether these neurons also participate in social behaviors. Additionally, it remains to be tested whether the role of Agrp neurons in feeding and/or repetitive/stereotypic behaviors are influenced by the social context. At present, these studies are extremely challenging to perform in mice (Anderson and Perona, 2014). With the advent of technology and emerging tools to analyze animal behavior, future studies dissecting the role of Agrp neurons (as well as

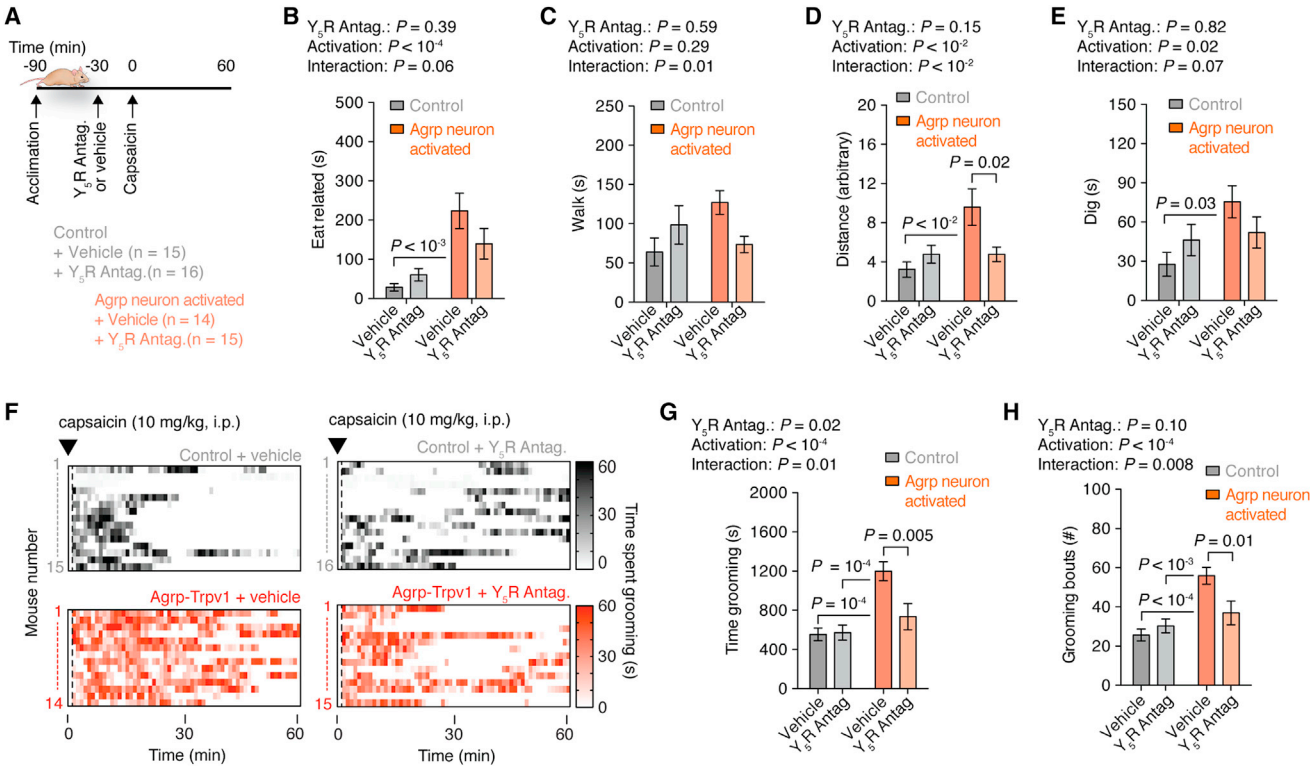

Figure 7. NPY_5 Receptor Signaling Is Necessary for Agrp-Neuron-Mediated Behaviors

(A) Protocol to record home-cage behaviors using CGP71683 (30 mg/kg, i.p.).

(B) Time spent in eating-related behaviors.

(C) Time spent walking.

(D) Total traveled distance.

(E) Time spent digging.

(F) Raster plots showing grooming behavior in individual mouse.

(G) Time spent grooming.

(H) Grooming bouts.

Error bars represent mean ± SEM. p values were calculated using two-way ANOVA followed by Holm-Sidak's multiple comparisons test and are reported in the panels. See also Figure S5.

other brain circuits) on behaviors in social settings are of utmost relevance and priority for our understanding of brain function.

Our data also suggest that these ancient brain regions play a role in psychiatric conditions. Specifically, misalignments between environmental cues (peripheral tissue function) and hypothalamic circuits may lead to maladaptive behaviors, including those associated with psychiatric and neurological disorders. Regarding the latter, we suggest that our results have implications for the etiology of anorexia nervosa. Patients suffering from this condition avoid ingesting calories despite the fact that they have elevated activity and a higher physiological state of hunger.

Because hunger signals activate Agrp neurons (Hahn et al., 1998; Liu et al., 2012; Takahashi and Cone, 2005; Yang et al., 2011), we postulate that, in individuals with a vulnerability to develop anorexia nervosa, Agrp neurons may respond to negative energy balance cues in an exacerbated manner and lead to repetitive and compulsive behaviors (Halmi et al., 2003; Matsunaga et al., 1999; Thiel et al., 1995). Future studies are needed to interrogate whether inert differences in Agrp neuronal excitability exist between vulnerable and invulnerable individuals. From this perspective, it is of interest to note that patients with anorexia nervosa have elevated circulating blood levels of Agrp compared to controls (Merle et al., 2011; Moriya et al., 2006) and that Agrp levels are associated with cognitive rigidity in these patients (Sarrar et al., 2011). Because NPY_5 receptor antagonists have been tested in humans (Erondu et al., 2006) and we found it to reverse many Agrp activation-triggered stereotypic behaviors, we suggest that human clinical trials with safe compounds can be initiated for addressing the behavioral aspects of anorexia nervosa as well as other neuropsychiatric diseases with both homeostatic and behavioral components.

EXPERIMENTAL PROCEDURES

Mice

All mice used in the experiments were 2–6 months old from both genders. We did not observe differences in the responses of males and females to capsaicin. Agrp-Trpv1 mice were: *AgrpCre$^{Tm/+}$::Trpv1$^{-/-}$::R26-LSL-Trpv1$^{Gt/+}$*; control animals were either Agrp-Trpv1 mice injected with vehicle (3.3% Tween 80 in saline) or *Trpv1$^{-/-}$:R26-LSL-Trpv1$^{Gt/+}$* mice injected with capsaicin. All

animals were littermates (Agrp neuron activated and controls) in the experiments. We did not observe any differences between the two control groups, and therefore, throughout the manuscript we referred to them as "controls." The following mouse lines were used in this study: *Agrptm1(cre)Lowl/J*, *Gt(ROSA)26Sortm1(Trpv1,ECFP)Mde/J*, *Trpv1tm1Jul/J*, *Rpl22tm1.1Psam/J*, *Tg(Npy-MAPT/Sapphire)1Rck/J*. All animals were kept in temperature- and humidity-controlled rooms, in a 12/12 hr light/dark cycle, with lights on from 7:00 AM–7:00 PM. Food and water were provided ad libitum unless otherwise stated. All procedures were approved by IACUC (Yale University).

Immunohistochemistry

Mice were deeply anesthetized and perfused with 0.9% saline containing heparin followed by freshly prepared fixative (paraformaldehyde 4%, picric acid 15%, in PB 0.1M [pH = 7.4]). Brains were post-fixed overnight in fixative. Coronal brain sections (50 μm) were washed several times in PB 0.1M (pH = 7.4) and pre-incubated with Triton X-100 for 30 min. Sections were then washed several times and blocked with 2% normal goat serum and incubated with chicken anti-GFP (1:8,000, 4°C, 48 hr; ABCAM), rabbit anti-cfos (1:20,000 at 4°C for 48 hr; Oncogene), and/or mouse anti-HA (1:1,000 dilution at RT for 24 hr; Covance). After, sections were extensively washed and incubated with secondary fluorescent Alexa antibodies (1:500). Sections were mounted, coverslipped, and visualized by a Zeiss microscope or an Olympus Confocal microscope.

Drugs

Drugs used were: capsaicin (3.33% Tween-80 in PBS; from Sigma), Bicuculline methiodide (in saline; from Sigma), and CGP71683 hydrochloride (in 5% DMSO, 5% Tween-80 in water; from Tocris). All drugs were injected in a volume of 10 ml/kg of body weight intraperitoneally (i.p.).

Food Intake

For the capsaicin dose-response experiment, mice were acclimated to metabolic chambers (TSE Systems) before recordings. Mice received vehicle or capsaicin (3, 10, and 30 mg/kg, i.p.), and food intake was automatically recorded (see Movie S1). Alternatively, food intake was manually recorded in single-housed mice. Bedding was changed 24 hr before the experiment, and animals were acclimated for at least 1 week with a minimum quantity of food in the cage to alleviate spillage. On the day of the experiments, food was removed 1 hr before the test and food intake was recorded before and 1 hr after capsaicin injection.

Electrophysiology

Four-week-old *Agrp-Cre$^{tm/+}$::Trpv1$^{-/-}$::R26-LSL-Trpv1$^{Gt/+}$::NpyGFP$^{Tg/+}$* mice were killed at the beginning of the light cycle, and the arcuate nucleus was sliced into 250 μm slices, containing GFP cells. After stabilization in ACSF, slices were transferred to the recording chamber and perfused with ACSF. Basal firing rate was recorded for at least 5 min. The slice was then incubated with a pulse of capsaicin (0.25 μM), followed by a washout. Whole-cell current-clamp recording was performed using low-resistance (3–4 MΩ) pipettes. The composition of the pipette solution was as follows (in mM): K-gluconate125, $MgCl_2$ 2, HEPES 10, EGTA 1.1, Mg-ATP 4, and Na_2-phosphocreatin 10, Na_2-GTP 0.5 (pH 7.3) with KOH. The composition of the bath solution was as follows (in mM): NaCl 124, KCl 3, $CaCl_2$ 2, $MgCl_2$ 2, NaH_2PO4 1.23, glucose 2.5, sucrose 7.5, $NaHCO_3$ 26. After a gigaohm (GΩ) seal and whole-cell access were achieved, membrane potential and action potentials were recorded under current clamp at 0 pA. All data were sampled at 3–10 kHz and filtered at 1–3 kHz. Electrophysiological data were analyzed with Axograph 4.9.

Home-Cage Behavior

Four-month-old Agrp-Trpv1 or control female mice were singly housed in their normal home cage 11 days prior to the start of the first behavioral study. Animals were acclimated to handling for 1 week before experiments. The day preceding the behavioral analysis, the mice were given fresh bedding. For a 1 hr acclimation period, cages were placed in front of the cameras of the HomeCageScan system (CleverSys, Reston, VA) and were backlit by IR light panels. Mice were injected with either 10 mg/kg capsaicin or vehicle and recorded for 1 hr. Food was removed for the acclimation period as well as the analysis period for groups reported as "no food." Mice in the fasted study were fasted for 16 hr prior to the experiment, and the re-fed group was given food at the time of injection. The NPY_5 receptor blocker (CGP71683 hydrochloride, 30 mg/kg, i.p.) was given to the animals 30 min prior to capsaicin injection. Videos were analyzed with the HomeCageScan software (v3.00).

Marble-Burying Test

Marble-burying test was as described (Deacon, 2006) with modifications. Mice were tested (baseline) and randomized to groups. Capsaicin (10 mg/kg, i.p.) was injected immediately before test. Drugs were injected 20 (for bicuculline) or 30 min (for CGP71683 hydrochloride) before capsaicin. Modified marble-burying test was performed in a rat cage containing 40 evenly distributed marbles. Place preference was performed in the same rat cage divided using a separator with an open door. Marble side contained 20 marbles. All studies were performed in cages containing 5 cm of corn-based animal bedding.

Calorie Restriction

Female mice (9 weeks old) were housed two-by-two to avoid chronic stress due to social isolation. We have used the balanced NIH-41 diet (3.34 kcal/g, protein 16.9%, fat 12.5%, fiber 3.8%, nitrogen-free extract 53.6%, vitamins, minerals) to avoid malnourishment during calorie restriction due to insufficient nutrient levels. Mice received 20% less calories than their ad libitum food intake baseline measurements. The marble-burying test was performed on the last days of the study (a baseline was recorded without injection, and on the next day mice were tested after capsaicin injection). We used the modified marble-burying test with a rat cage containing 40 marbles (as described above).

DREADD Experiment

Recombinant rAAV5-Ef1a-DIO-hm3D(Gq)-mcherry virus (500 nl from UNC Viral Core) was injected bilaterally into the arcuate nucleus of *Agrp-Cre* male mice (AP = 1.40 mm; DV = −5.90 mm; L = ± 0.30 mm). Animals were allowed to recover for 3 weeks. All mice were singly housed in their normal home cage 3 weeks prior to the start of the first home-cage behavioral study. Two days preceding the behavioral analysis, the mice were given fresh bedding. Home-cage behaviors were analyzed as above. Mice were injected (i.p.) with either 0.3 mg/kg CNO (n = 7) or saline (n = 4) and recorded during 2 hr with no food available. Mice were later tested for feeding response and showed robust induction of food intake after CNO injection (data not shown). Infection was confirmed by visualizing mCherry in the arcuate nucleus. Clozapine N-oxide (CNO) was from Enzo Life Science.

Locomotor Activity

Mice were allowed to explore a novel environment (a rat cage, 45 × 24 × 20 cm) for 120 min after capsaicin injection. To test the side effects of the receptor blockers in locomotor activity, animals received an injection of bicuculline methiodide (10 mg/kg, i.p) or vehicle (PBS) 20 min before experiment. CGP71683 hydrochloride (30 mg/kg, i.p) or vehicle (5% DMSO, 5% tween-80 in water) were injected 30 min prior to the experiment. Male mice were used in these experiments (n = 25, 3–4 months old) and were allowed to explore the apparatus for 30 min. The experiment was performed under dim light during the light cycle.

Two-Stages Open-Field Test

The apparatus consists of a Plexiglas open-field (37 × 37 × 37 cm). Mice were first put in the open field for 5 min ("exploratory stage"). Immediately after, mice were returned to their home cages for 2 min. A new object (a cylinder of 5 cm radius and 10 cm high) was placed in the center of the arena. Mice were then returned to the open field for an additional 5 min ("novelty stage"). The room was illuminated with infrared lights and dim red light.

Elevated Plus Maze and Zero Maze

The plus maze consisted of four elevated arms (40 cm from the floor, 25 cm long, and 5.2 cm wide) arranged at right angles. Two opposite arms were enclosed by 15-cm high walls, and the other two were open (no walls). Male control (n = 8) and Agrp-Trpv1 (n = 11) mice (3–4 months old) were placed on the 5 × 5 cm center section and allowed to explore the apparatus. The zero maze

consisted of an elevated circular platform with two opposite quadrants enclosed and two open, allowing uninterrupted exploration. The apparatus has a 50 cm diameter, 5 cm lane width, 15 cm wall height, and 40 cm elevation (from Stoeling, #68016). Capsaicin (10 mg/ kg, i.p.) was injected immediately before the experiments. Experiments were performed during the night cycle of the animals using infrared illumination and dim red light. Mice were recorded for 10 min and tracked using Any-Maze (Stoelting).

Statistical Analysis

Matlab R2009a, PASW Statistics 18.0, and Prism 6.0 were used to analyze data and plot figures. When homogeneity was assumed, a parametric analysis of variance test was used. The student's t test was used to compare two groups. One-, two-way, or two-way with repeated measures ANOVA were used as the other tests unless stated otherwise. When significant, a multiple comparisons post hoc test was used (Holm-Sidak's test). When homogeneity was not assumed, the Kruskal-Wallis nonparametric ANOVA was selected for multiple statistical comparisons. The Mann-Whitney U test was used to determine significance between groups. Statistical data are provided in the figures. $p < 0.05$ was considered statistically significant.

SUPPLEMENTAL INFORMATION

Supplemental Information includes five figures and five movies and can be found with this article online at http://dx.doi.org/10.1016/j.cell.2015.02.024.

AUTHOR CONTRIBUTIONS

M.O.D., M.R.Z., and J.B. performed the experiments. All authors designed, analyzed, and interpreted data. M.O.D. and T.L.H. wrote the manuscript.

ACKNOWLEDGMENTS

We thank Zhong-Wu Liu for electrophysiological recordings. We thank Marya Shanabrough for assistance. T.L.H. was supported by NIH (DP1 DK006850, R01AG040236, and P01NS062686), the American Diabetes Association, the Helmholtz Society (ICEMED), and by Conselho Nacional de Desenvolvimento Científico e Tecnológico (CNPq: 401476/2012-0, Brazil). M.O.D. received support from Brain and Behavior Research Foundation, NCATS (UL1 TR000142), and CNPq (487096/2013-4, Brazil). M.R.Z. was partially supported by a Science Without Borders fellowship from CNPq/Brazil.

Received: December 1, 2014
Revised: January 16, 2015
Accepted: January 30, 2015
Published: March 5, 2015

REFERENCES

Adamah-Biassi, E.B., Stepien, I., Hudson, R.L., and Dubocovich, M.L. (2013). Automated video analysis system reveals distinct diurnal behaviors in C57BL/6 and C3H/HeN mice. Behav. Brain Res. *243*, 306–312.

Ahmari, S.E., Spellman, T., Douglass, N.L., Kheirbek, M.A., Simpson, H.B., Deisseroth, K., Gordon, J.A., and Hen, R. (2013). Repeated cortico-striatal stimulation generates persistent OCD-like behavior. Science *340*, 1234–1239.

Amodeo, D.A., Jones, J.H., Sweeney, J.A., and Ragozzino, M.E. (2012). Differences in BTBR T+ tf/J and C57BL/6J mice on probabilistic reversal learning and stereotyped behaviors. Behav. Brain Res. *227*, 64–72.

Anderson, D.J., and Perona, P. (2014). Toward a science of computational ethology. Neuron *84*, 18–31.

Aponte, Y., Atasoy, D., and Sternson, S.M. (2011). AGRP neurons are sufficient to orchestrate feeding behavior rapidly and without training. Nat. Neurosci. *14*, 351–355.

Arenkiel, B.R., Klein, M.E., Davison, I.G., Katz, L.C., and Ehlers, M.D. (2008). Genetic control of neuronal activity in mice conditionally expressing TRPV1. Nat. Methods *5*, 299–302.

Atasoy, D., Betley, J.N., Su, H.H., and Sternson, S.M. (2012). Deconstruction of a neural circuit for hunger. Nature *488*, 172–177.

Barnett, S.A. (1956). Behaviour Components in the Feeding of Wild and Laboratory Rats. Behaviour *9*, 24–43.

Betley, J.N., Cao, Z.F., Ritola, K.D., and Sternson, S.M. (2013). Parallel, redundant circuit organization for homeostatic control of feeding behavior. Cell *155*, 1337–1350.

Broberger, C., Johansen, J., Johansson, C., Schalling, M., and Hökfelt, T. (1998). The neuropeptide Y/agouti gene-related protein (AGRP) brain circuitry in normal, anorectic, and monosodium glutamate-treated mice. Proc. Natl. Acad. Sci. USA *95*, 15043–15048.

Burguière, E., Monteiro, P., Feng, G., and Graybiel, A.M. (2013). Optogenetic stimulation of lateral orbitofronto-striatal pathway suppresses compulsive behaviors. Science *340*, 1243–1246.

Caterina, M.J., Schumacher, M.A., Tominaga, M., Rosen, T.A., Levine, J.D., and Julius, D. (1997). The capsaicin receptor: a heat-activated ion channel in the pain pathway. Nature *389*, 816–824.

Chaudhri, O., Small, C., and Bloom, S. (2006). Gastrointestinal hormones regulating appetite. Philos. Trans. R. Soc. Lond. B Biol. Sci. *361*, 1187–1209.

Clark, J.T., Kalra, P.S., Crowley, W.R., and Kalra, S.P. (1984). Neuropeptide Y and human pancreatic polypeptide stimulate feeding behavior in rats. Endocrinology *115*, 427–429.

Coll, A.P., Farooqi, I.S., and O'Rahilly, S. (2007). The hormonal control of food intake. Cell *129*, 251–262.

Deacon, R.M. (2006). Digging and marble burying in mice: simple methods for in vivo identification of biological impacts. Nat. Protoc. *1*, 122–124.

Dietrich, M.O., and Horvath, T.L. (2009). Feeding signals and brain circuitry. Eur. J. Neurosci. *30*, 1688–1696.

Dietrich, M.O., Bober, J., Ferreira, J.G., Tellez, L.A., Mineur, Y.S., Souza, D.O., Gao, X.B., Picciotto, M.R., Araújo, I., Liu, Z.W., and Horvath, T.L. (2012). AgRP neurons regulate development of dopamine neuronal plasticity and nonfood-associated behaviors. Nat. Neurosci. *15*, 1108–1110.

Dube, M.G., Horvath, T.L., Kalra, P.S., and Kalra, S.P. (2000). Evidence of NPY Y5 receptor involvement in food intake elicited by orexin A in sated rats. Peptides *21*, 1557–1560.

Erondu, N., Gantz, I., Musser, B., Suryawanshi, S., Mallick, M., Addy, C., Cote, J., Bray, G., Fujioka, K., Bays, H., et al. (2006). Neuropeptide Y5 receptor antagonism does not induce clinically meaningful weight loss in overweight and obese adults. Cell Metab. *4*, 275–282.

Gerald, C., Walker, M.W., Criscione, L., Gustafson, E.L., Batzl-Hartmann, C., Smith, K.E., Vaysse, P., Durkin, M.M., Laz, T.M., Linemeyer, D.L., et al. (1996). A receptor subtype involved in neuropeptide-Y-induced food intake. Nature *382*, 168–171.

Gropp, E., Shanabrough, M., Borok, E., Xu, A.W., Janoschek, R., Buch, T., Plum, L., Balthasar, N., Hampel, B., Waisman, A., et al. (2005). Agouti-related peptide-expressing neurons are mandatory for feeding. Nat. Neurosci. *8*, 1289–1291.

Grove, K.L., Brogan, R.S., and Smith, M.S. (2001). Novel expression of neuropeptide Y (NPY) mRNA in hypothalamic regions during development: region-specific effects of maternal deprivation on NPY and Agouti-related protein mRNA. Endocrinology *142*, 4771–4776.

Güler, A.D., Rainwater, A., Parker, J.G., Jones, G.L., Argilli, E., Arenkiel, B.R., Ehlers, M.D., Bonci, A., Zweifel, L.S., and Palmiter, R.D. (2012). Transient activation of specific neurons in mice by selective expression of the capsaicin receptor. Nat. Commun. *3*, 746.

Gyertyán, I. (1995). Analysis of the marble burying response: marbles serve to measure digging rather than evoke burying. Behav. Pharmacol. *6*, 24–31.

Hahn, T.M., Breininger, J.F., Baskin, D.G., and Schwartz, M.W. (1998). Coexpression of Agrp and NPY in fasting-activated hypothalamic neurons. Nat. Neurosci. *1*, 271–272.

Halmi, K.A., Sunday, S.R., Klump, K.L., Strober, M., Leckman, J.F., Fichter, M., Kaplan, A., Woodside, B., Treasure, J., Berrettini, W.H., et al. (2003).

Obsessions and compulsions in anorexia nervosa subtypes. Int. J. Eat. Disord. *33*, 308–319.

Horvath, T.L., Naftolin, F., Kalra, S.P., and Leranth, C. (1992). Neuropeptide-Y innervation of beta-endorphin-containing cells in the rat mediobasal hypothalamus: a light and electron microscopic double immunostaining analysis. Endocrinology *131*, 2461–2467.

Horvath, T.L., Bechmann, I., Naftolin, F., Kalra, S.P., and Leranth, C. (1997). Heterogeneity in the neuropeptide Y-containing neurons of the rat arcuate nucleus: GABAergic and non-GABAergic subpopulations. Brain Res. *756*, 283–286.

Horvath, T.L., Diano, S., and van den Pol, A.N. (1999). Synaptic interaction between hypocretin (orexin) and neuropeptide Y cells in the rodent and primate hypothalamus: a novel circuit implicated in metabolic and endocrine regulations. J. Neurosci. *19*, 1072–1087.

Jhuang, H., Garrote, E., Mutch, J., Yu, X., Khilnani, V., Poggio, T., Steele, A.D., and Serre, T. (2010). Automated home-cage behavioural phenotyping of mice. Nat. Commun. *1*, 68.

Kanatani, A., Mashiko, S., Murai, N., Sugimoto, N., Ito, J., Fukuroda, T., Fukami, T., Morin, N., MacNeil, D.J., Van der Ploeg, L.H., et al. (2000). Role of the Y1 receptor in the regulation of neuropeptide Y-mediated feeding: comparison of wild-type, Y1 receptor-deficient, and Y5 receptor-deficient mice. Endocrinology *141*, 1011–1016.

Karvat, G., and Kimchi, T. (2012). Systematic autistic-like behavioral phenotyping of 4 mouse strains using a novel wheel-running assay. Behav. Brain Res. *233*, 405–414.

Kheifets, A., and Gallistel, C.R. (2012). Mice take calculated risks. Proc. Natl. Acad. Sci. USA *109*, 8776–8779.

Krashes, M.J., DasGupta, S., Vreede, A., White, B., Armstrong, J.D., and Waddell, S. (2009). A neural circuit mechanism integrating motivational state with memory expression in Drosophila. Cell *139*, 416–427.

Krashes, M.J., Koda, S., Ye, C., Rogan, S.C., Adams, A.C., Cusher, D.S., Maratos-Flier, E., Roth, B.L., and Lowell, B.B. (2011). Rapid, reversible activation of AgRP neurons drives feeding behavior in mice. J. Clin. Invest. *121*, 1424–1428.

Krashes, M.J., Shah, B.P., Koda, S., and Lowell, B.B. (2013). Rapid versus delayed stimulation of feeding by the endogenously released AgRP neuron mediators GABA, NPY, and AgRP. Cell Metab. *18*, 588–595.

Kyzar, E.J., Pham, M., Roth, A., Cachat, J., Green, J., Gaikwad, S., and Kalueff, A.V. (2012). Alterations in grooming activity and syntax in heterozygous SERT and BDNF knockout mice: the utility of behavior-recognition tools to characterize mutant mouse phenotypes. Brain Res. Bull. *89*, 168–176.

Lam, T.K.T., Schwartz, G.J., and Rossetti, L. (2005). Hypothalamic sensing of fatty acids. Nat. Neurosci. *8*, 579–584.

Liu, T., Kong, D., Shah, B.P., Ye, C., Koda, S., Saunders, A., Ding, J.B., Yang, Z., Sabatini, B.L., and Lowell, B.B. (2012). Fasting activation of AgRP neurons requires NMDA receptors and involves spinogenesis and increased excitatory tone. Neuron *73*, 511–522.

Londei, T., Valentini, A.M., and Leone, V.G. (1998). Investigative burying by laboratory mice may involve non-functional, compulsive, behaviour. Behav. Brain Res. *94*, 249–254.

Luquet, S., Perez, F.A., Hnasko, T.S., and Palmiter, R.D. (2005). NPY/AgRP neurons are essential for feeding in adult mice but can be ablated in neonates. Science *310*, 683–685.

Matsunaga, H., Kiriike, N., Iwasaki, Y., Miyata, A., Yamagami, S., and Kaye, W.H. (1999). Clinical characteristics in patients with anorexia nervosa and obsessive-compulsive disorder. Psychol. Med. *29*, 407–414.

Merle, J.V., Haas, V., Burghardt, R., Döhler, N., Schneider, N., Lehmkuhl, U., and Ehrlich, S. (2011). Agouti-related protein in patients with acute and weight-restored anorexia nervosa. Psychol. Med. *41*, 2183–2192.

Moriya, J., Takimoto, Y., Yoshiuchi, K., Shimosawa, T., and Akabayashi, A. (2006). Plasma agouti-related protein levels in women with anorexia nervosa. Psychoneuroendocrinology *31*, 1057–1061.

Ollmann, M.M., Wilson, B.D., Yang, Y.K., Kerns, J.A., Chen, Y., Gantz, I., and Barsh, G.S. (1997). Antagonism of central melanocortin receptors in vitro and in vivo by agouti-related protein. Science *278*, 135–138.

Pedrazzini, T., Seydoux, J., Künstner, P., Aubert, J.F., Grouzmann, E., Beermann, F., and Brunner, H.R. (1998). Cardiovascular response, feeding behavior and locomotor activity in mice lacking the NPY Y1 receptor. Nat. Med. *4*, 722–726.

Rogan, S.C., and Roth, B.L. (2011). Remote control of neuronal signaling. Pharmacol. Rev. *63*, 291–315.

Rossi, M., Kim, M.S., Morgan, D.G., Small, C.J., Edwards, C.M., Sunter, D., Abusnana, S., Goldstone, A.P., Russell, S.H., Stanley, S.A., et al. (1998). A C-terminal fragment of Agouti-related protein increases feeding and antagonizes the effect of alpha-melanocyte stimulating hormone in vivo. Endocrinology *139*, 4428–4431.

Sarrar, L., Ehrlich, S., Merle, J.V., Pfeiffer, E., Lehmkuhl, U., and Schneider, N. (2011). Cognitive flexibility and Agouti-related protein in adolescent patients with anorexia nervosa. Psychoneuroendocrinology *36*, 1396–1406.

Stanley, B.G., Kyrkouli, S.E., Lampert, S., and Leibowitz, S.F. (1986). Neuropeptide Y chronically injected into the hypothalamus: a powerful neurochemical inducer of hyperphagia and obesity. Peptides *7*, 1189–1192.

Takahashi, K.A., and Cone, R.D. (2005). Fasting induces a large, leptin-dependent increase in the intrinsic action potential frequency of orexigenic arcuate nucleus neuropeptide Y/Agouti-related protein neurons. Endocrinology *146*, 1043–1047.

Thiel, A., Broocks, A., Ohlmeier, M., Jacoby, G.E., and Schüssler, G. (1995). Obsessive-compulsive disorder among patients with anorexia nervosa and bulimia nervosa. Am. J. Psychiatry *152*, 72–75.

Thomas, A., Burant, A., Bui, N., Graham, D., Yuva-Paylor, L.A., and Paylor, R. (2009). Marble burying reflects a repetitive and perseverative behavior more than novelty-induced anxiety. Psychopharmacology (Berl.) *204*, 361–373.

Witkin, J.M. (2008). Animal models of obsessive-compulsive disorder. Curr. Protoc. in Neurosci., Unit 9, 30.

Wolak, M.L., DeJoseph, M.R., Cator, A.D., Mokashi, A.S., Brownfield, M.S., and Urban, J.H. (2003). Comparative distribution of neuropeptide Y Y1 and Y5 receptors in the rat brain by using immunohistochemistry. J. Comp. Neurol. *464*, 285–311.

Wu, Q., Clark, M.S., and Palmiter, R.D. (2012). Deciphering a neuronal circuit that mediates appetite. Nature *483*, 594–597.

Xu, A.W., Kaelin, C.B., Morton, G.J., Ogimoto, K., Stanhope, K., Graham, J., Baskin, D.G., Havel, P., Schwartz, M.W., and Barsh, G.S. (2005). Effects of hypothalamic neurodegeneration on energy balance. PLoS Biol. *3*, e415.

Yang, Y., Atasoy, D., Su, H.H., and Sternson, S.M. (2011). Hunger states switch a flip-flop memory circuit via a synaptic AMPK-dependent positive feedback loop. Cell *146*, 992–1003.

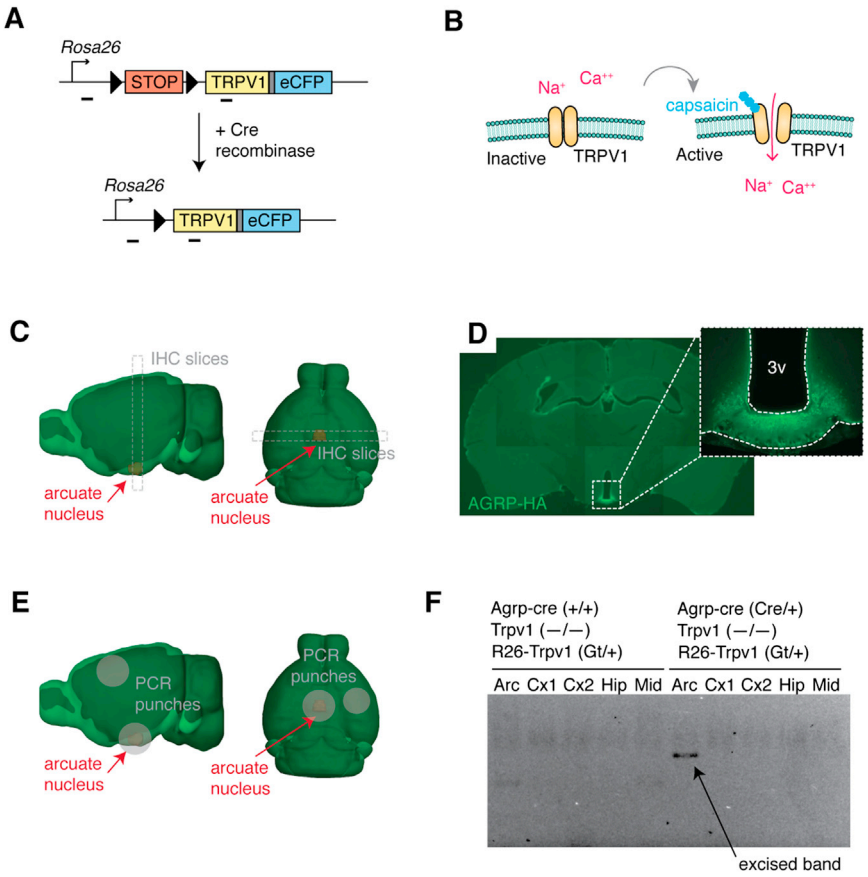

Figure S1. Specific Expression of Trpv1 in Agrp Neurons, Related to Figure 2

(A) Schematic of the conditional *R26-LSL-Trpv1-eCFP* mice used in the study. When bred to *Agrp-Cre* animals, the stop codon is excised and Trpv1 is expressed in Cre- expressing cells. Because the animals are backcrossed to a Trpv1 knockout background, expression of ectopic Trpv1 is selective to Agrp neurons. (B) Diagram showing Trpv1 are cation channels that are closed at resting state and open in response to the agonist, capsaicin, leading to neural cell activation. (C) Illustration showing the location of the arcuate nucleus of the hypothalamus, where Agrp neurons are located. (D) Because staining with antibodies against NPY and Agrp label fibers but not the soma, we used a reporter mouse that expresses –HA in Cre- expressing cells to confirm only Agrp neurons express Cre- recombinase. Noteworthy, in our experience, using this knock-in *Agrp-Cre* line in a B6 or B6.129 background we have < 5% animals showing ectopic expression of cre. Using a different *Agrp-Cre* transgenic line, in the same background, we get 30%–40% ectopic expression of Cre-recombinase in other neuronal areas. Thus, we used the publicly available *Agrp-Cre* knocking line for our studies. (Inset) Staining using an antibody against HA showing specific expression of the reporter in the arcuate nucleus of the hypothalamus. (E) Illustration showing brain regions used to genotype animals for the ectopic allele of *R26-LSL-Trpv1*. We punched different brain regions, extract DNA and genotype the cells using a combination of primers (illustrated as short lines in the panel A) for the ectopic Trpv1 allele. (F) Gel showing the excised allele is specifically expressed in the arcuate nucleus. We used the same set of primers to genotype the tail of every animal used in this study to confirm they were not ectopic expressing cre. Noteworthy, when cre is ectopically expressed in *Agrp-Cre* lines, it is also expressed in peripheral tissues. As stated above, less than 5% of the *Agrp-Cre* positive animals showed ectopic expression, and they were not included in our studies.

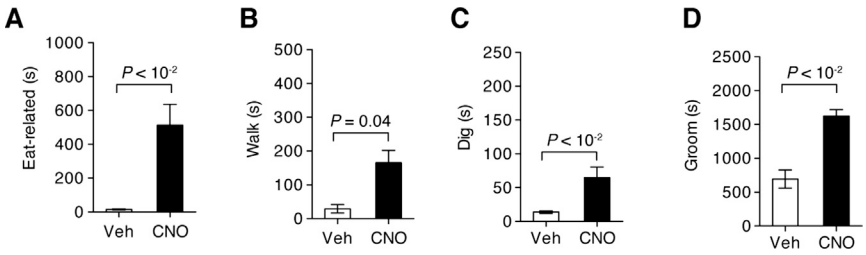

Figure S2. Home-Cage Behavior Analysis of Agrp-Neuronal-Activated Mice Using DREADD, Related to Figure 3

(A–D) In A–D, data from home-cage scan behavior phenotyping of mice with no food provided. Mice were injected with vehicle (saline, i.p., 10 ml/kg) or CNO (0.3 mg/kg, i.p.) and recorded for 2 hr after injection. (A) Eat-related behaviors, including time mice interacting with empty food container and time spent chewing (in the absence of food, mice chewed bedding material). (B) Time walking. (C) Time digging. (D) Time grooming. Bars represent mean ± SEM. Statistical significance (P) values are plotted in the figures. Statistical data derived from t test. Vehicle (n = 4), CNO (n = 7).

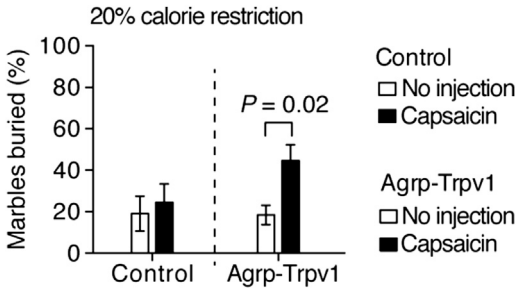

Figure S3. Activation of Agrp Neurons Induces Marble-Burying Behavior in Calorie-Restricted Mice, Related to Figure 4

Marble burying behavior in control and calorie-restricted mice. Mice were calorie-restricted 20% of their ad libitum diet for 4 weeks and then tested in the MBT in two consecutive days (no injection and capsaicin injection, 10 mg/kg, i.p.). Levels of marbles buried in the calorie-restricted group were equivalent to ad libitum fed mice (Figure 4C). Activation of Agrp neurons by capsaicin in Agrp-Trpv1 mice increases marble burying behavior. Bars represent mean ± SEM. Statistical significance (P) values are plotted in the figures. Statistical data derived from t test. Control (n = 7), Agrp-Trpv1 (n = 10).

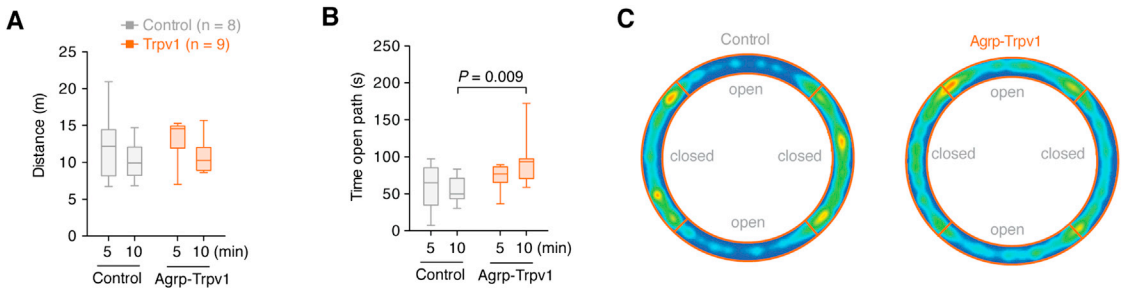

Figure S4. Anxiolytic Profile of Agrp Neuron Activation in the Zero-Maze Test, Related to Figure 5

Control and Agrp-Trpv1 mice were injected with capsaicin (10 mg/kg, i.p.) and immediately placed in the zero-maze for 10 min. (A) Total distance traveled in the apparatus. (B) Time spent in the open paths. (C) Occupancy plots of all animals in each group, showing the increased time Agrp neuron activated mice spent in the open paths. Box and whiskers represent median ± min/max. *P value*s were calculated using two-way ANOVA with repeated-measured followed by Holm-Sidak's multiple comparisons test.

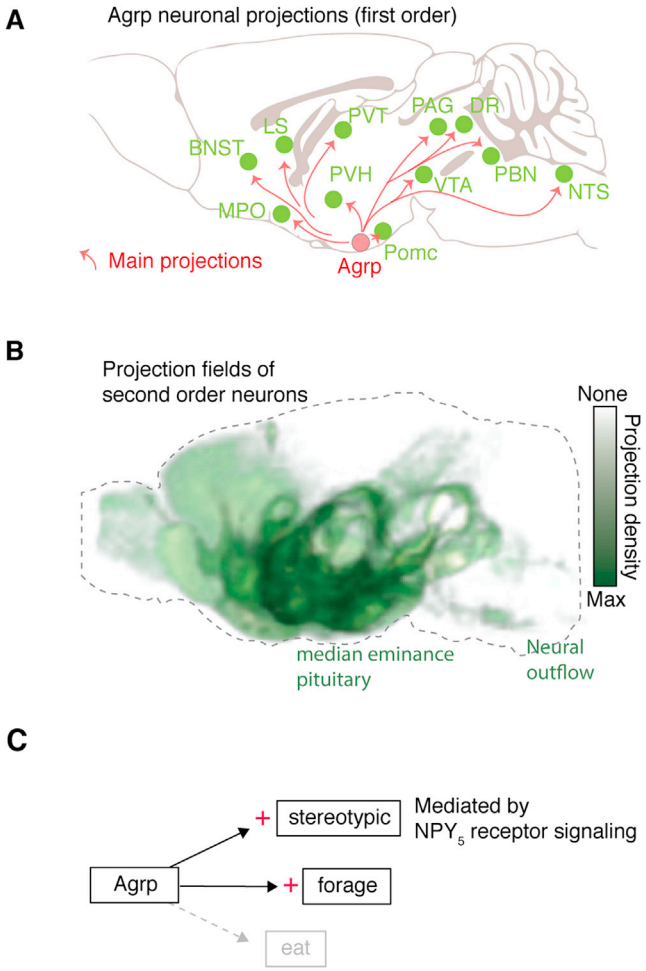

Figure S5. Summary of the Role of Agrp Neurons on Behaviors and Their Connectivity, Related to Figure 7

(A) Main projections from Agrp neurons (in red) to target brain areas. (B) Overlap of projection densities of second order nuclei with Agrp neurons as seed point. Even though it is not known exactly what neuronal subtypes in projecting areas receive inputs from Agrp neurons, this diagram gives a general idea of the capacity of Agrp neurons to influence a broad range of brain regions (including cortical and hippocampal regions) by acting in second order nuclei. (C) Diagram showing the participation of Agrp neurons in repetitive/stereotypic behaviors, a previously unsuspected role for these cells. These stereotypic behaviors are fully reversed by blockade of NPY_5 receptor signaling. In B, side views of 3D-rendered brains tracking projection density from specific brain areas (as follows) are overlapped. Bed nucleus of stria terminalis (BNST), experiment 175739085. Paraventricular nucleus of the thalamus (PVT), experiment 120875111. Lateral septal nucleus (LS), experiment 178486024. Medial preoptic area (MPO), experiment 119846838. Paraventricular hypothalamic nucleus (PVH), experiment 176432524. POMC neurons in the arcuate nucleus, experiment 175738378. Periaqueductal gray (PAG) and dorsal raphe (DR), experiment 114155190. Ventral tegmental area (VTA), experiment 156314762. All images were acquired from the Allen Mouse Brain Connectivity Atlas (Image credit: Allen Institute for Brain Science; ©2012 Allen Institute for Brain Science. Allen Mouse Brain Connectivity Atlas [Internet]. Available from: http://connectivity.brain-map.org/).

Chapter II. Activation of Agrp neurons modulates memory-related cognitive processes in mice

Scientific article published on *Pharmacological Research*.

Pharmacological Research 141 (2019) 303–309

Contents lists available at ScienceDirect

Pharmacological Research

journal homepage: www.elsevier.com/locate/yphrs

Activation of Agrp neurons modulates memory-related cognitive processes in mice

Marcelo R. Zimmer[a,c], Ariana E. Schmitz[a,d], Marcelo O. Dietrich[a,b,c,*]

[a] Program in Integrative Cell Signaling and Neurobiology of Metabolism, Department of Comparative Medicine, Yale University School of Medicine, New Haven, CT, 06520, USA
[b] Department of Neuroscience, Yale University School of Medicine, New Haven, CT, 06520, USA
[c] Graduate Program in Biochemistry, Universidade Federal do Rio Grande do Sul, Porto Alegre, RS, 90035, Brazil
[d] Department of Biochemistry, Universidade Federal de Santa Catarina, Florianópolis, SC, 88040, Brazil

ARTICLE INFO

Keywords:
Memory
Cognition
Animal model
Hypothalamus

ABSTRACT

Hypothalamic Agrp neurons are critical regulators of food intake in adult mice. In addition to food intake, these neurons have been involved in other cognitive processes, such as the manifestation of stereotyped behaviors. Here, we evaluated the extent to which Agrp neurons modulate mouse behavior in spatial memory-related tasks. We found that activation of Agrp neurons did not affect spatial learning but altered behavioral flexibility using a modified version of the Barnes Maze task. Furthermore, using the Y-maze test to probe working memory, we found that chemogenetic activation of Agrp neurons reduced spontaneous alternation behavior mediated by the neuropeptide Y receptor-5 signaling. These findings suggest novel functional properties of Agrp neurons in memory-related cognitive processes.

1. Introduction

Animals need to adapt different behavioral strategies in times of caloric needs to ensure survival. For instance, animals rely on spatial memory and working memory to exploit nutritional supplies and decision-making [1]. In fact, it is the strong influence of hunger on the behavior of the animal that has ignited the study of animal behavior since Pavlov [2,3]. Agouti-related protein (Agrp)-producing neurons, located in the arcuate nucleus of the hypothalamus, are critical regulators of food intake in mice [4–7]. In addition to food intake, Agrp neurons are involved in behaviors that are not proximally involved in food ingestion [8–10]. For example, chemogenetic activation of Agrp neurons elicits repetitive and compulsive behaviors when mice are tested in the absence of food [9]. Despite these previous findings, we still know little about the influence of Agrp neurons in memory-related cognitive functions.

Here, we performed behavioral assays to assess memory-related cognitive processes in mice under conditions of Agrp neuron activation. We found that chemogenetic activation of Agrp neurons modulate the performance of mice in behavior tasks involving spatial learning and working memory.

2. Methods

2.1. Animals

All mice used in the experiments were 4–8 months old from both genders. $Agrp^{Trpv1}$ mice and control animals are $AgrpCre^{Tm/+}::Trpv1^{-/-}::R26\text{-}LSL\text{-}Trpv1^{Gt}$ and $Trpv1^{-/-}:R26\text{-}LSL\text{-}Trpv1^{Gt/+}$, respectively [9,11]. Similarly, $Agrp^{Trpv1:VgatKO}$ and control animals are $AgrpCre^{Tm/+}::Trpv1^{-/-}::R26\text{-}LSL\text{-}Trpv1^{Gt/+}::Vgat^{Flox.Flox}$ and $Trpv1^{-/-}::R26\text{-}LSL\text{-}Trpv1^{Gt/+}::Vgat^{Flox.Flox}$. $Agrp^{Cre}$ and $R26^{LSL\text{-}Trpv1}$, respectively. $Vgat^{Flox.Flox}$ mice were backcrossed to $Trpv1^{KO}$ mice. All mice were kept in temperature- and humidity-controlled rooms, in a 12/12 h light/dark cycle, with lights on from 7:00 AM–7:00 PM. Food and water were provided ad libitum unless otherwise stated. All procedures were approved by IACUC (Yale University).

2.2. Drugs

Drugs used were: capsaicin (3.33% Tween-80 in PBS; from Sigma) and CGP71683 hydrochloride (hereinafter referred as neuropeptide Y receptor 5 (NPY_5R) antagonist) (in 5% DMSO, 5% Tween-80 in water; from Tocris). All drugs were injected in a volume of 10 ml/kg of body weight intraperitoneally (i.p.). Route of administration and dose of

* Corresponding author at: Yale University School of Medicine, 310 Cedar Street, Brady Memorial Laboratory, Suite 330C, New Haven, CT, 06520, USA.
E-mail address: marcelo.dietrich@yale.edu (M.O. Dietrich).

https://doi.org/10.1016/j.phrs.2018.12.024
Received 3 December 2018; Received in revised form 27 December 2018; Accepted 27 December 2018
Available online 02 January 2019

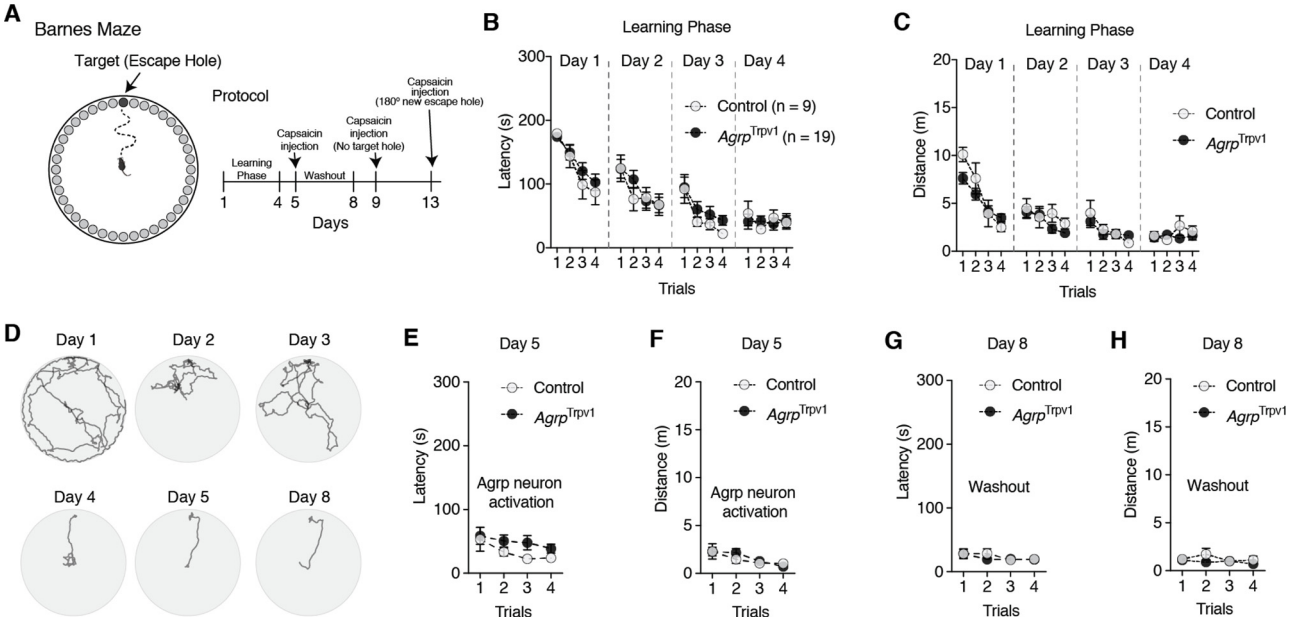

Fig. 1. Activation of Agrp neurons does not impair spatial learning. (A) Illustrative representation of Barnes Maze and experimental protocol. On days 5, 9, and 13 they received an injection of capsaicin (10 mg/kg, i.p.) before trials. Control (n = 9) and *Agrp*^{Trpv1} mice (n = 19) were tested. **(B–C)** Latency and distance traveled to reach the escape hole in the learning phase during trials across days. (**D**) Tracking data from a control animal representing one trial per day during the learning phase. **(E–F)** Latency and distance traveled to reach the escape hole upon Agrp neuron activation. (**G-H)** Latency and distance traveled to reach the escape hole three days after the injection of capsaicin, to probe the long-lasting effects of Agrp neuron activation. In B, C, E, F, G, and H symbols represent mean ± SEM. Statistically significant *P* values are provided in the panels.

drugs were established according to previous study published by our group [9].

2.3. Modified barnes maze

A schematic representation of the Barnes Maze is given in Fig. 1A. The Barnes Maze consists of a white elevated circular platform (91 x 122 cm) with 40 equidistant holes located around the edges. A dark Plexiglas escape chamber was placed under one of the holes (target hole) in which the animals could hide. Four reference cues were presented in the walls surrounding the maze. Animals were tested under a 300-watt light to create an aversive environment in the surface of the apparatus due to the bright illumination. Before each trial, mice were placed in a dark enclosed start box positioned in the center of the maze. Ten seconds later, the box was lifted, and animals were allowed to explore the maze. The protocol consisted of four days of training (learning or acquisition phase) in which animals were allowed to explore the apparatus for 180 s during each trial. During the intervals, animals returned to the home cage. At day 5, we tested the effect of activation of Agrp neurons in the recall of memory. Mice were not tested at days 6 and 7. At day 8, we re-tested mice in the maze to evaluate any long-lasting effects of Agrp neuron activation at day 5. At day 9, we performed the probe trial in which the escape chamber was removed, and animals were allowed to explore the maze for 180 s to evaluate exploratory behavior and behavior search strategy to find an alternative escape route upon activation of Agrp neurons. We performed four trials a day for each animal with an inter-trial interval of 15 min. During the inter-trial interval, mice were placed in the home cage and no food was provided. At day 13, we performed a reversal learning trial of 180 s after injection of capsaicin to all mice. Latency to reach the escape chamber and total distance traveled were recorded and measured automatically by a video tracking system (ANY-maze software, Stoelting Co, Wood Dale, IL).

2.4. Spontaneous alternation behavior (Y-Maze)

The Y-maze consisted of a black Plexiglas apparatus with three symmetrical enclosed arms (30 cm long, 8 cm wide and 15 cm high) at 120° angle from each other. The arms converged on an equilateral triangular center platform (5 × 5 x 5 cm). Animals were recorded under infrared illumination during the dark cycle. Prior to testing, animals received an injection of capsaicin (10 mg/kg, i.p.). Testing began when animals were placed in one arm of the Y-maze and allowed to explore the environment for 10 min. For *Agrp*$^{Trpv1:VgatKO}$ mice were placed in one arm of the Y-maze and allowed to explore the environment for 15 min. An animal was considered to enter an arm when 85% of the body surface was within the arm. The number of arm entries and the sequence of entries were recorded using a video tracking software (Any-Maze software, Stoelting Co., Wood Dale, IL). In the indicated experiments, NPY_5R antagonist (30 mg/kg, i.p.) or vehicle were administered 30 min prior injection of capsaicin. Spontaneous alternation behavior was calculated as the ratio of correct alternations (A) to possible alternations (number of arm entries – 2) (Fig. 3**A**). A correct alternation is considered when animals visit the three different arms of the Y-maze consecutively (e.g., ABC, ACB, CBA). The number of correct alternations is a conserved measure of working memory processes.

2.5. Statistical analysis and data plotting

Prism 8.0 was used to analyze data and plot figures. All figures were edited in Adobe Illustrator CS6/CC. Data were first subjected to a normality test using the D'Agostino & Pearson normality test or the Shapiro-Wilk normality test. When homogeneity was assumed, a parametric analysis of variance test was used. Two-way ANOVA with repeated measures was used to compare multiple groups and days/trials of testing. When necessary, Greenhouse-Geisser estimates of sphericity were used to correct for degrees of freedom. Holm-Sidak's multiple comparisons test was used to find post-hoc differences among groups. The student's *t*-test (paired and unpaired) and the Mann-Whitney U test were used to determine significance between two groups. Chi-square

test was used to analyze the differences in the use of search strategies in the Barnes Maze. Statistical data are provided in the figures. $P < 0.05$ was considered statistically significant.

3. Results

To investigate to what extent Agrp neurons influence cognitive performance in memory-related tests that do not involve food cues, we tested the effect of the chemogenetic activation of these neurons in a modified version of the Barnes Maze test (Fig. 1**A**). To activate Agrp neurons, we used $Agrp^{Trpv1}$ mice [9,11]. $Agrp^{Trpv1}$ mice expressed the Trpv1 receptor exclusively in the Agrp neurons. Trpv1 is a calcium receptor activated by capsaicin, its exogenous ligand. Thus, this animal model allows the chemogenetic activation of Agrp neurons by peripheral injection of capsaicin.

Unsurprisingly, during the learning phase both control and $Agrp^{Trpv1}$ mice decreased the latency to reach the escape chamber [Fig. 1**B** and **1D**; day 1 (effect of trial, $F_{3,78} = 22.31$, $P < 0.001$; effect of genotype, $F_{1,26} = 0.40$, $P = 0.53$; interaction, $F_{3,78} = 0.57$, $P = 0.64$); day 2 (effect of trial, $F_{3,78} = 7.65$, $P = 0.002$; effect of genotype, $F_{1,26} = 0.12$, $P = 0.73$; interaction, $F_{3,78} = 0.86$, $P = 0.47$); day 3 (effect of trial, $F_{3,78} = 11.02$, $P < 0.001$; effect of genotype, $F_{1,26} = 1.06$, $P = 0.31$; interaction, $F_{3,78} = 0.30$, $P = 0.83$); day 4 (effect of trial, $F_{3,78} = 0.74$, $P = 0.53$; effect of genotype, $F_{1,26} = 0.01$, $P = 0.91$; interaction, $F_{3,78} = 1.06$, $P = 0.37$)] and the distance traveled [Fig. 1**C**; day 1 (effect of trial, $F_{3,78} = 36.30$, $P < 0.001$; effect of genotype, $F_{1,26} = 0.76$, $P = 0.39$; interaction, $F_{3,78} = 3.32$, $P = 0.024$); day 2 (effect of trial, $F_{3,78} = 3.24$, $P = 0.027$; effect of genotype, $F_{1,26} = 1.25$, $P = 0.2743$; interaction, $F_{3,78} = 0.86$, $P = 0.46$); day 3 (effect of trial, $F_{3,78} = 6.72$, $P = 0.0004$; effect of genotype, $F_{1,26} = 0.05$, $P = 0.82$; interaction, $F_{3,78} = 0.92$, $P = 0.43$); day 4 (effect of trial, $F_{3,78} = 0.99$, $P = 0.40$; effect of genotype, $F_{1,26} = 0.49$, $P = 0.49$; interaction, $F_{3,78} = 2.17$, $P = 0.09$)] to a similar degree.

At day 5, chemogenetic activation of Agrp neurons by injection of capsaicin in $Agrp^{Trpv1}$ mice did not alter the performance of mice in the Barnes Maze as demonstrated by the latency to enter the escape chamber (Fig. 1**E**; effect of trial, $F_{3,78} = 3.46$, $P = 0.02$; effect of genotype, $F_{1,26} = 1.26$, $P = 0.27$; interaction, $F_{3,78} = 0.50$, $P = 0.68$) and the distance traveled in the apparatus (Fig. 1**F**; effect of trial, $F_{3,78} = 5.62$, $P = 0.0015$; effect of genotype, $F_{1,26} = 0.16$, $P = 0.69$; interaction, $F_{3,78} = 0.63$, $P = 0.60$). We then evaluated whether testing animals upon chemogenetic activation of Agrp neurons had any long-lasting effects on behavior performance. At day 8, we tested the animals once again for four trials without injection of capsaicin. We did not observe any statistical differences in the latency to reach the escape chamber (Fig. 1**G**; effect of trial, $F_{3,78} = 1.91$, $P = 0.13$; effect of genotype, $F_{1,26} = 0.15$, $P = 0.71$; interaction, $F_{3,78} = 0.65$, $P = 0.58$) or in the distance traveled in the apparatus (Fig. 1**H;** effect of trial, $F_{3,78} = 1.02$, $P = 0.39$; effect of genotype, $F_{1,26} = 1.22$, $P = 0.28$; interaction, $F_{3,78} = 1.22$, $P = 0.31$). Thus, in mice that learnt the contingency of a spatial memory task that does not involve food rewards, chemogenetic activation of Agrp neurons does not disrupt the retrieval of the memory, the motivation to perform the test, and the long-term retrieval of the memory.

Next, we performed a probe trial with no escape hole (Fig. 2**A**). Typically, the probe trial consists of a single short trial [12,13]. However, we opted to run four trials to investigate the dynamic changes in behavior upon chemogenetic activation of Agrp neurons. During the probe trials, mice searched around the target area for the escape chamber (Fig. 2**B-F** and **Movie S1**), corroborating activation of Agrp neurons did not alter memory recall (similar to Fig. 1). Compared to control mice, chemogenetic activation of Agrp neurons led to a relative increase in the exploration of the target quadrant of the apparatus where the escape hole was previously located (Fig. 2**G-H;** $P = 0.002$ using Holm-Sidak's multiple comparisons test after two-way ANOVA: effect of quadrant, $F_{2,52} = 184.6$, $P < 0.0001$; effect of genotype, $F_{1,26} = 2.52$, $P = 0.12$; interaction, $F_{2,52} = 6.41$, $P = 0.003$ – all trials combined) and a decrease in the time exploring adjacent quadrants (Fig. 2**G-H**; $P = 0.02$).

We also measured other indexes of exploratory behavior during the probe trials. The total number of hole entries (Fig. 2**I**; effect of trial, $F_{2.57,67.05} = 5.39$, $P = 0.003$; effect of genotype, $F_{1,26} = 11.73$, $P = 0.002$; interaction, $F_{3,78} = 0.46$, $P = 0.70$) and the total number of holes explored (Fig. 2**J**; effect of trial, $F_{2.46,63.99} = 23.50$, $P < 10^{-8}$; effect of genotype, $F_{1,26} = 12.24$, $P = 0.001$; interaction, $F_{3,78} = 0.96$, $P = 0.41$) were reduced upon chemogenetic activation of Agrp neurons. Concomitantly, the number of holes not explored across all four trials was increased in $Agrp^{Trpv1}$ mice (Fig. 2**K**; $t_{23.66} = 4.15$, $P = 0.004$, unpaired t test with Welch's correction). In line with the decreased investigation of alternative holes to exit the apparatus, chemogenetic activation of Agrp neurons significantly decreased the distance traveled compared to control mice (Fig. 2**L**; effect of trial, $F_{3,78} = 23.17$, $P < 0.0001$; effect of genotype, $F_{1,26} = 17.10$, $P = 0.0003$; interaction, $F_{3,78} = 0.39$, $P = 0.76$). Thus, in a probe trial with no escape chamber, chemogenetic activation of Agrp neurons seem to impair exploratory behavior and searching behavior for a new escape alternative, skewing mouse behavior towards previously acquired navigation strategies.

To further understand the consequences of these changes in search behavior, we ran another trial on day 13, in which we placed a new escape chamber at 180° from the original target hole (Fig. 2**M**). Four out of 9 control mice and 6 out of 19 $Agrp^{Trpv1}$ mice found the new escape chamber (Fig. 2**N;** ${x^2}_1 = 0.44$, $P_{1\text{-tail}} = 0.25$, chi-squared test; and Fig. 2**O-P**). We did not find a significant difference in the number of holes explored (Fig. 2**Q**; $t_8 = 1.03$, $P = 0.33$, unpaired t test) or the distance traveled in the apparatus between control and $Agrp^{Trpv1}$ mice that were able to enter the new escape chamber (Fig. 2**R**; $t_8 = 0.45$, $P = 0.66$, unpaired t test). We next analyzed the behavior of mice that did not enter the new escape chamber during the trial (Fig. 2**S-T**). In this subgroup of mice, chemogenetic activation of Agrp neurons decreased the total number of holes explored (Fig. 2**U**; $t_{16} = 4.102$, $P = 0.0008$, unpaired t test) and the distance traveled in the apparatus (Fig. 2**V**; $t_{16} = 2.43$, $P = 0.02$, unpaired t test) compared to control mice. Thus, the results from the modified Barnes Maze test implies that chemogenetic activation of Agrp neurons in mice suppresses the searching behavior to find an escape alternative, suggesting that in more natural conditions the overactivation of these neurons can reduce behavior flexibility.

One possibility for the reduced behavior flexibility upon chemogenetic activation of Agrp neurons in the Barnes Maze probe trials is altered working memory. To more directly test for working memory, we measured the spontaneous alternation behavior of mice (Fig. 3**A**). Spontaneous alternation is conserved across mammals [14,15] and comprises the tendency of animals to alternate arms when exploring a maze [16–18]. The Y-maze test used here evaluates the spontaneous alternation behavior as a measurement of spatial working memory [19–21], which is independent of previous training or the use of food rewards. Chemogenetic activation of Agrp neurons did not alter the number of arm entries (Fig. 3**B**; control: 45.75 ± 3.12, n = 8; $Agrp^{Trpv1}$: 41.00 ± 2.26, n = 11; $t_{17} = 1.26$, $P = 0.22$, unpaired t test) but led to a reduced proportion of correct spontaneous alternations towards random choices (Fig. 3**C**; control: 67.01 ± 2.69%; $Agrp^{Trpv1}$: 57.49 ± 2.42%; $t_{17} = 2.60$, $P = 0.01$, unpaired t test). This result suggest chemogenetic activation of Agrp neurons reduces the performance in a test of working memory in mice.

Next, we investigated whether GABA release by Agrp neurons was involved in the impaired spontaneous alternation behavior upon chemogenetic Agrp neuronal activation. We generated $Agrp^{Trpv1}$ mice with impaired GABA release selectively from Agrp neurons (Fig. 4**A**) [22]. Using this mouse model, chemogenetic activation of Agrp neurons did not significantly change the number of arm entries (Fig. 4**B**; control: 59.75 ± 4.92, n = 12; $Agrp^{Trpv1:VgatKO}$: 57.00 ± 5.91, n = 9;

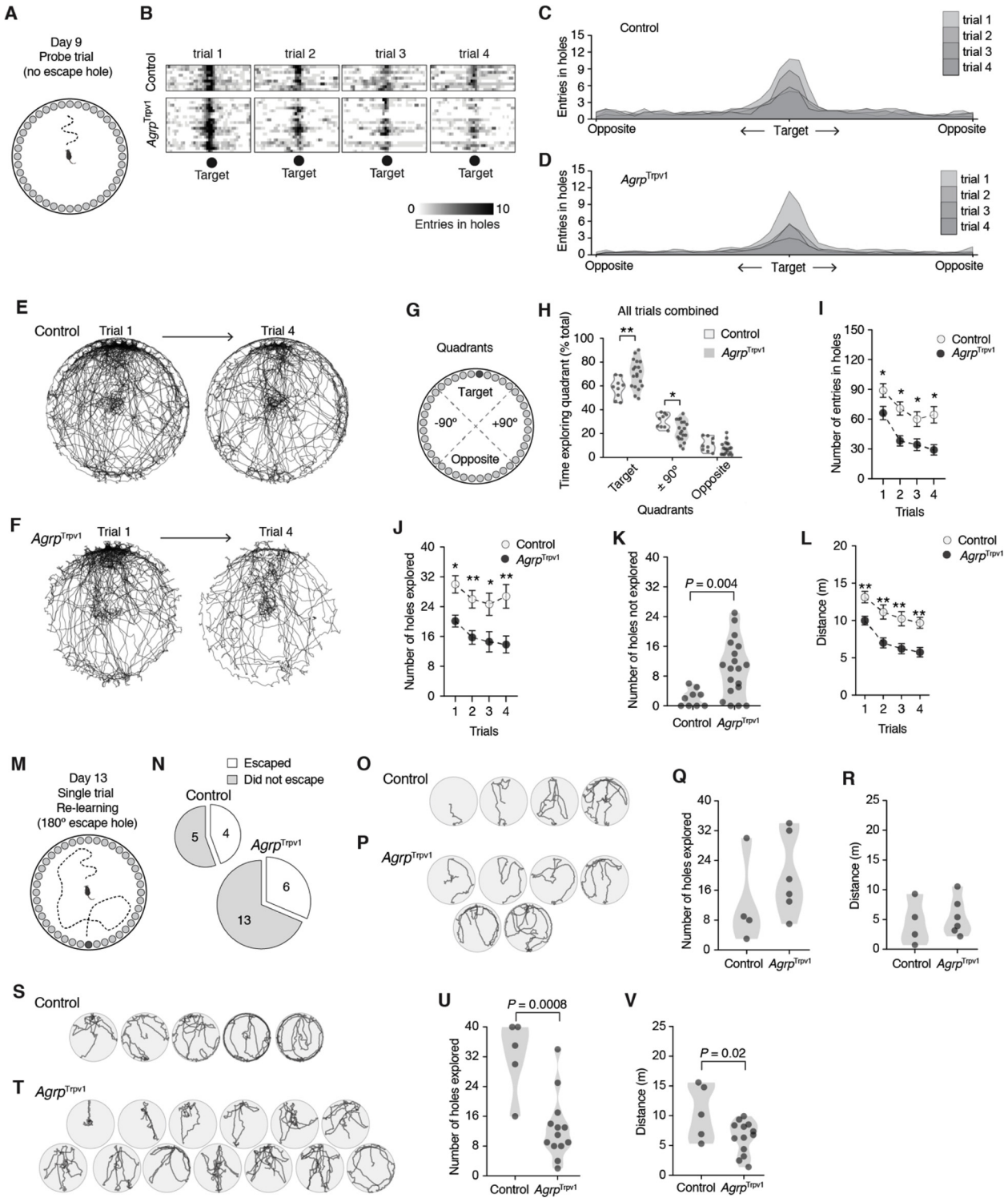

Fig. 2. Activation of Agrp neurons alters spatial navigation in probe trials.
(A) Illustration of the Barnes Maze in the probe trials with the removal of the escape hole. (**B**) Heat plot showing the number of entries in each hole (X axis) across the four trials at day 9 (each box is one trial; each row is one mouse). (**C-D**) Quantification of data from B in the form of histogram distribution. (**E-F**) Cumulative superimposed tracking plots of control (n = 9) and *Agrp*^{Trpv1} mice (n = 9 randomly displayed to equal the number of control mice) in the first and the fourth trials of the probe test. (**G**) Illustration of the quadrants in the Barnes Maze in the probe trial. (**H**) Proportion of time mice spent exploring the quadrants in all probe trials combined. (**I**) Total number of entries in holes across the probe trials. (**J**) Total number of holes explored (out of 40 total) across the probe trials. (**K**) Total number of holes not explored during the probe test (4 trials combined; out of 40 holes). (**L**) Total distance traveled across the probe trials. (**M**) Illustration of the reversal learning trial with a new escape chamber placed at 180° of the original target hole. (**N**) Proportion of mice that escaped the Barnes Maze by entering the new escape chamber. (**O-P**) Tracking plots of all mice that escaped the trial by entering the new escape chamber. (**Q**) Total number of holes explored (out of 40 total) in the trial by the animals that entered the new escape hole. (**R**) Similar to Q, but the total distance traveled in the trial. (**S-T**) Similar to O-P, tracking plots of all mice that did not escape the apparatus during the reversal learning trial. (**U**) Similar to Q, but for mice that did not escape. (**V**) Similar to R, but for mice that did not escape. In I, J, and L symbols represent mean ± SEM. In H, K, Q, R, U, and V symbols represent individual values. Statistically significant *P* values are provided in the panels. For multiple comparisons tests, * denotes $P < 0.05$ and ** denotes $P < 0.01$.

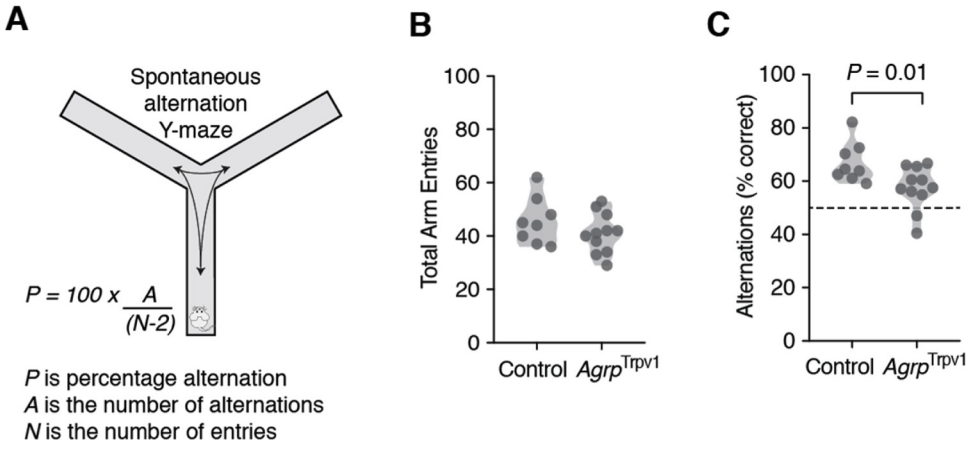

Fig. 3. Activation of Agrp neurons reduces spontaneous alternation behavior in mice. (A) Diagram illustrating the use of the Y-maze test to measure spontaneous alternation behavior in mice. Control (n = 8) and $Agrp^{Trpv1}$ mice (n = 11) were tested immediately after receiving an injection of capsaicin (10 mg/kg, i.p.). **(B)** Violin plots represent the distribution in the total number of arm entries between groups. **(C)** Violin plots represent the distribution in the proportion of correct alternations between groups. Symbols represent individual values. Statistically significant *P* values are provided in the panels.

$t_{19} = 0.35$, $P = 0.72$, unpaired *t* test) but decreased the number of spontaneous alternations (Fig. 4**C**; control: 69.87 ± 2.01%; $Agrp^{Trpv1:VgatKO}$: 62.14 ± 2.53%; $t_{19} = 2.42$, $P = 0.02$, unpaired *t* test) similar to our previous results (Fig. 3). Thus, GABA release by Agrp neurons does not seem to mediate the reduced spontaneous alternation behavior upon chemogenetic activation of Agrp neurons.

Agrp neurons also release neuropeptide Y (NPY), which signal mainly through downstream NPY_1 and NPY_5 receptors [23–26]. In a previous study, we demonstrated that repetitive behaviors driven by the chemogenetic activation of Agrp neurons were mediated by NPY_5

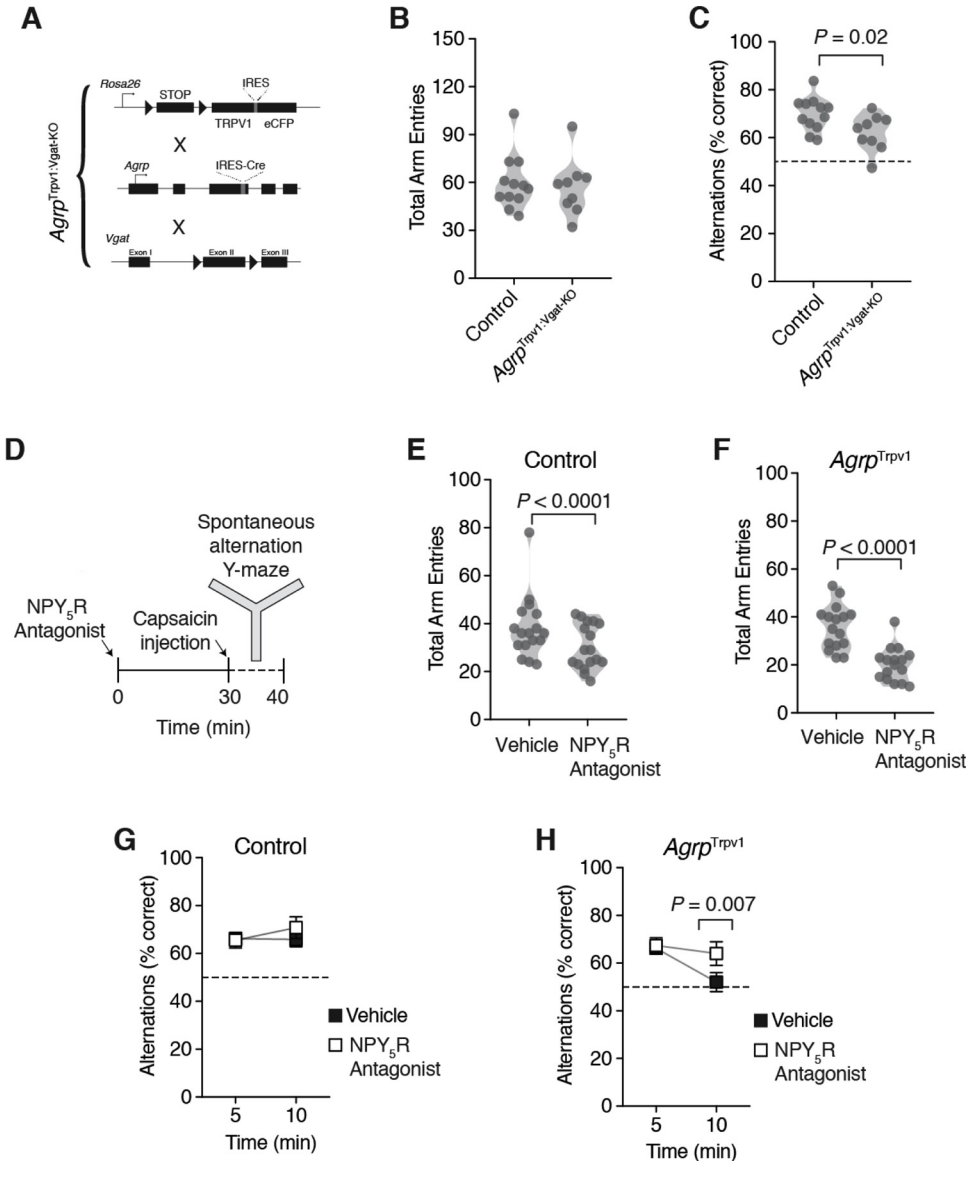

Fig. 4. NPY signaling, but not GABA release by Agrp neurons, blunts the effect of Agrp neuron activation on spontaneous alternation behavior. **(A)** Schematic strategy to generate the $Agrp^{Trpv1:VgatKO}$ mice. Mice are the result of a triple breeding cross; all lines were backcrossed to a Trpv1 knockout background. Control (n = 12) and $Agrp^{Trpv1:VgatKO}$ mice (n = 9) were tested immediately after receiving an injection of capsaicin (10 mg/kg, i.p.). **(B)** Violin plots represent the distribution in the total number of arm entries between groups. **(C)** Violin plots represent the distribution in the proportion of correct alternations between groups. **(D)** Study design showing pre-treatment of mice with the NPY_5 receptor antagonist (CGP71683, 30 mg/kg, i.p.) or vehicle thirty minutes before the injection of capsaicin (10 mg/kg, i.p.). Control (n = 17) and $Agrp^{Trpv1.}$
mice (n = 16) were tested in the Y-maze immediately after the injection of capsaicin. The same animals were tested twice, in response to vehicle or CGP71683. Mice were randomly assigned to the different groups using a crossover study design. **(E–F)** Violin plots represent the distribution in the total number of arm entries in control and $Agrp^{Trpv1}$ mice, respectively. **(G–H)** Proportion of correct alternations in five-minute bins in control and $Agrp^{Trpv1}$ mice, respectively. In B, C, E and F symbols represent individual values. In G and H, symbols represent mean ± SEM. Statistically significant *P* values are provided in the panels.

receptor signaling [9]. Hence, we sought to test the role of NPY_5 receptor signaling in spontaneous alternation behavior upon chemogenetic Agrp neuron activation (Fig. 4**D**). The NPY_5 receptor antagonist CGP71683 (30 mg/kg, i.p.) reduced the total number of arm entries in both control (Fig. 4**E;** vehicle: 38.18 ± 3.13, n = 17; NPY_5R antagonist: 30.35 ± 2.24, n = 17; $t_{16} = 3.17$, $P = 0.005$, paired *t* test) and $Agrp^{Trpv1}$ mice (Fig. 4**F;** vehicle: 35.88 ± 2.28, n = 16; NPY_5R antagonist: 20.25 ± 1.76, n = 16; $t_{15} = 5.91$, $P < 0.0001$, paired *t* test) compared to vehicle injected animals. In control animals, treatment with the NPY_5R antagonist did not significantly change spontaneous alternation behavior (Fig. 4**G;** effect of time, $F_{1,16} = 1.23$, $P = 0.28$; effect of drug treatment, $F_{1,16} = 0.31$, $P = 0.58$; interaction, $F_{1,16} = 0.41$, $P = 0.52$, two-way ANOVA with time as a repeated-measure). On the other hand, treatment of $Agrp^{Trpv1}$ mice with the NPY_5R antagonist blunted the reduction in spontaneous alternation behavior observed upon chemogenetic activation of Agrp neurons (Fig. 4**H**; effect of time, $F_{1,15} = 7.29$, $P = 0.01$; effect of drug treatment, $F_{1,15} = 2.15$, $P = 0.16$; interaction, $F_{1,15} = 4.70$, $P = 0.04$, two-way ANOVA with time as a repeated-measure). Together, these findings suggest that Agrp neurons are capable of altering cognitive performance in mice at least partially via NPY_5 receptor signaling in behavior tests that probe working memory and do not involve food related cues.

4. Discussion

Agrp neurons are classically involved in the promotion of hunger [5,6]. This study provides support for the capacity of hypothalamic Agrp neurons to alter cognitive processes in behavior tasks that do not involve food cues or food rewards. More specifically, our findings suggest that chemogenetic activation of Agrp neurons can acutely shift the behavior repertoire of mice in memory-related tests, impairing the use of working memory and suppressing exploratory searching behavior towards a non-food related escape goal.

Animals use spatial memory to navigate and to recall their past locations [27]. Spatial learning and memory are assessed in rodents using a variety of approaches, such as the Morris Water Maze, the Barnes Maze, and the Radial Arm Maze [27–33]. Here, we used the Barnes Maze test as the least stressful option compared to the Morris Water Maze as it does not require mice to swim in cold water. Additionally, the Barnes Maze does not require food rewards as often used in the Radial Arm Maze [13,34]. Using the Barnes Maze, we found that chemogenetic activation of Agrp neurons was capable of suppressing searching behavior for a new escape chamber when the previously memorized escape location was either removed or altered. This behavior could result from drive competition, in which activation of Agrp neurons would generate a motivational drive presumably for food that suppresses the drive to explore the aversive environment and find a new escape route [35]. However, (1) chemogenetic activation of Agrp neurons did not alter behavior performance during trials in which the escape chamber was at a previously memorized location; and (2) in the probe trials, mice in which the Agrp neurons were activated showed skewed exploration of the previously memorized escape hole compared to alternative holes. Thus, the motivation to find the escape chamber seem to be preserved upon chemogenetic activation of Agrp neurons, which would argue against a competition between motivational drives. An alternative explanation to these findings would be that activation of Agrp neurons alters behavioral flexibility [36–38] and working memory, favoring previously established memories.

The Y-maze test used to assess spontaneous alternation behavior [14–18] measures spatial working memory [19–21]. In this test, a score of 50% indicates random choice between two arms [39]. Performance below 50% indicates repetitive/perseverative choices [40,41], while a performance above 50% indicates use of working memory in making behavior choices [42]. We found that chemogenetic activation of Agrp neurons impairs the performance in the task towards 50% performance, suggesting random choices and impaired use of working memory. The impaired performance in the spontaneous alternation test was mediated, at least partially, by NPY_5 receptor signaling. These results are similar to a previous report from our laboratory demonstrating that chemogenetic activation of Agrp neurons led to repetitive, stereotypic behaviors via NPY_5 receptor signaling [9]. In our studies we used peripheral injection of a pharmacological antagonist of NPY_5 receptor signaling. Intriguingly, the same dose and route of administration of this pharmacological antagonist did not suppress Agrp neuron activation driven food intake in mice [9]. Together, these results suggest that the repetitive behaviors and reduced performance in the Y-maze test upon chemogenetic activation of Agrp neurons are likely not the product of the same cognitive processes involved in food intake. Alternatively, because NPY_5 receptors are expressed in several downstream targets of Agrp neurons [26,43] as well as in cortex and hippocampus [43–45], our studies cannot precisely identify which NPY_5 receptor expressing neurons are important to blunt the effects of Agrp neurons on spontaneous alternation behavior. It could be that upon activation of Agrp neurons in testing conditions with no food available, neurons that express the NPY_5 receptor - and are not direct targets of Agrp neurons - control the expression of these altered cognitive processes. Future studies should address this question using more specific tools to perform discrete manipulations of NPY signaling whilst conducting similar behavioral assessments of working memory.

Agrp neurons are considered *bona fide* motivational drivers of food intake. Our behavior results may suggest a broader view of the drive generated by the activity of these neurons, i.e. hunger. Agrp neuron activity seems to signal an 'energy storage' drive, rather than a drive specific to food appetite. In this case, the drive would be transmitted to other neuronal networks that would take the most adaptive solution to obtain energy, to decrease energy expenditure, and to store excess energy in body supplies (e.g., fat). In situations of increased food supply, food intake is the most adaptive solution to increase energy storage. Conversely, in conditions when food sources are scarcely available, decreasing the expenditure of energy in seemingly superfluous activities would be the most adaptive solution. Thus, in the case of the Barnes Maze test, when the escape chamber is removed or difficult to find (as in animals that did not enter the chamber in the reversal learning trial), Agrp neuron activity suppresses the search for the new solution, as this would presumably be the most cost-effective solution energetically. In support of this model, we and others have investigated the effects of Agrp neuron activity in a variety of behavior tests and have never found a strong suppression in the exploratory drive [9,35,46] as reported in the probe trials of the Barnes Maze. In fact, activation of Agrp neurons is typically related to increased activity levels that are interpreted as foraging activity in anticipation of food intake [9,35,46]. Comparisons between the physiological and behavioral processes controlled by Agrp neurons as well as other neurons involved in motivational states would help to clarify the extent to which this framework refers to what we denominate 'hunger' or refers to a more distinct motivational state. Were this model to hold, it would be intriguing to see the performance of mice in tests that involve food rewards, life-threatening conditions, and more naturalistic settings when the environment is less deterministic than that in the laboratory.

Our results highlight the involvement of evolutionarily conserved Agrp neurons in the mammalian hypothalamus in the coordination of complex cognitive functions in conditions that do not necessarily - or proximally in an ethological perspective - involve metabolic or appetite control. They provide experimental evidence to inquire about the functional organization of the mammalian brain and how neurons that generate motivational states communicate with neuronal networks involved in memory recall and executive functions. Moreover, our findings can raise novel insights in the understanding of several human conditions characterized by metabolic and cognitive dysfunctions, including obesity, anorexia nervosa, and Prader-Willi Syndrome. Since neuropeptide Y receptor-5 antagonists have been tested in clinical studies in humans, these compounds could be promptly tested in these

human conditions.

Authors' contribution

M.R.Z. performed the Y-maze experiments, designed the studies, analyzed the data and wrote the manuscript. A.S. performed the Barnes Maze experiments, designed the study, and analyzed the data. M.O.D. helped performing the Y-maze experiments, supervised the work, designed the studies, analyzed the data, and wrote the manuscript.

Conflict of interest

The authors declare no conflict of interest.

Acknowledgements

We thank lab members and Dr. Ifat Levy for their comments on this manuscript. M.O.D. was supported by a NARSAD Young Investigator Grant ID 22709 from the Brain & Behavior Research Foundation, by the National Institute Of Diabetes And Digestive And Kidney Diseases of the National Institutes of Health (R01DK107916), by a pilot grant from the Yale Diabetes Research Center (P30 DK045735), by the Yale Center for Clinical Investigation Scholar Award, by the Whitehall Foundation, by the Charles H. Hood Foundation, Inc. (Boston, MA) and by a pilot grant from the Modern Diet and Physiology Research Center (The John B. Pierce Laboratory). M.O.D. also received support from the Conselho Nacional de Desenvolvimento Científico e Tecnológico (CNPq) and Coordenadoria de Aperfeiçoamento de Pessoal de Nível Superior (CAPES), Brazil. M.R.Z. and A.S. were partially supported by scholarships from CNPq and CAPES. The authors declare no conflict of interest.

Appendix A. Supplementary data

Supplementary material related to this article can be found, in the online version, at doi:https://doi.org/10.1016/j.phrs.2018.12.024.

References

[1] K. Hulgard, J.M. Ratcliffe, Niche-specific cognitive strategies: object memory interferes with spatial memory in the predatory bat *Myotis nattereri*, J. Exp. Biol. 217 (18) (2014) 3293–3300.
[2] I.P. Pavlov, G.V. Anrep, Conditioned Reflexes, Dover Publications, 2003.
[3] M.O. Dietrich, T.L. Horvath, Limitations in anti-obesity drug development: the critical role of hunger-promoting neurons, Nat. Rev. Drug Discov. 11 (9) (2012) 675–691.
[4] J.R. Shutter, et al., Hypothalamic expression of ART, a novel gene related to agouti, is up-regulated in obese and diabetic mutant mice, Genes Dev. 11 (5) (1997) 593–602.
[5] T.M. Hahn, et al., Coexpression of Agrp and NPY in fasting-activated hypothalamic neurons, Nat. Neurosci. 1 (4) (1998) 271–272.
[6] M. Rossi, et al., A C-terminal fragment of Agouti-related protein increases feeding and antagonizes the effect of alpha-melanocyte stimulating hormone in vivo, Endocrinology 139 (10) (1998) 4428–4431.
[7] E. Gropp, et al., Agouti-related peptide-expressing neurons are mandatory for feeding, Nat. Neurosci. 8 (10) (2005) 1289–1291.
[8] C.J. Burnett, et al., Hunger-driven motivational state competition, Neuron 92 (1) (2016) 187–201.
[9] M.O. Dietrich, et al., Hypothalamic agrp neurons drive stereotypic behaviors beyond feeding, Cell 160 (6) (2015) 1222–1232.
[10] S.L. Padilla, et al., Agouti-related peptide neural circuits mediate adaptive behaviors in the starved state, Nat. Neurosci. 19 (5) (2016) 734–741.
[11] H.B. Ruan, et al., O-GlcNAc transferase enables AgRP neurons to suppress browning of white fat, Cell 159 (2) (2014) 306–317.
[12] B. Sunyer, et al., Barnes Maze, a Useful Task to Assess Spatial Reference Memory in the Mice, (2007).
[13] C.A. Barnes, Memory deficits associated with senescence: a neurophysiological and behavioral study in the rat, J. Comp. Physiol. Psychol. 93 (1) (1979) 74–104.
[14] A. Nguyen, et al., Spontaneous alternation behavior in humans, Proceedings of the 23rd ACM Symposium on Virtual Reality Software and Technology (2017) 1–4.
[15] C.L. Richman, et al., Spontaneous alternation behavior in animals: A review, Curr. Psychol. Res. Rev. 5 (4) (1986) 358–391.
[16] E.C. Tolman, Purpose and cognition: the determiners of animal learning, Psychol. Rev. 32 (4) (1925) 285–297.
[17] R. Lalonde, The neurobiological basis of spontaneous alternation, Neurosci. Biobehav. Rev. 26 (1) (2002) 91–104.
[18] W.N. Dember, H. Fowler, Spontaneous alternation behavior, Psychol. Bull. 55 (6) (1958) 412–428.
[19] W.G. Drew, L.L. Miller, E.L. Baugh, Effects of delta9-THC, LSD-25 and scopolamine on continuous, spontaneous alternation in the Y-maze, Psychopharmacologia 32 (2) (1973) 171–182.
[20] M. Sarter, G. Bodewitz, D.N. Stephens, Attenuation of scopolamine-induced impairment of spontaneous alteration behaviour by antagonist but not inverse agonist and agonist beta-carbolines, Psychopharmacology (Berl.) 94 (4) (1988) 491–495.
[21] M. Hiramatsu, T. Hyodo, T. Kameyama, U-50488H, a selective kappa-opioid receptor agonist, improves carbon monoxide-induced delayed amnesia in mice, Eur. J. Pharmacol. 315 (2) (1996) 119–125.
[22] Q. Tong, et al., Synaptic release of GABA by AgRP neurons is required for normal regulation of energy balance, Nat. Neurosci. 11 (9) (2008) 998–1000.
[23] C. Gerald, et al., A receptor subtype involved in neuropeptide-Y-induced food intake, Nature 382 (6587) (1996) 168–171.
[24] T. Pedrazzini, et al., Cardiovascular response, feeding behavior and locomotor activity in mice lacking the NPY Y1 receptor, Nat. Med. 4 (6) (1998) 722–726.
[25] A. Kanatani, et al., Role of the Y1 receptor in the regulation of neuropeptide Y-mediated feeding: comparison of wild-type, Y1 receptor-deficient, and Y5 receptor-deficient mice, Endocrinology 141 (3) (2000) 1011–1016.
[26] M.L. Wolak, et al., Comparative distribution of neuropeptide Y Y1 and Y5 receptors in the rat brain by using immunohistochemistry, J. Comp. Neurol. 464 (3) (2003) 285–311.
[27] S.D. Healy, C. Jozet-Alves, Spatial memory, in: M.D. Breed, J. Moore (Eds.), Encyclopedia of Animal Behavior, Academic Press, Oxford, 2010, pp. 304–307.
[28] C.J. Cole, S.A. Josselyn, 4.27 - transcription regulation of memory: CREB, CaMKIV, Fos/Jun, CBP, and SRF, in: J.H. Byrne (Ed.), Learning and Memory: A Comprehensive Reference, Academic Press, Oxford, 2008, pp. 547–566.
[29] J.D. Sweatt, Chapter 4 - rodent behavioral learning and memory models, in: J.D. Sweatt (Ed.), Mechanisms of Memory (Second Edition), Academic Press, London, 2010, pp. 76–103.
[30] M. Carter, J. Shieh, Chapter 2 - animal behavior, in: M. Carter, J. Shieh (Eds.), Guide to Research Techniques in Neuroscience (Second Edition), Academic Press, San Diego, 2015, pp. 39–71.
[31] S.L. Inman-Wood, et al., Effects of prenatal cocaine on Morris and Barnes maze tests of spatial learning and memory in the offspring of C57BL/6J mice, Neurotoxicol. Teratol. 22 (4) (2000) 547–557.
[32] A. Holmes, et al., Behavioral profiles of inbred strains on novel olfactory, spatial and emotional tests for reference memory in mice, Genes Brain Behav. 1 (1) (2002) 55–69.
[33] R. D'Hooge, P.P. De Deyn, Applications of the Morris water maze in the study of learning and memory, Brain Res. Rev. 36 (1) (2001) 60–90.
[34] M.E. Bach, et al., Impairment of spatial but not contextual memory in CaMKII mutant mice with a selective loss of hippocampal LTP in the range of the theta frequency, Cell 81 (6) (1995) 905–915.
[35] C.J. Burnett, et al., Hunger-driven motivational state competition, Neuron 92 (1) (2016) 187–201.
[36] S.A. Laredo, et al., Effects of defeat stress on behavioral flexibility in males and females: modulation by the mu-opioid receptor, Eur. J. Neurosci. 41 (4) (2015) 434–441.
[37] R.S. Reiserer, et al., Impaired spatial learning in the APPSwe + PSEN1DeltaE9 bigenic mouse model of Alzheimer's disease, Genes Brain Behav. 6 (1) (2007) 54–65.
[38] M. Yasumura, et al., IL1RAPL1 knockout mice show spine density decrease, learning deficiency, hyperactivity and reduced anxiety-like behaviours, Sci. Rep. 4 (2014) 6613.
[39] L. Kokkinidis, H. Anisman, Interaction between cholinergic and catecholaminergic agents in a spontaneous alternation task, Psychopharmacology (Berl.) 48 (3) (1976) 261–270.
[40] L. Kokkinidis, H. Anisman, Perseveration and rotational behavior elicited by d-amphetamine in a Y-maze exploratory task: differential effects of intraperitoneal and unilateral intraventricular administration, Psychopharmacology (Berl.) 52 (2) (1977) 123–128.
[41] L. Kokkinidis, H. Anisman, Abatement of stimulus perseveration following repeated d-amphetamine treatment: absence of behaviorally augmented tolerance, Pharmacol. Biochem. Behav. 8 (5) (1978) 557–563.
[42] H. Anisman, L.J.P. Kokkinidis, Effects of scopolamine, d-amphetamine and other drugs affecting catecholamines on spontaneous alternation and locomotor activity in mice, Psychopharmacologia 45 (1) (1975) 55–63.
[43] A. Kask, et al., The neurocircuitry and receptor subtypes mediating anxiolytic-like effects of neuropeptide Y, Neurosci. Biobehav. Rev. 26 (3) (2002) 259–283.
[44] K.L. Grove, et al., Neuropeptide Y Y5 receptor protein in the cortical/limbic system and brainstem of the rat: expression on γ-aminobutyric acid and corticotropin-releasing hormone neurons, Neuroscience 100 (4) (2000) 731–740.
[45] C. Aoki, V.M. Pickel, Neuropeptide Y in cortex and striatum, Ann. N. Y. Acad. Sci. 611 (1) (1990) 186–205.
[46] M.J. Krashes, et al., Rapid, reversible activation of AgRP neurons drives feeding behavior in mice, J. Clin. Invest. 121 (4) (2011) 1424–1428.

Chapter III. Functional ontogeny of hypothalamic Agrp neurons in neonatal mouse behaviors

Scientific article published in the journal *Cell*.

Article

Cell

Functional Ontogeny of Hypothalamic Agrp Neurons in Neonatal Mouse Behaviors

Graphical Abstract

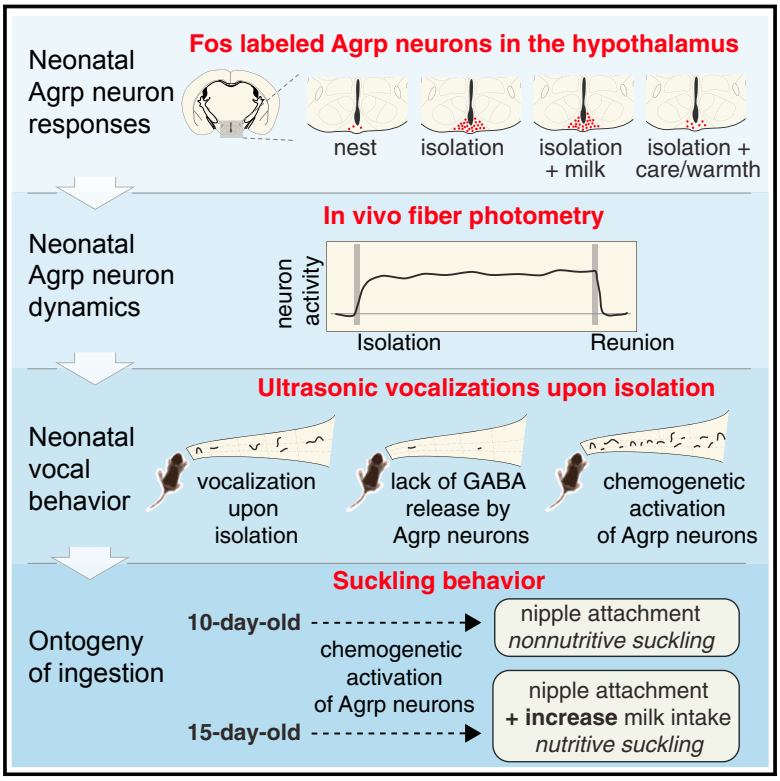

Highlights

- Isolation from the nest activates Agrp neurons in neonatal mice
- Care and warmth, but not milk, blunts activation of Agrp neurons
- Neonatal Agrp neurons modulate isolation-induced ultrasonic vocalizations
- Agrp neurons increase milk ingestion in 15- but not in 10-day-old mice

Authors

Marcelo R. Zimmer, Antonio H.O. Fonseca, Onur Iyilikci, Rafael Dai Pra, Marcelo O. Dietrich

Correspondence

marcelo.dietrich@yale.edu

In Brief

Hypothalamic Agrp neurons play a role in offspring-to-caregiver bonding independent of their role in food ingestion.

Zimmer et al., 2019, Cell *178*, 1–16
June 27, 2019
https://doi.org/10.1016/j.cell.2019.04.026

CellPress

Please cite this article in press as: Zimmer et al., Functional Ontogeny of Hypothalamic Agrp Neurons in Neonatal Mouse Behaviors, Cell (2019), https://doi.org/10.1016/j.cell.2019.04.026

Article

Cell

Functional Ontogeny of Hypothalamic Agrp Neurons in Neonatal Mouse Behaviors

Marcelo R. Zimmer,[1,3] Antonio H.O. Fonseca,[1,4] Onur Iyilikci,[1] Rafael Dai Pra,[1,3] and Marcelo O. Dietrich[1,2,3,5,*]
[1]Program in Integrative Cell Signaling and Neurobiology of Metabolism, Department of Comparative Medicine, Yale University School of Medicine, New Haven, CT 06520, USA
[2]Department of Neuroscience, Yale University School of Medicine, New Haven, CT 06520, USA
[3]Graduate Program in Biological Sciences-Biochemistry, Universidade Federal do Rio Grande do Sul, Porto Alegre, RS 90035, Brazil
[4]Graduate Program in Microelectronics, Universidade Federal do Rio Grande do Sul, Porto Alegre, RS 15064, Brazil
[5]Lead Contact
*Correspondence: marcelo.dietrich@yale.edu
https://doi.org/10.1016/j.cell.2019.04.026

SUMMARY

Hypothalamic Agrp neurons regulate food ingestion in adult mice. Whether these neurons are functional before animals start to ingest food is unknown. Here, we studied the functional ontogeny of Agrp neurons during breastfeeding using postnatal day 10 mice. In contrast to adult mice, we show that isolation from the nursing nest, not milk deprivation or ingestion, activated Agrp neurons. Non-nutritive suckling and warm temperatures blunted this effect. Using *in vivo* fiber photometry, neonatal Agrp neurons showed a rapid increase in activity upon isolation from the nest, an effect rapidly diminished following reunion with littermates. Neonates unable to release GABA from Agrp neurons expressed blunted emission of isolation-induced ultrasonic vocalizations. Chemogenetic overactivation of these neurons further increased emission of these ultrasonic vocalizations, but not milk ingestion. We uncovered important functional properties of hypothalamic Agrp neurons during mouse development, suggesting these neurons facilitate offspring-to-caregiver bonding.

INTRODUCTION

Agouti-related peptide (Agrp) neurons in the arcuate nucleus of the hypothalamus serve as a central coordinator to regulate food intake. Ablation of these neurons leads to aphagia in adult mice (Gropp et al., 2005; Luquet et al., 2005), but not in neonates, suggesting that Agrp neurons do not contribute to ingestive behaviors early in development. In support of this view, Agrp neurons show delayed development in rodents (Nilsson et al., 2005; Padilla et al., 2010), when the final maturation of Agrp neuronal circuitry coincides with weaning (Grove and Smith, 2003). However, impairing development of Agrp neurons during the first postnatal week in mice has persistent consequences to metabolism and behavior (Dietrich et al., 2012; Joly-Amado et al., 2012), suggesting an unidentified function for Agrp neurons during early development.

Here, we assessed the functional ontogeny of Agrp neurons in early postnatal development of mice at postnatal day 10 (P10) and during the weaning period during postnatal days 15–21 (P15–P21).

RESULTS

Isolation from the Nursing Nest, Not Nutrient Intake, Activates Agrp Neurons in Neonates

In adult mice, nutrient deprivation activates Agrp neurons (Hahn et al., 1998; Takahashi and Cone, 2005). So, we investigated the extent to which Agrp neurons respond to a lack of nutrients in neonatal mice. To test this, we isolated P10 mice from the nest for 90 min or 8 h to prevent nutrient intake via milk ingestion (Figure 1A). A 90-min time from onset of separation maximizes Fos expression (Barros et al., 2015). Both periods of isolation increased Agrp neuronal activity, as indicated by the increased number of Fos positive Agrp neurons upon isolation (nest: 3.14 ± 0.96%, n = 9; isolation/90 min: 31.19 ± 1.89%, n = 10; isolation/8 h: 46.19 ± 2.04%, n = 3; $F_{2,\ 19} = 128.6$, $p < 10^{-11}$, one-way ANOVA; Figures 1B–1D).

Because 90 min significantly increased Fos positive Agrp neurons, we tested whether this period of isolation also stimulated milk intake. We measured milk intake by calculating the change in body weight in animals that remained in the nest for 90 min compared to animals isolated for 90 min followed by re-introduction to the nest for an additional 90-min period (Figure 1E). In this protocol, we did not observe significant differences in the body-weight changes between the two experimental conditions (nest: 62.1 ± 15.4 mg, n = 12; reunion: 76.2 ± 14.4 mg, n = 12; $t_{22} = 0.65$, p = 0.51, unpaired *t* test; Figure 1F). Thus, activation of Agrp neurons after 90 min of isolation from the nest in P10 mice is not significant to increase milk intake. Moreover, the increased activation of Agrp neurons does not seem to arise from a generalized stress response, as corticosterone levels did not increase after isolation (nest: 9.96 ± 1.85 ng/mL, n = 7; isolation: 12.40 ± 1.85 ng/mL, n = 11; $t_{16} = 0.88$, p = 0.39, unpaired t test; Figure 1G), and testing pups in the presence of a predator odor for 90 min did not alter Fos labeling in Agrp neurons (nest: 1.19 ± 0.92%, n = 2; isolation: 23.82 ± 4.78%,

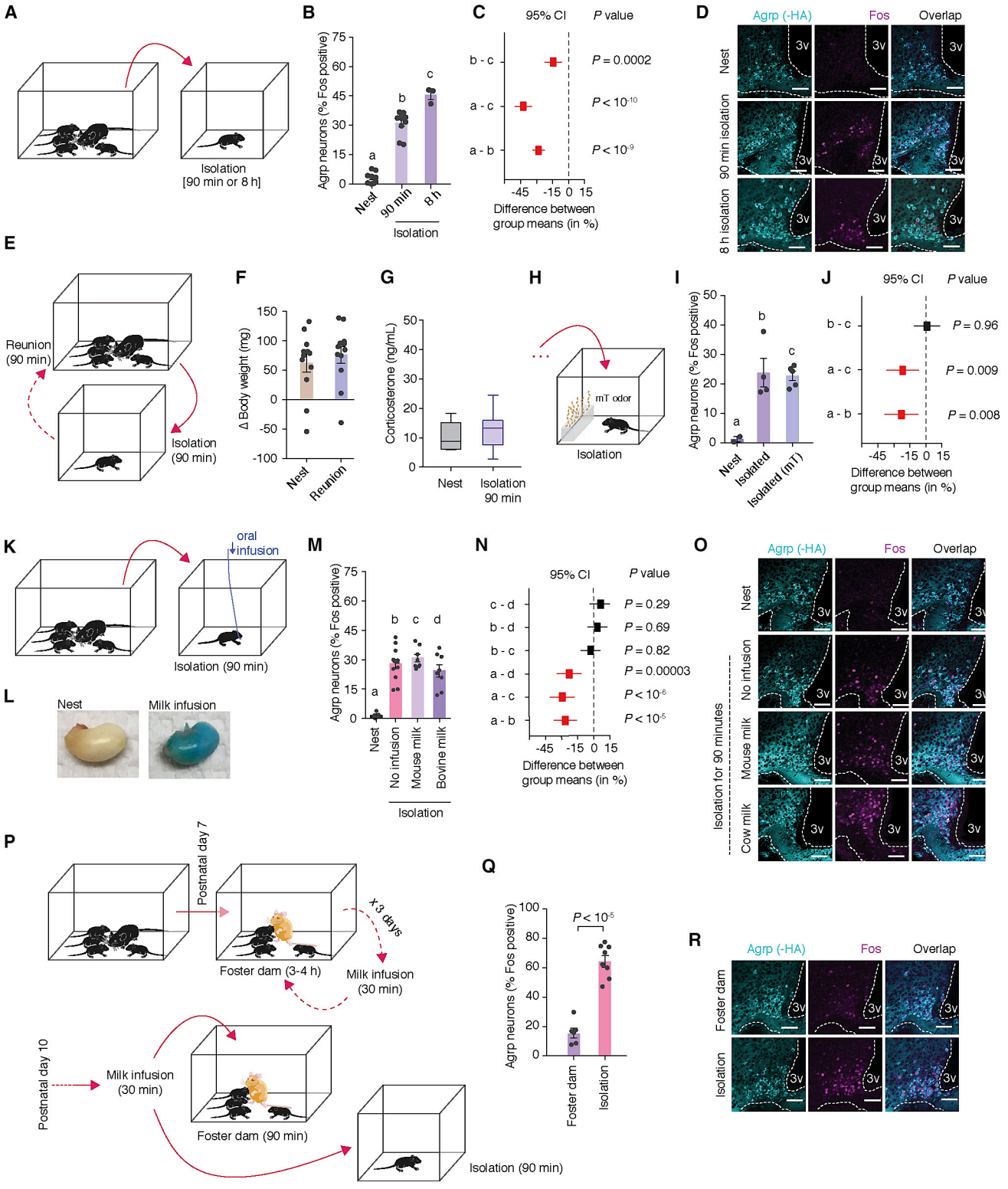

Figure 1. Fos Labels Agrp Neuron Activation in P10 Mice upon Social Isolation

(A) P10 mice were socially isolated for 90 min or 8 h.

(B) Agrp neurons positive for Fos immunoreactivity (nest, n = 9; isolation/90 min, n = 10; isolation/8 h, n = 3, one-way ANOVA, $p < 10^{-11}$).

(legend continued on next page)

n = 4; isolation and predator odor: 22.71 ± 1.59%, n = 5; $F_{2, 8}$ = 9.73, p = 0.007, one-way ANOVA; Figures 1H–1J).

To evaluate whether the activation of Agrp neurons upon isolation from nest is due to caloric deprivation, we isolated P10 mice while orally infusing bovine or mouse derived milk (Figure 1K). We confirmed milk ingestion by adding a colored dye to the milk to verify its presence in the stomach (Figure 1L). Surprisingly, our results showed no significant difference between the activation of Agrp neurons between the groups that received an oral infusion of milk and the control group that received a passive oral probe with no milk infusion (nest: 1.51 ± 0.65%, n = 5; isolation and no infusion: 27.88 ± 2.39%, n = 12; isolation and mouse milk: 30.73 ± 1.93%, n = 8; isolation and bovine milk: 24.24 ± 3.14%, n = 8; $F_{3, 29}$ = 19.38, p < 10^{-6}, one-way ANOVA; Figures 1M–1O).

Next, we tested the hypothesis that Agrp neuron activity in P10 mice increases upon separation in anticipation of future nutrient deprivation. To this end, we investigated the extent to which isolation from the nest activates Agrp neurons when dissociating milk intake and the nest. P7 mice were housed with a foster non-lactating dam and were manually fed milk by an investigator (Figure 1P). All neonates quickly developed locomotor activity toward the investigator at feeding onset, which suggests a learned association that the milk source was outside the home nest. We then assessed activation of Agrp neurons at P10 at either isolation or return to the home cage with the foster dam for a period of 90 min after all pups were previously fed with equal volumes of milk. Similar to our previous experiments, isolation from the home nest strongly increased the number of Fos positive Agrp neurons compared to mice that returned to the home cage (foster dam: 15.59 ± 3.26%, n = 6; isolation: 64.39 ± 3.94%, n = 8; t_{12} = 9.06, p < 10^{-5}, unpaired t test; Figures 1Q and 1R). Taken together, these results suggest that activation of Agrp neurons in P10 mice following isolation from the nest does not require milk deprivation or anticipation of milk deprivation, which stands in contrast to adult mice.

Non-nutritive Suckling and Thermal Support Blunt Agrp Neuron Activation in Neonates

Our next goal was to evaluate the relative importance of different components of the nest environment and mother-infant interaction that contribute to Agrp neuron activation in P10 mice after isolation from the nest. In the nursing nest, pups receive care from the dam. An important feature of maternal care is neonatal attachment to the mother's nipple and suckling. So, we investigated the extent to which suckling alters the activation of Agrp neurons. We fostered P10 mice with non-lactating dams, non-lactating dams with protruded nipples, and lactating dams (Figure 2A). In all cases, foster dams promptly retrieved the pups and placed them in the nest. All foster dams displayed maternal behaviors, such as grooming and licking and arched-back "nursing" of pups, as expected. Interestingly, all foster dams blunted the activation of Agrp neurons in P10 mice compared to isolated pups (nest: 2.10 ± 0.21%, n = 6; isolation: 26.47 ± 1.57%, n = 6; non-lactating foster dam: 16.59 ± 1.64%, n = 7; non-lactating foster dam with protruded nipples: 8.66 ± 1.26%, n = 6; lactating foster dam: 10.29 ± 0.65%, n = 4; $F_{4, 24}$ = 50.29, p < 10^{-10}, one-way ANOVA; Figures 2B and 2C). Attachment of pups to the foster dam's nipples further decreased the number of Fos-labeled Agrp neurons compared to pups placed with a foster dam with non-protruded nipples to prevent nipple attachment (Figures 2B and 2C). The effect of nipple attachment was irrespective of milk availability, as the expression of Fos in pups showed a similar magnitude when placed with lactating and non-lactating foster dams with protruded nipples (Figures 2B and 2C). Overall, activation of Agrp neurons in P10 mice is blunted by non-nutritive suckling, an important component of maternal care, and is not further reduced by availability of milk in the dam's nipples.

(C) Tukey-Kramer's multiple comparisons test of the difference between means (95% confidence intervals from B), representing effect sizes.
(D) Representative images of immunohistochemistry for HA (cyan, labels Agrp neurons in *Agrp*$^{Rpl22\text{-}HA}$ mice), Fos (magenta), and overlap. Scale bars represent 50 μm.
(E) Effect of isolation (90 min) on milk intake upon reunion with the dam and litter for an additional 90 min.
(F) Delta body weight as a measure of milk intake during 90 min in P10 mice (control, n = 12; reunion, n = 12, unpaired t test, p = 0.51).
(G) Plasma corticosterone levels in P10 mice after 90-min isolation (control, n = 7; reunion, n = 11, unpaired t test, p = 0.39). Boxplot represents median, 1st/3rd quartiles, and min and max values.
(H) Effect of exposure to predator odor (mT) during 90-min isolation in P10 mice.
(I) Quantification of Agrp neurons positive for Fos (nest, n = 2; isolation, n = 4; isolation/mT, n = 5, one-way ANOVA, p = 0.007).
(J) Tukey-Kramer's multiple comparisons test of the difference between means (95% confidence intervals from I), representing effect sizes.
(K) Effect of milk infusion (mouse or bovine) in the activation of Agrp neurons in isolated P10 mice.
(L) Infused milk was labeled with a blue dye to confirm ingestion. Post-mortem images of the stomach of P10 mice.
(M) Quantification of Agrp neurons positive for Fos (nest, n = 5; isolation with no infusion, n = 12; isolation with infusion of mouse milk, n = 8; isolation with infusion of cow milk, n = 8, one-way ANOVA, p < 10^{-6}).
(N) Tukey-Kramer's multiple comparisons test of the difference between means (95% confidence intervals from M), representing effect sizes.
(O) Representative images of immunohistochemistry for HA (cyan, labeling Agrp neurons in *Agrp*$^{Rpl22\text{-}HA}$ mice), Fos (magenta), and overlap. Scale bars represent 50 μm.
(P) Effect of artificial rearing mice on Fos upon isolation. P7 mice were fostered with a non-lactating dam, while hand-fed every 3–4 h for 3 days. At P10, all mice were hand-fed and separated in two groups: reunited with the foster dam or isolated for 90 min.
(Q) Quantification of Agrp neurons positive for Fos (foster dam, n = 6; isolation, n = 8, unpaired t test, p < 10^{-5}).
(R) Representative images of immunohistochemistry for HA (cyan, labeling Agrp neurons in *Agrp*$^{Rpl22\text{-}HA}$ mice), Fos (magenta), and overlap. Scale bars represent 50 μm.
In (B), (F), (I), (M), and (Q), bars indicate mean ± SEM. Circles represent individual values. In (C), (J) and (N), symbols represent mean ± SEM; red denotes statistically significant differences.

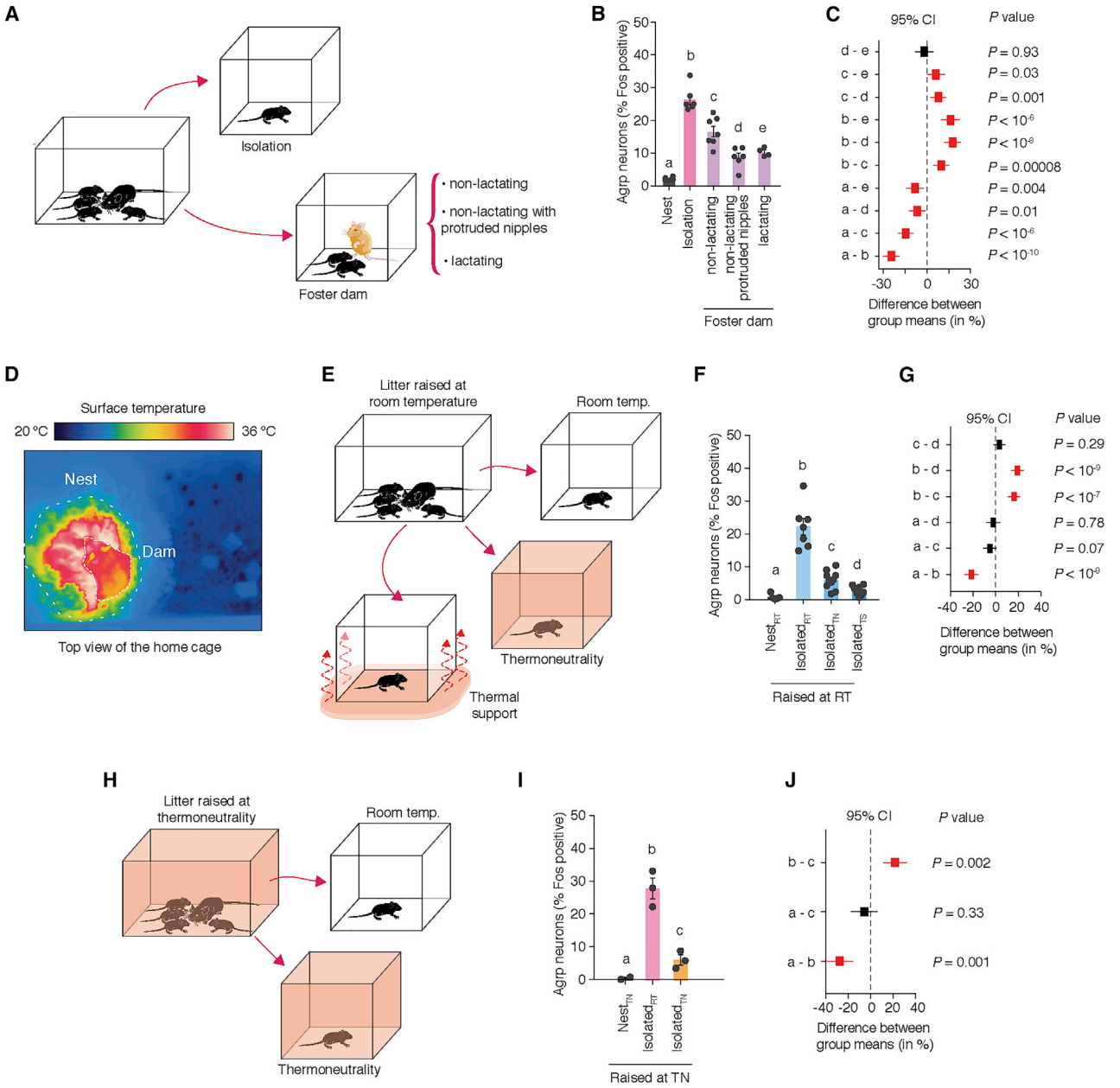

Figure 2. Warm Temperatures Blunt Activation of Agrp Neurons in P10 Mice

(A) Study design: P10 mice were either fostered with non-lactating dams, with non-lactating dams with protruded nipples, or with lactating dams for 90 min. A control group was not manipulated (nest) and a second group was isolated (isolation).

(B) Quantification of Agrp neurons positive for Fos (nest, n = 6; isolation, n = 6; non-lactating foster dam, n = 7; non-lactating foster dam with protruded nipples, n = 6; lactating foster dam, n = 4, one-way ANOVA, $p < 10^{-10}$).

(C) Tukey-Kramer's multiple comparisons test of the difference between means (95% confidence intervals from B), representing effect sizes.

(D) Thermo-photography of the nursing nest. Lactating dam is on the top of P10 offspring. Nest temperature is approximately 34°C–36°C.

(E) Offspring raised at room temperature (RT) were isolated either at room temperature, at thermoneutrality (TN, in a climate chamber set to 35°C) or at room temperature with a thermal support (TS) irradiating heat from underneath the cage (≈35°C).

(F) Quantification of Agrp neurons positive for Fos (nest and room temperature, n = 5; isolation and room temperature, n = 7; isolation and thermoneutrality, n = 10; isolation and thermal support, n = 8, one-way ANOVA, $p = 10^{-10}$).

(G) Tukey-Kramer's multiple comparisons test of the difference between means (95% confidence intervals from F) representing effect sizes.

(H) Offspring raised at thermoneutrality (climate chamber at 35°C) were isolated for 90 min at room temperature or thermoneutrality.

(legend continued on next page)

The nursing nest provides critical thermal insulation, which reduces heat loss from neonates that have not fully developed homeostatic mechanisms for thermoregulation. Dams contribute to thermal insulation by building a nest and skin-to-skin contact with pups (Figure 2D). To test the effects of thermal insulation on the activation of Agrp neurons, we isolated P10 mice at room temperature or at a thermoneutral temperature (≈35°C; Figure 2E). Because temperature exchanges in the nest occur by skin-to-skin contact, we included an additional control group, in which we provided thermal support by irradiating heat (≈35°C) from underneath (Figure 2E). 90 min of isolation at thermoneutrality or with thermal support strongly suppressed activation of Agrp neurons in P10 mice as assayed by Fos labeling compared with pups isolated at room temperature (nest: 0.77 ± 0.39%, n = 5; isolation and room temperature: 22.19 ± 2.53%, n = 7; isolation and thermoneutrality: 5.90 ± 0.86%, n = 10; isolation and thermal support: 2.75 ± 0.51%, n = 8; $F_{3, 26}$ = 47.31, p = 10^{-10}, one-way ANOVA; Figures 2F and 2G). Thus, Agrp neurons in P10 mice respond to the withdrawal of thermal insulation when isolated from the nursing nest. This factor holds primary importance for the responses of these neurons to isolation.

Next, we tested the extent to which the response of Agrp neurons in P10 mice to the withdrawal of thermal insulation was dependent on prior experience with drops in ambient temperature. To prevent mice from experiencing ambient temperatures lower than nest temperatures, we repeated the experiments in animals born and raised in a thermoneutral environment (Figure 2H). P10 mice raised at thermoneutrality showed increased Fos-labeled Agrp neurons when isolated at room temperature but not at thermoneutrality (nest and thermoneutrality: 0.62 ± 0.33%, n = 2; isolation and room temperature: 27.94 ± 3.13%, n = 3; isolation and thermoneutrality: 6.16 ± 1.54%, n = 3; $F_{2, 5}$ = 37.91, p = 0.001, one-way ANOVA; Figures 2I and 2J). Thus, the response of Agrp neurons to withdrawal of thermal insulation in P10 mice does not require previous experiences with drops in ambient temperature.

Neonatal Agrp Neurons Undergo Rapid Activity Changes

In the previous experiments, we could not elucidate the temporal dynamics of physiological activation of Agrp neurons. For example, Agrp neurons after isolation (Figure 3A) could slowly increase their activity similar to a homeostat (Figure 3B). Alternatively, these neurons could rapidly respond to isolation (Figure 3C) similar to an alarm and reflexive system. A third alternative suggests that Agrp neurons could show delayed activation (Figure 3D), suggesting a thresholding mechanism triggers these neurons in neonates.

To better understand the natural activity dynamics of Agrp neurons early in postnatal development, we injected an adeno-associated virus encoding jGCaMP7s in a *Cre*-dependent manner in newborn *Agrp*$^{Cre/Cre}$ mice (Figures 3E–G) (Dana et al., 2018). We then used fiber photometry to measure calcium transients originating from Agrp neurons upon isolation-reunion in P13–14 pups (Figure 3A). We found that pup isolation from the nest increased activity of Agrp neurons that occurred within seconds (Figures 3H and 3I) and persisted throughout the isolation period (10 min). After this initial separation, reunion of the isolated animal with the litter immediately decreased the activity of Agrp neurons (Figures 3H and 3I). The suppression of Agrp neuronal activity was robust and rapid, normalizing the detected signal to pre-isolation levels in less than 30 s (Figures 3H and 3I). All animals tested showed this response to isolation-reunion, suggesting a general model in which Agrp neurons in neonates rapidly respond to disruptions in the nest conditions (Figure 3C).

Neonatal Agrp Neurons Modulate the Emission of Ultrasonic Vocalizations

In most neonatal mammals, including mice, disruptions in the nest condition lead to infant vocalization (Hofer, 1994). In mice and rats, neonates emit ultrasonic vocalizations (USVs) when separated from the dam (Noirot, 1966, 1968; Zippelius and Schleidt, 1956) (Figures 4A and 4B). We investigated whether activation of Agrp neurons in neonates upon isolation from the nest could modulate emission of USVs.

First, we confirmed that isolation from the nest induced vocal behavior in P10 mice (Figure 4A). We then investigated whether isolation at thermoneutrality would influence USVs, since these conditions blunt activation of Agrp neurons upon isolation (Figure 2). Analysis of vocal behavior showed a rapid increase in USV emission upon isolation from the nest (Figures 4B–4E), an effect that blunted at thermoneutrality (nest, n = 3; isolated and room temperature, n = 16; isolated and thermoneutrality, n = 4; $F_{2,20}$ = 18.08, p < 10^{-4}, one-way ANOVA; Figures 4C–4E). Thus, vocal behavior dynamics in neonatal mice follow the dynamics of Agrp neuron activation upon isolation in these experimental conditions.

To test the extent to which Agrp neurons contribute to vocal behavior of P10 mice upon isolation, we tested animals lacking the transmitters released by Agrp neurons (NPY and GABA) (Hahn et al., 1998; Horvath et al., 1997). We recorded the emission of USVs in *Npy*^{KO} and *Agrp*$^{Vgat\text{-}KO}$ mice and their littermate controls following 10 minutes isolation in P10 mice. Animals lacking NPY exhibited a similar number of USVs after isolation compared to controls (control: 343.4 ± 56.8 USVs, n = 12; *Npy*$^{KO/+}$: 384.5 ± 69.3 USVs, n = 17; *Npy*$^{KO/KO}$: 348.0 ± 91.7 USVs, n = 7; p = 0.74, Kruskal-Wallis [KW] test; Figure 4F). In contrast, *Agrp*$^{Vgat\text{-}KO}$ mice had a significant decrease in emission of USVs upon isolation (control: 321.0 ± 50.4 USVs, n = 10; *Agrp*$^{Vgat\text{-}KO}$: 57.7 ± 14.6 USVs, n = 14; *U* = 2, p < 10^{-5}, Mann-Whitney test; Figures 4G and 4H).

We further analyzed the spectro-temporal characteristics of 3,427 USVs from control mice and 786 USVs from *Agrp*$^{Vgat\text{-}KO}$ mice. We characterized individual USVs by changes in

(I) Quantification of Agrp neurons positive for Fos (nest and thermoneutrality, n = 2; isolation and room temperature, n = 3; isolation and thermoneutrality, n = 3, one-way ANOVA, p = 0.001).

(J) Tukey-Kramer's multiple comparisons test of the difference between means (95% confidence intervals from I), representing effect sizes.

In (B), (F), and (I), bars represent mean ± SEM; round symbols represent individual values. In (C), (G), and (J), symbols represent mean ± SEM; red denotes statistically significant differences.

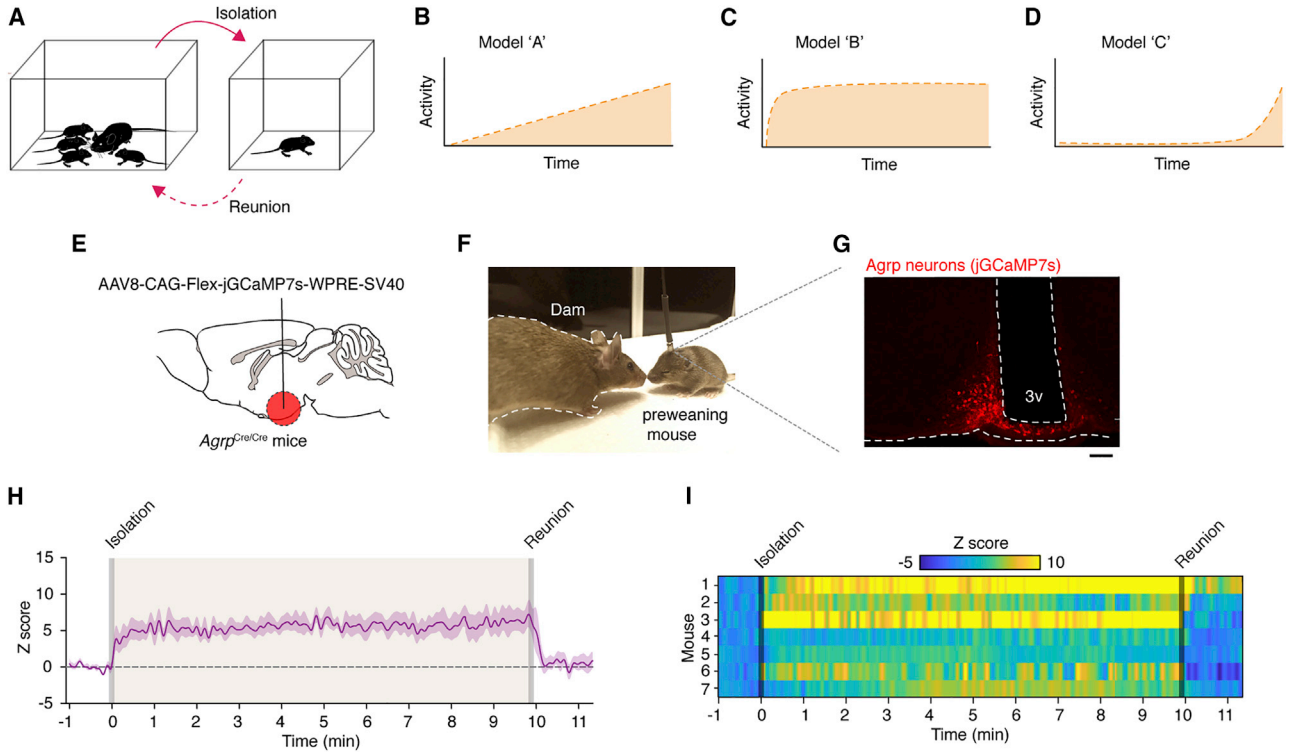

Figure 3. Rapid Dynamics of Agrp Neuronal Activity in Mice during Early Development

(A) Experimental model of isolation and reunion in neonates, which activates Agrp neurons after 90 min. Three theoretical models of activity changes of these neurons are illustrated in (B)–(D).

(B) Model A: activity of Agrp neurons gradually increases during the 90-min isolation.

(C) Model B: activity of Agrp neurons rapidly increases upon isolation.

(D) Model C: activity of Agrp neurons increases in isolation after a delay.

(E) In newborn *Agrp*$^{Cre/Cre}$ mice, an adeno-associated virus was injected in the arcuate nucleus of the hypothalamus to express jGCaMP7s in Agrp neurons (AAV-CAG-Flex-jGCaMP7s).

(F) Preweaning mouse connected to an optic fiber and its dam.

(G) Expression of jGCaMP7s in Agrp neurons of a P14 mouse.

(H) *Z* score of Agrp neuronal activity in P13–14 mice. Baseline was recorded for 1 min and then pups were isolated for 10 min. Subsequently, pups were reunited with the litter. Plot represents mean ± SEM (n = 7 animals).

(I) Heat plot representing individual responses to isolation and reunion.

spectro-temporal characteristics, such as duration, frequency, and bandwidth. Compared to control mice, USVs from *Agrp*$^{Vgat\text{-}KO}$ mice decreased in duration of 9.5 ms (control: 37.84 ± 0.45 ms; *Agrp*$^{Vgat\text{-}KO}$: 28.31 ± 0.84 ms; $D = 0.176$, $p = 10^{-15}$, Kolmogorov-Smirnov [KS] test; Figure 4I), in mean frequency of 1.9 kHz (control: 82.20 ± 0.28 kHz; *Agrp*$^{Vgat\text{-}KO}$: 80.24 ± 0.55 kHz; $D = 0.10$, $p = 10^{-15}$, KS test; Figure 4J), and in bandwidth of 5.6 kHz (control: 22.86 ± 0.35 kHz; *Agrp*$^{Vgat\text{-}KO}$: 17.20 ± 0.67 kHz; $D = 0.17$, $p = 10^{-15}$, KS test; Figure 4K). We also found an overall decrease in the number of vocalizations across most USV categories (Figures 4L–4X) (Grimsley et al., 2011). However, we observed an increase in the incidence of "short" vocalizations, when analyzing the relative frequency of USV categories (Figure 4Y). This syllable represents the simplest form of vocalization by neonatal mice based on spectro-temporal characteristics (Figures 4L–4V). Thus, lacking GABA release from Agrp neurons, P10 *Agrp*$^{Vgat\text{-}KO}$ mice led to fewer and simpler USVs compared to control animals. Taken together, these findings indicate Agrp neurons are critically positioned to modulate the emission of USVs in neonatal mice.

Chemogenetic Activation of Agrp Neurons Increases USV Emission

We further tested whether chemogenetic activation of Agrp neurons could modulate emission of USV in isolated P10 pups using *Agrp*^{Trpv1} mice (Dietrich et al., 2015; Ruan et al., 2014; Arenkiel et al., 2008; Güler et al., 2012) (Figure 5A; Figure S1). Subcutaneous injection of capsaicin (10 mg/kg) in *Agrp*^{Trpv1} mice robustly activated Agrp neurons in young pups (Figure 5B; n = 5 mice per group; $U = 0$, $p = 0.004$, Mann-Whitney test). Chemogenetic activation of Agrp neurons using the *Agrp*^{Trpv1} animal model induced a 61% increase in USV emission in P10 mice (control: 686.7 ± 50.22 USVs, n = 32; *Agrp*^{Trpv1}: 1040.0 ± 66.56 USVs, n = 24; $t_{51} = 4.318$, $p < 0.0001$; 2-tailed unpaired *t* test; Figures 5C–5E).

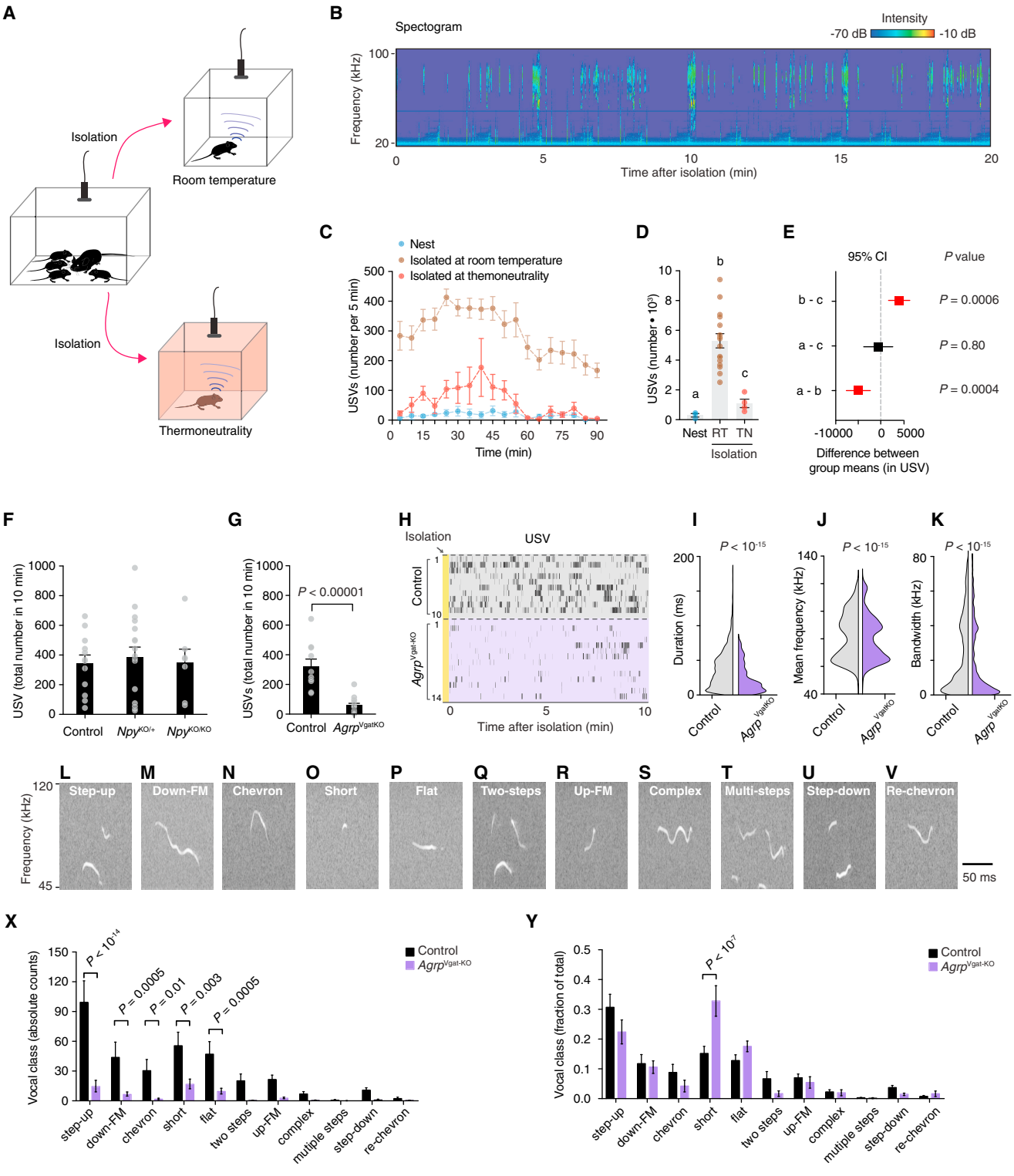

Figure 4. Agrp Neurons in P10 Mice Modulate Emission of Ultrasonic Vocalizations via GABA Release

(A) Experimental model of isolation in P10 mice at room temperature (RT) or at thermoneutral conditions (thermoneutrality; climate chamber set at 35°C).

(B) Representative spectrogram of ultrasonic vocalizations (USVs) in P10 mice recorded in isolation.

(C) Number of USVs in five-minute bins during isolation at room temperature or thermoneutrality and control group recorded in the nest.

(legend continued on next page)

We also analyzed the spectro-temporal characteristics of a total of 21,019 USVs from control mice and 24,976 vocalizations from *Agrp*^{Trpv1} mice. Upon activation of Agrp neurons, the USV duration decreased by 4 ms (control: 51.42 ± 0.23 ms; *Agrp*^{Trpv1}: 47.09 ± 0.19 ms; $D = 0.077$, $p = 10^{-15}$, KS test; Figure 5F), the mean frequency increased by 3 kHz (control: 77.50 ± 0.08 kHz; *Agrp*^{Trpv1}: 80.96 ± 0.07 kHz; $D = 0.12$, $p = 10^{-15}$, KS test; Figure 5G), and the bandwidth increased by 2 kHz (control: 27.31 ± 0.13 kHz; *Agrp*^{Trpv1}: 29.84 ± 0.12 kHz; $D = 0.07$, $p = 10^{-15}$, KS test; Figure 5H). The selected categories of USVs induced by activation of Agrp neurons (Figure 5I) showed a higher complexity compared to those suppressed in *Agrp*$^{Vgat\text{-}KO}$ mice (Figure 4).

Interestingly, when we analyzed the relative frequency of USV categories, we found a selective increase in the frequency of "chevrons" upon chemogenetic activation of Agrp neurons (Figures 5J and 4N). To further corroborate these findings, we used a second software tool MUPET to classify vocalizations based on their shape (Van Segbroeck et al., 2017). We found six clusters of vocalizations that showed a more than 2.5-fold increase upon activation of Agrp neurons (Figures 5K and 5L). These clusters were very similar to each other, resembling our previous analysis (Figures 4G and 4H). We also found that activation of Agrp neurons suppressed vocalizations in cluster 39 (Figures 5K and 5M). The USVs in cluster 39 were simpler in shape, resembling vocalizations predominantly emitted by *Agrp*$^{Vgat\text{-}KO}$ pups (Figure 4). In contrast to mice lacking GABA release by Agrp neurons, chemogenetic activation of these neurons stimulated USV emission at a higher rate and with higher complexity. Together, these results strongly suggest a model in which neonatal Agrp neurons are rapidly activated upon isolation from the nest, which modulates USV emission, presumably to attract the dam.

Chemogenetic Activation of Agrp Neurons in Neonatal Mice Modulates the Behavior of Dams

Neonatal behavior is linked to maternal behavior, as the former can enhance and entrain the behavior of the latter. Based on our previous results, we expected that chemogenetic activation of Agrp neurons in the neonate would change the response of the dam toward the neonate. We devised a test to assess maternal responsiveness to P10 mice, the "maternal preference test" (Figure 5N). In this test, maternal responsiveness was measured as the time of dam-pup interaction. We found maternal exploratory behavior was strongly skewed toward *Agrp*^{Trpv1} pups compared to controls (preference index - control: 44.96 ± 13.68 s, n = 25; *Agrp*^{Trpv1}: 125.1 ± 21.74 s, n = 25; $t_{24} = 2.69$; p = 0.01, 2-tailed paired *t* test; Figures 5O and 5P). These results support the model in which neonatal Agrp neurons modulate vocal behaviors signaling the dam should return to the nest.

Chemogenetic Activation of Neonatal Agrp Neurons Increases Odds for Nipple Attachment

In young pups, contact with the dam is critical for suckling behavior and ingestion of breast milk. Thus, we next devised behavior experiments to test whether activation of Agrp neurons in pups would drive behaviors toward the dam, including exploratory activity, suckling, and milk intake. We eliminated active participation by the dam as the driver of these behaviors by examining the behavior of P10 mice toward anesthetized dams (Figure 6A). In anesthetized dams, milk ejection decreases considerably (Lincoln et al., 1973), so suckling under these conditions is considered non-nutritive. Indeed, we did not observe the stretching reflex in pups that suckled during our experiments, which is a pathognomonic sign of milk ejection and ingestion (Vorherr et al., 1967).

Activation of Agrp neurons in P10 mice increased the total number of pups that attached to the dam's nipples (control: 9 out of 22; *Agrp*^{Trpv1}: 13 out of 15; p = 0.005, chi-square test; Figure 6B) and increased the distance traveled in the testing chamber (control: 0.75 ± 0.14 m, n = 22; *Agrp*^{Trpv1}: 1.20 ± 0.21 m, n = 15; $U = 94$, p = 0.027, Mann-Whitney test; Figures 6C and 6D). We then compared nipple attachment behavior of P10 mice, excluding animals that did not attach to the dam's nipples from post hoc analysis. Chemogenetic activation of Agrp neurons did not change the frequency (control: 3.11 ± 1.23; *Agrp*^{Trpv1}: 3.61 ± 0.83; $U = 51$, p = 0.63, Mann-Whitney test; Figure 6E), latency (control: 279.9 ± 57.4 s; *Agrp*^{Trpv1}: 485.4 ± 86.2 s; $U = 35$, p = 0.12, Mann-Whitney test; Figure 6F), or the duration of nipple attachment (control: 719.4 ± 128.0 s; *Agrp*^{Trpv1}: 529.8 ± 99.86 s; $U = 39$, p = 0.20, Mann-Whitney test; Figure 6G). Thus, while chemogenetic activation of Agrp neurons in P10 mice increased the probability of attaching to the dam's nipples, it did not change the observable microstructure of nipple attachment behavior.

(D) Total number of USVs during recording from (C) (nest, n = 3; isolation and room temperature, n = 16, isolation and thermoneutrality, n = 4; one-way ANOVA, $p < 10^{-4}$).
(E) Tukey-Kramer's multiple comparisons test of the difference between means (95% confidence intervals from D), representing effect sizes.
(F) The total number of vocalizations upon isolation (10 min) in *Npy*$^{+/+}$ (n = 12), *Npy*$^{KO/+}$ (n = 17), and *Npy*$^{KO/KO}$ (n = 7) P10 mice; Kruskall-Wallis test, p = 0.74.
(G) Similar to (F) but using P10 mice knockout for *Vgat* specifically in Agrp neurons (*Agrp*$^{Vgat\text{-}KO}$) and their littermate controls (control, n = 10; *Agrp*$^{Vgat\text{-}KO}$, n = 14; Mann-Whitney test, $p < 10^{-5}$).
(H) Raster plots; ticks represent USVs. Each row represents an animal.
(I–K) Violin plots representing the distribution of USV characteristics in control (n = 3,427 USVs) and *Agrp*$^{Vgat\text{-}KO}$ mice (n = 786 USVs) in (I) duration, (J) mean frequency of the main component, and (K) the bandwidth; p values calculated using the Kolmogorov-Smirnov test.
(L–V) Types of USVs labeled in this study. Each panel represents the spectrogram of one type of vocal call as followed: (L) Step-up, (M) Down-frequency modulation, (N) Chevron, (O) Short, (P) Flat, (Q) Two-steps, (R) Up-frequency modulation, (S) Complex, (T) Multi-steps, (U) Step-down and (V) Reverse chevron.
(X) Distribution of absolute counts of each vocal call type.
(Y) Similar to (X) but vocal types normalized to total counts. In (X) and (Y), multiple t tests with p values corrected for multiple comparisons using the Holm-Sidak method.
In (C), symbols represent mean ± SEM. In (D), (F), (G), (X), and (Y), bars represent mean ± SEM. In (E), symbols represent mean ± 95% CI. In (I)–(K), data distribution is plotted. In (D), (F), and (G), symbols represent individual data. Statistically significant p values are displayed in the panels.

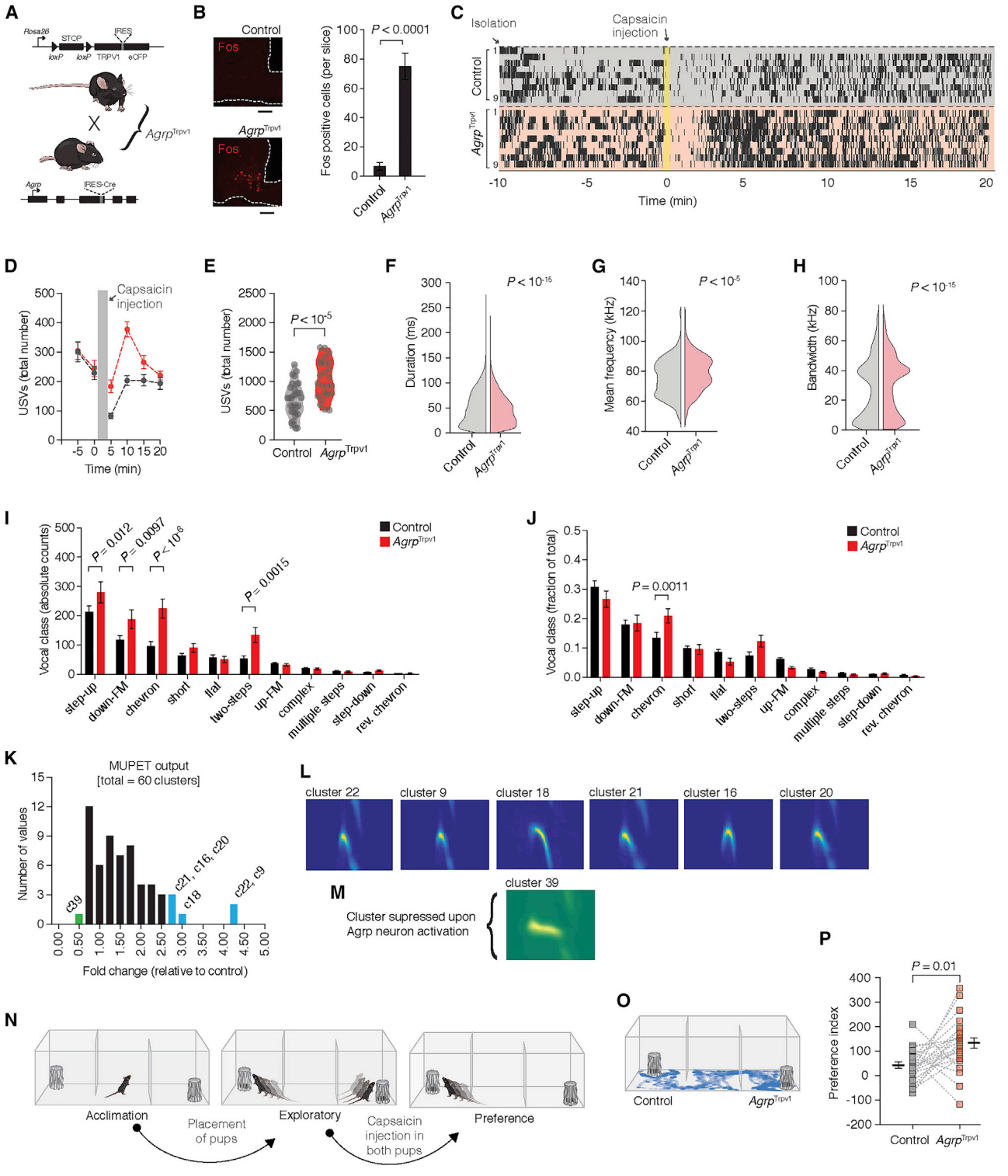

Figure 5. Activation of Agrp Neurons in P10 Mice Increases USV Emission and Alters the Dam's Behavior

(A) Generation of *Agrp*^{Trpv1} mice.

(B) Fos in the arcuate nucleus of P15 *Agrp*^{Trpv1} mice upon injection of capsaicin (10 mg/kg, s.c.; n = 5 mice per group). Scale bar corresponds to 50 μm. Bars and symbols represent mean ± SEM.

(C) Raster plots show USV in isolated P10 controls (n = 32) and *Agrp*^{Trpv1} mice (n = 24). A tick represents a USV.

(D) Related to (C), number of USVs (in 5-min bins).

(legend continued on next page)

Next, we investigated the influence of the environmental temperature on nipple attachment behavior (Figure 6H). Thermal support from underneath the testing chamber completely suppressed nipple attachment behavior in P10 control mice (0 out of 11 pups tested attached), while 4 out of 10 pups with activated Agrp neurons attached to the dam's nipples ($p = 0.019$, chi-square test; Figure 6I). Interestingly, the arousal response of P10 mice upon activation of Agrp neurons was intact, as measured by the distance traveled during the test (control: 0.30 ± 0.07 m, n = 11; *Agrp*^{Trpv1}: 1.03 ± 0.19 m, n = 10; $U = 13$, $p = 0.002$, Mann-Whitney test; Figures 6J and 6K). When we analyzed the different components of nipple attachment behavior of the four P10 mice that successfully attached, we found the frequency of attachments was largely suppressed with mice only attaching once during the test (Figure 6L). The latency to attach (386.5 ± 49.62 s; Figure 6M) was similar to the other experimental conditions (Figures 6F and 6S). The duration animals remained attached to the nipples (787.9 ± 48.20 s; Figure 6N) was within the range of our other experiments (Figures 6G and 6T). We conclude providing warmth did not blunt the arousal response after activating Agrp neurons but did suppress nipple attachment behavior of P10 mice. Taken together, our behavioral experiments further support the importance of a thermal stimulus in neonates to modulate the functional properties of Agrp neurons.

We then assessed whether a lactating anaesthetized dam would alter attachment by P10 mice. Oxytocin triggers the milk ejection reflex following nipple stimulation by the pups during suckling (Lincoln and Paisley, 1982). To facilitate milk ejection, we injected a group of anesthetized dams with oxytocin immediately before testing each pup (Figure 6O) (Singh and Hofer, 1978; Vorherr et al., 1967). Similar to non-lactating dams, activation of Agrp neurons in P10 mice increased the number of mice that attached to the dam's nipples (control: 8 out of 18; *Agrp*^{Trpv1}: 13 out of 15; $p = 0.012$, chi-square test; Figure 6P). The total distance traveled during the test was not different between groups (control: 0.87 ± 0.22 m, n = 18; *Agrp*^{Trpv1}: 1.13 ± 0.28 m, n = 15; $U = 100.5$, $p = 0.21$, Mann-Whitney test; Figure 6Q). When comparing the behavior of animals that attached to the dam's nipples, we did not find statistical differences in the frequency (control: 5.25 ± 0.99, n = 8; *Agrp*^{Trpv1}: 8.38 ± 1.52, n = 13; $U = 34$, $p = 0.20$, Mann-Whitney test; Figure 6R) or duration of attachments (control: 515.7 ± 78.68 s, n = 8; *Agrp*^{Trpv1}: 502.6 ± 91.98 s, n = 13; $U = 50$, $p = 0.91$, Mann-Whitney test; Figure 6T), but we found a decrease in the latency of attachment (control: 501.9 ± 68.91 s, n = 8; *Agrp*^{Trpv1}: 335.2 ± 55.52 s, n = 13; $U = 21$, $p = 0.02$, Mann-Whitney test; Figure 6S). Since dams were lactating, we also measured body-weight changes in the pups as a measure of milk intake. Interestingly, upon activation of Agrp neurons, P10 mice ingested a lower amount of milk than controls during the test (control: 91.2 ± 19.9 mg; *Agrp*^{Trpv1}: 43.7 ± 10.0 mg; pups that did not attach: −10.0 ± 2.9 mg, n = 12; $F_{2,30} = 19.35$, $p < 10^{-5}$, one-way ANOVA; Figures 6U and 6V). These results suggest that activated Agrp neurons increase dam-seeking behavior but not necessarily increase ingestion of milk.

Chemogenetic Activation of Agrp Neurons Increases Ingestive Behaviors in P15 Mice

Mice rapidly transition from breastfeeding to independent feeding during weaning period. At approximately P15, mice begin experimenting with food sources but still rely on breastfeeding for nutrition (Hammond et al., 1996). We next examined the behavior of P15 mice toward the dam to investigate the ontogeny of Agrp neuron function. All tested P15 mice attached to the nipples of the anesthetized dam regardless of chemogenetic activation of Agrp neurons (n = 19 mice per group; Figure 7A). Activating Agrp neurons did not significantly change the distance traveled in the testing chamber (control: 2.03 ± 0.34 m; *Agrp*^{Trpv1}: 2.20 ± 0.22 m; $U = 145$, $p = 0.31$, Mann-Whitney test; Figure 7B). In contrast to P10 mice, chemogenetic activation of Agrp neurons in P15 mice showed a striking increase in the number of attachments to the dam's nipples compared to control (control: 3.68 ± 1.02; *Agrp*^{Trpv1}: 11.74 ± 1.80; $U = 72.5$, $p = 0.001$; Mann-Whitney test; Figures 7C and 7D). We observed no statistical difference in the latency of the first attachment (control: 226.6 ± 50.8 s; *Agrp*^{Trpv1}: 123.0 ± 16.92 s; $U = 116$, $p = 0.06$; Mann-Whitney test; Figure 7E) or the total duration of nipple attachment (control: 711.6 ± 85.2 s; *Agrp*^{Trpv1}: 798.9 ± 79.02 s; $U = 143$, $p = 0.28$; Mann-Whitney test; Figure 7F).

Since P15 mice displayed numerous nipple attachments (Figure 7D), we could track and quantify the number of nipples

(E) Related to (C) and (D), total number of USVs in the 20 min after activating Agrp neurons in isolated pups (control, n = 32; *Agrp*^{Trpv1}, n = 24; p value calculated using a 2-tailed unpaired *t* test).

(F–H) Violin plots representing the distribution of USV characteristics in control (n = 22,168 USVs) and *Agrp*^{Trpv1} mice (n = 24,971 USVs) in (F) duration, (G) mean frequency of the main component of the USV, and (H) the bandwidth; p values calculated using the Kolmogorov-Smirnov test.

(I) Distribution of absolute counts of each vocal call type.

(J) Similar to (I), but vocal types normalized to total counts. In (I) and (J), multiple *t* tests with p values corrected for multiple comparisons using the Holm-Sidak method.

(K) Distribution of the fold change (number of USVs from *Agrp*^{Trpv1} mice related to number of USVs from control mice) in each of the 60 output clusters analyzed by MUPET (see STAR Methods). Shown in blue are 6 clusters highly enriched in USVs from *Agrp*^{Trpv1} mice. Shown in green is 1 cluster enriched in USVs from controls.

(L) Related to (K), images represent the 6 clusters enriched in USVs from *Agrp*^{Trpv1} mice.

(M) Related to (K), image represents the cluster enriched in USVs from control mice.

(N) Maternal preference test (MPT).

(O) Representative tracking (in blue) of a dam in the preference stage.

(P) Preference index (in seconds) during MPT (n = 25 pairs; p value calculated using a 2-tailed paired *t* test).

In (D), symbols represent mean ± SEM. In (B), (I), and (J), bars represent mean ± SEM. In (F)–(H), data distribution is plotted. In (E) and (P), symbols represent individual data. In (P), black lines indicate mean ± SEM. See also Figure S1.

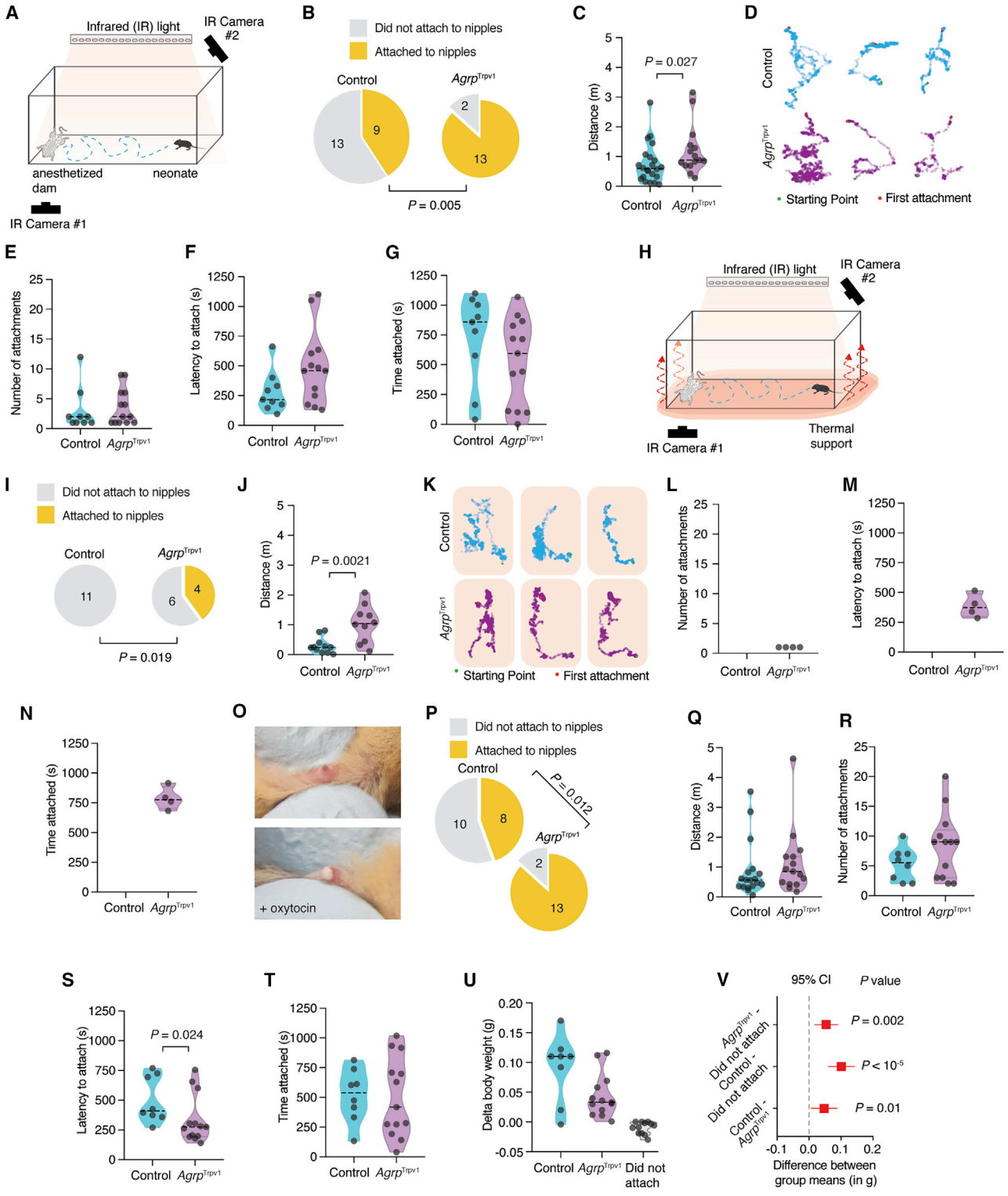

Figure 6. Agrp Neuron Activation and Suckling Behavior in P10 Mice

(A) Chamber to assay suckling behavior in mice.

(B–G) Quantification of suckling behavior in P10 mice tested with an anesthetized, non-lactating dam. In (B), proportion of mice displaying nipple attachment. In (C), total distance traveled. In (D), tracking of locomotor activity (bottom: starting point; top: anesthetized dam). In (E)–(G), data only considering mice that attached to nipples. In (E), number of nipple attachments. In (F), latency to the first attachment. In (G), total time attached to nipples.

(legend continued on next page)

explored to measure nipple-shifting behavior (Figure 7G) (Cramer et al., 1980). Chemogenetic activation of Agrp neurons in P15 mice increased the total number of different nipples explored during the test (control: 2.68 ± 0.57 nipples; $Agrp^{Trpv1}$: 5.21 ± 0.62 nipples; U = 92.5, p = 0.007; Mann-Whitney test; Figure 7H). In these experiments, mice did not show a nipple preference (n = 38 mice; p = 0.42, one-way ANOVA; Figures 7I and 7J), which is a phenomenon observed in other species (Erwin et al., 1975; Hudson et al., 2009; Tomaszycki et al., 1998).

We repeated the above experiments using anesthetized dams injected with oxytocin during a 10-min test. In control mice, 50% of P15 mice attached to the dam's nipples (4 out of 8 mice), while 91% of $Agrp^{Trpv1}$ mice displayed the same behavior (11 out of 12 mice; p = 0.035, chi-square test; Figure 7K). Activating Agrp neurons did not significantly change the distance traveled in the testing chamber (control: 1.13 ± 0.26 m; $Agrp^{Trpv1}$: 1.56 ± 0.21 m; U = 31, p = 0.20, Mann-Whitney test; Figure 7L) but strongly increased the number of nipple attachments (control: 2.00 ± 0.70; $Agrp^{Trpv1}$: 9.90 ± 1.82; U = 2.5, p = 0.007, Mann-Whitney test; Figure 7M). The latency to the first nipple attachment (control: 162.0 ± 33.1 s; $Agrp^{Trpv1}$: 119.9 ± 27.1 s; U = 14, p = 0.34, Mann-Whitney test; Figure 7N) and the total duration of nipple attachment (control: 332.2 ± 11.9 s; $Agrp^{Trpv1}$: 388.0 ± 34.7 s; U = 20, p = 0.85, Mann-Whitney test; Figure 7O) were not changed upon chemogenetic activation of Agrp neurons. In contrast to P10 mice, chemogenetic activation of Agrp neurons in P15 mice did significantly increase milk intake in mice that attached to the nipples of lactating dams (control: 17.2 ± 26.1 mg; $Agrp^{Trpv1}$: 109.5 ± 38.7 mg; U = 7, p = 0.02, Mann-Whitney test; Figure 7P).

We also tested the extent to which activation of Agrp neurons induces ingestion of solid food during the weaning period. We did not observe changes in food intake in P15 mice, but we observed increased food intake in P18 and P21 mice upon chemogenetic activation of Agrp neurons (Figure 7Q). Similarly, we only found changes in body weight during the feeding test in P21 mice (Figure 7R). Together, this set of behavioral experiments suggest that Agrp neurons in P10 mice are not proximally involved in milk intake or signaling milk ingestion. We propose that these functional properties of Agrp neurons rapidly change (or appear) as mice approach weaning age.

DISCUSSION

Overall, our results reveal functional properties of Agrp neurons in neonatal mice. These insights demonstrate developmental differences that emerge during ontogeny, so studying any complex system may remain incomplete without assessing its developmental properties (Tinbergen, 1963).

Our experiments unexpectedly revealed that Agrp neurons are functional during the first 2 postnatal weeks in mice despite their immature characteristics (Nilsson et al., 2005; Padilla et al., 2010). We showed that Agrp neurons in P10 mice did not respond to milk intake and their activation did not directly increase milk intake. Conversely, non-nutritive suckling and thermal insulation were key factors modulating the activity of Agrp neurons. These results are compatible with the physiology of breastfeeding in neonatal mammals. During breastfeeding, mice, like most other mammals, do not receive continuous milk ejection. Milk ejection remains under control of a neuroendocrine reflex (Cross and Harris, 1952) and occurs at random intervals, as demonstrated in rats (Lincoln et al., 1973). In spite of milk ejection patterns, neonatal rats stay attached to the dam's nipple for at least 12 h a day in the first days of life (Lincoln et al., 1973). In fact, homeostatic sensing of milk deprivation to modulate nutritive suckling behavior only develops later as shown in laboratory rodents (Ellis et al., 1984; Hall and Rosenblatt, 1978; Kenny et al., 1979). Thus, these studies strongly imply that nipple attachment serves as a stimulus for more than milk ejection. In fact, neonatal rodents develop filial huddling to dams triggered by thermotactile stimulation rather than provision of milk (Alberts, 2007; Alberts and May, 1984). Similar to rodents, neonatal monkeys prefer a cloth mother that provides thermal and tactile stimuli to a wired mother with a nursing bottle (Harlow, 1958), establishing that maternal comfort has a superior importance compared to milk intake in driving neonatal affectional responses. We posit that Agrp neurons of neonates drive this milk-independent encoding of the offspring-to-caregiver bond.

In our studies, thermal insulation was the primary factor modulating the activation of Agrp neurons in neonates following isolation from the nest. Notably, experiencing previous thermal challenges was not significant to activate neonatal Agrp neurons following isolation from the nest, which suggests an ''innate'' property of Agrp neurons. Intriguingly, foster dams also provide thermal insulation for the neonates, but they do not suppress activation of Agrp neurons after isolation from

(H) Suckling behavior using thermal support (≈35°C).
(I–N) Quantification of suckling behavior in P10 mice tested with an anesthetized, non-lactating dam (as displayed in H). In (I), proportion of mice that attached to the nipples. In (J), total distance traveled. In (K), tracking of locomotor activity (bottom: starting point; top: anesthetized dam). In (L), number of nipple attachments. In (M), latency to the first attachment. In (N), total time attached to nipples.
(O) Milk letdown prior to and after oxytocin injection in anesthetized dams.
(P–T) Quantification of suckling behavior in P10 mice tested with an anesthetized, lactating dam. In (P), proportion of P10 mice that attached to the nipples. In (Q), total distance traveled. In (R)–(T), data only reflect pups that attached to nipples. In (R), number of nipple attachments. In (S), latency to the first attachment. In (T), the total time attached to nipples.
(U) Delta body weight after suckling assay (control, n = 8; $Agrp^{Trpv1}$, n = 13; pups that did not attach, n = 12; one-way ANOVA, $p < 10^{-5}$).
(V) Tukey-Kramer's multiple comparisons test of the difference between means (95% confidence intervals from U), representing effect sizes.
In (B), (I), and (P), statistical analysis was performed using the chi-square test (2-tailed). In yellow, proportion of mice that attached to the dam's nipples are shown. In gray, mice that did not attach are shown.
In (C), (E)–(G), (J), (L)–(N), and (Q)–(U), violin plots represent the distribution of the data. Symbols represent individual values. Statistical analysis was performed using Mann-Whitney test, with the exception of (U). p values are provided in the panels when statistically significant.

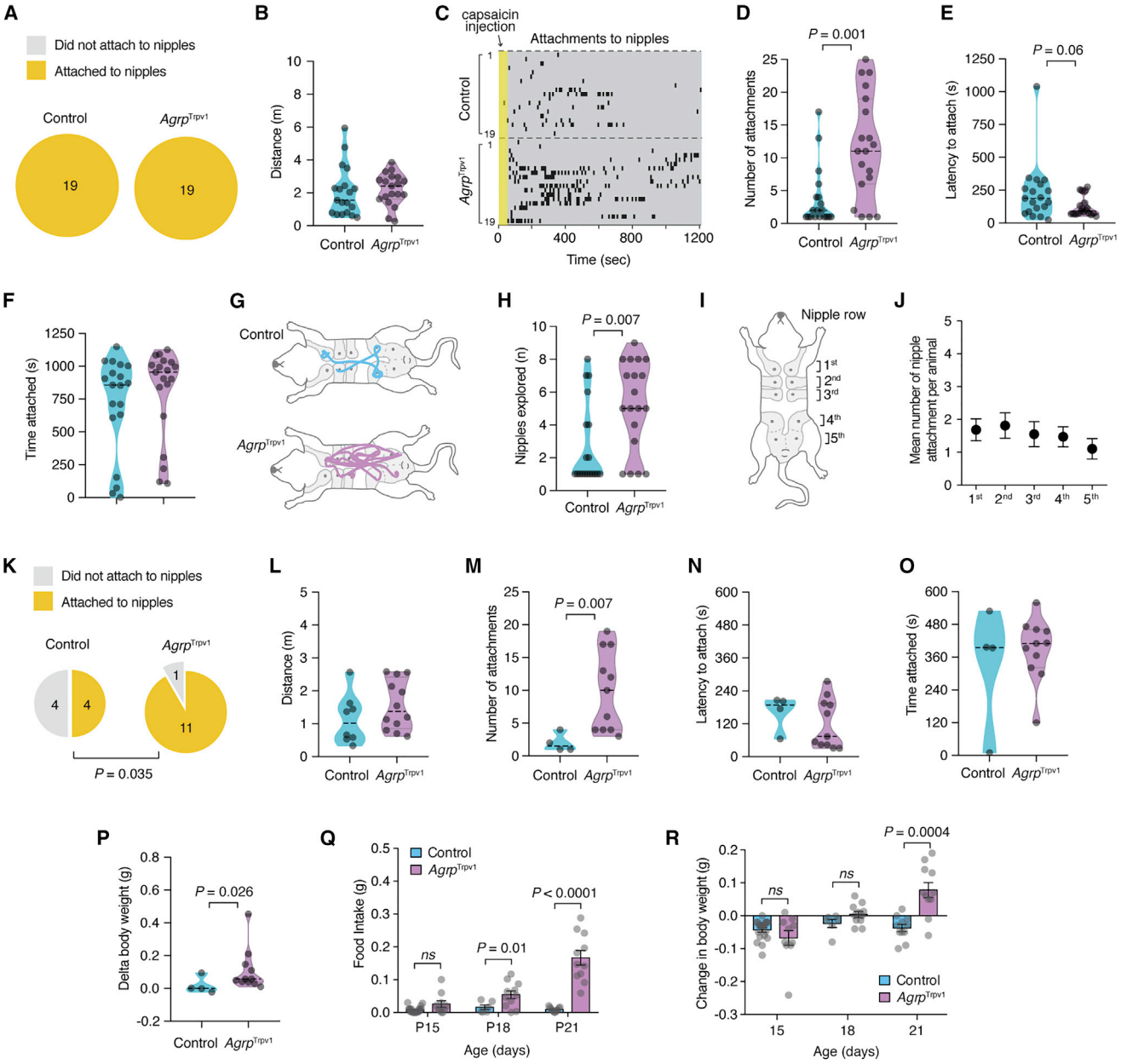

Figure 7. Ontogeny of Ingestive Behaviors in Mice

(A–J) Suckling behavior in P15 mice using anesthetized non-lactating dams during a 20-min test. (A) All pups attached to the dam's nipples during the test. (B) Total distance traveled. (C) Raster plot, ticks indicate nipple attachment. (D) Number of nipple attachments. (E) Latency to the first nipple attachment. (F) Total time attached to nipples. (G) Representative tracking data of nipple attachment. (H) Number of nipples explored. (I) Illustration of the location and number of nipples in the dam and (J) nipple preference as measured by the number of nipple attachments per nipple row in P15 mice (n = 38; both control and *Agrp*^{Trpv1} mice were included).

(K–O) Suckling behavior in P15 mice using anesthetized lactating dams during a 10-min test. (K) Proportion of P15 mice that attached to the nipples of lactating dams. In (L), total distance traveled during the test. In (M)–(O), only showing mice that attached to nipples. In (M), the number of nipple attachments is shown. In (N), latency to the first attachment is shown. In (O), total time attached to nipples is shown.

(P) Delta body weight after the suckling assay (control, n = 4; *Agrp*^{Trpv1} n = 11).

(Q) Chow intake during 30 min after activation of Agrp neurons in mice at 15, 18, and 21 days of age.

(R) Delta body weight in the same animals as in (Q).

In (A) and (K), statistical analysis performed using the chi-square test (2-tailed). In yellow, proportion of mice that attached to the dam's nipples. In gray, mice that did not attach. In (B), (D)–(F), (H), and (L)–(P), violin plots represent the distribution of the data. Symbols represent individual values. Statistical analysis performed using Mann-Whitney test. In (Q) and (R), differences tested using unpaired t test with Welch's correction (unequal SDs) are shown. p values provided in the panels when statistically significant. Bars and symbols (in J, Q, and R) represent mean ± SEM.

the nest to the same degree as thermal support. This observation suggests that neonates integrate several sensory signatures coupled to the nest environment, such as sensory cues from the dam, siblings, home-nest odors, or from all these sources, to create and build expectations of the external world. We unexpectedly propose that activity of Agrp neurons partially encodes this information. Future studies should address the exact nature of this information and the combination of sensory modalities needed to modulate the activity of neonatal Agrp neurons.

Our results provide further evidence to the proposal that Agrp neurons serve as motivational drivers in the mammalian brain. In adult mice, Agrp neurons may encode negative valence (Betley et al., 2015). Under this proposal, these neurons when active would generate an unpleasant state of hunger leading the adult mouse to engage in behaviors to eat and suppress this state (Betley et al., 2015). Our results support this functional property of Agrp neurons in encoding an overall negative state beginning in early development. Clearly, isolation from the nursing nest serves as a negative stimulus for the neonate, which triggers a rapid activation of Agrp neurons and emission of vocalizations. Conversely, reunion then serves as a positive stimulus for the isolated neonate, which immediately suppresses the activity of Agrp neurons. By studying the functional ontogeny of Agrp neurons, our results support a model by which Agrp neurons generate a motivational drive to suppress an overall negative state.

In our studies, we could not find increases in corticosterone levels upon isolation or an enhanced activation of Agrp neurons (as labeled by Fos) in the presence of predator odor. Despite these negative results, we cannot rule out the possibility that Agrp neurons early in life are responsive to general stressors.

Upon parental separation, some infant mammals and birds respond with protest, despair, and emit sounds to attract them (Hofer, 1994). Our results demonstrated that neonatal Agrp neurons are a critical component of the circuit modulating vocal behavioral response in mice. These findings provide further insight into the underlying neural pathways subserving neonatal vocal behavior (Curry et al., 2013; Mosienko et al., 2015; Winslow et al., 2000). Investigating downstream circuits linking Agrp neurons to brain regions involved in the emission of USVs (Arriaga and Jarvis, 2013; Arriaga et al., 2012) will reveal how the neonatal brain encodes sensory information and internal state-dependent variables to generate behavioral responses (Boulanger-Bertolus et al., 2017; Hofer, 1996).

Our results have a broad impact to understand the functional ontogeny of hypothalamic neurons and the importance of the neonatal period in brain and behavior development. Additionally, these studies establish a mechanistic substrate underlying infant-caregiver interaction, which suggests an initial population of neurons underlying the long-sought nature of this social bond in mammals (Harlow, 1958; Lewis et al., 2007).

STAR★METHODS

Detailed methods are provided in the online version of this paper and include the following:

ACKNOWLEDGMENTS

We thank Jeremy Bober for technical support. We thank lab members as well as Dr. Ruslan Medzhitov, Dr. Ivan de Araujo, and Dr. Esther Florsheim for critical insights in the manuscript. M.O.D. was supported by a NARSAD Young Investigator Grant ID 22709 from the Brain & Behavior Research Foundation, by the National Institute of Diabetes and Digestive and Kidney Diseases of the NIH (R01DK107916), by a pilot grant from the Yale Diabetes Research Center (P30 DK045735), by the Yale Center for Clinical Investigation Scholar Award, by the Whitehall Foundation, by the Charles H. Hood Foundation, Inc. (Boston, MA), and by a pilot grant from the Modern Diet and Physiology Research Center (The John B. Pierce Laboratory). M.O.D. also received support from the Conselho Nacional de Desenvolvimento Científico e Tecnológico (CNPq) and Coordenadoria de Aperfeiçoamento de Pessoal de Nível Superior (CAPES), Brazil. M.R.Z., A.H.O.F., and R.D.P. were partially supported by scholarships from CNPq and CAPES. We thank Life Science Editors for editorial assistance.

AUTHOR CONTRIBUTIONS

M.R.Z. performed the experiments, designed the studies, analyzed the data, and helped write the manuscript. A.H.O.F. developed a tool for ultrasonic vocalization analysis in neonates and analyzed the data. R.D.P. performed part of the Fos and behavior experiments. O.I. performed the fiber photometry experiment. M.O.D. supervised the work, designed the studies, analyzed the data, and wrote the manuscript.

DECLARATION OF INTERESTS

The authors declare no competing interests.

Received: January 22, 2019
Revised: March 25, 2019
Accepted: April 12, 2019
Published: May 16, 2019

REFERENCES

Alberts, J.R. (2007). Huddling by rat pups: ontogeny of individual and group behavior. Dev. Psychobiol. *49*, 22–32.

Alberts, J.R., and May, B. (1984). Nonnutritive, thermotactile induction of filial huddling in rat pups. Dev. Psychobiol. *17*, 161–181.

Arenkiel, B.R., Klein, M.E., Davison, I.G., Katz, L.C., and Ehlers, M.D. (2008). Genetic control of neuronal activity in mice conditionally expressing TRPV1. Nat. Methods *5*, 299–302.

Arriaga, G., and Jarvis, E.D. (2013). Mouse vocal communication system: are ultrasounds learned or innate? Brain Lang. *124*, 96–116.

Arriaga, G., Zhou, E.P., and Jarvis, E.D. (2012). Of mice, birds, and men: the mouse ultrasonic song system has some features similar to humans and song-learning birds. PLoS ONE *7*, e46610.

Barros, V.N., Mundim, M., Galindo, L.T., Bittencourt, S., Porcionatto, M., and Mello, L.E. (2015). The pattern of c-Fos expression and its refractory period in the brain of rats and monkeys. Front. Cell. Neurosci. *9*, 72.

Betley, J.N., Xu, S., Cao, Z.F.H., Gong, R., Magnus, C.J., Yu, Y., and Sternson, S.M. (2015). Neurons for hunger and thirst transmit a negative-valence teaching signal. Nature *521*, 180–185.

Boulanger-Bertolus, J., Rincón-Cortés, M., Sullivan, R.M., and Mouly, A.M. (2017). Understanding pup affective state through ethologically significant ultrasonic vocalization frequency. Sci. Rep. *7*, 13483.

Cramer, C.P., Blass, E.M., and Hall, W.G. (1980). The ontogeny of nipple-shifting behavior in albino rats: mechanisms of control and possible significance. Dev. Psychobiol. *13*, 165–180.

Cross, B.A., and Harris, G.W. (1952). The role of the neurohypophysis in the milk-ejection reflex. J. Endocrinol. *8*, 148–161.

Curry, T., Egeto, P., Wang, H., Podnos, A., Wasserman, D., and Yeomans, J. (2013). Dopamine receptor D2 deficiency reduces mouse pup ultrasonic vocalizations and maternal responsiveness. Genes Brain Behav. *12*, 397–404.

Dana, H., Sun, Y., Mohar, B., Hulse, B., Hasseman, J.P., Tsegaye, G., Tsang, A., Wong, A., Patel, R., Macklin, J.J., et al. (2018). High-performance GFP-based calcium indicators for imaging activity in neuronal populations and microcompartments. bioRxiv. https://doi.org/10.1101/434589.

Dietrich, M.O., Bober, J., Ferreira, J.G., Tellez, L.A., Mineur, Y.S., Souza, D.O., Gao, X.B., Picciotto, M.R., Araújo, I., Liu, Z.W., and Horvath, T.L. (2012). AgRP neurons regulate development of dopamine neuronal plasticity and nonfood-associated behaviors. Nat. Neurosci. *15*, 1108–1110.

Dietrich, M.O., Zimmer, M.R., Bober, J., and Horvath, T.L. (2015). Hypothalamic Agrp neurons drive stereotypic behaviors beyond feeding. Cell *160*, 1222–1232.

Ellis, S., Axt, K., and Epstein, A.N. (1984). The arousal of ingestive behaviors by chemical injection into the brain of the suckling rat. J. Neurosci. *4*, 945–955.

Erwin, J., Anderson, B., and Bunger, D. (1975). Nursing behavior of infant pigtail monkeys (Macaca nemestrina): preferences for nipples. Percept. Mot. Skills *40*, 592–594.

Girish, V., and Vijayalakshmi, A. (2004). Affordable image analysis using NIH Image/ImageJ. Indian J. Cancer *41*, 47.

Görs, S., Kucia, M., Langhammer, M., Junghans, P., and Metges, C.C. (2009). Technical note: Milk composition in mice–methodological aspects and effects of mouse strain and lactation day. J. Dairy Sci. *92*, 632–637.

Grimsley, J.M., Monaghan, J.J., and Wenstrup, J.J. (2011). Development of social vocalizations in mice. PLoS ONE *6*, e17460.

Gropp, E., Shanabrough, M., Borok, E., Xu, A.W., Janoschek, R., Buch, T., Plum, L., Balthasar, N., Hampel, B., Waisman, A., et al. (2005). Agouti-related peptide-expressing neurons are mandatory for feeding. Nat. Neurosci. *8*, 1289–1291.

Grove, K.L., and Smith, M.S. (2003). Ontogeny of the hypothalamic neuropeptide Y system. Physiol. Behav. *79*, 47–63.

Güler, A.D., Rainwater, A., Parker, J.G., Jones, G.L., Argilli, E., Arenkiel, B.R., Ehlers, M.D., Bonci, A., Zweifel, L.S., and Palmiter, R.D. (2012). Transient activation of specific neurons in mice by selective expression of the capsaicin receptor. Nat. Commun. *3*, 746.

Hahn, T.M., Breininger, J.F., Baskin, D.G., and Schwartz, M.W. (1998). Coexpression of Agrp and NPY in fasting-activated hypothalamic neurons. Nat. Neurosci. *1*, 271–272.

Hall, W.G., and Rosenblatt, J.S. (1978). Development of nutritional control of food intake in suckling rat pups. Behav. Biol. *24*, 413–427.

Hammond, K.A., Lloyd, K.C., and Diamond, J. (1996). Is mammary output capacity limiting to lactational performance in mice? J. Exp. Biol. *199*, 337–349.

Harlow, H.F. (1958). The nature of love. Am. Psychol. *13*, 673–685.

Hofer, M.A. (1994). Hidden regulators in attachment, separation, and loss. Monogr. Soc. Res. Child Dev. *59*, 192–207.

Hofer, M.A. (1996). Multiple regulators of ultrasonic vocalization in the infant rat. Psychoneuroendocrinology *21*, 203–217.

Horvath, T.L., Bechmann, I., Naftolin, F., Kalra, S.P., and Leranth, C. (1997). Heterogeneity in the neuropeptide Y-containing neurons of the rat arcuate nucleus: GABAergic and non-GABAergic subpopulations. Brain Res. *756*, 283–286.

Hudson, R., Raihani, G., González, D., Bautista, A., and Distel, H. (2009). Nipple preference and contests in suckling kittens of the domestic cat are unrelated to presumed nipple quality. Dev. Psychobiol. *51*, 322–332.

Joly-Amado, A., Denis, R.G., Castel, J., Lacombe, A., Cansell, C., Rouch, C., Kassis, N., Dairou, J., Cani, P.D., Ventura-Clapier, R., et al. (2012). Hypothalamic AgRP-neurons control peripheral substrate utilization and nutrient partitioning. EMBO J. *31*, 4276–4288.

Kenny, J.T., Stoloff, M.L., Bruno, J.P., and Blass, E.M. (1979). Ontogeny of preference for nutritive over nonnutritive suckling in albino rats. J. Comp. Physiol. Psychol. *93*, 752–759.

Lewis, T., Amini, F., and Lannon, R. (2007). A General Theory of Love (Knopf Doubleday Publishing Group).

Lincoln, D.W., and Paisley, A.C. (1982). Neuroendocrine control of milk ejection. J. Reprod. Fertil. *65*, 571–586.

Lincoln, D.W., Hill, A., and Wakerley, J.B. (1973). The milk-ejection reflex of the rat: an intermittent function not abolished by surgical levels of anaesthesia. J. Endocrinol. *57*, 459–476.

Luquet, S., Perez, F.A., Hnasko, T.S., and Palmiter, R.D. (2005). NPY/AgRP neurons are essential for feeding in adult mice but can be ablated in neonates. Science *310*, 683–685.

Mosienko, V., Beis, D., Alenina, N., and Wöhr, M. (2015). Reduced isolation-induced pup ultrasonic communication in mouse pups lacking brain serotonin. Mol. Autism *6*, 13.

Nilsson, I., Johansen, J.E., Schalling, M., Hökfelt, T., and Fetissov, S.O. (2005). Maturation of the hypothalamic arcuate agouti-related protein system during postnatal development in the mouse. Brain Res. Dev. Brain Res. *155*, 147–154.

Noirot, E. (1966). Ultra-sounds in young rodents. I. Changes with age in albino mice. Anim. Behav. *14*, 459–462.

Noirot, E. (1968). Ultrasounds in young rodents. II. Changes with age in albino rats. Anim. Behav. *16*, 129–134.

Padilla, S.L., Carmody, J.S., and Zeltser, L.M. (2010). Pomc-expressing progenitors give rise to antagonistic neuronal populations in hypothalamic feeding circuits. Nat. Med. *16*, 403–405.

Ruan, H.B., Dietrich, M.O., Liu, Z.W., Zimmer, M.R., Li, M.D., Singh, J.P., Zhang, K., Yin, R., Wu, J., Horvath, T.L., and Yang, X. (2014). O-GlcNAc transferase enables AgRP neurons to suppress browning of white fat. Cell *159*, 306–317.

Schindelin, J., Arganda-Carreras, I., Frise, E., Kaynig, V., Longair, M., Pietzsch, T., Preibisch, S., Rueden, C., Saalfeld, S., Schmid, B., et al. (2012). Fiji: an open-source platform for biological-image analysis. Nat. Methods *9*, 676–682.

Singh, P.J., and Hofer, M.A. (1978). Oxytocin reinstates maternal olfactory cues for nipple orientation and attachment in rat pups. Physiol. Behav. *20*, 385–389.

Takahashi, K.A., and Cone, R.D. (2005). Fasting induces a large, leptin-dependent increase in the intrinsic action potential frequency of orexigenic arcuate nucleus neuropeptide Y/Agouti-related protein neurons. Endocrinology *146*, 1043–1047.

Tinbergen, N. (1963). On aims and methods of Ethology. Z. Tierpsychol. *20*, 410–433.

Tomaszycki, M., Cline, C., Griffin, B., Maestripieri, D., and Hopkins, W.D. (1998). Maternal cradling and infant nipple preferences in rhesus monkeys (Macaca mulatta). Dev. Psychobiol. *32*, 305–312.

Van Segbroeck, M., Knoll, A.T., Levitt, P., and Narayanan, S. (2017). MUPET-Mouse Ultrasonic Profile ExTraction: A Signal Processing Tool for Rapid and Unsupervised Analysis of Ultrasonic Vocalizations. Neuron *94*, 465–485.

Vorherr, H., Kleeman, C.R., and Lehman, E. (1967). Oxytocin-induced stretch reaction in suckling mice and rats: a semiquantitative bio-assay for oxytocin. Endocrinology *81*, 711–715.

Winslow, J.T., Hearn, E.F., Ferguson, J., Young, L.J., Matzuk, M.M., and Insel, T.R. (2000). Infant vocalization, adult aggression, and fear behavior of an oxytocin null mutant mouse. Horm. Behav. *37*, 145–155.

Zippelius, H.-M., and Schleidt, W.M. (1956). Ultraschall-Laute bei jungen Mäusen. Naturwissenschaften *43*, 502.

STAR★METHODS

KEY RESOURCES TABLE

REAGENT or RESOURCE	SOURCE	IDENTIFIER
Antibodies		
Rabbit polyclonal anti-c-Fos	Santa Cruz Biotechnologies	Cat# sc-52-G; RRID: AB_2629503
Rabbit monoclonal anti-c-Fos (9F6)	Cell Signaling Technology	Cat# 2250; RRID: AB_2247211
Mouse polyclonal anti-HA	BioLegend	Cat# 901503; RRID: AB_2565005
Donkey anti-mouse IgG (H+L), Alexa Fluor 488	Thermo Fisher Scientific	Cat# A-21202; RRID: AB_141607
Donkey anti-rabbit IgG (H+L), Alexa Fluor 594	Thermo Fisher Scientific	Cat# A-21207; RRID: AB_141637
Donkey anti-rabbit IgG (H+L), Alexa Fluor 647	Thermo Fisher Scientific	Cat# A-31573; RRID: AB_2536183
Bacterial and Virus Strains		
AAV8-CAG-Flex-jGCaMP7s-WPRE-SV40	Janelia Research Campus	Addgene, 104495
Biological Samples		
N/A		
Chemicals, Peptides, and Recombinant Proteins		
Capsaicin	Sigma-Aldrich	Cat# M2028-1G
Oxytocin	Sigma-Aldrich	Cat# O4375-250IU
Critical Commercial Assays		
Corticosterone ELISA kit	Enzo Life Sciences	ADI-900-097
Deposited Data		
N/A		
Experimental Models: Cell Lines		
N/A		
Experimental Models: Organisms/Strains		
Mouse: *Agrp*^{Cre}, Agrptm1(cre)Lowl/J	The Jackson Laboratory	JAX: 012899
Mouse: *R26*$^{LSL\text{-}Trpv1}$, B6;129P2-Gt(ROSA)26Sortm1 (Trpv1,ECFP)Mde/J	The Jackson Laboratory	JAX: 008513
Mouse: *Trpv1*^{KO}, B6.129X1-Trpv1tm1Jul/J	The Jackson Laboratory	JAX: 003770
Mouse: *Rpl22*$^{LSL\text{-}HA}$, B6N.129-Rpl22tm11Psam/J	The Jackson Laboratory	JAX: 011029
Mouse: *Npy*^{KO}, 129S-*Npy*^{tm1Rpa}/J	The Jackson Laboratory	JAX: 004545
Mouse: *Vgat*$^{Flox/Flox}$, *Slc32a1*^{tm1Lowl}	The Jackson Laboratory	JAX: 012897
Oligonucleotides		
Trpv1 knockout Wild type (5′-TGGCTCATATTTG CCTTCAG-3′)	Yale Keck Oligonucleotide Synthesis	Custom preparation
Trpv1 knockout Common (5′-CAGCCCTAGGAG TTGATGGA-3′)	Yale Keck Oligonucleotide Synthesis	Custom preparation
Trpv1 knockout Mutant (5′-TAAAGCGCATGCTC CAGACT-3′)	Yale Keck Oligonucleotide Synthesis	Custom preparation
Ectopic Trpv1 allele F (5′-TCCCAAAGTCGCTC TGAGTT-3′)	Yale Keck Oligonucleotide Synthesis	Custom preparation
Ectopic Trpv1 ectopic (5′-TGGCTTGCAGTTAG GGTCTC-3′)	Yale Keck Oligonucleotide Synthesis	Custom preparation
Recombinant DNA		
N/A		
Software and Algorithms		
ImageJ/Fiji	Girish and Vijayalakshmi, 2004; Schindelin et al., 2012	https://imagej.nih.gov/ij/, RRID:SCR_002285
MUPET	Van Segbroeck et al., 2017	https://sail.usc.edu/mupet

(*Continued on next page*)

Continued

REAGENT or RESOURCE	SOURCE	IDENTIFIER
Any-Maze	Stoelting Co	http://www.anymaze.co.uk/index.htm, RRID:SCR_014289
GraphPad Prism 8.0	GraphPad	https://www.graphpad.com/scientific-software/prism/,RRID:SCR_002798
Sound Recording Software Avisoft-RECORDER	Avisoft	https://www.avisoft.com/recorder.htm, RRID:SCR_014436
MATLAB 2016a	MathWorks	https://www.mathworks.com/products/matlab.html,RRID:SCR_001622
Other		
Micro-Renathane® Tubing	Braintree Scientific, Inc	MRE-033
Promethion CAB-8 Temperature Control Cabinet	Sables Systems International	N/A
UltraSoundGate 416 USGH	Avisoft Bioacoustics	34163
UltraSoundGate Condenser Microphone CM 16	Avisoft Bioacoustics	40011
2.5 μL Microliter Syringe Model 62 RN	Hamilton Company	7632-01
32 gauge, Small Hub RN Needle, 15 mm, 15°	Hamilton Company	7803-04
Optic Cannulae	Doric	MFC-400/430-0.48-RM2-FLT
Optic Fibers	Doric	MFP-400/460/1100_FCM-CM2
Attenuator Fiberoptic Patchcode	Doric	MFP-400/430/LWMJ-0.48_FCM-FCM_T0.05
Fluorescence MiniCube	Doric	FMC4_AE(405)_E(460-490)_F(500-550)
LED Driver	Doric	RVP_2CH_1A
405 nm LED	Doric	CLED_405
465 nm LED	Doric	CLED_465
Fiber Photometry Processor	Tucker-Davis Technology	RZ5P
Half & Half cow's milk	Organic Valley	UPC# 0 93966 00033 7

CONTACT FOR REAGENT AND RESOURCE SHARING

Further information and requests for reagents should be direct to and will be fulfilled by the Lead Contact, Marcelo Dietrich (marcelo.dietrich@yale.edu).

EXPERIMENTAL MODELS AND SUBJECT DETAILS

All preweaning mice used in the experiments were 10-21 days old from both genders. Dams used were 2 – 6 months old. In this study, we used the following mouse lines from The Jackson Laboratories: *Agrptm1(cre)Lowl/J* (*Agrp*^{Cre}) (JAX: 012899); B6;129P2-*Gt(ROSA)26Sortm1(Trpv1,ECFP)Mde/J* (*R26*$^{LSL\text{-}Trpv1}$) (JAX: 008513); B6.129X1-*Trpv1tm1Jul/J* (*Trpv1*^{KO}) (JAX: 003770); B6N.129-*Rpl22tm11Psam/J* (*Rpl22*$^{LSL\text{-}HA}$) (JAX: 011029); 129S-*Npy*^{tm1Rpa}/J (*Npy*^{KO}) (JAX: 004545); and *Slc32a1*^{tm1Lowl} (*or Vgat*$^{Flox/Flox}$) (JAX: 012897).

Agrp^{Trpv1} mice were: *AgrpCre*$^{Tm/+}$*::Trpv1*$^{-/-}$*::R26-LSL-Trpv1*$^{Gt/+}$; control animals were *Trpv1*$^{-/-}$*:R26-LSL-Trpv1*$^{Gt/+}$ mice injected with capsaicin. *Agrp*^{Cre} and *R26*$^{LSL\text{-}Trpv1}$ mice were backcrossed to *Trpv1*^{KO} mice to avoid the peripheral actions of capsaicin when injected systemically to activate Agrp neurons (Arenkiel et al., 2008; Dietrich et al., 2015; Güler et al., 2012; Ruan et al., 2014). We have thoroughly characterized *Agrp*^{Trpv1} mice previously (Dietrich et al., 2015). *Agrp*^{HA} mice were generated by crossing *Agrp*^{Cre} to *Rpl22*$^{LSL\text{-}HA}$ mice. Analysis of ectopic expression of Cre was performed by using a specific set of primers against the excised conditional allele, as characterized before (Dietrich et al., 2015); mice with ectopic expression of the excised allele were not used in the studies. *Agrp*$^{Vgat\text{-}KO}$ mice were generated by crossing *Agrp*^{Cre} to *Vgat*$^{Flox/Flox}$ mice to finally generate *Agrp*$^{Cre/+}$*:: Vgat*$^{Flox/Flox}$. Controls were Cre negative littermates. All mice were kept in temperature- and humidity-controlled rooms, in a 12/12 hr light/dark cycle, with lights on from 7:00 AM–7:00 PM. Food (Teklad 2018S, Envigo) and water were provided *ad libitum* unless otherwise stated. All procedures were approved by IACUC (Yale University).

METHOD DETAILS

Drugs

capsaicin (10 mg/kg, s.c. or i.p.; 3.33% Tween-80 in PBS; from Sigma) and oxytocin (5mg/kg, 15 IU/mg dissolved in PBS; from Sigma).

Immunohistochemistry

Mice were deeply anesthetized and perfused with freshly prepared fixative (paraformaldehyde 4%, in PBS 1x [pH = 7.4]). Brains were post-fixed overnight in fixative and sectioned on a vibratome. Coronal brain sections (50 μm) were washed several times in PBS 1x (pH = 7.4) and pre-incubated with Triton X-100 (0.3% in PBS 1x) for 30 min. Sections were then incubated in a blocking solution (Triton 0.3%, Donkey Serum 10%, Glycine 0.3M in PBS 1x) for one hour. Sections were then incubated with rabbit polyclonal anti-Fos (1:200; sc-52, Santa Cruz Biotechnologies) or rabbit monoclonal anti-Fos (1:1000, #2250; Cell Signaling Technology) and mouse polyclonal anti-HA (1:1000; 901503, Biolegend) for 16 hr. After, sections were extensively washed in 0.3% Triton in PBS and incubated with secondary fluorescent Alexa antibodies (1:500). Sections were mounted and visualized by a Leica TCS SP5 Spectral Confocal Microscope (Center for Cellular e Molecular Imaging, Yale University). During the entire procedure, investigators were blinded to the experimental groups. The ImageJ analysis program (version 1.51h, NIH, USA) (Girish and Vijayalakshmi, 2004; Schindelin et al., 2012) was utilized to count the number of –HA positive (*Agrp*^{HA} neurons) and Fos-positive neurons manually.

Isolation from the nest (Figures 1A–1D):

At postnatal day 10 (P10), neonates (*Agrp*^{HA}) were divided into three conditions: (1) kept with the biological mother and littermates (nest); (2) isolated for 90 minutes and (3) isolated for 8 hours. Isolated animals were single-housed and placed in a clean chamber with fresh bedding. Pups were sacrificed and expression of Fos was evaluated. Samples were prepared for immunohistochemistry as described above. *Agrp*^{HA} pups were used in these studies to allow identification of Agrp neurons. All samples were prepared and counted blinded for the experimental groups.

Milk intake in the nursing nest (Figures 1E and 1F):

when ten days of age (P10), pups were divided into two groups: kept with the biological mother or isolated for 90 minutes. Isolated pups were reintroduced to the biological mother for another 90 minutes after isolation. Body weight was measured prior and after 90 minutes. To ensure that animals within each group had similar milk availability, they were tested using an equal number of animals. Upon reintroduction of the isolated pups to the home cage, pups that stayed with the dam were removed to avoid competition. These experiments were not blinded.

Measurement of corticosterone levels (Figure 1G):

At postnatal day 10, neonates were divided into two groups: kept with the biological mother or isolated for 90 minutes. After testing, neonates were deeply anesthetized, and blood samples were collected through cardiac puncture. A total of 150 μl of blood was collected. Blood samples were left at room temperate for one hour and centrifuged at 5000 rpm for 20 minutes. Plasma was collected and stored at −80°C. Corticosterone level was measured using an enzyme immunoassay (ELISA) kit (Enzo Life Sciences, Farmingdale, NY, USA) according to the manufacturer's instructions.

Isolation from the nest in the presence of a predator odor (Figures 1H–1J):

At postnatal day 10 (P10), pups (*Agrp*^{HA}) were divided into three conditions: (1) kept with the biological mother and littermates (nest); (2) isolated for 90 minutes and (3) isolated for 90 minutes in the presence of a synthetic predator odor (2,4,5-Trimethylthiazole (mT), Sigma-Aldrich). Isolated animals were single-housed and placed in a clean chamber with fresh bedding. Ten microliters of mT odor were pipetted onto a small square nesting material (2 × 2 cm). To avoid contact with the odor, the chamber was divided by a wire mesh resulting in two small compartments, allowing the pups to smell the odor.

Isolation from the nest with milk infusion (Figures 1K–1O):

The procedure of milk infusion consisted in the insertion of a polyurethane-based catheter tubing (Micro-Renathane® Tubing, MRE-033, Braintree Scientific, Inc.) attached to a pump. To avoid an invasive procedure, the inserted tube end was heated and bent to create a small U shape at its end tip. After insertion into the mouth, the tube was attached to the fur on the outside of the cheek using a small drop of crazy glue to hold it in place. The whole procedure did not require anesthesia and last less than 30 s. A total of 200 μl of milk was infused during the 90 minutes (15 μl ejections, every 5-15 minutes). The following types of milk were used: (1) commercial Half & Half cow's milk (Organic Valley, Ultra Pasteurized Grade A); an (2) mouse milk collected from lactating dams. To confirm that milk was infused, a tasteless blue dye (Erioglaucine disodium salt, Sigma-Aldrich, Cat. 861146) was added (< 1 mg/mL) to the milk prior infusion. The stomach was excised to confirm the blue color indicating milk ingestion.

Mouse milk collection

The milk collection was performed on lactating dams with litters between the ages of P8-P12. Dams were separated from their litter for 6 hours prior collection to ensure adequate milk production. Dams were lightly anesthetized with isoflurane and oxytocin (5 mg/kg, i.p) was administered to promote milk release. Milk was expressed from the nipples using pressure from the thumb and forefinger to gently massage and squeeze the mammary tissue in an upward motion until a visible bead of milk begins to form at the base of the teat. Then, milk was collected using a 20 μl calibrated pipette, pipetted into a 1.5 mL Eppendorf tube and stored at −20°C until the day of the test. The duration of the milk collection lasts less than 10 minutes.

Artificial feeding protocol (Figures 1P–1R):

when seven days old, neonates were separated from the biological dam and kept with a non-lactating foster dam. Every 3-4 hours, the neonates were separated from the foster dam and milk was provided for ~30 minutes by the experimenter using a surrogate nipple attached to a tip in a 100 μL pipette. The volume of intake in each session varied between 80 μl to 150 μl of milk. Because of the limitation in getting mouse milk, we performed the artificial feeding using a more caloric formula of cow milk (Heavy Whipping Cream, Organic Valley) that resembles the nutrition facts of a mouse milk (Görs et al., 2009). At postnatal day 10, milk was provided for 30 minutes and immediately after neonates were separated into two groups: kept with the non-lactating foster dam and littermates (nest) or isolated for 90 minutes. All other procedures for Fos counting were as described above.

Assessment of maternal components with foster dams (Figures 2A–2C):

At postnatal day 10, neonates were separated from the biological dam and placed in the cage of a foster dam. Foster dams in different lactation conditions were used: (1) non-lactating foster dam; (2) non-lactating foster dam with protruded nipples; (3) lactating foster dam. Dam rodents have the nipples still distended without milk release permitting suckling for two weeks after weaning if the female is not pregnant again. Lactating foster dams were chosen in a similar postnatal day of lactation, and their offspring was removed immediately before placing the alien/unfamiliar neonates. Neonates were divided into five groups: (1) kept with the biological dam and littermates (nest); (2) kept with a non-lactating foster dam; (3) kept with a non-lactating foster dam with protruded nipple; (4) kept with lactating foster dam with protruded nipple and (5) isolated for 90 minutes. All other procedures for Fos counting were as described above.

Isolation from the nest with thermal support (Figures 2D–2G):

When ten-day-old, neonates were separated from the biological dam, and thermal support was provided using two different conditions. In the first condition, neonates were placed in a humidity and temperature-controlled climate chamber (70%–80% of humidity, 35°C, Sables Systems). In the second condition, a thermal support device set at 35°C was placed underneath the chamber in which the neonates were separated. We confirmed appropriated thermal conditions by monitoring the temperature throughout testing using calibrated thermometers. Neonates were divided into four groups: (1) kept with the biological dam and littermates (nest); (2) isolated for 90 minutes at thermoneutrality; (3) isolated for 90 minutes in the thermal support device; and (4) isolated for 90 minutes without thermal support (room temperature). All other procedures for Fos counting were as described above.

Isolation from the nest in pups raised at thermoneutrality (Figures 2H–2J):

The lactating dam was placed in a humidity and temperature-controlled climate chamber (70%–80% of humidity, 35°C, Sables Systems) two weeks before delivery to acclimate to the new environment. Temperature and humidity in the climate chamber were monitored twice a day until testing. At postnatal day 10, neonates were divided into three groups: (1) kept with the biological dam and littermates (nest); (2) isolated for 90 minutes at room temperature; and (3) isolated for 90 minutes at thermoneutrality. All other procedures for Fos counting were as described above.

Fiber photometry (Figure 3):

Agrp$^{Cre/Cre}$ mouse neonates (P0-P1) were cryo-anesthetized. Neonates were placed on ice, using aluminum foil as a barrier to prevent direct contact with the ice. After 8 minutes, neonates were removed from the ice and placed onto a chilled rat/mouse neonatal frame (Stoelting Co., Wood Dale, IL). A Cre-dependent adeno-associated virus (AAV) encoding the calcium sensor jGCaMP7s (AAV8-CAG-Flex-jGCaMP7s-SV40, Penn Vector Core) was injected unilaterally at a volume of 300 nL using following coordinates from lambda: AP = +.98 ML, lateral = −0.3mm, DV = −4.1mm. On postnatal day 12, a fiber optic cannula (NA = 0.48, core diameter = 400 μm from Doric Lenses) was placed over the arcuate nucleus using following coordinates from bregma: AP = −1.38 mm, lateral = −0.3mm, DV = −5.8 mm. One to two days after placing the fiber optic cannula, experimental mice were placed in a Plexiglas cage (10 cm x 8 cm x 6 cm) with 4 siblings and bedding from home cage. After 5 minutes of baseline fiber photometry recordings (see below), mice connected to the fiber photometry system were moved to an identical adjacent Plexiglas cage for a period of ten minutes of isolation. Subsequently, experimental mice were return to the cage with the siblings for 5 minutes. The fiber photometry system consisted of two different sets of LEDs: 405 nm LED sinusoidally modulated at 211 Hz and a 460 nm LED sinusoidally modulated at 333 Hz. Both light streams were merged into an optical fiber patch using a minicube (Doric Systems). The fiber optic patch was connected to the cannula on the mouse pup. Fluorescence emitted by jGCaMP7s in response to light excitation was collected with same fiber patch cord and focused into a photodetector (Newport). The signal collected at the photodetector was

collected in a digital fiber photometry processor (RZ5P, Tucker-Davis Technologies). Signal was processed and pre-analyzed using the Synapse Software Suite (Tucker-Davis Technologies). The data were exported to MATLAB for post-processing. First, the isosbestic channel (405 nm excitation) was fitted to the calcium-dependent channel (460 nm excitation, denoted as *F*) using first order polynomial fitting (F_0 denotes the fitted isosbestic). The calcium fluorescence activity was calculated as: $(F - F_0)/F_0$. The high-frequency components of the fluorescence activity were then filtered out by a low pass filter at 0.5 Hz. We then down sampled the signal by averaging it in non-overlapping windows of 0.1 s. The Z-score was calculated considering the minute before isolation as the baseline.

Recording of ultrasonic vocalizations (Figures 4 and 5):

P10 mice were separated from the dam and placed in a soundproof chamber. In the thermoneutrality experiment, pups were divided into two groups: (1) isolated for 90 minutes at room temperature or (2) isolated for 90 minutes at thermoneutrality (70%–80% of humidity, 35°C, Sables Systems). USVs were recorded for 90 minutes. In experiments with the Npy^{KO} and $Agrp^{Vgat\text{-}KO}$ mice, USVs were recorded for ten minutes immediately following separation from the dam in the soundproof chamber. In the experiment with $Agrp^{Trpv1}$ mice, this initial ten minutes was considered as a baseline before activation of Agrp neurons. Then, P10 mice were injected with capsaicin (10 mg/kg, s.c) and USVs were recorded for an additional twenty minutes. USVs were recorded using an UltraSoundGate Condenser Microphone CM 16 (Avisoft Bioacoustics, Berlin, Germany) placed 10 cm above the animals. The microphone was connected via an UltraSoundGate 416 USGH audio device and recorded with a sampling rate of 250,000 Hz by the software Avisoft RECORDER (version 4.2.16; Avisoft Bioacoustics).

Maternal preference test (Figures 5N–5P):

The maternal preference test was performed in a three-chamber apparatus (65 × 42 × 23 cm) and comprised of three stages: Stage 1 – acclimation: the dam was allowed to explore the apparatus without the presence of pups for ten minutes. Stage 2 – exploration: two P10 mice (control and $Agrp^{Trpv1}$, n = 25 pairs) were placed on each side of the apparatus inside of an inverted metal wire cup and the dam was allowed to explore the pups for ten minutes. Stage 3 - preference: dam was restricted to the center compartment, pups were injected with capsaicin (10 mg.kg, s.c) and placed in the cups and then the dam was allowed to explore all compartments for 20 minutes. Groups were randomly alternated between both sides to avoid preference for one side of the chamber. Time spent interacting with the pups was measured using Any-maze (Stoelting Co., Wood Dale, IL).

Analysis of ultrasonic vocalizations

Ultrasonic vocalizations (USV) were automatically extracted from the audio recordings by using spectral analysis through image processing. Each audio file was analyzed in segments of 1 minute long and then Short Fourier transformed with a Hamming windowing function (window = 256), NFFT = 1024 sampling points and an overlap between successive windows equal to half of the window size. These parameters generate a spectrogram with resolution of 0.5 ms and 244 Hz. The spectrograms were converted to grayscale images and the USVs were segmented on the spectrogram through a sequence of image processing techniques, which included the contrast enhancement of the image (γ = 1), the application of an adaptive threshold (sensitivity of 20%) followed by a series of morphological operations and identification of connected components. The segmented USV candidates were then analyzed by a local median filtering (LMF) to eliminate segmentation noise based on the contrast between an USV candidate and its background. The minimum contrast acceptable between an USV candidate and its background was automatically estimated based on a differential geometry analysis of the contrast of all the USV candidates detected in an audio recording. USVs less than 10 ms apart were considered as part of the same syllable. Next, all the USVs were classified in 11 distinct call types (Grimsley et al., 2011) by a Convolutional Neural Network, which had the AlexNet architecture as starting point. The network was trained for USV classification with over 14,000 samples of real USVs, which were then augmented in order to increase the variability of the samples, resulting in > 57,000 samples. The output consisted of a table summarizing the main features of the USVs detected. This table contains the start and end time of the USVs, as well as its mean, maximum and minimum frequency, mean intensity and other relevant spectral features such as the existence of harmonic components. Each vocalization received a label based on the most likely call type label attributed by the Convolutional Neural Network. The label of each USV is also available as a probability distribution function over all the call types. The software was custom developed in our laboratory and is available upon request. The details of the software will be published elsewhere.

Mouse pup behavior toward the anesthetized dam (Figures 6A–6G and 7A–7J):

Animals were recorded under infrared illumination and assessed for 20 minutes at postnatal day 10 (P10) and postnatal day 15 (P15). Each animal was tested at one age only. Before the experiment, the dam was anesthetized (100 mg/kg Ketamine + 10 mg/kg Xylazine). The maximum number of pups tested per dam was eight. Animals received an injection of capsaicin (10 mg/kg, s.c.) before the experiment. We used a custom built-chamber (20 × 15 cm built in opaque Plexiglas). The dam was placed at an angle of 45° on her back along the edge. Pups were placed on the other edge of the chamber, ~20 cm away from their dam. Parameters such as latency to attach to the dam's nipple, distance traveled, and the number of nipple attachments were assessed using Any-Maze (Stoelting Co., Wood Dale, IL). Experiments were performed blinded for the genotype.

Mouse pup behavior toward the anesthetized dams injected with oxytocin (Figures 6P–6V and 7K–7P):

In anesthetized dams, milk ejection is largely decreased, and dams are considered non-lactating (Lincoln et al., 1973). To circumvent this issue, we performed a similar experiment as described above but injected the anesthetized dams with oxytocin (5 mg/kg, i.p) immediately before each test. Nipples were manually expressed to confirm that there was milk ejection before the experiment. P10 mice received an injection of capsaicin (10 mg/kg, s.c) and were subsequently assessed for 20 minutes. In this assay, a second injection of oxytocin (5 mg/kg, i.p) was given at 10 minutes of test. P15 mice received an injection of capsaicin (10 mg/kg, s.c) and were subsequently assessed for 10 minutes. The duration of the testing period was shorter because P15 mice quickly attached to the dam's nipple in preliminary experiments. Parameters such as latency to attach to the dam's nipple, distance traveled, and the number of nipple attachments were analyzed using Any-Maze (Stoelting Co., Wood Dale, IL). Body weight was measured prior and after testing. Experiments were performed blinded for the genotype.

Independent feeding (Figures 7Q and 7R):

Mice were tested at postnatal days P15, P18, and P21. Naive animals were used for each postnatal age and mice were acclimated to the behavior room for one-hour before the experiment. Food was left inside the cage to prevent a state of deprivation. Animals were tested in a mouse cage filled with home bedding and two Petri dishes placed in opposite corners. After the acclimation period (1 hour), the experiment was performed. Animals were removed from the cage, received an injection of capsaicin (10 mg/kg, i.p.) and were returned to the cage. One Petri dish was empty; the other had a pellet of chow diet. Body weight and food intake were evaluated after 30 minutes. Experiments were performed blinded for the genotype.

QUANTIFICATION AND STATISTICAL ANALYSIS

MATLAB (2016a or above) and Prism 8.0 were used to analyze data and plot figures. All figures were edited in Adobe Illustrator CS6/CC. Illustrations were designed by Mind the Graph (MindtheGraph.com). Data were first subjected to a normality test using the D'Agostino & Pearson normality test or the Shapiro-Wilk normality test. When homogeneity was assumed, a parametric analysis of variance test was used. The Student's t test was used to compare two groups. Welch's correction was used when standard deviations were unequal between groups. ANOVA was used to compare multiple groups. Tukey-Kramer's multiple comparisons test was used to find post hoc differences among groups and calculate 95% confidence intervals to report effect size. When 95% confidence intervals were not calculated, then the Holm-Sidak's multiple comparisons test was used. When homogeneity was not assumed, the Kruskal-Wallis nonparametric ANOVA was selected for multiple statistical comparisons. The Mann-Whitney U test was used to determine significance between groups. Two sample Kolmogorov–Smirnov test was used to calculate the statistical differences between features of ultrasonic vocalizations. Chi-square test was used to find differences in the number of pups that attached to nipples in the behavior tests performed in neonates. One- or two-tail tests were used based on prior experimental hypothesis. Statistical data are provided in text and in the figures. In the text, values are provided as mean ± SEM $p < 0.05$ was considered statistically significant.

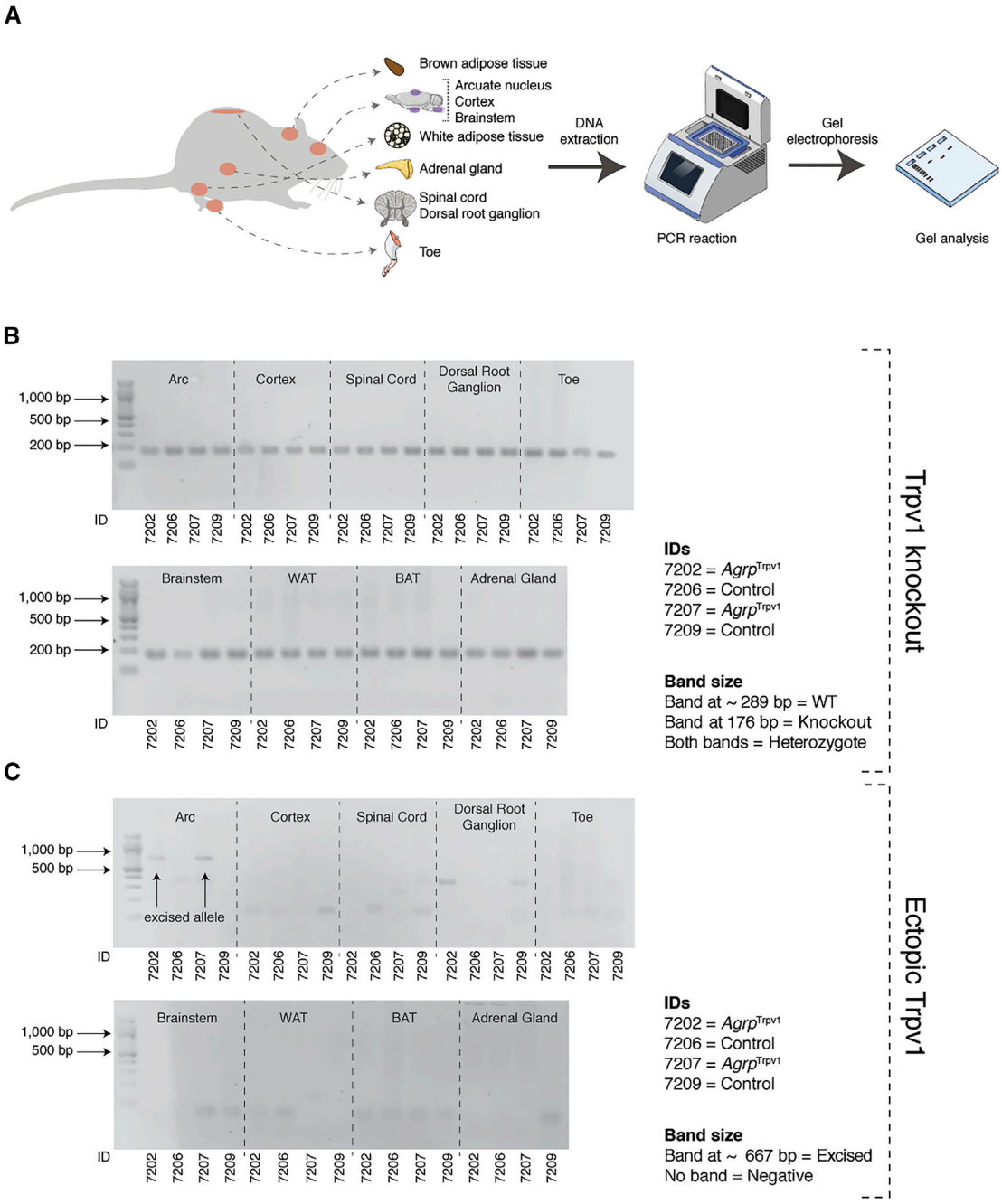

Figure S1. PCR-Based Analysis for Genotyping *Agrp*^{trpv1} and Control Mice, Related to Figure 5

(A) Illustrative diagram of the tissue collection and PCR-based analysis genotyping.

(B) Genomic DNA samples from P15 mice were extracted and amplified using primers for Trpv1 knockout allele. The lower band is the knockout allele for the Trpv1 gene.

(C) Genomic DNA samples from P15 mice were extracted and amplified using primers for ectopic Trpv1 allele. The upper band (667 bp) shows that the excised allele for Trpv1 is specifically expressed in the arcuate nucleus of the hypothalamus.

PART III

Discussion of the results presented in each chapter.

Discussion

In chapter I, I described experiments demonstrating the capacity for Agrp neurons to induce behaviors that are not proximally involved in food intake. These behaviors were repetitive motor actions, resembling displacement behaviors. Animals tend to exhibit displacement behaviors as an attempt to attenuate a particular motivation during a scenario of frustration (Delius, 1967; Tinbergen, 1940). For instance, in times of caloric need when food is not easily obtained, animals display behaviors not directly involved in food consumption (e.g. grooming) to reduce an unpleasant state (e.g. hunger) due to the frustration of the consummatory act (feeding). Thus, I interpreted that animals upon activation of Agrp neurons, when food is unavailable, display behaviors to reduce the feeling of hunger. Recently, studies have shown that activation of Agrp neurons triggers a negative-valence signal (Betley et al., 2015), suggesting that activation of these neurons transmits an unpleasant state (e.g. hunger) that animals try to avoid. Our data support this view since Agrp neuron activation in the presence of food largely suppressed the occurrence of repetitive, stereotyped behaviors.

Interestingly, activation of Agrp neurons increased the expression of behaviors, such as marble-burying and grooming. These behaviors are found in animal models of obsessive-compulsive disorder (OCD) (Alonso et al., 2015). Patients with neuropsychiatric disorders such as Anorexia Nervosa exhibit high activity accompanied by compulsive behaviors (Gummer et al., 2015; Halmi et al., 2003; Matsunaga et al., 1999; Serpell et al., 2002; Thiel et al., 1995). At the brain level, Anorexia Nervosa is proposed to be caused by hypothalamic dysfunction (Mecklenburg et al., 1974; Nilsson et al., 2013). Interestingly, it has been reported increased levels of plasma NPY and AGRP in patients with Anorexia Nervosa (Goldstone et al., 2002; Moriya et al., 2006). Our findings support the hypothesis that hyperactivation of Agrp neurons might be involved in Anorexia Nervosa.

The manifestation of repetitive-obsessive-compulsive-like-behaviors induced by activation of Agrp neurons in our studies was not caused by higher levels of anxiety. On the contrary, activation of Agrp neurons had an anxiolytic effect when animals were tested in different paradigms used to measure anxiety in mice. We interpreted our findings as suggestive that activation of Agrp neurons decreased risk assessment, and animals were more susceptible to explore unfamiliar environments. A recent study, using optogenetic activation of Agrp neurons, found similar results and support this interpretation showing that risk assessment is changed upon Agrp neuron activation (Padilla et al., 2016).

In chapter II, I described a set of experiments demonstrating that Agrp neurons are also involved in memory-related cognitive processes. Activation of Agrp neurons disrupted spontaneous working memory whereas it did not influence the recall of spatial memory in mice. These findings provide useful insight into the understanding of several human conditions characterized by metabolic and cognitive dysfunctions, as we have discussed above. Perhaps of particular interest is the symptomatology of Prader-Willy syndrome (Cassidy and Driscoll, 2009; Ho and Dimitropoulos, 2010). This disorder is characterized by perseverance traits, cognitive impairment, and obesity later in life (Cassidy and Driscoll, 2009; Dykens, 2004; Ho and Dimitropoulos, 2010; Whittington et al., 2004). Albeit speculative, our results might provide an entry point to understand the underlying neural mechanisms leading to cognitive impairment in Prader-Willy syndrome. In spite of these speculative arguments, our findings primarily reinforce the view that modulation of a neuronal population in the mammalian brain can affect broadly multiple brains areas and generate behaviors that go beyond their primary function. It also strengths the view that mammalian brain is organized by highly connected networks of neurons.

In chapter III, we assessed the functional ontogeny of Agrp neurons in modulating neonatal behaviors in mice. Previous findings suggested that Agrp neurons were not functional

during early mouse development. First, Luquet and colleagues reported that ablation of Agrp neurons in neonatal mice did not impair the development and survival of the animals (Luquet et al., 2005). Second, the projections of Agrp neurons onto other brain areas are under development until the third postnatal week, and it was suggested that the function of these neurons in feeding occur only at weaning, coinciding with their final maturation (Bouret et al., 2004; Nilsson et al., 2005). Third, previous studies demonstrated that nutrient sensing to milk deprivation is not developed early in life (Blass and Teicher, 1980; Blass, 1979; Hall, 1985; Hall et al., 1977). Despite these previous findings and against the dogma, we found that Agrp neurons play an essential role during the early postnatal development of mice, influencing critical aspects of the infant behavior that are ultimately involved in the infant-to-mother attachment.

Our results were unexpected and surprising. We first revealed that Agrp neurons are activated upon maternal separation in ten days old mice independently of milk intake. Our findings suggested that thermal cues are the primary stimulus encoded at the level of Agrp neurons in these young mice, signaling maternal separation. These findings illustrate the functional properties of neonatal Agrp neurons that contrast to adult mice, in which Agrp neurons are activated upon prolonged periods of food deprivation (Hahn et al., 1998; Knight et al., 2012; Wu et al., 2014).

Upon maternal separation, rodent neonates emit calls in the ultrasonic range (Noirot, 1966, 1968; Zippelius and Schleidt, 1956). This vocal behavior is rapidly triggered upon maternal separation and helps the mother to find and retrieve the neonates (Del Vecchio et al., 2009; Hofer, 1973; Hofer, 1994; Newman, 2007). Our results demonstrated that Agrp neurons mediate the vocal behavior of neonates acting as an alarm-system to attract the mother's attention. The meaning of these calls was not unraveled but several studies demonstrated that infant vocalizations go beyond a source of communication; they depict the infant affective state

(Hofer, 1994). Furthermore, our results provide additional insights into a behavior widely seen among mammals, including humans. For instance, when separated from their mothers, human babies emit audible sounds (crying) which serves as a potent stimulus to bring the mother's attention (Bowlby, 1969; Formby, 1967; Hofer, 1994; Valanne et al., 1967).

Our findings just scratched the surface of the functional ontogeny of hypothalamic Agrp neurons. What downstream targets are involved in their functional properties, how these neurons modulate neonatal behaviors, and the extent to which the reported mechanisms are conserved across other mammals remain to be addressed in future studies. However, I would like to argue that the reported studies can serve as an entry point to understand the development of physiological processes in mammals, including the ontogeny of offspring-to-caregiver bonding.

Conclusion

The results of this thesis revealed a role of hunger-promoting Agrp neurons in repetitive behaviors and cognitive processes in adult animals, in addition to key functional properties of these neurons early in the postnatal development of mice. Altogether, our results can help elucidate key features of mammals, including (1) the co-existence of metabolic and neuropsychiatric disorders in the human population and (2) the ontogeny of social relationships, starting from the attachment of the infant to its caregiver.

References

Abramowitz, J.S., and Jacoby, R.J. (2015). Obsessive-compulsive and related disorders: a critical review of the new diagnostic class. Annu Rev Clin Psychol *11*, 165-186.

Adan, R.A., Tiesjema, B., Hillebrand, J.J., la Fleur, S.E., Kas, M.J., and de Krom, M. (2006). The MC4 receptor and control of appetite. Br J Pharmacol *149*, 815-827.

Al Ain, S., Belin, L., Schaal, B., and Patris, B. (2013). How does a newly born mouse get to the nipple? Odor substrates eliciting first nipple grasping and sucking responses. Dev Psychobiol *55*, 888-901.

Al-Goblan, A.S., Al-Alfi, M.A., and Khan, M.Z. (2014). Mechanism linking diabetes mellitus and obesity. Diabetes Metab Syndr Obes *7*, 587-591.

Alberts, J.R. (1978). Huddling by rat pups: multisensory control of contact behavior. J Comp Physiol Psychol *92*, 220-230.

Alford, B.R., and Ruben, R.J. (1963). Physiological, behavioral and anatomical correlates of the development of hearing in the mouse. Ann Otol Rhinol Laryngol *72*, 237-247.

Alonso, P., Lopez-Sola, C., Real, E., Segalas, C., and Menchon, J.M. (2015). Animal models of obsessive-compulsive disorder: utility and limitations. Neuropsychiatr Dis Treat *11*, 1939-1955.

Anand, B.K., and Brobeck, J.R. (1951a). Hypothalamic control of food intake in rats and cats. Yale J Biol Med *24*, 123-140.

Anand, B.K., and Brobeck, J.R. (1951b). Localization of a “Feeding Center” in the Hypothalamus of the Rat. Proceedings of the Society for Experimental Biology and Medicine *77*, 323-325.

Aponte, Y., Atasoy, D., and Sternson, S.M. (2011). AGRP neurons are sufficient to orchestrate feeding behavior rapidly and without training. Nat Neurosci *14*, 351-355.

Arias-Carrion, O., and Poppel, E. (2007). Dopamine, learning, and reward-seeking behavior. Acta Neurobiol Exp (Wars) *67*, 481-488.

Atasoy, D., Betley, J.N., Su, H.H., and Sternson, S.M. (2012). Deconstruction of a neural circuit for hunger. Nature *488*, 172-177.

Baquero, A.F., de Solis, A.J., Lindsley, S.R., Kirigiti, M.A., Smith, M.S., Cowley, M.A., Zeltser, L.M., and Grove, K.L. (2014). Developmental switch of leptin signaling in arcuate nucleus neurons. J Neurosci *34*, 9982-9994.

Barnes, A.S. (2011). The epidemic of obesity and diabetes: trends and treatments. Tex Heart Inst J *38*, 142-144.

Benito, K., and Storch, E.A. (2011). Assessment of obsessive–compulsive disorder: review and future directions. Expert Review of Neurotherapeutics *11*, 287-298.

Betley, J.N., Cao, Z.F., Ritola, K.D., and Sternson, S.M. (2013). Parallel, redundant circuit organization for homeostatic control of feeding behavior. Cell *155*, 1337-1350.

Betley, J.N., Xu, S., Cao, Z.F.H., Gong, R., Magnus, C.J., Yu, Y., and Sternson, S.M. (2015). Neurons for hunger and thirst transmit a negative-valence teaching signal. Nature *521*, 180.

Bewick, G.A., Gardiner, J.V., Dhillo, W.S., Kent, A.S., White, N.E., Webster, Z., Ghatei, M.A., and Bloom, S.R. (2005). Post-embryonic ablation of AgRP neurons in mice leads to a lean, hypophagic phenotype. FASEB J *19*, 1680-1682.

Blass, E.M. (1990). Suckling: Determinants, changes, mechanisms, and lasting impressions. Developmental Psychology *26*, 520-533.

Blass, E.M., and Teicher, M.H. (1980). Suckling. Science *210*, 15-22.

Blass, E.M.H., W. G.; Teicher, M. H. (1979). The ontogeny of suckling and ingestive behaviors. Prog Psychobio Physiol Psychol, 243-299.

Bondar, C. (2018). Wild Moms : Motherhood in the Animal Kingdom (Pegasus Books).

Bouret, S.G., Draper, S.J., and Simerly, R.B. (2004). Formation of projection pathways from the arcuate nucleus of the hypothalamus to hypothalamic regions implicated in the neural control of feeding behavior in mice. J Neurosci *24*, 2797-2805.

Bowlby, J. (1969). *Attachment and Loss: Vol. I:Attachment.* (New York: Basic Books).

Brake, S.C., Wolfson, V., and Hofer, M.A. (1979). Electromyographic patterns associated with nonnutritive sucking in 11–13-day-old rat pups. J Comp Physiol Psych *93*, 760-770.

Brambilla, F., Perna, G., Bussi, R., and Bellodi, L. (2000). Dopamine function in obsessive compulsive disorder: cortisol response to acute apomorphine stimulation. Psychoneuroendocrinology *25*, 301-310.

Brecher, G., and Waxler, S.H. (1949). Obesity in albino mice due to single injections of goldthioglucose. Proc Soc Exp Biol Med *70*, 498-501.

Brobeck, J.R. (1946). Mechanism of the development of obesity in animals with hypothalamic lesions. Physiol Rev *26*, 541-559.

Broberger, C., Johansen, J., Johansson, C., Schalling, M., and Hokfelt, T. (1998). The neuropeptide Y/agouti gene-related protein (AGRP) brain circuitry in normal, anorectic, and monosodium glutamate-treated mice. Proc Natl Acad Sci U S A *95*, 15043-15048.

Brockmeyer, T., Friederich, H.C., and Schmidt, U. (2018). Advances in the treatment of anorexia nervosa: a review of established and emerging interventions. Psychological Medicine *48*, 1228-1256.

Bultman, S.J., Michaud, E.J., and Woychik, R.P. (1992). Molecular characterization of the mouse agouti locus. Cell *71*, 1195-1204.

Cansell, C., Denis, R.G., Joly-Amado, A., Castel, J., and Luquet, S. (2012). Arcuate AgRP neurons and the regulation of energy balance. Front Endocrinol (Lausanne) *3*, 169.

Cassidy, S.B., and Driscoll, D.J. (2009). Prader-Willi syndrome. Eur J Hum Genet *17*, 3-13.

Castelhano-Carlos, M.J., Sousa, N., Ohl, F., and Baumans, V. (2010). Identification methods in newborn C57BL/6 mice: a developmental and behavioural evaluation. Lab Anim *44*, 88-103.

Chen, H.Y., Trumbauer, M.E., Chen, A.S., Weingarth, D.T., Adams, J.R., Frazier, E.G., Shen, Z., Marsh, D.J., Feighner, S.D., Guan, X.M.*, et al.* (2004). Orexigenic action of peripheral ghrelin is mediated by neuropeptide Y and agouti-related protein. Endocrinology *145*, 2607-2612.

Chen, Y., Lin, Y.-C., Kuo, T.-W., and Knight, Zachary A. (2015). Sensory Detection of Food Rapidly Modulates Arcuate Feeding Circuits. Cell *160*, 829-841.

Clark, J.T., Kalra, P.S., and Kalra, S.P. (1985). Neuropeptide Y Stimulates Feeding but Inhibits Sexual Behavior in Rats. Endocrinology *117*, 2435-2442.

Clarke, D.J., Boer, H., Whittington, J., Holland, A., Butler, J., and Webb, T. (2002). Prader–Willi syndrome, compulsive and ritualistic behaviours: the first population-based survey. British Journal of Psychiatry *180*, 358-362.

Coëffier, M., Achamrah, N., and Déchelotte, P. (2016). Physical activity in patients with anorexia nervosa. Nutrition Reviews *74*, 301-311.

Cone, R.D. (2005). Anatomy and regulation of the central melanocortin system. Nature Neuroscience *8*, 571.

Cone, R.D. (2006). Studies on the physiological functions of the melanocortin system. Endocr Rev *27*, 736-749.

Cools, R. (2008). Role of dopamine in the motivational and cognitive control of behavior. Neuroscientist *14*, 381-395.

Cowley, M.A., Smart, J.L., Rubinstein, M., Cerdán, M.G., Diano, S., Horvath, T.L., Cone, R.D., and Low, M.J. (2001). Leptin activates anorexigenic POMC neurons through a neural network in the arcuate nucleus. Nature *411*, 480.

Cowley, M.A., Smith, R.G., Diano, S., Tschop, M., Pronchuk, N., Grove, K.L., Strasburger, C.J., Bidlingmaier, M., Esterman, M., Heiman, M.L.*, et al.* (2003). The distribution and mechanism of action of ghrelin in the CNS demonstrates a novel hypothalamic circuit regulating energy homeostasis. Neuron *37*, 649-661.

Cramer, C.P., Thiels, E., and Alberts, J.R. (1990). Weaning in rats: I. Maternal behavior. Dev Psychobiol *23*, 479-493.

Del Vecchio, T., Walter, A., and O'Leary, S.G. (2009). Affective and physiological factors predicting maternal response to infant crying. Infant Behavior and Development *32*, 117-122.

Delius, J.D. (1967). Displacement Activities and Arousal. Nature *214*, 1259-1260.

Dicken, M.S., Tooker, R.E., and Hentges, S.T. (2012). Regulation of GABA and glutamate release from proopiomelanocortin neuron terminals in intact hypothalamic networks. J Neurosci *32*, 4042-4048.

Dietrich, M.O., Bober, J., Ferreira, J.G., Tellez, L.A., Mineur, Y.S., Souza, D.O., Gao, X.B., Picciotto, M.R., Araujo, I., Liu, Z.W.*, et al.* (2012). AgRP neurons regulate development of dopamine neuronal plasticity and nonfood-associated behaviors. Nature Neuroscience *15*, 1108-1010.

Dietrich, M.O., Zimmer, M.R., Bober, J., and Horvath, T.L. (2015). Hypothalamic Agrp neurons drive stereotypic behaviors beyond feeding. Cell *160*, 1222-1232.

Dykens, E.M. (2004). Maladaptive and compulsive behavior in Prader-Willi syndrome: new insights from older adults. Am J Ment Retard *109*, 142-153.

Ellacott, K.L., and Cone, R.D. (2006). The role of the central melanocortin system in the regulation of food intake and energy homeostasis: lessons from mouse models. Philos Trans R Soc Lond B Biol Sci *361*, 1265-1274.

Finkelstein, E.A., Trogdon, J.G., Cohen, J.W., and Dietz, W. (2009). Annual medical spending attributable to obesity: payer-and service-specific estimates. Health Aff (Millwood) *28*, w822-831.

Formby, D. (1967). Maternal recognition of infant's cry. Dev Med Child Neurol *9*, 293-298.

Fox, M.W. (1966). Neuro-Behavioral ontogeny: A synthesis of ethological and neurophysiological concepts. Brain Research *2*, 3-20.

Frohlich, A. (1901). Ein Fall von Tumor der Hypophysis cerebri ohne Akromegalie. Wien Klin Rundschau *15*, 883-886, 906-908.

Gantz, I., Konda, Y., Tashiro, T., Shimoto, Y., Miwa, H., Munzert, G., Watson, S.J., DelValle, J., and Yamada, T. (1993a). Molecular cloning of a novel melanocortin receptor. J Biol Chem *268*, 8246-8250.

Gantz, I., Miwa, H., Konda, Y., Shimoto, Y., Tashiro, T., Watson, S.J., DelValle, J., and Yamada, T. (1993b). Molecular cloning, expression, and gene localization of a fourth melanocortin receptor. J Biol Chem *268*, 15174-15179.

Gantz, I., Shimoto, Y., Konda, Y., Miwa, H., Dickinson, C.J., and Yamada, T. (1994). Molecular Cloning, Expression, and Characterization of a Fifth Melanocortin Receptor. Biochemical and Biophysical Research Communications *200*, 1214-1220.

German, R.Z., and Crompton, A.W. (2000). CHAPTER 14 - The Ontogeny of Feeding in Mammals. In Feeding, K. Schwenk, ed. (San Diego: Academic Press), pp. 449-457.

Goldstone, A.P. (2006). The hypothalamus, hormones, and hunger: alterations in human obesity and illness. In Progress in Brain Research, A. Kalsbeek, E. Fliers, M.A. Hofman, D.F. Swaab, E.J.W. van Someren, and R.M. Buijs, eds. (Elsevier), pp. 57-73.

Goldstone, A.P., Unmehopa, U.A., Bloom, S.R., and Swaab, D.F. (2002). Hypothalamic NPY and agouti-related protein are increased in human illness but not in Prader-Willi syndrome and other obese subjects. J Clin Endocrinol Metab *87*, 927-937.

Griffon, N., Mignon, V., Facchinetti, P., Diaz, J., Schwartz, J.C., and Sokoloff, P. (1994). Molecular Cloning and Characterisation of the Rat Fifth Melanocortin Receptor. Biochemical and Biophysical Research Communications *200*, 1007-1014.

Gropp, E., Shanabrough, M., Borok, E., Xu, A.W., Janoschek, R., Buch, T., Plum, L., Balthasar, N., Hampel, B., Waisman, A.*, et al.* (2005). Agouti-related peptide-expressing neurons are mandatory for feeding. Nature Neuroscience *8*, 1289-1291.

Grove, K.L., Allen, S., Grayson, B.E., and Smith, M.S. (2003). Postnatal development of the hypothalamic neuropeptide Y system. Neuroscience *116*, 393-406.

Grove, K.L., and Smith, M.S. (2003). Ontogeny of the hypothalamic neuropeptide Y system. Physiol Behav *79*, 47-63.

Gummer, R., Giel, K.E., Schag, K., Resmark, G., Junne, F.P., Becker, S., Zipfel, S., and Teufel, M. (2015). High Levels of Physical Activity in Anorexia Nervosa: A Systematic Review. Eur Eat Disord Rev *23*, 333-344.

Gungor, N.K. (2014). Overweight and obesity in children and adolescents. J Clin Res Pediatr Endocrinol *6*, 129-143.

Hagan, M.M., Rushing, P.A., Pritchard, L.M., Schwartz, M.W., Strack, A.M., Van Der Ploeg, L.H., Woods, S.C., and Seeley, R.J. (2000). Long-term orexigenic effects of AgRP-(83---132) involve mechanisms other than melanocortin receptor blockade. Am J Physiol Regul Integr Comp Physiol *279*, R47-52.

Hahn, T.M., Breininger, J.F., Baskin, D.G., and Schwartz, M.W. (1998). Coexpression of Agrp and NPY in fasting-activated hypothalamic neurons. Nat Neurosci *1*, 271-272.

Hall, W.G. (1985). What we know and don't know about the development of independent ingestion in rats. Appetite *6*, 333-356.

Hall, W.G., Cramer, C.P., and Blass, E.M. (1975). Developmental changes in suckling of rat pups. Nature *258*, 318-320.

Hall, W.G., Cramer, C.P., and Blass, E.M. (1977). Ontogeny of Suckling in Rats - Transitions toward Adult Ingestion. J Comp Physiol Psych *91*, 1141-1155.

Halmi, K.A., Sunday, S.R., Klump, K.L., Strober, M., Leckman, J.F., Fichter, M., Kaplan, A., Woodside, B., Treasure, J., Berrettini, W.H.*, et al.* (2003). Obsessions and compulsions in anorexia nervosa subtypes. Int J Eat Disord *33*, 308-319.

Haskell-Luevano, C., and Monck, E.K. (2001). Agouti-related protein functions as an inverse agonist at a constitutively active brain melanocortin-4 receptor. Regulatory Peptides *99*, 1-7.

Hentges, S.T., Nishiyama, M., Overstreet, L.S., Stenzel-Poore, M., Williams, J.T., and Low, M.J. (2004). GABA release from proopiomelanocortin neurons. J Neurosci *24*, 1578-1583.

Hentges, S.T., Otero-Corchon, V., Pennock, R.L., King, C.M., and Low, M.J. (2009). Proopiomelanocortin expression in both GABA and glutamate neurons. J Neurosci *29*, 13684-13690.

Hetherington, A.W., and Ranson, S.W. (1940). Hypothalamic lesions and adiposity in the rat. The Anatomical Record *78*, 149-172.

Hetherington, A.W., and Ranson, S.W. (1942). The relation of various hypothalamic lesions to adiposity in the rat. The Journal of comparative neurology *76*, 475-499.

Heyman, I., Mataix-Cols, D., and Fineberg, N.A. (2006). Obsessive-compulsive disorder. BMJ *333*, 424-429.

Hill, J.O., Wyatt, H.R., and Peters, J.C. (2013). The Importance of Energy Balance. Eur Endocrinol *9*, 111-115.

Ho, A.Y., and Dimitropoulos, A. (2010). Clinical management of behavioral characteristics of Prader-Willi syndrome. Neuropsychiatr Dis Treat *6*, 107-118.

Hofer, M.A. (1973). Maternal separation affects infant rats' behavior. Behavioral Biology *9*, 629-633.

Hofer, M.A. (1994). Hidden regulators in attachment, separation, and loss. Monogr Soc Res Child Dev *59*, 192-207.

Horvath, T., Naftolin, F., Kalra, S., and Leranth, C. (1992). Neuropeptide-Y innervation of beta-endorphin-containing cells in the rat mediobasal hypothalamus: a light and electron microscopic double immunostaining analysis. Endocrinology *131*, 2461-2467.

Horvath, T.L., Bechmann, I., Naftolin, F., Kalra, S.P., and Leranth, C. (1997). Heterogeneity in the neuropeptide Y-containing neurons of the rat arcuate nucleus: GABAergic and non-GABAergic subpopulations. Brain Research *756*, 283-286.

Howard, A.D., Chen, A.S., MacNeil, D.J., Marsh, D.J., Weingarth, D.T., Frazier, E.G., Adams, J.R., Van der Ploeg, L.H.T., Trumbauer, M.E., Qian, S.*, et al.* (2004). Orexigenic Action of Peripheral Ghrelin Is Mediated by Neuropeptide Y and Agouti-Related Protein. Endocrinology *145*, 2607-2612.

Kenny, J.T., Stoloff, M.L., Bruno, J.P., and Blass, E.M. (1979). Ontogeny of preference for nutritive over nonnutritive suckling in albino rats. J Comp Physiol Psych *93*, 752-759.

Kleitman, N., and Satinoff, E. (1982). Thermoregulatory behavior in rat pups from birth to weaning. Physiology & Behavior *29*, 537-541.

Knight, Z.A., Tan, K., Birsoy, K., Schmidt, S., Garrison, J.L., Wysocki, R.W., Emiliano, A., Ekstrand, M.I., and Friedman, J.M. (2012). Molecular profiling of activated neurons by phosphorylated ribosome capture. Cell *151*, 1126-1137.

Krashes, M.J., Koda, S., Ye, C., Rogan, S.C., Adams, A.C., Cusher, D.S., Maratos-Flier, E., Roth, B.L., and Lowell, B.B. (2011). Rapid, reversible activation of AgRP neurons drives feeding behavior in mice. J Clin Invest *121*, 1424-1428.

Lam, B.Y.H., Cimino, I., Polex-Wolf, J., Nicole Kohnke, S., Rimmington, D., Iyemere, V., Heeley, N., Cossetti, C., Schulte, R., Saraiva, L.R.*, et al.* (2017). Heterogeneity of hypothalamic pro-opiomelanocortin-expressing neurons revealed by single-cell RNA sequencing. Mol Metab *6*, 383-392.

Lamoreux, M.L., and Mayer, T.C. (1975). Site of gene action in the development of hair pigment in recessive yellow (ee) mice. Developmental Biology *46*, 160-166.

Lehrman, J.S.R.D.S. (1963). Maternal behavior in mammals (Oxford, England: Wiley).

Leon, M. (1986). Development of Thermoregulation. In Developmental Psychobiology and Developmental Neurobiology, E.M. Blass, ed. (Boston, MA: Springer US), pp. 297-322.

Leonard, H.L., Swedo, S.E., Allen, A.J., and Rapoport, J.L. (1994). Obsessive-Compulsive Disorder. In International Handbook of Phobic and Anxiety Disorders in Children and Adolescents, T.H. Ollendick, N.J. King, and W. Yule, eds. (Boston, MA: Springer US), pp. 207-221.

Lincoln, D.W., Hill, A., and Wakerley, J.B. (1973). The milk-ejection reflex of the rat: an intermittent function not abolished by surgical levels of anaesthesia. J Endocrinol *57*, 459-476.

Lincoln, D.W., and Paisley, A.C. (1982). Neuroendocrine control of milk ejection. J Reprod Fertil *65*, 571-586.

Logan, D.W., Brunet, L.J., Webb, W.R., Cutforth, T., Ngai, J., and Stowers, L. (2012). Learned recognition of maternal signature odors mediates the first suckling episode in mice. Curr Biol *22*, 1998-2007.

Lu, D., Willard, D., Patel, I.R., Kadwell, S., Overton, L., Kost, T., Luther, M., Chen, W., Woychik, R.P., Wilkison, W.O.*, et al.* (1994). Agouti protein is an antagonist of the melanocyte-stimulating-hormone receptor. Nature *371*, 799-802.

Luquet, S., Perez, F., Hnasko, T., and Palmiter, R. (2005). NPY/AgRP neurons are essential for feeding in adult mice but can be ablated in neonates. Science *310*, 683-685.

Mandelblat-Cerf, Y., Ramesh, R.N., Burgess, C.R., Patella, P., Yang, Z., Lowell, B.B., and Andermann, M.L. (2015). Arcuate hypothalamic AgRP and putative POMC neurons show opposite changes in spiking across multiple timescales. eLife *4*, e07122.

Marshall, N.B., Barrnett, R.J., and Mayer, J. (1955). Hypothalamic lesions in goldthioglucose injected mice. Proc Soc Exp Biol Med *90*, 240-244.

Matsunaga, H., Kiriike, N., Iwasaki, Y., Miyata, A., Yamagami, S., and Kaye, W.H. (1999). Clinical characteristics in patients with anorexia nervosa and obsessive-compulsive disorder. Psychol Med *29*, 407-414.

Mayer, J., and Marshall, N.B. (1956). Specificity of Gold Thioglucose for Ventromedial Hypothalamic Lesions and Hyperphagia. Nature *178*, 1399.

Mecklenburg, R.S., Loriaux, D.L., Thompson, R.H., Andersen, A.E., and Lipsett, M.B. (1974). Hypothalamic dysfunction in patients with anorexia nervosa. Medicine (Baltimore) *53*, 147-159.

Miller, M.W., Duhl, D.M., Vrieling, H., Cordes, S.P., Ollmann, M.M., Winkes, B.M., and Barsh, G.S. (1993). Cloning of the mouse agouti gene predicts a secreted protein ubiquitously expressed in mice carrying the lethal yellow mutation. Genes Dev *7*, 454-467.

Mohr, B. (1840). Hypertrophie der Hypophysis cerebri und adurch bedingter Druck auf die Hirngrundflache, ins besondere auf die Sehnerven, das Chiasma derselben und den linkseitigen Hirnschinkel. Wschr des Heilk *6*, 565-571.

Mori, Y. (2001). [Regulation of appetite by melanocortin and its receptors]. Nihon Rinsho *59*, 431-436.

Moriya, J., Takimoto, Y., Yoshiuchi, K., Shimosawa, T., and Akabayashi, A. (2006). Plasma agouti-related protein levels in women with anorexia nervosa. Psychoneuroendocrinology *31*, 1057-1061.

Morley, J.E., Hernandez, E.N., and Flood, J.F. (1987a). Neuropeptide Y increases food intake in mice. Am J Physiol *253*, R516-522.

Morley, J.E., Levine, A.S., Gosnell, B.A., Kneip, J., and Grace, M. (1987b). Effect of neuropeptide Y on ingestive behaviors in the rat. Am J Physiol *252*, R599-609.

Mountjoy, K.G., Mortrud, M.T., Low, M.J., Simerly, R.B., and Cone, R.D. (1994). Localization of the melanocortin-4 receptor (MC4-R) in neuroendocrine and autonomic control circuits in the brain. Molecular Endocrinology *8*, 1298-1308.

Mountjoy, K.G., Robbins, L.S., Mortrud, M.T., and Cone, R.D. (1992). The cloning of a family of genes that encode the melanocortin receptors. Science *257*, 1248-1251.

Newman, J.D. (2007). Neural circuits underlying crying and cry responding in mammals. Behavioural Brain Research *182*, 155-165.

Nilsson, I., Johansen, J.E., Schalling, M., Hokfelt, T., and Fetissov, S.O. (2005). Maturation of the hypothalamic arcuate agouti-related protein system during postnatal development in the mouse. Brain Res Dev Brain Res *155*, 147-154.

Nilsson, I.A.K., Lindfors, C., Schalling, M., Hökfelt, T., and Johansen, J.E. (2013). Chapter Two - Anorexia and Hypothalamic Degeneration. In Vitamins & Hormones, G. Litwack, ed. (Academic Press), pp. 27-60.

Noirot, E. (1966). Ultra-sounds in young rodents. I. Changes with age in albino mice. Animal Behaviour *14*, 459-462.

Noirot, E. (1968). Ultrasounds in young rodents. II. Changes with age in albino rats. Animal Behaviour *16*, 129-134.

Nowak, R. (2006). Suckling, Milk, and the Development of Preferences Toward Maternal Cues by Neonates: From Early Learning to Filial Attachment? In Advances in the study of behavior (Elsevier Inc.).

Ollmann, M.M., Wilson, B.D., Yang, Y.K., Kerns, J.A., Chen, Y.R., Gantz, I., and Barsh, G.S. (1997). Antagonism of central melanocortin receptors in vitro and in vivo by Agouti-related protein. Science *278*, 135-138.

Olney, J.W. (1969). Brain lesions, obesity, and other disturbances in mice treated with monosodium glutamate. Science *164*, 719-721.

Olney, J.W., Adamo, N.J., and Ratner, A. (1971). Monosodium glutamate effects. Science *172*, 294.

Oosterom, J., Nijenhuis, W.A.J., and Adan, R.A.H. (2001). AgRP(83–132) Acts as an Inverse Agonist on the Human-Melanocortin-4 Receptor. Molecular Endocrinology *15*, 164-171.

Padilla, S.L., Qiu, J., Soden, M.E., Sanz, E., Nestor, C.C., Barker, F.D., Quintana, A., Zweifel, L.S., Ronnekleiv, O.K., Kelly, M.J.*, et al.* (2016). Agouti-related peptide neural circuits mediate adaptive behaviors in the starved state. Nat Neurosci *19*, 734-741.

Pauls, D.L., Abramovitch, A., Rauch, S.L., and Geller, D.A. (2014). Obsessive–compulsive disorder: an integrative genetic and neurobiological perspective. Nature Reviews Neuroscience *15*, 410.

Pinto, S., Roseberry, A.G., Liu, H., Diano, S., Shanabrough, M., Cai, X., Friedman, J.M., and Horvath, T.L. (2004). Rapid rewiring of arcuate nucleus feeding circuits by leptin. Science *304*, 110-115.

Raj, M., and Kumar, R.K. (2010). Obesity in children & adolescents. Indian J Med Res *132*, 598-607.

Rau, A.R., and Hentges, S.T. (2017). The Relevance of AgRP Neuron-Derived GABA Inputs to POMC Neurons Differs for Spontaneous and Evoked Release. J Neurosci *37*, 7362-7372.

Roselli-Rehfuss, L., Mountjoy, K.G., Robbins, L.S., Mortrud, M.T., Low, M.J., Tatro, J.B., Entwistle, M.L., Simerly, R.B., and Cone, R.D. (1993). Identification of a receptor for gamma melanotropin and other proopiomelanocortin peptides in the hypothalamus and limbic system. Proc Natl Acad Sci U S A *90*, 8856-8860.

Rossi, M., Kim, M.S., Morgan, D.G., Small, C.J., Edwards, C.M., Sunter, D., Abusnana, S., Goldstone, A.P., Russell, S.H., Stanley, S.A.*, et al.* (1998). A C-terminal fragment of Agouti-related protein increases feeding and antagonizes the effect of alpha-melanocyte stimulating hormone in vivo. Endocrinology *139*, 4428-4431.

Serpell, L., Livingstone, A., Neiderman, M., and Lask, B. (2002). Anorexia nervosa: Obsessive–compulsive disorder, obsessive–compulsive personality disorder, or neither? Clinical Psychology Review *22*, 647-669.

Shutter, J.R., Graham, M., Kinsey, A.C., Scully, S., Luthy, R., and Stark, K.L. (1997). Hypothalamic expression of ART, a novel gene related to agouti, is up-regulated in obese and diabetic mutant mice. Genes Dev *11*, 593-602.

Silvers, W.K. (1958). An experimental approach to action of genes at the agouti locus in the mouse. III. Transplants of newborn Aw-, A-and at-skin to Ay-, Aw-, A-and aa hosts. J Exp Zool *137*, 189-196.

Silvers, W.K. (1979). The Coat Colors of Mice (New York, NY: Springer New York).

Singh, P.J., and Tobach, E. (1975). Olfactory bulbectomy and nursing behavior in rat pups (Wistar DAB). Dev Psychobiol *8*, 151-164.

Singh, P.J., Tucker, A.M., and Hofer, M.A. (1976). Effects of nasal ZnSO4 irrigation and olfactory bulbectomy on rat pups. Physiology & Behavior *17*, 373-382.

Sohn, J.W., and Williams, K.W. (2012). Functional heterogeneity of arcuate nucleus pro-opiomelanocortin neurons: implications for diverging melanocortin pathways. Mol Neurobiol *45*, 225-233.

Spanswick, D., Smith, M.A., Groppi, V.E., Logan, S.D., and Ashford, M.L.J. (1997). Leptin inhibits hypothalamic neurons by activation of ATP-sensitive potassium channels. Nature *390*, 521.

Stanley, B.G., Chin, A.S., and Leibowitz, S.F. (1985). Feeding and drinking elicited by central injection of neuropeptide Y: Evidence for a hypothalamic site(s) of action. Brain Research Bulletin *14*, 521-524.

Stanley, B.G., and Leibowitz, S.F. (1985). Neuropeptide Y injected in the paraventricular hypothalamus: a powerful stimulant of feeding behavior. Proc Natl Acad Sci U S A *82*, 3940-3943.

Sternson, S.M., and Atasoy, D. (2014). Agouti-related protein neuron circuits that regulate appetite. Neuroendocrinology *100*, 95-102.

Teicher, M.H., and Blass, E.M. (1977). First suckling response of the newborn albino rat: the roles of olfaction and amniotic fluid. Science *198*, 635-636.

Thiel, A., Broocks, A., Ohlmeier, M., Jacoby, G.E., and Schussler, G. (1995). Obsessive-compulsive disorder among patients with anorexia nervosa and bulimia nervosa. Am J Psychiatry *152*, 72-75.

Thiels, E., and Alberts, J.R. (1991). Weaning in the Norway rat: relation between suckling and milk, and suckling and independent ingestion. Dev Psychobiol *24*, 19-38.

Tinbergen, N. (1940). Die Übersprungbewegung. Zeitschrift für Tierpsychologie *4*, 1-40.

Treasure, J., Zipfel, S., Micali, N., Wade, T., Stice, E., Claudino, A., Schmidt, U., Frank, G.K., Bulik, C.M., and Wentz, E. (2015). Anorexia nervosa. Nature Reviews Disease Primers *1*, 15074.

Valanne, E.H., Vuorenkoski, V., Partanen, T.J., Lind, J., and Wasz-Hockert, O. (1967). The ability of human mothers to identify the hunger cry signals of their own new-born infants during the lying-in period. Experientia *23*, 768-769.

van den Top, M., Lee, K., Whyment, A.D., Blanks, A.M., and Spanswick, D. (2004). Orexigen-sensitive NPY/AgRP pacemaker neurons in the hypothalamic arcuate nucleus. Nature Neuroscience *7*, 493.

Wang, L., Saint-Pierre, D.H., and Taché, Y. (2002). Peripheral ghrelin selectively increases Fos expression in neuropeptide Y – synthesizing neurons in mouse hypothalamic arcuate nucleus. Neuroscience Letters *325*, 47-51.

Whittington, J., Holland, A., Webb, T., Butler, J., Clarke, D., and Boer, H. (2004). Cognitive abilities and genotype in a population-based sample of people with Prader-Willi syndrome. J Intellect Disabil Res *48*, 172-187.

Williams, K.W., Margatho, L.O., Lee, C.E., Choi, M., Lee, S., Scott, M.M., Elias, C.F., and Elmquist, J.K. (2010). Segregation of acute leptin and insulin effects in distinct populations of arcuate proopiomelanocortin neurons. J Neurosci *30*, 2472-2479.

Wolff, P.H. (1968). Sucking Patterns of Infant Mammals. Brain, Behavior and Evolution *1*, 354-367.

Wu, Q., Boyle, M., and Palmiter, R. (2009). Loss of GABAergic signaling by AgRP neurons to the parabrachial nucleus leads to starvation. Cell *137*, 1225-1234.

Wu, Q., Lemus, M.B., Stark, R., Bayliss, J.A., Reichenbach, A., Lockie, S.H., and Andrews, Z.B. (2014). The temporal pattern of cfos activation in hypothalamic, cortical, and brainstem nuclei in response to fasting and refeeding in male mice. Endocrinology *155*, 840-853.

Zippelius, H.-M., and Schleidt, W.M. (1956). Ultraschall-Laute bei jungen M‰usen. Naturwissenschaften Naturwissenschaften *43*, 502.

ANNEXES A

Here are presented the scientific articles that were not part of the main body of the dissertation.

Annex A-1. Leptin signaling in astrocytes regulates hypothalamic neuronal circuits and feeding

Scientific article published on *Nature Neuroscience*.

Leptin signaling in astrocytes regulates hypothalamic neuronal circuits and feeding

Jae Geun Kim[1], Shigetomo Suyama[1], Marco Koch[1,2], Sungho Jin[1], Pilar Argente-Arizon[3], Jesús Argente[3], Zhong-Wu Liu[1], Marcelo R Zimmer[1], Jin Kwon Jeong[1,4], Klara Szigeti-Buck[1], Yuanqing Gao[5], Cristina Garcia-Caceres[5], Chun-Xia Yi[5], Natalina Salmaso[6], Flora M Vaccarino[6,7], Julie Chowen[3], Sabrina Diano[1,4,7], Marcelo O Dietrich[1], Matthias H Tschöp[5] & Tamas L Horvath[1,4,7]

We found that leptin receptors were expressed in hypothalamic astrocytes and that their conditional deletion led to altered glial morphology and synaptic inputs onto hypothalamic neurons involved in feeding control. Leptin-regulated feeding was diminished, whereas feeding after fasting or ghrelin administration was elevated in mice with astrocyte-specific leptin receptor deficiency. These data reveal an active role of glial cells in hypothalamic synaptic remodeling and control of feeding by leptin.

Astrocytes are the most abundant cells in the CNS, yet they have often been relegated to a less than prominent role in the control of complex brain functions supported by neuronal circuits[1,2]. The regulation of food intake and energy expenditure is tightly linked to the synaptic plasticity of hypothalamic neural circuits[3,4], processes in which glial cells have also been implicated[5,6]. It has not yet been explored whether this involvement of glia is secondary or has an active role in the promotion of these processes initiated by leptin[7].

Previously, the long form of leptin receptors (*Lepr*) was located in astrocytes via immunocytochemistry[8,9]. However, because of questions regarding antibody specificity, it remains controversial whether astrocytes express functional *Lepr*. We found immunolabeling of glial fibrillary acidic protein (GFAP) in a subset of *Lepr*-driven EGFP-expressing cells (**Supplementary Fig. 1**). *Lepr* mRNA was detected from translating ribosomes of astrocytes (**Supplementary Fig. 1**). Finally, we found that mRNA of *Lepr* was expressed in purified mouse hypothalamic astrocytes using astrocyte primary culture (**Supplementary Fig. 2**).

To test the role of the long form of leptin receptors in glial cells, we generated a genetic mouse model in which leptin receptors are time-specifically ablated in astrocytes. Because glial cells are the progenitor cells for neurogenesis during brain development[10], we used a tamoxifen-inducible *Cre-ERT2* system to allow cell- and time-specific knockout of leptin receptor in adult astrocytes (**Supplementary Fig. 2**). To assess whether functional Cre protein was restricted to astrocytes and induced by tamoxifen injection, we crossed GFAP-CreERT2 mice with tdTomato-loxP reporter mice, which express red fluorescent protein. We confirmed successful Cre-mediated recombination in GFAP-positive cells by detecting tdTomato-positive cells after injection of tamoxifen (**Supplementary Fig. 3**). This recombination was found to be specific to astrocytes, as the tdTomato-positive cells did not express Iba-1 (a marker for microglia) or NeuN (a marker for neurons) (**Supplementary Fig. 3**). In addition, we combined *in situ* hybridization with immunohistochemistry to validate the selective loss of functional leptin receptors from GFAP-positive cells in GFAP-Cre transgenic mice that are homozygous for a *loxP*-flanked *Lepr* allele (**Fig. 1a** and **Supplementary Fig. 1**). We further confirmed the deletion of leptin receptor exon 17 in astrocyte primary cells of *Gfap-Lepr*$^{-/-}$ mice by reverse transcription (RT)-PCR (**Supplementary Fig. 2**).

Given that we previously found that leptin affects glial morphology[6,11], we first analyzed astrocytes in the arcuate nucleus of mice following leptin receptor knockout (**Fig. 1b**). Astrocyte-specific loss of leptin receptors did not alter the total number of GFAP-positive cells in the hypothalamus (**Fig. 1c**). However, *Gfap-Lepr*$^{-/-}$ mice showed fewer numbers (**Fig. 1d**) and shorter lengths (**Fig. 1e**) of primary astrocytic projections. We also analyzed astrocytes in the hippocampus. Notably, we detected *Lepr* mRNA in the hippocampus (**Supplementary Fig. 4a**), but there were no changes regarding the number and morphology of GFAP-positive cells (**Supplementary Fig. 4b–e**).

Previously, we reported that astrocytic processes are involved in synaptic plasticity of feeding circuits, including those comprising the proopiomelanocortin (POMC) neurons that secrete α-melanocyte stimulating hormone (α-MSH) and AgRP (agouti-related protein) neurons that co-produce neuropeptide Y (NPY) and GABA[5,6]. This led us to evaluate the patterns of glial ensheathment onto the perikaryal membranes of POMC and unlabeled neurons in the arcuate nucleus by electron microscopy. *Gfap-Lepr*$^{-/-}$ mice had lower glial coverage on the perikaryal membranes of POMC (**Fig. 1f** and **Supplementary Fig. 5a**) and unlabeled neurons (**Fig. 1g**) than control mice. We then analyzed glial coverage of POMC and AgRP cells of *Gfap-Lepr*$^{-/-}$ mice using double immunofluorescence: GFAP immonolabeled with red fluorescence in association with green fluorescent protein (GFP)-labeled POMC or AgRP neurons (*Npy-hrGFP* mice were used for the latter; these mice allow visualization of AgRP neurons through coexpression of NPY and AgRP in these cells). We found that direct contacts were lower between astrocytes and either POMC (**Supplementary Fig. 5b**,**c**) or AgRP (**Supplementary Fig. 5d**,**e**) neurons in *Gfap-Lepr*$^{-/-}$ mice relative to control values.

[1]Program in Integrative Cell Signaling and Neurobiology of Metabolism, Section of Comparative Medicine, Yale University School of Medicine, New Haven, Connecticut, USA. [2]Institute of Anatomy, University of Leipzig, Leipzig, Germany. [3]Hospital Infantil Universitario Niño Jesús, Department of Endocrinology, Instituto de Investigación La Princesa and Centro de Investigación Biomédica en Red de la Fisiopatología (CIBER) de Fisiopatología de Obesidad y Nutrición, Instituto de Salud Carlos III, Madrid, Spain. [4]Department of Obstetrics, Gynecology, and Reproductive Sciences, Yale University School of Medicine, New Haven, Connecticut, USA. [5]Institute for Diabetes and Obesity, Helmholtz Zentrum München & Technische Universität München, Germany. [6]Child Study Center, Yale University School of Medicine, New Haven, Connecticut, USA. [7]Department of Neurobiology, Yale University School of Medicine, New Haven, Connecticut, USA. Correspondence should be addressed to T.L.H. (tamas.horvath@yale.edu).

Received 16 February; accepted 24 April; published online 1 June 2014; doi:10.1038/nn.3725

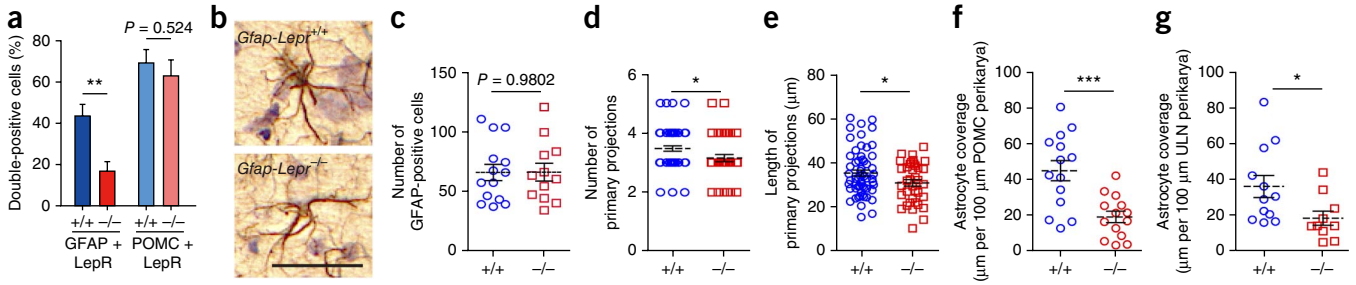

Figure 1 Cell autonomous impairment of leptin receptor (LepR) signaling alters astrocyte morphology and reduces astrocytic coverage onto melanocortin cells. (**a**) Bar graphs show the number of astrocytes or POMC cells expressing *Lepr* mRNA in the Arc (GFAP + LepR, $n = 6$ slices for *Gfap-Lepr*$^{+/+}$ (+/+), $n = 6$ slices for *Gfap-Lepr*$^{-/-}$ (–/–), $P = 0.0041$, $t_{10} = 3.699$; POMC + LepR, $n = 6$ slices for *Gfap-Lepr*$^{+/+}$, $n = 6$ slices for *Gfap-Lepr*$^{-/-}$, $P = 0.524$, $t_{10} = 0.6603$). (**b**) Representative image of GFAP immunolabeling in the Arc of *Gfap-Lepr*$^{+/+}$ and *Gfap-Lepr*$^{-/-}$ mice. Scale bar represents 100 µm. (**c**–**e**) The number of GFAP-positive cells did not differ between *Gfap-Lepr*$^{+/+}$ and *Gfap-Lepr*$^{-/-}$ mice ($n = 14$ slices for *Gfap-Lepr*$^{+/+}$, $n = 12$ slices for *Gfap-Lepr*$^{-/-}$, $P = 0.9802$, $t_{24} = 0.02503$; **c**), but the number of primary projections ($n = 59$ cells for *Gfap-Lepr*$^{+/+}$, $n = 39$ cells for *Gfap-Lepr*$^{-/-}$, $P = 0.0334$, $t_{96} = 2.158$; **d**) and their length ($n = 59$ cells for *Gfap-Lepr*$^{+/+}$, $n = 37$ cells for *Gfap-Lepr*$^{-/-}$, $P = 0.0403$, $t_{94} = 2.079$; **e**) were less in *Gfap-Lepr*$^{-/-}$ mice than in *Gfap-Lepr*$^{+/+}$ mice. (**f**,**g**) POMC cells ($n = 14$ cells for *Gfap-Lepr*$^{+/+}$, $n = 14$ cells for *Gfap-Lepr*$^{-/-}$, $P = 0.0005$, $t_{26} = 3.989$; **f**), and unlabeled neurons (ULN) ($n = 12$ cells for *Gfap-Lepr*$^{+/+}$, $n = 10$ cells for *Gfap-Lepr*$^{-/-}$, $P = 0.0316$, $t_{20} = 1.967$; **g**) in their vicinity, of *Gfap-Lepr*$^{-/-}$ mice had less coverage of their perikaryal membranes by astrocytic processes compared with controls. $^*P < 0.05$, $^{**}P < 0.01$, $^{***}P < 0.001$ versus *Gfap-Lepr*$^{+/+}$. Data are presented as means ± the s.e.m. *P* values for unpaired comparisons were analyzed by two-tailed Student's *t* test.

Next, we assessed whether reduced astrocyte coverage affects synapse number on arcuate nucleus neurons. First, we analyzed synapse number and type by electron microscopy. We found that there were elevated numbers of both symmetric and asymmetric synapses on both POMC (**Fig. 2a**,**b**) and unlabeled neuronal perikarya (**Fig. 2c**) in *Gfap-Lepr*$^{-/-}$ mice relative to controls. Accordingly, we found an elevated frequency of miniature inhibitory postsynaptic currents onto POMC neurons (mIPSCs; **Fig. 2d**), but there was no change in the frequency of miniature excitatory postsynaptic currents onto POMC neurons (mEPSCs) onto POMC cells (**Fig. 2e**). AgRP neurons had an increase in the frequency of both mIPSCs and mEPSCs (**Fig. 2f**,**g**). Taken together, these data indicate that leptin receptor signaling in astrocytes regulates the synaptic input organization of AgRP and POMC cells. We also observed an increase in the amplitudes of both mIPSCs and mEPSCs onto the POMC neurons of *Gfap-Lepr*$^{-/-}$ mice (**Supplementary Fig. 6c**,**d**). On the other hand, there was no alteration in the amplitude of miniature postsynaptic currents onto the AgRP neurons (**Supplementary Fig. 6a**,**b**). These findings suggest that the reduced astrocyte coverage may affect the signaling pathways linked to the postsynaptic receptors of POMC neurons, presumably by buffering trophic factors in the respective synaptic cleft area.

We previously found that the synaptic input organization of the melanocortin system predicts the behavioral output of the melanocortin system in the face of a changing metabolic milieu[3,5,12]. Thus, we next assessed the metabolic phenotype of *Gfap-Lepr*$^{-/-}$ mice and their littermate controls but found them to be normal in phenotypes

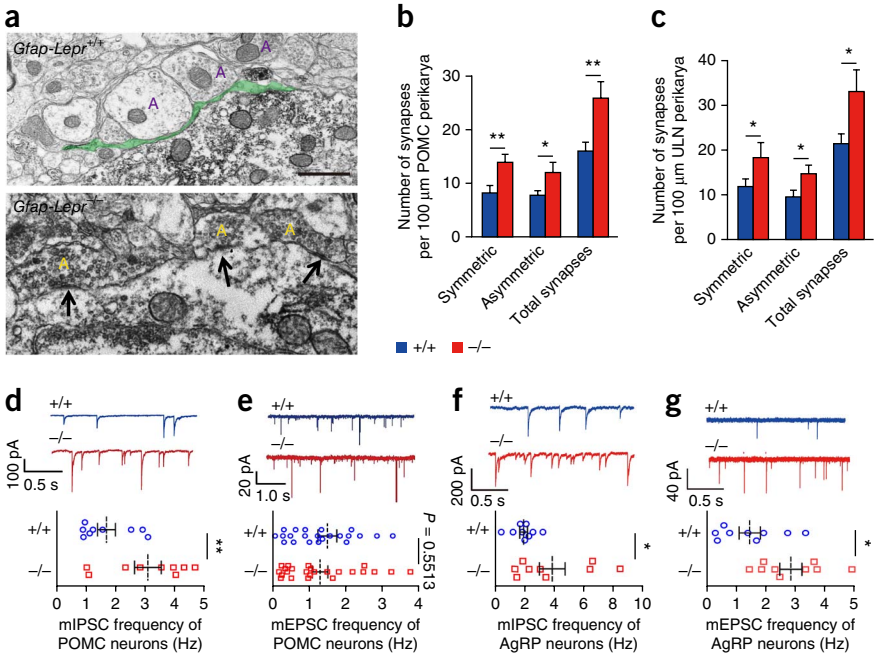

Figure 2 Impaired leptin receptor signaling in astrocytes increases the number of synapses onto POMC and AgRP neurons. (**a**) Representative electron micrograph showing astrocyte coverage (green pseudo-color) and synapses (black arrows) onto POMC-labeled cells. Scale bar represent 1 µm. A, axon. (**b**,**c**) POMC cells ($n = 19$ cells for *Gfap-Lepr*$^{+/+}$ (+/+), $n = 15$ cells for *Gfap-Lepr*$^{-/-}$ (–/–); $P = 0.0097$, $t_{32} = 2.751$ for symmetric; $P = 0.0311$, $t_{32} = 2.255$ for asymmetric; $P = 0.0047$, $t_{32} = 3.039$ for total; **b**), as well as unlabeled neurons (ULN; **c**) ($n = 12$ cells for *Gfap-Lepr*$^{+/+}$, $n = 10$ cells for *Gfap-Lepr*$^{-/-}$; $P = 0.0466$, $t_{20} = 1.763$ for symmetric; $P = 0.0352$, $t_{20} = 2.259$ for asymmetric; $P = 0.0297$, $t_{20} = 2.341$ for total) in their vicinity, of *Gfap-Lepr*$^{-/-}$ mice had elevated numbers of symmetric, asymmetric and, thus, total synapses on their perikaryal membrane compared with controls. (**d**,**e**) POMC neurons (identified by *Pomc*-driven *GFP* labeling) of *Gfap-Lepr*$^{-/-}$ mice had an elevated frequency of mIPSCs ($n = 9$ cells for *Gfap-Lepr*$^{+/+}$, $n = 9$ cells for *Gfap-Lepr*$^{-/-}$, $P = 0.0203$, $t_{16} = 2.576$; **d**), but we found no changes in the frequency of mEPSCs ($n = 23$ cells for *Gfap-Lepr*$^{+/+}$, $n = 25$ cells for *Gfap-Lepr*$^{-/-}$, $P = 0.5513$, $t_{45} = 0.6003$; **e**). (**f**,**g**) AgRP neurons (identified by *NPY*-driven *hrGFP* labeling) of *Gfap-Lepr*$^{-/-}$ mice had an elevated frequency of mIPSCs ($n = 9$ cells for *Gfap-Lepr*$^{+/+}$, $n = 9$ cells for *Gfap-Lepr*$^{-/-}$, $P = 0.0493$, $t_{16} = 2.127$; **f**) and mEPSCs ($n = 9$ cells for *Gfap-Lepr*$^{+/+}$, $n = 9$ cells for *Gfap-Lepr*$^{-/-}$, $P = 0.0164$, $t_{16} = 2.681$; **g**). $^*P < 0.05$, $^{**}P < 0.01$ versus (+/+). Data are presented as means ± the s.e.m. *P* values for unpaired comparisons were analyzed by two-tailed Student's *t* test.

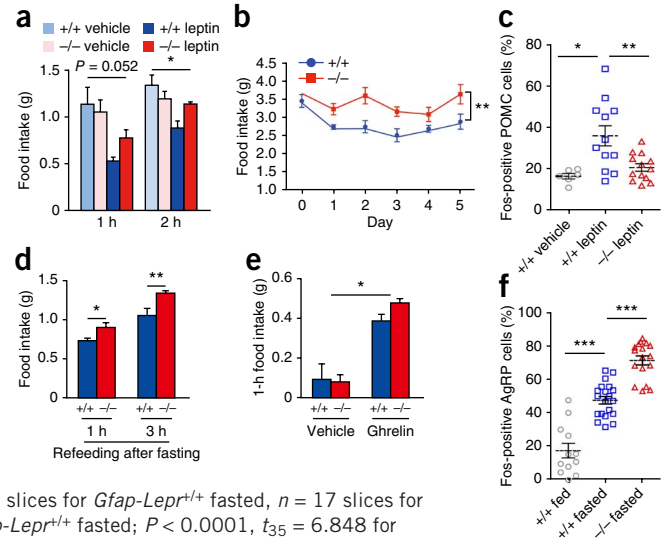

Figure 3 Impairment of leptin receptor signaling in astrocytes blunts leptin-induced anorexia and enhances fasting or ghrelin-induced hyperphagia. (**a**,**b**) *Gfap-Lepr*$^{-/-}$ (–/–) mice showed blunted suppression of feeding in response to leptin administration (**a**: $n = 5$ mice for *Gfap-Lepr*$^{+/+}$ (+/+) + vehicle, *Gfap-Lepr*$^{-/-}$ + vehicle and *Gfap-Lepr*$^{-/-}$ + leptin, $n = 6$ mice for *Gfap-Lepr*$^{+/+}$ + leptin; $P = 0.052$, $F_{1,17} = 4.386$ for 1 h; $P = 0.018$, $F_{1,17} = 6.873$ for 2 h; **b**: $n = 6$ mice per group, $P = 0.0095$, $F_{9,36} = 2.971$). (**c**) Number of Fos-positive POMC cells induced by leptin treatment was reduced in *Gfap-Lepr*$^{-/-}$ mice ($n = 6$ slices for *Gfap-Lepr*$^{+/+}$ + vehicle, $n = 12$ slices for *Gfap-Lepr*$^{+/+}$ + leptin, $n = 13$ slices for *Gfap-Lepr*$^{-/-}$ + leptin; $P = 0.013$, $t_{16} = 2.788$ for *Gfap-Lepr*$^{+/+}$ + vehicle versus *Gfap-Lepr*$^{+/+}$ + leptin; $P = 0.0056$, $t_{23} = 3.055$ for *Gfap-Lepr*$^{+/+}$ + leptin versus *Gfap-Lepr*$^{-/-}$ + leptin). (**d**–**f**) *Gfap-Lepr*$^{-/-}$ mice showed increased feeding after fasting or ghrelin administration (**d**: $n = 6$ mice for *Gfap-Lepr*$^{+/+}$, $n = 7$ mice for *Gfap-Lepr*$^{-/-}$; $P = 0.0378$, $t_{11} = 2.361$ for 1 h; $P = 0.0092$, $t_{11} = 3.150$ for 3 h; **e**: $n = 5$ mice for *Gfap-Lepr*$^{+/+}$ + vehicle, $n = 6$ mice for *Gfap-Lepr*$^{-/-}$ + vehicle, $n = 12$ mice for *Gfap-Lepr*$^{+/+}$ + ghrelin, $n = 11$ mice for *Gfap-Lepr*$^{-/-}$ + ghrelin, $P = 0.04$, $F_{1,32} = 4.57$). (**f**) The number of Fos-positive AgRP cells induced by overnight fasting was enhanced in *Gfap-Lepr*$^{-/-}$ mice ($n = 12$ slices for *Gfap-Lepr*$^{+/+}$ fed, $n = 20$ slices for *Gfap-Lepr*$^{+/+}$ fasted, $n = 17$ slices for *Gfap-Lepr*$^{-/-}$ fasted; $P < 0.0001$, $t_{30} = 6.721$ for *Gfap-Lepr*$^{+/+}$ fed versus *Gfap-Lepr*$^{+/+}$ fasted; $P < 0.0001$, $t_{35} = 6.848$ for *Gfap-Lepr*$^{+/+}$ fasted versus *Gfap-Lepr*$^{-/-}$ fasted). White arrows indicate double-labeled cells. $^{*}P < 0.05$, $^{**}P < 0.01$, $^{***}P < 0.001$ versus (+/+), leptin or fasted. Data are presented as means ± the s.e.m. *P* values for unpaired comparisons were analyzed by two-tailed Student's *t* test. Two-way ANOVA was performed to detect significant interaction between genotype and treatment (leptin or ghrelin). Two-way repeated-measures ANOVA was performed to detect significant interaction between genotype and time (multiple injections of leptin).

of 3-month-old *Gfap-Lepr*$^{-/-}$ mice under standard feeding conditions (**Supplementary Fig. 7a–h**). However, the effects of both single and multiple injections of leptin to suppress feeding were diminished in *Gfap-Lepr*$^{-/-}$ mice relative to controls (**Fig. 3a**,**b**). Consistent with these results, leptin-stimulated Fos activity was attenuated in the *Gfap-Lepr*$^{-/-}$ mice (**Fig. 3c** and **Supplementary Fig. 8a**). These findings are consistent with the observed increase in the number of inhibitory inputs onto the POMC neurons in these mice, as it has been shown that leptin exerts its effect on POMC neurons, at least in part, by the suppression of their inhibitory inputs[13,14]. The effect of the selective knockout of *Lepr* in astrocytes on mIPSCs (but not on mEPSCs) recapitulated the effects of leptin that we previously observed in *Lep*$^{ob/ob}$ mice. However, the lack of a measurable effect of leptin on mEPSCs of POMC cells was not reflected in morphological alterations regarding putative excitatory inputs. These discrepancies may be a result of the fact that leptin signaling is more broadly affected in *Lep*$^{ob/ob}$ mice, but they also highlight the idea that the interrogation of circuit integrity and function cannot be reliably asserted by a single approach.

Next, we determined the responses of *Gfap-Lepr*$^{-/-}$ mice to fasting or ghrelin, a gut hormone that is elevated during negative energy balance and that promotes feeding behavior[15,16]. Fasting-induced hyperphagia was enhanced in these mice compared with controls (**Fig. 3d**). *Gfap-Lepr*$^{-/-}$ mice also showed elevated ghrelin-induced food intake (**Fig. 3e**). Consistent with these findings, AgRP neurons of *Gfap-Lepr*$^{-/-}$ mice exhibited an increased number of Fos-expressing nuclei in response to fasting than controls (**Fig. 3f** and **Supplementary Fig. 8b**). These observations are consistent with the findings that food deprivation or ghrelin administration elevates AgRP neuronal activity, at least in part, by mediation of presynaptic excitatory inputs[17], which we found to be controlled by astrocytes.

Collectively, we found that that leptin receptor signaling in astrocytes has a previously underappreciated active role at the arcuate nucleus interface between afferent hormones, hypothalamic synaptic adaptations and strength, and CNS control of feeding. The extent to which these processes may be involved in the development of obesity in response to overnutrition and the identity of the intercellular signaling modalities that enables glial cells to alter synaptology need to be determined.

METHODS

Methods and any associated references are available in the online version of the paper.

Note: Any Supplementary Information and Source Data files are available in the online version of the paper.

ACKNOWLEDGMENTS

This work was supported by the US National Institutes of Health (DP1 DK098058, R01AG040236, P01NS062686 and R01 DK097566), the American Diabetes Association, the Helmholtz Society (ICEMED) and the Klarmann Family Foundation.

AUTHOR CONTRIBUTIONS

J.G.K., M.O.D. and T.L.H. designed the study. J.G.K., M.H.T. and T.L.H. interpreted the results. J.G.K. and S.J. performed the experiments and analyzed the data. M.K. and K.S.-B. contributed to **Figures 1h,j** and **2a–c**. J.K.J. and S.D. contributed to **Figure 1c**. S.S. and Z.-W.L. contributed to **Figure 2d–g** and **Supplementary Figure 6**. M.R.Z., N.S. and F.M.V. contributed to **Supplementary Figures 1** and **4a**. P.A.-A., J.C. and J.A. contributed to **Supplementary Figure 2b**. Y.G., C.G.-C. and C.-X.Y. contributed to the generation of the animal model. J.G.K. and T.L.H. wrote the paper with input from the other authors.

COMPETING FINANCIAL INTERESTS

The authors declare no competing financial interests.

1. Bélanger, M., Allaman, I. & Magistretti, P.J. *Cell Metab.* **14**, 724–738 (2011).
2. Allaman, I., Belanger, M. & Magistretti, P.J. *Trends Neurosci.* **34**, 76–87 (2011).
3. West, M.J. & Gundersen, H.J. *J. Comp. Neurol.* **296**, 1–22 (1990).
4. Diano, S., Naftolin, F. & Horvath, T.L. *J. Neuroendocrinol.* **10**, 239–247 (1998).
5. Horvath, T.L. *et al. Proc. Natl. Acad. Sci. USA* **107**, 14875–14880 (2010).
6. Fuente-Martín, E. *et al. J. Clin. Invest.* **122**, 3900–3913 (2012).
7. Sholl, D.A. *J. Anat.* **93**, 143–158 (1959).
8. Hsuchou, H., Pan, W., Barnes, M.J. & Kastin, A.J. *Peptides* **30**, 2275–2280 (2009).
9. Hsuchou, H. *et al. Brain* **132**, 889–902 (2009).
10. Ganat, Y.M. *et al. J. Neurosci.* **26**, 8609–8621 (2006).
11. García-Cáceres, C. *et al. Endocrinology* **152**, 1809–1818 (2011).
12. Gao, Q. & Horvath, T.L. *Annu. Rev. Neurosci.* **30**, 367–398 (2007).
13. Cowley, M.A. *et al. Nature* **411**, 480–484 (2001).
14. Vong, L. *et al. Neuron* **71**, 142–154 (2011).
15. Cowley, M.A. *et al. Neuron* **37**, 649–661 (2003).
16. Andrews, Z.B. *et al. Nature* **454**, 846–851 (2008).
17. Yang, Y., Atasoy, D., Su, H.H. & Sternson, S.M. *Cell* **146**, 992–1003 (2011).

ONLINE METHODS

Animal. Two transgenic mice lines (GFAP-CreERT2 and *Lepr*$^{loxP/loxP}$ mice) were obtained and crossed. GFAP-CreERT2 mice[10], which are inducible transgenic mice under control of human *GFAP* promoter and estrogen (C57BL/6J background, generated by F.M. Vaccarino, Yale University School of Medicine) were mated with *Lepr*$^{loxP/loxP}$ mice[18] (generated by S. Chua, Albert Einstein College of Medicine), and breeding cages were maintained by mating *Lepr*$^{loxP/loxP}$ and *Lepr*$^{loxP/loxP}$; GFAP-CreERT2 mice. To excise *loxP* sites by Cre recombination, 5-week-old male mice were administrated tamoxifen twice a day (100 mg per kg of body weight, intraperitoneal) for 5 d. Tamoxifen (Sigma-Aldrich) was dissolved in sunflower oil at a final concentration of 10 mg ml^{-1} at 37 °C, and then filter sterilized and stored for up to 7 d at 4 °C in the dark. All control groups were tamoxifen-injected littermate control mice (*Lepr*$^{loxP/loxP}$). Genotyping was done by PCR using primer sets binding to *Cre* (Cre-1084, 5′-GCG GTC TGG CAG TAA AAA CTA TC-3′; Cre-1085, 5′-GTG AAA CAG CAT TGC TGT CAC TT-3′; Cre-42, 5′-CTA GGC CAC AGA ATT GAA AGA TCT-3′, Cre-43, 5′-GTA GGT GGA AAT TCT AGC ATC ATC C-3′) and crossing the *loxP* site (65A, 5′-AGA ATG AAA AAG TTG TTT TGG GA-3′; 105, 5′-ACA GGC TTG AGA ACA TGA ACA C-3′; 106, 5′-GTC TGA TTT GAT AGA TGG TCT T-3′). To generate POMC or NPY neuron-specific GFP-labeled mice, *Lepr*$^{loxP/loxP}$; GFAP-CreERT2 mice were mated with transgenic mice expressing GFP in POMC neurons (#008322, Jackson Laboratories) or hrGFP in NPY neurons (#006417, Jackson Laboratories). To confirm specific Cre-mediated recombination in GFAP-positive cell, inducible *Cre* expression was screened by mouse line (GFAP-CreERT2 + *Gt(ROSA)26Sor*$^{tm14(CAG-tdTomato)Hze}$ (#007914, Jackson Laboratories)) with injection of tamoxifen (100 mg per kg, intraperitoneal) twice a day for 5 consecutive days. To identify expression of leptin receptor in astrocyte, we used a mouse model[19] (*Lepr-Cre* + Rosa26 ^{EGFP}; obtained from M.G. Myers Jr., University of Michigan) that expresses EGFP in leptin receptor–positive cells. All animals were kept in temperature- and humidity-controlled rooms on a 12-h:12-h light:dark cycle, with lights on from 7:00 a.m. to 7:00 p.m. Mice were group housed (3–5 mice per cage) and food and water were provided *ad libitum*. All procedures were approved by the Institutional Animal Care and Use Committee of Yale University.

Food intake measurement. All mice used in these studies were 2-month-old males and were individually caged 5 d before the start of feeding studies to allow the animals to acclimatize to their new environment. For the fasting-induced feeding behavior, 1- and 3-h rebounded food intake were measured after 18-h food deprivation (beginning at 2 h before the dark cycle). For the ghrelin-induced feeding, mice received ghrelin (3 mg per kg, intraperitoneal) at the early light cycle (ZT 3). Food pellets were weighted and added to the mouse cage 30 min after ghrelin injection and 1-h food intake was measured. To determine the leptin response on feeding behavior, mice were food deprived for overnight (18 h) and then received leptin (3 mg per kg, intraperitoneal) 2 h after the dark cycle (ZT 14). 1- and 2-h food intake were measured 30 min after leptin injection. To determine the effect of repetitive injection of leptin on daily food intake, food intake was measured every day for 5 d after daily administration of leptin (3 mg per kg, intraperitoneal).

Analysis of metabolic phenotype. 3-month-old male mice were acclimated in metabolic chambers (TSE Systems) for 4 d before the start of the recordings. Mice were continuously recorded for 3 d with the following measurements being taken every 30 min: water intake, food intake, ambulatory activity (in X and Z axes) and gas exchange (O_2 and CO_2) (using the TSE LabMaster system). VO_2, VCO_2 and energy expenditure were calculated according to the manufacturer's guidelines (PhenoMaster Software, TSE Systems). Body composition was measured using magnetic resonance imaging (EchoMRI).

Electron microscopy. Under deep anesthesia, 3-month-old male mice were killed by perfusion (4% paraformaldehyde (wt/vol), 0.1% glutaraldehyde (vol/vol), and 15% picric acid (vol/vol) in phosphate buffer (PB)), and their brains were processed for immunolabeling for electron microscopy studies. Ultrathin sections were cut on a Leica Ultra-Microtome, collected on Formvar-coated single-slot grids and analyzed with a Tecnai 12 Biotwin electron microscope (FEI). The electron microscopy photographs (×11,500) were used to measure astrocytic coverage and the numbers of synapses on perikaryal membrane of POMC and unlabeled neurons. The analysis of synapse number was performed in an unbiased fashion as described elsewhere[3,20]. The analysis of the astrocytic coverage was performed as described previously[5,6]. All investigators were blinded to the experimental groups during the entire procedure.

Electrophysiology. *Gfap-Lepr*$^{+/+}$ and *Gfap-Lepr*$^{-/-}$ mice (4-week-old male) labeled with the *Pomc-GFP* or *Npy-hrGFP* were killed at the beginning of the dark cycle, and the ARC was sliced into 250 µm slices (two per mouse), containing the *Pomc-GFP* or *Npy-hrGFP* cells. Slices were then incubated with artificial cerebrospinal fluid at 35 °C for 4 h. After stabilization in artificial cerebrospinal fluid, slices were transferred to the recording chamber for recording mIPSCs and mEPSCs as described previously[3,21].

Immunohistochemistry. 3-month-old male mice were anesthetized and transcardially perfused with 0.9% saline (wt/vol) containing heparin (10 mg l^{-1}) followed by fixative (4% paraformaldehyde, 15% picric acid, 0.1% glutaraldehyde in 0.1 M PB). Brains were collected and post-fixed overnight before coronal sections were taken at every 50 µm. Sections were washed and then treated with 1% H_2O_2 (vol/vol) for 15 min to remove endogenous peroxidase activity. After washing and blocking with 2% normal horse serum (vol/vol), sections were incubated with primary antibodies (antibody to mouse GFAP, 1:1,000 for 2 h at 20–22 °C, Sigma, G3893; antibody to rabbit c-fos, 1:2,000 for overnight at 20–22 °C, Millipore, ABE457; antibody to chicken GFP, 1:2,000 for overnight at 20–22 °C, Abcam, ab13970; antibody to mouse NeuN, 1:1,000 for overnight at 20–22 °C, Millipore, MAB377; antibody to rabbit Iba-1, 1:2,000 for overnight at 20–22 °C, Wako, 019-19741). The following day, sections were extensively washed and incubated in biotinylated secondary antibody to rabbit, ABC reagent and diaminobenzidine (DAB) substrate (Vector Laboratories). Crystal violet staining was performed to detect cell nuclei. Immunofluorescence was performed with a combination of Alexa Fluor 488–labeled secondary antibodies to rabbit, chicken or mouse (1:500 for 1 h at 20–22 °C, Invitrogen, #A21206, #A11039, #A21202) or Alexa Fluor 594–labeled secondary antibodies to rabbit or mouse (1:500 for 1 h at 20–22 °C, Invitrogen, #A21207, #A21203). Representative images were selected from experiments that had been repeated at least three times.

Quantification of astrocyte number and projections. For the quantitative evaluation of astrocytes, six sections throughout the arcuate nucleus per animal were analyzed. Astrocytes were detected by DAB-based immunohistochemistry with GFAP antibody followed by crystal violet staining to identify their nuclei. Images were captured with a 40× objective using a digital camera and analyzed using ImageJ software. Cells were counted according to the optical disector technique[3]. The number of primary projections was determined for each GFAP-positive cell that was included entirely in the field of analysis and Sholl's analysis[7] was performed to assess differences in the extension of glial processes as described previously[22].

Detection of *Lepr* mRNA in astrocyte (*in situ* hybridization). To verify our animal model with specific deletion of leptin receptor expression in astrocytes, we combined *in situ* hybridization with immunohistochemistry using astrocyte-specific leptin receptor knockout (*Gfap-Lepr*$^{-/-}$) mice and their control mice (*Gfap-Lepr*$^{+/+}$). To this end, we designed leptin receptor–specific riboprobes to specifically recognize mRNA region corresponding to *Lepr*-delta exon 17 allele (NM_146146, NCBI GenBank). The riboprobes were labeled with S^{35} and purified with a spin RNA column (Roche Diagnostics). Brain tissues from *Gfap-Lepr*$^{-/-}$ and control animals were quickly removed, frozen in liquid nitrogen, coronally sectioned at 20-µm thickness using a cryostat, and stored in −80 °C until use. First, we performed radioactive *in situ* hybridization using the S^{35}-labeled riboprobes as above following the protocol reported previously[23]. Briefly, sections were fixed with 3% paraformaldehyde solution, acetylated (2.7 ml of triethanolamine and 0.5 ml of acetic anhydride in 200 ml of RNase-free water), dehydrated through a series of alcohols, and then hybridized with the riboprobes at 52 °C for overnight. The next day, the sections were washed through regular washing steps[23], and were ready for immunohistochemistry to visualize astrocyte using a GFAP antibody as a molecular marker for astrocyte. After the washing steps, the sections were incubated with a milk blocking buffer (3% fat-free milk, 0.3% Triton X-100 in 0.1 M PB) at 20–22 °C for 30 min. Next, a series of antibody incubations was performed as following: antibody to mouse GFAP (1:1,000 for 2 h

doi:10.1038/nn.3725

at 20–22 °C, Sigma), antibody to rabbit POMC (1:1,000 for overnight at 20–22 °C, Phoenix pharmaceuticals, H-029-30) and Alexa 594–conjugated antibody to mouse IgG (1:250 dilution in 0.1 M PB, Invitrogen, #A21203) at 20–22 °C for 1 h. Regular 0.1 M PB washing was performed between antibody incubations. The sections were then finally subjected for emulsion autoradiography and further microscopy.

Astrocyte primary culture. Mice at postnatal day 3 were killed by decapitation and the hypothalamus was collected in DMEM F12 (Gibco) plus 1% antibiotics-antimycotics (Gibco). The hypothalamus was dissociated and the suspension was centrifuged for 7 min at 201*g*. The pellet was resuspended with DMEM F12 plus 10% fetal bovine serum (Gibco by Life Technologies) and 1% antibiotics-antimycotics. This media was used to seed and grow cells in 25-cm^3 culture treated flasks at 37 °C and 5% CO_2. The media was changed every 2 d until the cells reached the desired confluence. Once confluence was reached, between days 7 and 9 *in vitro*, the flasks were place in an incubator shaker at 280 r.p.m. at 37 °C overnight. After shaking, the cells were then washed with phosphate-buffered saline (Gibco), trypsinized and resuspended in DMEM F12 plus 10% fetal bovine serum and 1% antibiotics-antimycotics. The suspension was centrifuged for 5 min at 266*g*. After cell counting, the cells were seeded in poly-L-lysine hydrobromide–coated (10 μg ml^{-1}, Sigma-Aldrich) six-well plates at a concentration of 130,000 cells per well. The cells were grown for 24 h in DMEM F12 containing 10% fetal bovine serum and 1% antibiotics-antimycotics and then treated with 4-hydroxytamoxifen at a concentration of 1 μM or vehicle during 3 consecutive days. Cells were then collected for RNA extraction and PCR analysis.

RT-PCR and ribosome profiling. RNA was extracted using QIAGEN RNeasy Micro Kit (#74004). cDNA was synthetized using QIAGEN Whole Transcriptome Kit (#207043). RT-PCR was performed in a Roche 480 LightCycler using Taqman probes (*Agrp* (Mm00475829_g1); *Leprb* (Mm01262069_m1); *NeuN* (Mm01248771_m1); *s100β* (Mm00485897_m1)). To validate the deletion of exon 17 in cording region of the leptin receptor gene, we designed specific primer set (forward, 5′-TCG ACA AGC AGC AGA ATG AC -3′; reverse, 5′-CTG CTG GGA CCA TCT CAT C-3′) and performed RT-PCR with tamoxifen-treated astrocyte primary cells.

Translating ribosome affinity purification (TRAP) was conducted in homogenate samples of hippocampus and hypothalamus obtained from *AldH-EGFP-L10a* mice, which express green fluorescent protein in the ribosomes of $AldH^+$ cells and mice with *loxP*-flanked *Rpl22* (ribosome protein subunit 22)[24] crossed with the *Agrp-cre* line, which express Rpl22 and HA proteins in ribosomes of AgRP neurons, thereby allowing for the immunoprecipitation of polysomes directly from astrocytes and AgRP neurons[24]. TRAP methods were conducted as previously published[25–27]. After RNA isolation, we obtained approximately 10–25 ng of RNA per sample. RT-PCR was performed as described above.

Statistical analyses. Statistical analyses were performed by use of Prism 6.0 software (GraphPad). Data distribution was assumed to be normal, but this was not formally tested. No statistical methods were used to predetermine sample sizes, but our sample sizes are similar to those reported in previous publication[16,28]. All analyses were performed in a blinded manner. No randomization was used to assign experimental groups or to collect data but mice and cells were assigned to specific experimental groups without bias. Unpaired *t* test was performed to analyze significance between two experimental groups. Two-way ANOVA analysis was performed to detect interaction between treatment and genotype. Two-way repeated-measures ANOVA analysis was used to detect interaction between time and genotype. Significance was taken at $P < 0.05$.

A **Supplementary Methods checklist** is available.

18. McMinn, J.E. *et al. Am. J. Physiol. Endocrinol. Metab.* **289**, E403–E411 (2005).
19. Patterson, C.M., Leshan, R.L., Jones, J.C. & Myers, M.G. Jr. *Brain Res.* **1378**, 18–28 (2011).
20. Diano, S. *et al. Nat. Neurosci.* **9**, 381–388 (2006).
21. Caron, E., Sachot, C., Prevot, V. & Bouret, S.G. *J. Comp. Neurol.* **518**, 459–476 (2010).
22. Del Cerro, S., Garcia-Estrada, J. & Garcia-Segura, L.M. *Glia* **14**, 65–71 (1995).
23. Jeong, J.K., Chen, Z., Tremere, L.A. & Pinaud, R. *J. Vis. Exp.* **42**, 2102 (2010).
24. Sanz, E. *et al. Proc. Natl. Acad. Sci. USA* **106**, 13939–13944 (2009).
25. Heiman, M. *et al. Cell* **135**, 738–748 (2008).
26. Doyle, J.P. *et al. Cell* **135**, 749–762 (2008).
27. Dougherty, J.D., Schmidt, E.F., Nakajima, M. & Heintz, N. *Nucleic Acids Res.* **38**, 4218–4230 (2010).
28. Dietrich, M.O. *et al. Nat. Neurosci.* **15**, 1108–1110 (2012).

doi:10.1038/nn.3725

Annex A-2. O-GlcNAc Transferase Enables AgRP Neurons to Suppress Browning of White Fat

Scientific article published on *Cell*.

Cell

O-GlcNAc Transferase Enables AgRP Neurons to Suppress Browning of White Fat

Hai-Bin Ruan,[1,2] Marcelo O. Dietrich,[1,2,5,6] Zhong-Wu Liu,[1,2] Marcelo R. Zimmer,[1,2,6] Min-Dian Li,[1,2,3] Jay Prakash Singh,[1,2] Kaisi Zhang,[1,2,3] Ruonan Yin,[1,2] Jing Wu,[1,2] Tamas L. Horvath,[1,2,4,5,*] and Xiaoyong Yang[1,2,3,*]
[1]Program in Integrative Cell Signaling and Neurobiology of Metabolism
[2]Section of Comparative Medicine
[3]Department of Cellular and Molecular Physiology
[4]Department of Obstetrics, Gynecology and Reproductive Sciences
[5]Department of Neurobiology
Yale University School of Medicine, 333 Cedar Street, New Haven, CT 06520, USA
[6]Department of Biochemistry, Universidade Federal do Rio Grande do Sul, Porto Alegre, RS 93042, Brazil
*Correspondence: tamas.horvath@yale.edu (T.L.H.), xiaoyong.yang@yale.edu (X.Y.)
http://dx.doi.org/10.1016/j.cell.2014.09.010

SUMMARY

Induction of beige cells causes the browning of white fat and improves energy metabolism. However, the central mechanism that controls adipose tissue browning and its physiological relevance are largely unknown. Here, we demonstrate that fasting and chemical-genetic activation of orexigenic AgRP neurons in the hypothalamus suppress the browning of white fat. O-linked β-N-acetylglucosamine (O-GlcNAc) modification of cytoplasmic and nuclear proteins regulates fundamental cellular processes. The levels of O-GlcNAc transferase (OGT) and O-GlcNAc modification are enriched in AgRP neurons and are elevated by fasting. Genetic ablation of OGT in AgRP neurons inhibits neuronal excitability through the voltage-dependent potassium channel, promotes white adipose tissue browning, and protects mice against diet-induced obesity and insulin resistance. These data reveal adipose tissue browning as a highly dynamic physiological process under central control, in which O-GlcNAc signaling in AgRP neurons is essential for suppressing thermogenesis to conserve energy in response to fasting.

INTRODUCTION

Overweight and obesity develop when energy intake exceeds energy expenditure, storing excess calories in the adipose tissue (Spiegelman and Flier, 2001). The adipose organ comprises white (WAT) and brown adipose tissues (BAT). WAT primarily stores energy as triglycerides and its excess and dysfunction lie at the core of obesity and associated metabolic disorders. In contrast, BAT-mediated adaptive thermogenesis dissipates chemical energy as heat, and protects against obesity in both rodents and humans (Cinti, 2012; Kajimura and Saito, 2013; Nedergaard et al., 2010; Smorlesi et al., 2012). Emerging evidence has demonstrated that "brown-like" adipocytes, so-called beige/brite cells, exist in specific WAT depots and differ from classic brown adipocytes in their origin and molecular identity (Petrovic et al., 2010; Rosen and Spiegelman, 2014; Wu et al., 2012). Multiple intrinsic factors and secreted molecules have been identified that modulate the development and function of beige/brite adipocytes and thus metabolic health in animals (Bartelt and Heeren, 2013; Wu et al., 2013). However, whether and how the central nervous system controls WAT browning is almost completely unknown.

Orexigenic neurons expressing agouti-related protein (AgRP)/neuropeptide Y (NPY) and anorexigenic neurons expressing proopiomelanocortin (POMC) reside in the arcuate nucleus of the hypothalamus. These neurons are regulated by peripheral hormones and nutrients and are critical for maintenance of energy homeostasis and glucose metabolism. During food deprivation, AgRP neurons are strongly activated to promote hunger (Hahn et al., 1998; Liu et al., 2012; Takahashi and Cone, 2005), an effect vastly mediated by ghrelin signaling in these neurons (Andrews et al., 2008; Chen et al., 2004; Yang et al., 2011). Despite the involvement of other hypothalamic areas in the control of thermogenesis in classic BAT (Nogueiras et al., 2008; Scherer and Buettner, 2011; Yasuda et al., 2004), it is not known whether hunger-promoting AgRP neurons are involved in the control of adaptive thermogenesis and/or browning of WAT.

Thousands of cytoplasmic and nuclear proteins are modified by a single O-linked β-N-acetylglucosamine (O-GlcNAc) moiety at serine or threonine residues, termed O-GlcNAcylation (Hart et al., 2007; Torres and Hart, 1984). This dynamic and reversible modification is emerging as a key regulator of diverse cellular processes, such as signal transduction, transcription, translation, and proteasomal degradation (Love and Hanover, 2005; Ruan et al., 2013a; Yang et al., 2002). Perturbations in protein O-GlcNAcylation are implicated in various human diseases including diabetes mellitus, neurodegeneration, and cancer

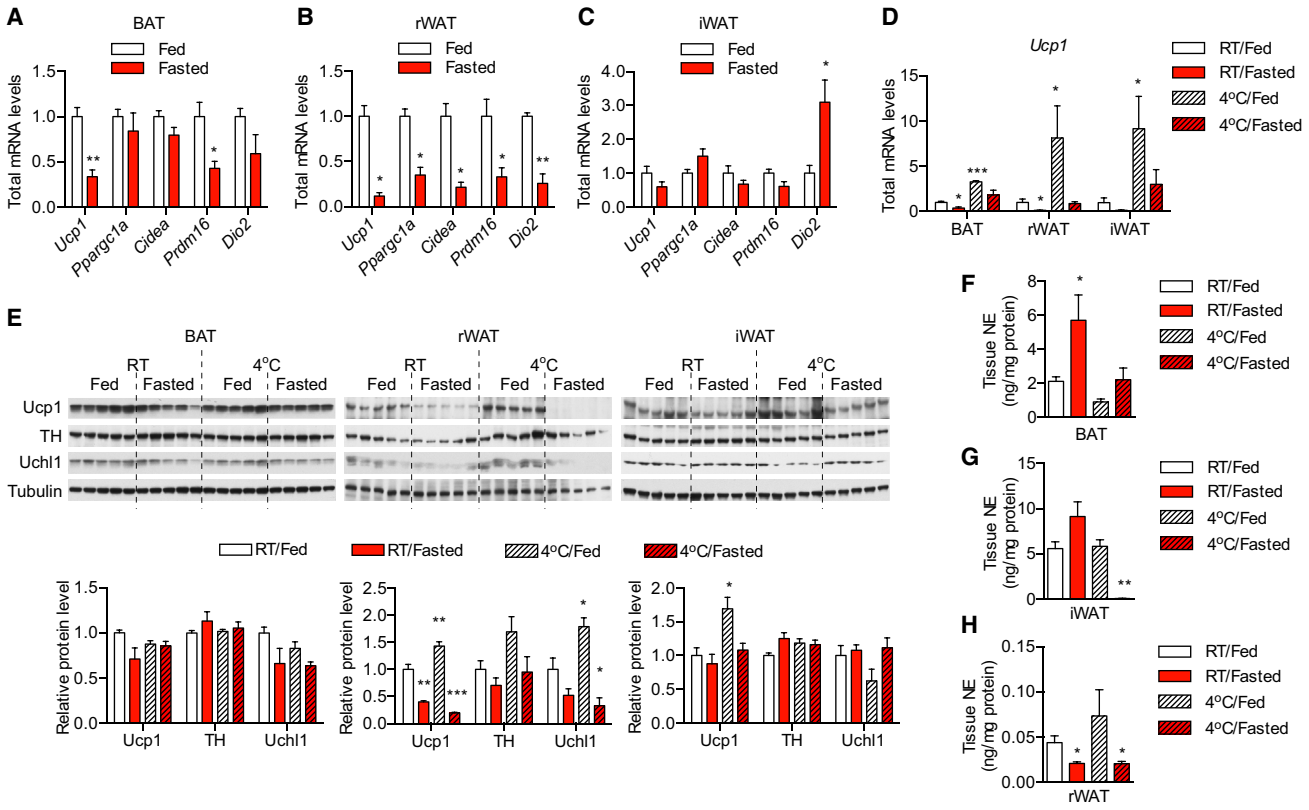

Figure 1. Fasting and AgRP Neurons Suppress WAT Browning

(A–C) Expression of thermogenic genes in different fat depots from ad libitum fed or 24 hr-fasted mice (n = 5). Same amount of RNA was used for reverse transcription followed by real-time PCR. Gene expression was first normalized to *36b4* and then relative mRNA amount per depot was calculated based on total RNA levels (Figure S1A). Total levels of thermogenic genes per depot in BAT (A), rWAT (B), and iWAT (C) are shown.

(D–H) Mice were either fed ad libitum or fasted overnight at room temperature (RT) or 4°C. (D) Expression of *Ucp1* transcript in different fat depots (n = 5). Values represent fold change relative to the RT/Fed group within each fat depot. (E) Immunoblotting showing protein levels of Ucp1, TH, and Uchl1. Densitometric analyses are shown at the bottom. (F–H) NE levels in (F) BAT, (G) iWAT, and (H) rWAT. Data are shown as mean ± SEM. *p < 0.01; **p < 0.01 by unpaired Student's t test.

See also Figure S1.

(Hart et al., 2007; Love and Hanover, 2005; Ruan et al., 2013b). Key components of insulin signaling can be O-GlcNAcylated (Ruan et al., 2013b; Whelan et al., 2010), and O-GlcNAcylation is a negative regulator of insulin signaling (Yang et al., 2008). Transgenic mice overexpressing OGT in skeletal muscle and fat exhibit elevated circulating insulin levels and insulin resistance (McClain et al., 2002). O-GlcNAcylation of transcription factors and cofactors such as FOXO1, CRTC2, and PGC-1α promotes the expression of gluconeogenic genes in liver (Dentin et al., 2008; Housley et al., 2008; Housley et al., 2009; Ruan et al., 2012). These studies demonstrate a vital role for O-GlcNAc signaling in metabolic regulation in peripheral tissues. However, the central roles of O-GlcNAc signaling in metabolic regulation have not been explored.

Here, we show that OGT expression is enriched in hypothalamic AgRP neurons and induced by fasting and ghrelin. Pharmacogenetical activation of AgRP neurons suppresses the thermogenic program in WAT, while the selective knockout of *Ogt* in AgRP neurons inhibits neuronal activity, promotes WAT browning, and protects mice against diet-induced obesity.

RESULTS

Fasting Suppresses Thermogenic Program in WAT

A major component of energy homeostasis is to adjust energy expenditure according to the level of energy intake (Apfelbaum et al., 1971; Shibata and Bukowiecki, 1987; Welle and Campbell, 1983). Given that WAT browning is an emerging regulator of energy expenditure, we test whether food availability regulates the browning process. Four adipose depots including classic BAT, gonadal WAT (gWAT), and two major depots that have the potential of browning—retroperitoneal and inguinal WAT (rWAT and iWAT)—from ad libitum fed and 24 hr-fasted mice were collected (Fisher et al., 2012; Guerra et al., 1998; Nedergaard and Cannon, 2013). Fasting reduced total RNA level in most depots (Figure S1A available online), thus thermogenic gene expression was determined by relative real-time PCR and calculated as total level per depot (Nedergaard and Cannon, 2013). *Ucp1* expression was significant decreased in BAT and rWAT (Figures 1A and 1B) and showed a tendency of reduction in iWAT and gWAT in fasted mice as compared to fed controls

(Figures 1C and S1B). The expression of other thermogenic genes including *Ppargc1a*, *Prdm16*, *Cidea*, and *Dio2* during fasting was significantly suppressed in rWAT, but mainly unchanged in BAT, iWAT, and gWAT (Figures 1A–1C and S1B). These data suggest that rWAT is the major depot responsible for the inhibitory effect of fasting on thermogenesis.

Cold exposure has been extensively shown as a physiological stimulator of BAT activation and WAT browning (Cinti, 2012). However, cold exposure did not efficiently induce *Ucp1* transcription in any fat depots when animals were deprived of food, indicating that fasting diminishes the effect of cold on thermogenesis (Figures 1D and S1C). When we examined the levels of Ucp1 protein in these fat depots, we found that fasting downregulated Ucp1 in rWAT but not in BAT and iWAT (Figure 1E). Sympathetic outflow to BAT and WAT controls the expression of thermogenic genes and heat production in brown and beige fat (Harms and Seale, 2013). Thus we hypothesized that changes in sympathetic nerve activity in response to stimuli determine the thermogenic program in different depots. Fasting increased levels of norepinephrine (NE) in serum (Figure S1D), BAT, and iWAT (Figures 1F and 1G). However, NE level only in rWAT was decreased during fasting (Figure 1H), correlated with the reduction in thermogenic gene expression. Fasting also dampened the induction of NE level in rWAT by cold (Figure 1H). In addition, fasting downregulated while cold upregulated the levels of tyrosine hydroxylase (TH), a marker of sympathetic nerve, and ubiquitin carboxyl-terminal esterase L1 (Uchl1), a general marker for peripheral neurons in rWAT (Figure 1E) (Burgi et al., 2011; Wilkinson et al., 1989). Taken together, these data suggest that fasting controls sympathetic outflow and regulates browning in rWAT.

Acute Activation of AgRP Neurons Suppresses Thermogenic Program in WAT

Orexigenic AgRP/NPY neurons in the hypothalamus are critical for energy homeostasis and glucose metabolism in response to nutrient and hormonal cues (Belgardt et al., 2009). During fasting, the activation of AgRP neurons provokes animals to seek food and simultaneously suppresses energy expenditure (Dietrich and Horvath, 2012; Small et al., 2001). To determine whether AgRP neurons regulate WAT browning, we took advantage of a chemical genetics approach that allows for acute, cell type-specific control of neuronal activity in vivo. Specifically, we generated mice expressing the cation channel Trpv1 only in AgRP neurons (Figure 2A) (Arenkiel et al., 2008). Capsaicin is a Trpv1 agonist that will induce the depolarization and activation of AgRP neurons in *Trpv1*$^{-/-}$*;AgRP-Cre*$^{+}$*;R26*^{Trpv1} mice. Acute activation of AgRP neurons by systemic injection of capsaicin (10 mg/kg, intraperitoneally [i.p.]) for only 1 hr strongly inhibited the expression of thermogenic genes including *Ucp1*, *Ppargc1a*, *Prdm16*, and *Cidea* in rWAT, and to a less extent in iWAT, but not in classic BAT or visceral gWAT in *Trpv1*$^{-/-}$*;AgRP-Cre*$^{+}$*;R26*^{Trpv1} mice (Figure 2B). Activation of AgRP neurons significantly reduced energy expenditure in *Trpv1*$^{-/-}$*;AgRP-Cre*$^{+}$*;R26*^{Trpv1} mice, compared to *Trpv1*$^{-/-}$*;AgRP-Cre*$^{-}$*;R26*^{Trpv1} mice (Figure 2C). Food was removed during these studies to eliminate the effect of diet-induced thermogenesis. Thus far, these data indicate that acute activation of AgRP neurons decreases energy expenditure and thermogenenic gene expression profile in selected fat depots.

To test the physiological importance of AgRP neuron-regulated browning, capsaicin-injected mice were immediately placed at 4°C. Core body temperature dropped lower in *Trpv1*$^{-/-}$*;AgRP-Cre*$^{+}$*;R26*^{Trpv1} mice (Figure 2D), suggesting that AgRP activation inhibits cold-induced thermogenesis. Gene expression analyses showed that cold promoted *Ucp1* transcription in BAT (Figure 2E), but not in rWAT (Figure 2F) of *Trpv1*$^{-/-}$*;AgRP-Cre*$^{+}$*;R26*^{Trpv1} mice, indicating that thermogenic program in rWAT is specifically inhibited by AgRP neurons. Acute activation of AgRP neurons did not change serum levels of NE (Figure 2G). However, we observed a reduction of NE level specifically in rWAT of *Trpv1*$^{-/-}$*;AgRP-Cre*$^{+}$*;R26*^{Trpv1} mice (Figure 2H). Treatment with a selective β3 agonist, CL-316, 243 rescued the decrease in body temperature and *Ucp1* expression in rWAT of capsaicin-injected *Trpv1*$^{-/-}$*;AgRP-Cre*$^{+}$*;R26*^{Trpv1} mice (Figures 2I and 2J). These data demonstrate that acute activation of hunger-promoting AgRP neurons suppresses browning in rWAT by regulating sympathetic activity.

OGT Controls AgRP Neuronal Activity

We then sought to determine possible nutrient sensors in AgRP neurons that respond to fasting. Previously, we have shown that O-GlcNAcylation of insulin signaling proteins and transcriptional regulators in peripheral tissues is important for glucose and lipid metabolism (Li et al., 2013; Ruan et al., 2012, 2013b; Yang et al., 2008). Expression of OGT and overall O-GlcNAc levels (Figures S2A and S2B) in the hypothalamus are significantly higher than peripheral tissues such as liver, WAT, and muscle. However, little is known about the role of O-GlcNAc modification in the hypothalamic regulation of metabolism. To determine the relative levels of *Ogt* transcripts in AgRP neurons, we isolated AgRP neuron-specific ribosome-associated mRNAs from the arcuate nucleus of *AgRP-Cre*$^{+}$*;RPL22*^{HA} mice by immunoprecipitation of the actively translating polyribosomes that were tagged with hemagglutinin (HA) epitope (Sanz et al., 2009). *Ogt* transcripts showed a 4-fold enrichment in AgRP neurons (Figure 3A). Consistently, immunohistochemistry demonstrated that a subset of AgRP/NPY neurons have relatively high levels of OGT proteins and O-GlcNAcylation (Figures 3B and 3C). Food deprivation for 24 hr increased OGT expression and O-GlcNAc levels in AgRP neurons (Figures 3B and 3C). Ghrelin is a hormone released by the empty stomach that promotes hunger by activating AgRP neurons in the hypothalamus (Andrews et al., 2008; Chen et al., 2004; Liu et al., 2012; Luquet et al., 2007; Wiedmer et al., 2011). We found that ghrelin increased O-GlcNAc levels in AgRP neurons (Figure 3D) and reduced levels of Ucp1 protein in rWAT (Figure S2C). These data point to the possibility that O-GlcNAcylation functions as a fasting signal in AgRP neurons.

To determine the physiological role of O-GlcNAc signaling in AgRP neurons, we generated AgRP neuron-specific *Ogt* knockout (KO) mice (Figure S2D). Immunofluorescent staining of OGT on *Npy-hrGFP* hypothalamus showed that OGT was specifically deleted in AgRP neurons (Figure S2E). Real-time PCR and western blot analyses confirmed that OGT was not ectopically deleted in the whole hypothalamus, cortex, or other peripheral metabolic tissues (Figures S2F and S2G). To identify AgRP neurons during electrophysiological studies, *AgRP-Ogt* KO mice were cross-bred into the *Npy-hrGFP* background (Figure 3E).

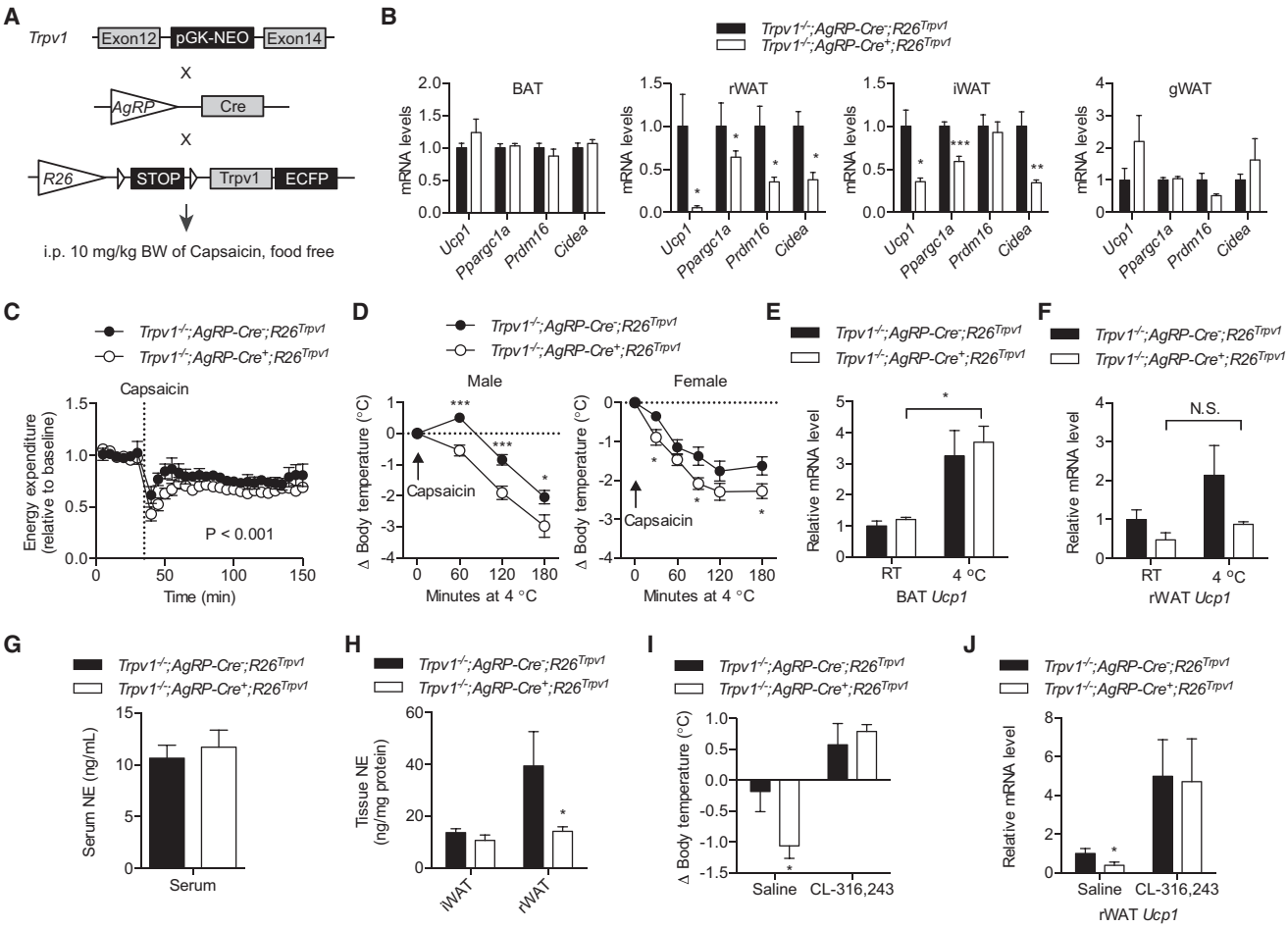

Figure 2. Acute Activation of AgRP Neurons Suppresses the Thermogenic Program in WAT

(A) Ten mg/kg body weight of capsaicin was injected to *Trpv1*$^{-/-}$;*AgRP-Cre*$^{-}$;*R26*^{Trpv1} (control) or *Trpv1*$^{-/-}$;*AgRP-Cre*$^{+}$;*R26*^{Trpv1} transgenic mice. Food was removed during all the experiments.

(B) Thermogenic gene expression in adipose tissues, 1 hr after capsaicin injection (n = 4).

(C) Changes in energy expenditure of mice after capsaicin injection (n = 4).

(D) Body temperature of mice during cold challenge immediately after capsaicin injection (n = 9–11).

(E and F) *Ucp1* expression in BAT (E) and rWAT (F) of capsaicin-injected mice at RT or 4°C for 2 hr (n = 4–6).

(G) Serum levels of NE of mice after 2 hr of capsaicin injection (n = 8).

(H) Levels of NE in iWAT and rWAT of mice after 2 hr of capsaicin injection (n = 8).

(I and J) Mice were injected with saline or 1 mg/kg body weight of CL-316, 243 at the same time with capsaicin. (I) Change in core body temperature (n = 6–8). (J) Levels of *Ucp1* transcript in rWAT (n = 4–6). Data are shown as mean ± SEM. *p < 0.05; **p < 0.01; ***p < 0.001 by unpaired Student's t tests.

Whole-cell current clamp measurements demonstrated that the membrane potential of AgRP neurons was similar between control (CT) and KO mice (Figure 3F). However, the spontaneous firing rate was reduced in KO mice (Figures 3G and 3H).

OGT Modulates the Potassium Channel in AgRP Neurons

Voltage-dependent potassium (K_V) channels mediate the repolarization and after-hyperpolarization phases of action potential, and defects in K_V current lead to dampened activity but intact membrane potential in neurons (Bean, 2007). Electrophysiological analyses showed a reduction in outward K^+ current in AgRP neurons from KO mice compared to CT mice (Figures 4A and 4B). The K^+ current in AgRP neurons was slowly inactivated, suggesting a possible involvement of delayed rectifier K_V channels. Kcnq3 (K_V7.3), mediating delayed rectifier K^+ current, is expressed in AgRP neurons (Ren et al., 2012). We found that OGT interacted with Kcnq3 in the hypothalamus, and fasting enhanced their interaction (Figure 4C). Kcnq3 has been shown to be O-GlcNAc-modified at murine synapse (Trinidad et al., 2012), and mutation of the O-GlcNAc site Threonine 655 to Alanine (T655A) almost abolished O-GlcNAcylation on Kcnq3 (Figure 4D). Then we assessed Kcnq3 activity and found that T655A mutant channel showed a significant reduction in K^+ current compared to the wild-type Kcnq3 (Figures 4E and 4F), suggesting that O-GlcNAcylation of this K_V channel is a key

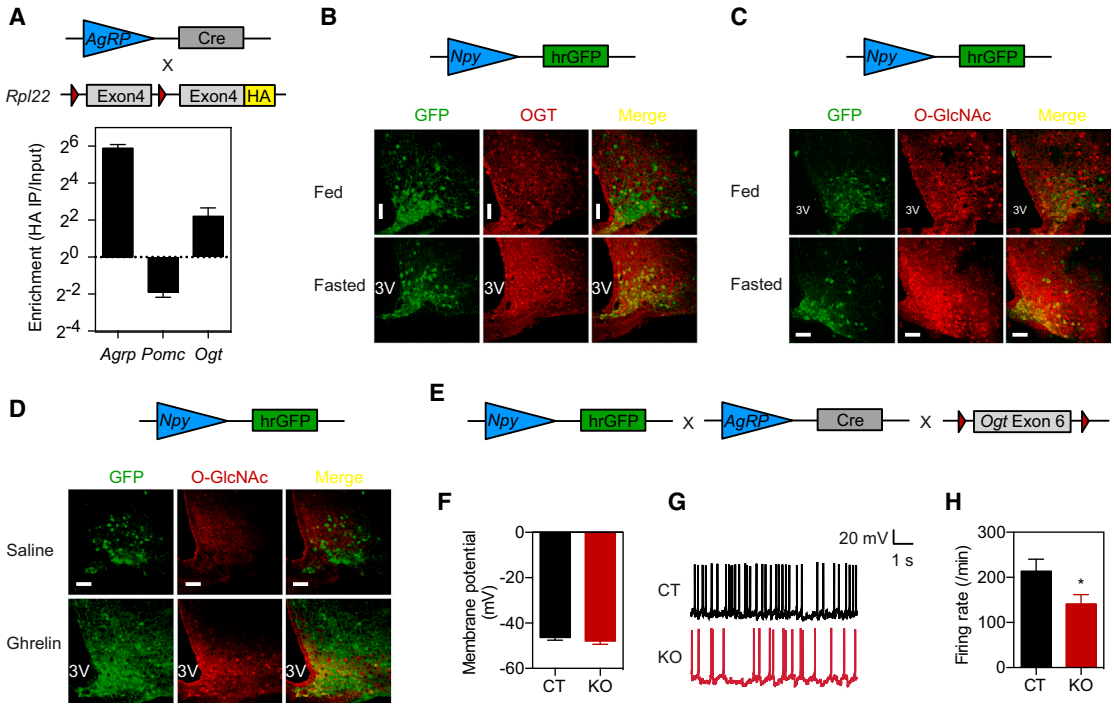

Figure 3. OGT Is Required for AgRP Neuronal Activity

(A) Ribosome-associated mRNAs were isolated from the arcuate nucleus of *AgRP-Cre*$^{+}$*; RPL22*^{HA} mice, and real-time PCR was performed to determine the enrichment of *Ogt* transcripts in HA immunoprecipitation compared to the input (n = 4). *Agrp* and *Pomc* transcripts were used as controls.

(B) Immunostaining of OGT in the hypothalamus of fed and overnight-fasted *Npy-hrGFP* mice.

(C) Immunostaining of O-GlcNAc in the hypothalamus of fed and overnight-fasted *Npy-hrGFP* mice.

(D) Immunostaining of O-GlcNAc in the hypothalamus of *Npy-hrGFP* mice injected with saline or 120 mmol/kg body weight of ghrelin for 1 hr.

(E) *AgRP-Cre*$^{-}$*;Ogt*^{flox} (CT) and *AgRP-Cre*$^{+}$*;Ogt*^{flox} (KO) mice were crossbred onto *Npy-hrGFP* background for the whole-cell current-clamp recordings.

(F) Basal membrane potential of AgRP neurons (n = 19).

(G) Representative tracing of action potentials of AgRP neurons.

(H) Firing rate of AgRP neurons (n = 19). Data are shown as mean ± SEM. *p < 0.05 by unpaired Sstudent's t test. 3V, 3rd ventricle. Scale bar represents 50 μm. See also Figure S2.

regulatory mechanism underlying cellular excitability. Taken together, *AgRP-Ogt* KO mice are intrinsically defective in the activity of K_V channels and neuronal firing, serving as a model to study metabolic roles of AgRP neurons.

Ogt Knockout in AgRP Neurons Promotes Thermogenic Program in WAT

Acute activation of AgRP neurons specifically suppressed rWAT browning (Figure 2), thus we hypothesized that impaired AgRP neuronal activity in *AgRP-Ogt* knockout mice would induce a thermogenic gene program in rWAT. As expected, the levels of *Ucp1* and *Cidea* mRNA were significantly increased in rWAT (Figure 5A), but remained unchanged in BAT of KO mice as compared to CT mice (Figure 5B). Consistently, uncoupled oxygen consumption rate (OCR) in BAT remained the same, while uncoupled OCR in rWAT was higher, when comparing KO mice to CT mice (Figure 5C). Blocking the β3 adrenergic receptor by SR59230A restored *Ucp1* expression in rWAT (Figure 5D), strengthening the notion that AgRP neurons control rWAT browning through SNS.

BAT of KO mice remained susceptible to the suppression of thermogenic genes by fasting (Figure 5E, compared to Figure 1A). In contrast, this suppression was abolished in rWAT of KO mice (Figure 5F, compared to Figure 1B). Ghrelin also failed to downregulate Ucp1 protein levels in rWAT of KO mice (Figure S3A). These data demonstrate that O-GlcNAc signaling in AgRP neurons is required for the regulation of WAT browning by fasting and ghrelin. As a result, *AgRP-Ogt* KO mice showed less reduction in energy expenditure than CT mice during the first 24 hr of fasting (Figure 5G) with concomitant increase in weight loss (Figure 5H). Nevertheless, there was no significant reduction in body weight of ad libitum KO mice (Figure S3B).

The defect in AgRP neuronal activity is normally associated with decreased feeding behavior (Dietrich et al., 2010). However, there was no change in food intake in *AgRP-Ogt* KO mice (Figure S3C). This is possibly due to the overproduction of *Agrp* and *Npy* transcripts via unknown compensatory mechanisms (Figure S3D), and/or the OGT-positive subset of AgRP neurons does not directly modulate feeding. Cold exposure did not affect OGT expression in AgRP neurons (Figure S3E), and *AgRP-Ogt* KO mice and control mice under fed conditions showed similar core body temperature during cold challenge (Figure S3F), indicating that the silencing of AgRP neurons either by feeding or by OGT deletion abolishes the impact of this neural circuit on cold-induced thermogenesis.

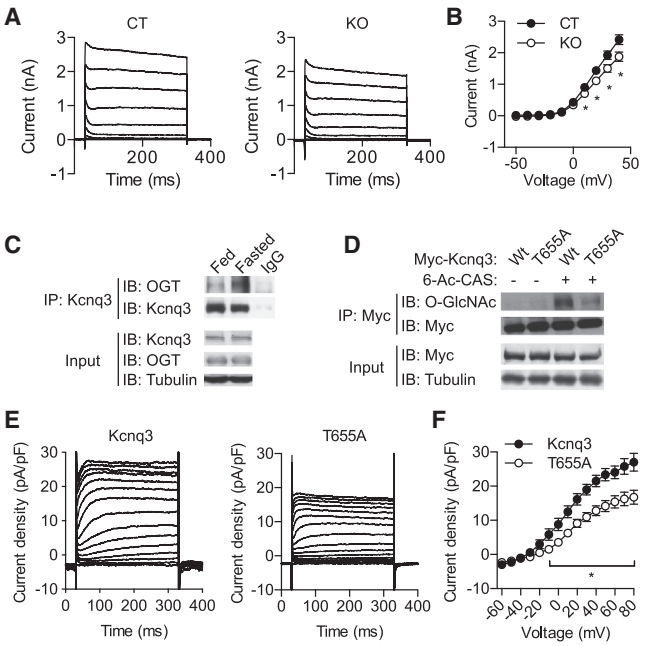

Figure 4. O-GlcNAcylation Modulates the Voltage-Dependent Kcnq3 Channel

(A) Ten mV-stepwise whole-cell voltage-clamp (−50 mV to 40 mV) was performed to record K^+ current in *Npy-hrGFP*-positive cells (n = 6–8).

(B) Current-voltage curve of K^+ currents at 300 ms in (A).

(C) Immunoprecipitation showing interaction between OGT and Kcnq3 in fed and fasted hypothalamus.

(D) Myc-tagged wild-type and T655A Kcnq3 were expressed in HEK293 cells. O-GlcNAc levels were determined by Myc immunoprecipitation followed by western blotting. 6-Ac-CAS, a specific inhibitor of O-GlcNAcase to increase O-GlcNAc levels.

(E) HEK293 cells were transfected with wild-type or T655A Kcnq, K^+ currents were recorded by whole-cell voltage-clamp (−60 to 80 mV) and then current density was calculated.

(F) Current density-voltage curve of wild-type and T655A Kcnq3 at 300 ms in E. Data are shown as mean ± SEM. *$p < 0.05$ by unpaired Student's t test.

It is reported that AgRP neurons regulate hepatic gluconeogenesis and that the browning of WAT improves glucose metabolism in mice (Könner et al., 2007; Qian et al., 2013; Seale et al., 2011). We observed a decrease in hepatic expression of gluconeogenic genes including *Ppargc1a*, *G6pc*, and *Pck1* in KO mice (Figure 5I). Gluconeogenesis in *AgRP-Ogt* KO mice was downregulated as shown by decreased blood glucose levels during pyruvate tolerance test and glucose tolerance test (Figures 5J and 5K). No changes in insulin levels or insulin sensitivity were observed (Figures S3G and S3H). These data demonstrate that *Ogt* knockout in AgRP neurons improves glucose metabolism in mice.

Ogt Knockout in AgRP Neurons Protects against Diet-Induced Obesity and Insulin Resistance

Next, we challenged the mice with high fat diet (HFD). Consistent with the findings in mice on NC, thermogenic genes including *Ucp1*, *Ppargc1a*, *Prdm16*, and *Cidea* were dramatically increased in rWAT of *AgRP-Ogt* KO mice (Figure 6A). There were more "brown-like" adipocytes and less fat exist in rWAT of KO mice (Figures 6B and 6C). Although BAT and iWAT showed a reduction in fat weight and content (Figures 6B and 6C), the expression of thermogenic genes was comparable between KO and CT groups (Figure 6A). We did not observe any changes in weight, morphology, or gene expression in gWAT (Figures 6A–6C). We also observed that protein levels of Ucp1 and tyrosine hydroxylase were markedly elevated in rWAT of KO mice (Figure 6D). These mice also exhibited increased NE levels in rWAT but not in BAT or iWAT (Figure 6E). These data demonstrate that *Ogt* knockout in AgRP neurons selectively activates browning in rWAT of mice fed on HFD.

Consistent with the activated thermogenic program, heat production in KO mice was significantly increased compared to CT mice, as demonstrated by the metabolic cage study (Figure 6F). As a result, both female and male KO mice gained significantly less body weight and fat mass compared to CT mice (Figures 7A, 7B, S4A, and S4B), despite consuming a similar amount of HFD (Figure 7C). Although levels of fasting glucose and insulin were not significantly different (Figures 7D, 7E, S4C, and S4D), there was a reduction in the values of the homeostasis model assessment of insulin resistance (HOMA-IR) in both female and male KO mice (Figures 7F and S4E). Consistent with these observations, glucose tolerance test and insulin tolerance test showed that *AgRP-Ogt* KO mice were more glucose-tolerant and insulin-sensitive than CT mice (Figures 7G, 7H, and S4F). Taken together, these data reveal that *Ogt* deficiency in AgRP neurons increases WAT browning and protects mice from diet-induced obesity and insulin resistance.

DISCUSSION

Studies in the past few years have greatly expanded our knowledge of beige adipocytes. There is no doubt that beige fat is metabolically important, especially during cold exposure and nutrient overload. Stimulating the browning process protects mice from diet-induced obesity, whereas the ablation of beige adipocytes causes metabolic dysfunction (Cohen et al., 2014; Seale et al., 2011). In this study, we identify fasting as a negative, physiological regulator of the thermogenic program in beige adipocytes. Intriguingly, fasting diminishes the effect of cold exposure on thermogenesis, suggesting that fasting is a predominant regulator of browning in order to conserve energy for survival.

The hypothalamus has been long proposed to regulate adaptive thermogenesis in BAT, independently on its regulation on food intake (Kong et al., 2012; Vogt and Brüning, 2013). Neuropeptides AgRP and NPY have been shown to inhibit BAT function, while α-MSH increases SNS activity and BAT function (Shi et al., 2013; Yasuda et al., 2004). It is not known whether these circuits also control WAT browning. In this study, we demonstrate that chemical-genetic activation of AgRP neurons acutely suppresses the thermogenic program in beige fat, demonstrating that white fat browning is a highly dynamic and reversible process. Conversely, impairment in AgRP neuronal activity abolishes fasting-mediated inhibition of WAT browning. These results reveal the dynamic nature of WAT browning and identify a specific neuronal population that negatively regulates this process.

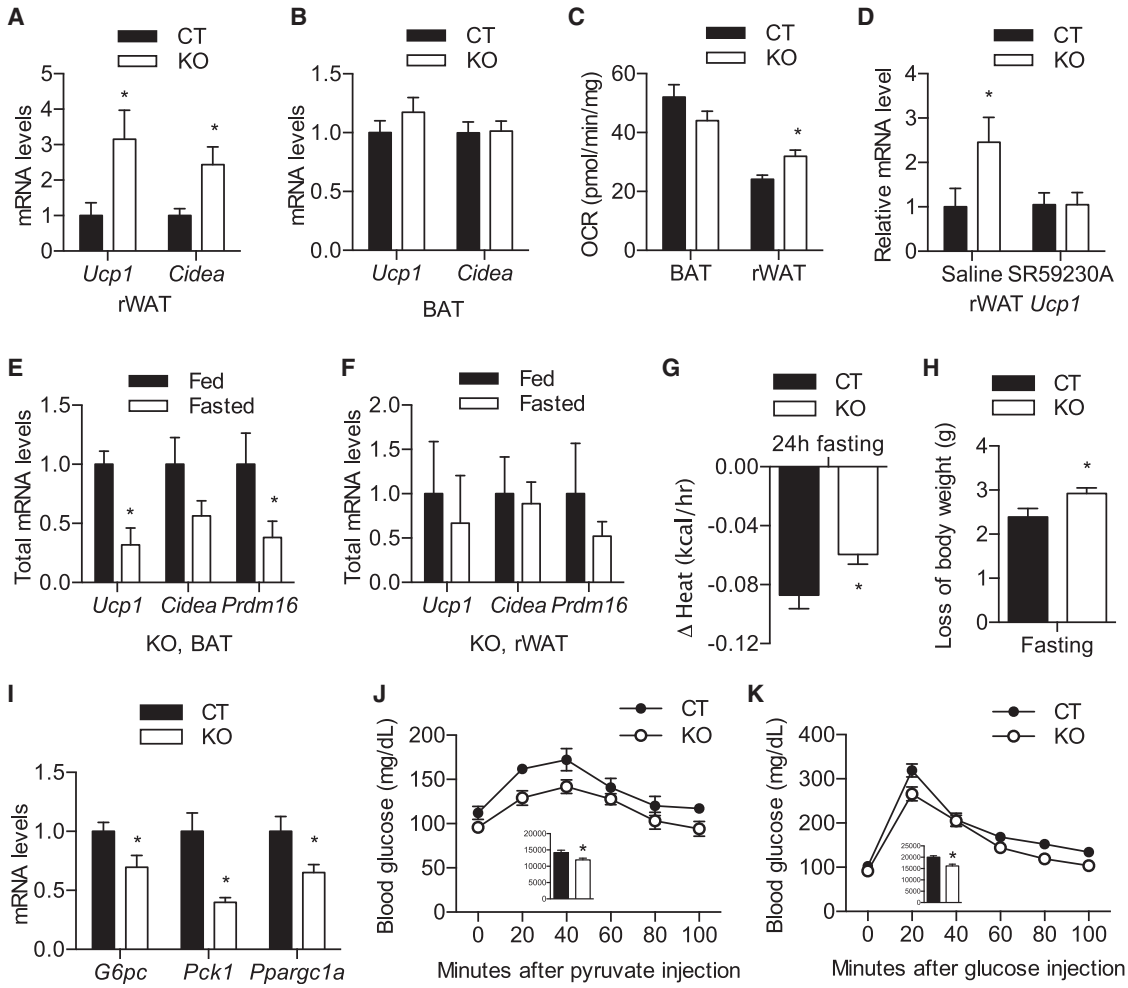

Figure 5. Loss of *Ogt* in AgRP Neurons Promotes Browning and Improves Glucose Metabolism in Mice Fed on Normal Chow

(A and B) Expression of thermogenic genes in rWAT (A) and BAT (B) of 6-month-old female mice (n = 4).

(C) Oxygen consumption rate of BAT and rWAT in the presence of oligomycin, an ATPase inhibitor (n = 8).

(D) Expression of *Ucp1* in rWAT from mice treated with 3 days of saline or SR59230A (n = 4–6).

(E and F) Expression of thermogenic genes in BAT (E) and rWAT (F) from fed and 24 hr-fasted *AgRP-Ogt* KO female mice (n = 3–4). Total amounts of mRNA were calculated based on relative mRNA levels and total amounts of RNA isolated.

(G and H) Loss of energy expenditure (G) and body weight (H) in CT and KO female mice after fasting for 24 hr (n = 6–15).

(I) Expression of gluconeogenic genes in liver of 6-month-old female mice (n = 3–4).

(J) Pyruvate tolerance test in 5-month-old female mice (n = 4–7). Insert, area under curve (AUC).

(K) Glucose tolerance test in 5-month-old female mice (n = 8–12). Inset, AUC. Data are shown as mean ± SEM. *p < 0.05 by unpaired Student's t test.

See also Figure S3.

Fasting and AgRP neuronal activation appear to regulate browning preferentially in rWAT, to a much less extent in other WAT depots but not in BAT. We demonstrate that uniquely in rWAT, sympathetic nerve activity correlates with thermogenic gene expression and browning during cold and fasting stimuli. In this regard, mapping the neuronal circuits linking AgRP neurons to sympathetic innervation onto different WAT depots would provide further insights. It is also possible that other mechanisms may mediate the effect of AgRP neurons on WAT browning. Although as a relative small depot, rWAT responds much quicker than BAT and other WAT depots after cold exposure or food deprivation. This suggests that browning in rWAT may function as a first line of defense to maintain energy homeostasis when food availability and environmental temperature are fluctuant.

O-GlcNAc signaling has long been proposed as a nutrient sensor in multiple peripheral tissues. Hyperglycemia-associated elevation in O-GlcNAc levels mediates many aspects of glucotoxicity (Ruan et al., 2013b). On the other hand, O-GlcNAc levels can also be increased by glucose deprivation in several cell types (Cheung and Hart, 2008; Kang et al., 2009; Taylor et al., 2008). Consistent with the latter observations, we demonstrate that OGT expression and O-GlcNAc modification increase in AgRP neurons in response to fasting and ghrelin, although the molecular mechanism has yet to be defined. Genetic ablation

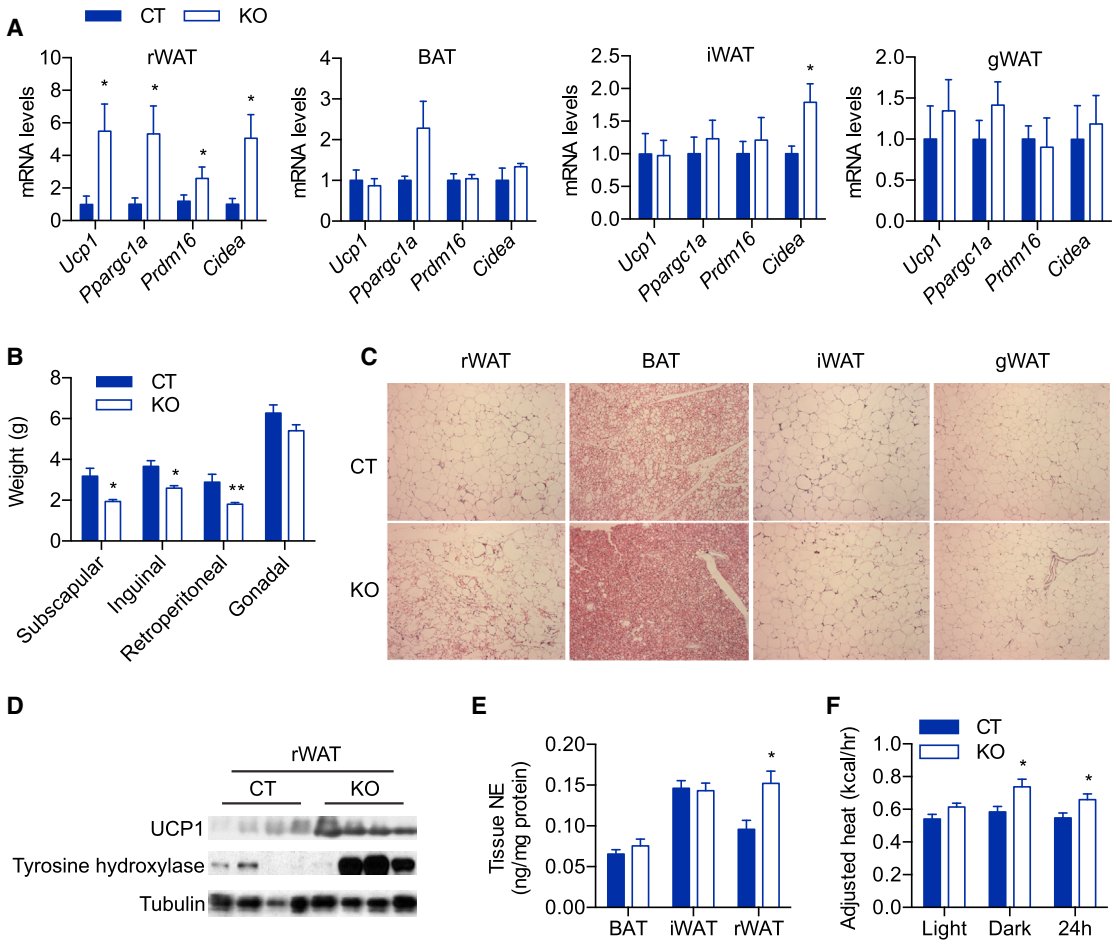

Figure 6. Browning Phenotypes in *AgRP-Ogt* Mice on HFD

(A) Thermogenic gene expression in different fat depots from 10-month-old female HFD mice (n = 5–7).

(B) Weight of fat depots in 10-month-old female HFD mice (n = 5–6).

(C) H&E staining of adipose tissues from 10-month-old female HFD mice.

(D) Immunoblotting of UCP1 and tyrosine hydroxylase in rWAT of 10-month-old female HFD mice.

(E) Norepinephrine levels in fat depots (n = 12).

(F) Energy expenditure in 6-month-old female HFD mice determined by metabolic cage study followed by regressing to body weight using ANCOVA analysis (n = 11). Data are shown as mean ± SEM. *p < 0.05; **p < 0.01 by unpaired Student's t test.

of OGT in AgRP neurons promotes WAT browning, thus leading to improved glucose and energy metabolism. Mouse models with defective BAT often fail to maintain their body temperature upon cold exposure (Feldmann et al., 2009). However, OGT expression in AgRP is not affected by cold, and *AgRP-Ogt* KO mice maintain a normal core temperature upon cold exposure. These observations prompt the hypothesis that brown fat primarily maintains homeothermy to combat cold, whereas beige fat regulates energy metabolism in response to nutrient stress. This notion is supported by the recent finding that PRDM16 ablation in beige fat does not affect body temperature in mice (Cohen et al., 2014).

Neuronal circuits in the arcuate nucleus of the hypothalamus are relatively tolerant to perturbations, especially during developmental and neonatal stages. Neonatal ablation of AgRP neurons has minimal effects on feeding, although ablation of these neurons in adults causes rapid starvation (Luquet et al., 2005). Genetic knockout of *Agrp* gene in mice also does not affect food intake (Qian et al., 2002). These data suggest that neuronal plasticity can compensate for the loss of *Agrp* gene or AgRP neurons. In our study, the deletion of *Ogt* in AgRP neurons occurs early during development. Although neuronal activity is decreased in *AgRP-Ogt* KO mice, the expression of *Agrp* and *Npy* transcripts is elevated, which may contribute to the maintenance of normal food intake.

Hunger and cold are two life-history variables during the development and evolution of mammals. We have observed that food deprivation (the negative regulator) dominates over cold exposure (the positive regulator) in the central control of WAT browning. This regulatory system may be evolutionarily important as it can reduce heat production to maintain energy balance during fasting. Modulating the hypothalamic control of WAT browning

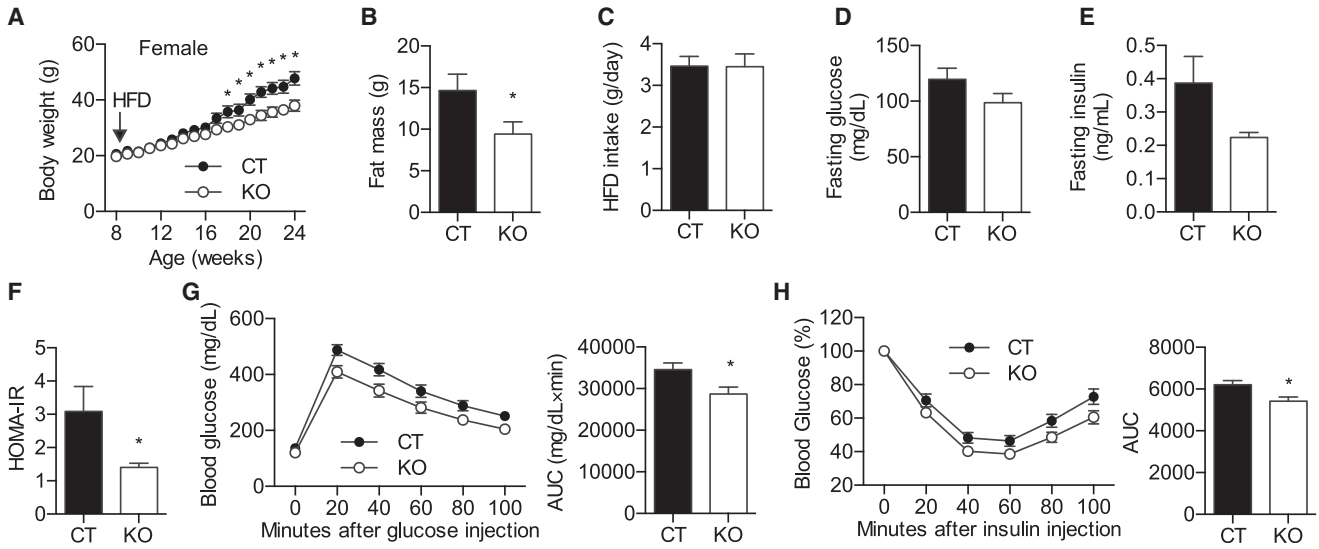

Figure 7. Loss of *Ogt* in AgRP Neurons Protects Mice from Diet-Induced Obesity and Insulin Resistance

(A) Growth curve of female mice fed with HFD (n = 12–13).

(B) Fat mass of 5-month-old female HFD mice (n = 12–13).

(C) Daily intake of HFD in 2-month-old female mice (n = 6).

(D–F) Fasting blood glucose (D), fasting serum insulin (E), and HOMA-IR (F) in 6-month-old female HFD mice (n = 6).

(G) Glucose tolerance test in 5-month-old female HFD mice. Area under curve (AUC) is shown to the right (n = 17–19).

(H) Insulin tolerance test in 5-month-old female HFD mice. Area under curve (AUC) is shown to the right (n = 12–13). Data are shown as mean ± SEM. *$p < 0.05$ by unpaired Student's t test.

See also Figure S4.

represents a potential strategy to combat obesity and associated morbidity.

EXPERIMENTAL PROCEDURES

Mice

Ogt-floxed mice on C57BL/6 background (Shafi et al., 2000) were kindly provided by Dr. Steven Jones (University of Louisville). *AgRP-Cre* mice, kindly donated by Alison Xu (University of California San Francisco), have been maintained in our colony on a mixed background (Xu et al., 2005). *Trpv1*^{tm1Jul}/J mice (#003770), *Gt(ROSA)26Sor*$^{tm1(Trpv1,ECFP)Mde}$/J (#008513), and *Npy-hrGFP* mice (#006417), which express humanized *Renilla* GFP under the control of the mouse *Npy* promoter, were from Jackson Laboratory. To express Trpv1 selectively in AgRP neurons, we have bred both Trpv1 colonies to a second *AgRP-Cre* line (*Agrp*$^{tm1(cre)Lowl}$/J, #012899, Jackson Laboratory). All animals were kept on a 12 hr:12 hr light:dark cycle. Mice were free to access water and either fed on a standard chow diet or 60% high fat diet (Research Diets). Ten mg/kg body weight (BW) of capsaicin, 1 mg/kg BW of CL-316, 243 (R&D Systems), and 120 mmol/kg BW of ghrelin (Enzo) were i.p. injected when indicated. Indicated mice were treated with 5 mg/kg BW of SR59230A (Abcam) for 3 consecutive days, and tissues were collected 2 hr after the final injection. All procedures have been approved by the Institutional Animal Care and Use Committee of Yale University.

Metabolic Assays

Body weights were recorded every week. Body composition was assessed using an EchoMRI system. For food intake measurement, mice were individually housed for at least 1 week for environmental habituation, and food consumption was weighed every morning for 7 consecutive days. For the metabolic cage study, mice were acclimated in metabolic chambers (TSE Systems) for 3 days and then gas exchange, food intake, and ambulatory activity were recorded continuously for another 3 days. Heat production was calculated and adjusted to body weight (Tschöp et al., 2012). Body temperature was measured rectally using a thermo-coupler (Physitemp). For pyruvate-, glucose-, and insulin-tolerance tests, 16-hour-fasted mice were injected with intraperitoneally with sodium pyruvate (1.5 g/kg body weight) or glucose (1.5 g/kg body weight); 6 hr fasted mice were injected with insulin (1 U/kg body weight). Blood glucose from tail-vein blood collected at the designated times was measured using a Nova Max Glucometer. Insulin (Millipore) and norepinephrine (Abnova) were determined using ELISA kits.

Electrophysiology

Mice were anesthetized with isoflurane and sacrificed by decapitation. The brain was gently removed from the skull and chilled in 4°C oxygenated high-sucrose solution containing (mM): sucrose 220, KCl 2.5, NaH_2PO_4 1.23, $NaHCO_3$ 26, $CaCl_2$1, $MgCl_2$ 6 and glucose 10, pH 7.3 with NaOH. The brain was trimmed to a large block containing the hypothalamus and then sliced on a vibrating microtome. Coronal, 300 μm, slices were cut through the full extent of the arcuate nucleus/lateral hypothalamus. Slices were maintained in artificial cerebrospinal fluid (ACSF, containing in mM: NaCl, 126; KCl, 2.5; $MgCl_2$, 1.2; $CaCl_2 \times 2H_2O$, 2; $NaH_2PO_4 \times H_2O$, 1.2; $NaHCO_3$, 26; glucose, 10) for 1 hr at room temperature in 95% O_2 5% CO_2 saturated ACSF prior to recordings. Perforated whole-cell current clamp were used to observe spontaneous action potentials. Slices were maintained at 34°C and perfused continuously with ACSF (bubbled with 5% CO_2 and 95% O_2) containing (in mM): NaCl, 124; KCl, 3; $CaCl_2$, 2; $MgCl_2$, 2; NaH_2PO_4, 1.23; $NaHCO_3$, 26; glucose, 2.5; sucrose 7.5; pH 7.4 with NaOH. Tetrodotoxin (0.001 mM) and CdCl2 (0.05 mM) were added in ACSF for Kv current recording. All data were sampled at 3–10 kHz and filtered at 1–3 kHz. Whole-cell voltage clamp recordings were obtained with a Multiclamp 700B amplifier. The patch pipette was made of borosilicate glass with a Sutter puller. The tip resistance of the recording pipettes was 2–4 MΩ after filling with a pipette solution containing (mM): potassium methanesulfonate 135, $MgCl_2$ 2, HEPES 10, EGTA 1.1, Mg-ATP 2, and Na_2-phosphocreatin 10, Na_2-GTP 0.3, pH 7.3 with KOH. Cells were held at –80 mV and step depolarized to +40 mV with 10 mV increments. All data were sampled and analyzed with Axograph X.

Ribosome RNA Enrichment

For ribosome profiling, the methods used here were in accordance with the original description of the animal model with minor modifications (Dietrich et al., 2013; Sanz et al., 2009). Fifty-day-old mice (from both genders) were sacrificed and five or six hypothalami were pooled for each n. A total of n = 4 was used. After RNA isolation, we obtained ~25 ng of RNA per sample. Only samples with high enrichment for *Agrp* and *Npy* were used for *Ogt* gene expression analyzes.

RNA and Real-Time PCR

Total RNA was extracted from mouse tissues using TRIzol reagent (Invitrogen). cDNA was reverse transcribed (Bio-Rad) and amplified with SYBR Green Supermix (Bio-Rad) using a LightCycler 480 real-time PCR system (Roche). All data were normalized to the expression of *18 s* and *36b4*. Primer sequences are available on request. When comparing gene expression between fed and fasted animals, total amounts of mRNA were calculated based on relative mRNA levels and total amounts of RNA isolated from specific depots (Nedergaard and Cannon, 2013).

Cell Culture

HEK293T cells were cultured in DMEM with 10% fetal bovine serum (FBS). Transfection was performed using FuGENE HD (Promega) according to the manufacture's manual. For immunoprecipitation, whole-cell lysates were mixed with the Myc or Kcnq3 antibody and precipitated by Protein A/G agarose beads (Santa Cruz).

Western Blotting

Anti-OGT (ab96718), anti-O-GlcNAc (RL2, ab2739), and anti-UCP1 (ab10983) were from Abcam. Anti-tyrosine hydroxylase (#2792) and anti-UCHL1 (#3524) were from Cell Signaling Technology. Anti-Myc (sc-40) was from Santa Cruz Biotechnology. Anti-Kcnq3 (NBP1-74102) was from Novus. Tissues were lysed in buffer containing 1% Nonidet P-40, 50 mM Tris × HCl, 0.1 mM EDTA, 150 mM NaCl, proteinase inhibitors and protein phosphatase inhibitors. Equal amounts of protein lysate were electrophoresed on SDS-PAGE gels and transferred to PVDF membrane. Primary antibodies were incubated at 4°C for overnight. Western blotting was visualized by peroxidase conjugated secondary antibodies and ECL chemiluminescent substrate.

Histology

Mice were anesthetized for intracardial perfusion of PBS, followed by 4% paraformaldehyde. Brain and adipose depots were dissected and postfixed in 4% paraformaldehyde overnight. Coronal brain sections (50 μm) were prepared using a vibrating microtome. Paraffin sections of fat tissues were stained with hematoxylin and eosin staining (H&E). For immunofluorescence, tissue slides were blocked with 3% BSA, 0.2% TWEEN 20 in PBS, incubated with primary antibodies (1:100 dilution) overnight and secondary antibodies (Alexa Fluor 488 anti-Rabbit IgG, Alexa Fluor 594 anti-Rabbit IgG, and Alexa Fluor 594 anti-Mouse IgG, 1:400) for 1 hr. An Olympus confocal system was used for fluorescence detection.

Statistical Analyses

Results are shown as mean ± SEM. The comparisons were carried out using two-tailed unpaired Student's t test or one-way ANOVA followed by post hoc comparisons using Tukey corrections.

SUPPLEMENTAL INFORMATION

Supplemental Information includes four figures and can be found with this article online at http://dx.doi.org/10.1016/j.cell.2014.09.010.

AUTHOR CONTRIBUTIONS

H.-B.R. designed and performed most of the experiments. Z.-W.L. designed and performed electrophysiological studies. M.O.D. and T.L.H. generated essential animal models and designed and executed experiments. M.R.Z. performed ribosome-mRNA profiling. M.L., J.P.S., K.Z., R.Y., and J.W. assisted in experiments. X.Y. conceived, designed, and supervised the project. H.-B.R. and X.Y. wrote the manuscript.

ACKNOWLEDGMENTS

We thank Dr. Steven Jones from University of Louisville for providing *Ogt*-flox mice and Dr. Alison Xu from University of California at San Francisco for donating *AgRP*-Cre mice. This work was supported by NIH R01 DK089098, American Diabetes Association, and Ellison Medical Foundation to X.Y., American Heart Association Scientist Development Grant to H.-B.R., NIH DP1 DK098058 and ADA Mentor-Based Fellowship to T.L.H., and CNPq/Brazil to M.O.D. and M.R.Z.

Received: February 22, 2014
Revised: July 12, 2014
Accepted: September 2, 2014
Published: October 9, 2014

REFERENCES

Andrews, Z.B., Liu, Z.W., Walllingford, N., Erion, D.M., Borok, E., Friedman, J.M., Tschöp, M.H., Shanabrough, M., Cline, G., Shulman, G.I., et al. (2008). UCP2 mediates ghrelin's action on NPY/AgRP neurons by lowering free radicals. Nature *454*, 846–851.

Apfelbaum, M., Bostsarron, J., and Lacatis, D. (1971). Effect of caloric restriction and excessive caloric intake on energy expenditure. Am. J. Clin. Nutr. *24*, 1405–1409.

Arenkiel, B.R., Klein, M.E., Davison, I.G., Katz, L.C., and Ehlers, M.D. (2008). Genetic control of neuronal activity in mice conditionally expressing TRPV1. Nat. Methods *5*, 299–302.

Bartelt, A., and Heeren, J. (2013). Adipose tissue browning and metabolic health. Nat. Rev. Endocrinol. *10*, 24–36.

Bean, B.P. (2007). The action potential in mammalian central neurons. Nat. Rev. Neurosci. *8*, 451–465.

Belgardt, B.F., Okamura, T., and Brüning, J.C. (2009). Hormone and glucose signalling in POMC and AgRP neurons. J. Physiol. *587*, 5305–5314.

Burgi, K., Cavalleri, M.T., Alves, A.S., Britto, L.R., Antunes, V.R., and Michelini, L.C. (2011). Tyrosine hydroxylase immunoreactivity as indicator of sympathetic activity: simultaneous evaluation in different tissues of hypertensive rats. Am. J. Physiol. Regul. Integr. Comp. Physiol. *300*, R264–R271.

Chen, H.Y., Trumbauer, M.E., Chen, A.S., Weingarth, D.T., Adams, J.R., Frazier, E.G., Shen, Z., Marsh, D.J., Feighner, S.D., Guan, X.M., et al. (2004). Orexigenic action of peripheral ghrelin is mediated by neuropeptide Y and agouti-related protein. Endocrinology *145*, 2607–2612.

Cheung, W.D., and Hart, G.W. (2008). AMP-activated protein kinase and p38 MAPK activate O-GlcNAcylation of neuronal proteins during glucose deprivation. J. Biol. Chem. *283*, 13009–13020.

Cinti, S. (2012). The adipose organ at a glance. Dis. Model. Mech. *5*, 588–594.

Cohen, P., Levy, J.D., Zhang, Y., Frontini, A., Kolodin, D.P., Svensson, K.J., Lo, J.C., Zeng, X., Ye, L., Khandekar, M.J., et al. (2014). Ablation of PRDM16 and beige adipose causes metabolic dysfunction and a subcutaneous to visceral fat switch. Cell *156*, 304–316.

Dentin, R., Hedrick, S., Xie, J., Yates, J., 3rd, and Montminy, M. (2008). Hepatic glucose sensing via the CREB coactivator CRTC2. Science *319*, 1402–1405.

Dietrich, M.O., and Horvath, T.L. (2012). Limitations in anti-obesity drug development: the critical role of hunger-promoting neurons. Nat. Rev. Drug Discov. *11*, 675–691.

Dietrich, M.O., Antunes, C., Geliang, G., Liu, Z.W., Borok, E., Nie, Y., Xu, A.W., Souza, D.O., Gao, Q., Diano, S., et al. (2010). Agrp neurons mediate Sirt1's action on the melanocortin system and energy balance: roles for Sirt1 in neuronal firing and synaptic plasticity. J. Neurosci. *30*, 11815–11825.

Dietrich, M.O., Liu, Z.W., and Horvath, T.L. (2013). Mitochondrial dynamics controlled by mitofusins regulate Agrp neuronal activity and diet-induced obesity. Cell *155*, 188–199.

Feldmann, H.M., Golozoubova, V., Cannon, B., and Nedergaard, J. (2009). UCP1 ablation induces obesity and abolishes diet-induced thermogenesis in mice exempt from thermal stress by living at thermoneutrality. Cell Metab. *9*, 203–209.

Fisher, F.M., Kleiner, S., Douris, N., Fox, E.C., Mepani, R.J., Verdeguer, F., Wu, J., Kharitonenkov, A., Flier, J.S., Maratos-Flier, E., and Spiegelman, B.M. (2012). FGF21 regulates PGC-1α and browning of white adipose tissues in adaptive thermogenesis. Genes Dev. *26*, 271–281.

Guerra, C., Koza, R.A., Yamashita, H., Walsh, K., and Kozak, L.P. (1998). Emergence of brown adipocytes in white fat in mice is under genetic control. Effects on body weight and adiposity. J. Clin. Invest. *102*, 412–420.

Hahn, T.M., Breininger, J.F., Baskin, D.G., and Schwartz, M.W. (1998). Coexpression of Agrp and NPY in fasting-activated hypothalamic neurons. Nat. Neurosci. *1*, 271–272.

Harms, M., and Seale, P. (2013). Brown and beige fat: development, function and therapeutic potential. Nat. Med. *19*, 1252–1263.

Hart, G.W., Housley, M.P., and Slawson, C. (2007). Cycling of O-linked beta-N-acetylglucosamine on nucleocytoplasmic proteins. Nature *446*, 1017–1022.

Housley, M.P., Rodgers, J.T., Udeshi, N.D., Kelly, T.J., Shabanowitz, J., Hunt, D.F., Puigserver, P., and Hart, G.W. (2008). O-GlcNAc regulates FoxO activation in response to glucose. J. Biol. Chem. *283*, 16283–16292.

Housley, M.P., Udeshi, N.D., Rodgers, J.T., Shabanowitz, J., Puigserver, P., Hunt, D.F., and Hart, G.W. (2009). A PGC-1alpha-O-GlcNAc transferase complex regulates FoxO transcription factor activity in response to glucose. J. Biol. Chem. *284*, 5148–5157.

Kajimura, S., and Saito, M. (2013). A New Era in Brown Adipose Tissue Biology: Molecular Control of Brown Fat Development and Energy Homeostasis. Annu Rev Physiol.

Kang, J.G., Park, S.Y., Ji, S., Jang, I., Park, S., Kim, H.S., Kim, S.M., Yook, J.I., Park, Y.I., Roth, J., and Cho, J.W. (2009). O-GlcNAc protein modification in cancer cells increases in response to glucose deprivation through glycogen degradation. J. Biol. Chem. *284*, 34777–34784.

Kong, D., Tong, Q., Ye, C., Koda, S., Fuller, P.M., Krashes, M.J., Vong, L., Ray, R.S., Olson, D.P., and Lowell, B.B. (2012). GABAergic RIP-Cre neurons in the arcuate nucleus selectively regulate energy expenditure. Cell *151*, 645–657.

Könner, A.C., Janoschek, R., Plum, L., Jordan, S.D., Rother, E., Ma, X., Xu, C., Enriori, P., Hampel, B., Barsh, G.S., et al. (2007). Insulin action in AgRP-expressing neurons is required for suppression of hepatic glucose production. Cell Metab. *5*, 438–449.

Li, M.D., Ruan, H.B., Hughes, M.E., Lee, J.S., Singh, J.P., Jones, S.P., Nitabach, M.N., and Yang, X. (2013). O-GlcNAc signaling entrains the circadian clock by inhibiting BMAL1/CLOCK ubiquitination. Cell Metab. *17*, 303–310.

Liu, T., Kong, D., Shah, B.P., Ye, C., Koda, S., Saunders, A., Ding, J.B., Yang, Z., Sabatini, B.L., and Lowell, B.B. (2012). Fasting activation of AgRP neurons requires NMDA receptors and involves spinogenesis and increased excitatory tone. Neuron *73*, 511–522.

Love, D.C., and Hanover, J.A. (2005). The hexosamine signaling pathway: deciphering the "O-GlcNAc code". Sci. STKE *2005*, re13.

Luquet, S., Perez, F.A., Hnasko, T.S., and Palmiter, R.D. (2005). NPY/AgRP neurons are essential for feeding in adult mice but can be ablated in neonates. Science *310*, 683–685.

Luquet, S., Phillips, C.T., and Palmiter, R.D. (2007). NPY/AgRP neurons are not essential for feeding responses to glucoprivation. Peptides *28*, 214–225.

McClain, D.A., Lubas, W.A., Cooksey, R.C., Hazel, M., Parker, G.J., Love, D.C., and Hanover, J.A. (2002). Altered glycan-dependent signaling induces insulin resistance and hyperleptinemia. Proc. Natl. Acad. Sci. USA *99*, 10695–10699.

Nedergaard, J., and Cannon, B. (2013). UCP1 mRNA does not produce heat. Biochim. Biophys. Acta *1831*, 943–949.

Nedergaard, J., Bengtsson, T., and Cannon, B. (2010). Three years with adult human brown adipose tissue. Ann. N Y Acad. Sci. *1212*, E20–E36.

Nogueiras, R., Wilson, H., Rohner-Jeanrenaud, F., and Tschöp, M.H. (2008). Central nervous system regulation of adipocyte metabolism. Regul. Pept. *149*, 26–31.

Petrovic, N., Walden, T.B., Shabalina, I.G., Timmons, J.A., Cannon, B., and Nedergaard, J. (2010). Chronic peroxisome proliferator-activated receptor gamma (PPARgamma) activation of epididymally derived white adipocyte cultures reveals a population of thermogenically competent, UCP1-containing adipocytes molecularly distinct from classic brown adipocytes. J. Biol. Chem. *285*, 7153–7164.

Qian, S., Chen, H., Weingarth, D., Trumbauer, M.E., Novi, D.E., Guan, X., Yu, H., Shen, Z., Feng, Y., Frazier, E., et al. (2002). Neither agouti-related protein nor neuropeptide Y is critically required for the regulation of energy homeostasis in mice. Mol. Cell. Biol. *22*, 5027–5035.

Qian, S.W., Tang, Y., Li, X., Liu, Y., Zhang, Y.Y., Huang, H.Y., Xue, R.D., Yu, H.Y., Guo, L., Gao, H.D., et al. (2013). BMP4-mediated brown fat-like changes in white adipose tissue alter glucose and energy homeostasis. Proc. Natl. Acad. Sci. USA *110*, E798–E807.

Ren, H., Orozco, I.J., Su, Y., Suyama, S., Gutierrez-Juarez, R., Horvath, T.L., Wardlaw, S.L., Plum, L., Arancio, O., and Accili, D. (2012). FoxO1 target Gpr17 activates AgRP neurons to regulate food intake. Cell *149*, 1314–1326.

Rosen, E.D., and Spiegelman, B.M. (2014). What we talk about when we talk about fat. Cell *156*, 20–44.

Ruan, H.B., Han, X., Li, M.D., Singh, J.P., Qian, K., Azarhoush, S., Zhao, L., Bennett, A.M., Samuel, V.T., Wu, J., et al. (2012). O-GlcNAc transferase/host cell factor C1 complex regulates gluconeogenesis by modulating PGC-1α stability. Cell Metab. *16*, 226–237.

Ruan, H.B., Nie, Y., and Yang, X. (2013a). Regulation of protein degradation by O-GlcNAcylation: crosstalk with ubiquitination. Mol. Cell. Proteomics *12*, 3489–3497.

Ruan, H.B., Singh, J.P., Li, M.D., Wu, J., and Yang, X. (2013b). Cracking the O-GlcNAc code in metabolism. Trends Endocrinol. Metab. *24*, 301–309.

Sanz, E., Yang, L., Su, T., Morris, D.R., McKnight, G.S., and Amieux, P.S. (2009). Cell-type-specific isolation of ribosome-associated mRNA from complex tissues. Proc. Natl. Acad. Sci. USA *106*, 13939–13944.

Scherer, T., and Buettner, C. (2011). Yin and Yang of hypothalamic insulin and leptin signaling in regulating white adipose tissue metabolism. Rev. Endocr. Metab. Disord. *12*, 235–243.

Seale, P., Conroe, H.M., Estall, J., Kajimura, S., Frontini, A., Ishibashi, J., Cohen, P., Cinti, S., and Spiegelman, B.M. (2011). Prdm16 determines the thermogenic program of subcutaneous white adipose tissue in mice. J. Clin. Invest. *121*, 96–105.

Shafi, R., Iyer, S.P., Ellies, L.G., O'Donnell, N., Marek, K.W., Chui, D., Hart, G.W., and Marth, J.D. (2000). The O-GlcNAc transferase gene resides on the X chromosome and is essential for embryonic stem cell viability and mouse ontogeny. Proc. Natl. Acad. Sci. USA *97*, 5735–5739.

Shi, Y.C., Lau, J., Lin, Z., Zhang, H., Zhai, L., Sperk, G., Heilbronn, R., Mietzsch, M., Weger, S., Huang, X.F., et al. (2013). Arcuate NPY controls sympathetic output and BAT function via a relay of tyrosine hydroxylase neurons in the PVN. Cell Metab. *17*, 236–248.

Shibata, H., and Bukowiecki, L.J. (1987). Regulatory alterations of daily energy expenditure induced by fasting or overfeeding in unrestrained rats. J. Appl. Physiol. *63*, 465–470.

Small, C.J., Kim, M.S., Stanley, S.A., Mitchell, J.R., Murphy, K., Morgan, D.G., Ghatei, M.A., and Bloom, S.R. (2001). Effects of chronic central nervous system administration of agouti-related protein in pair-fed animals. Diabetes *50*, 248–254.

Smorlesi, A., Frontini, A., Giordano, A., and Cinti, S. (2012). The adipose organ: white-brown adipocyte plasticity and metabolic inflammation. Obes. Rev. *13* (*Suppl 2*), 83–96.

Spiegelman, B.M., and Flier, J.S. (2001). Obesity and the regulation of energy balance. Cell *104*, 531–543.

Takahashi, K.A., and Cone, R.D. (2005). Fasting induces a large, leptin-dependent increase in the intrinsic action potential frequency of orexigenic arcuate

nucleus neuropeptide Y/Agouti-related protein neurons. Endocrinology *146*, 1043–1047.

Taylor, R.P., Parker, G.J., Hazel, M.W., Soesanto, Y., Fuller, W., Yazzie, M.J., and McClain, D.A. (2008). Glucose deprivation stimulates O-GlcNAc modification of proteins through up-regulation of O-linked N-acetylglucosaminyltransferase. J. Biol. Chem. *283*, 6050–6057.

Torres, C.R., and Hart, G.W. (1984). Topography and polypeptide distribution of terminal N-acetylglucosamine residues on the surfaces of intact lymphocytes. Evidence for O-linked GlcNAc. J. Biol. Chem. *259*, 3308–3317.

Trinidad, J.C., Barkan, D.T., Gulledge, B.F., Thalhammer, A., Sali, A., Schoepfer, R., and Burlingame, A.L. (2012). Global identification and characterization of both O-GlcNAcylation and phosphorylation at the murine synapse. Mol. Cell. Proteomics *11*, 215–229.

Tschöp, M.H., Speakman, J.R., Arch, J.R., Auwerx, J., Brüning, J.C., Chan, L., Eckel, R.H., Farese, R.V., Jr., Galgani, J.E., Hambly, C., et al. (2012). A guide to analysis of mouse energy metabolism. Nat. Methods *9*, 57–63.

Vogt, M.C., and Brüning, J.C. (2013). CNS insulin signaling in the control of energy homeostasis and glucose metabolism - from embryo to old age. Trends Endocrinol. Metab. *24*, 76–84.

Welle, S., and Campbell, R.G. (1983). Stimulation of thermogenesis by carbohydrate overfeeding. Evidence against sympathetic nervous system mediation. J. Clin. Invest. *71*, 916–925.

Whelan, S.A., Dias, W.B., Thiruneelakantapillai, L., Lane, M.D., and Hart, G.W. (2010). Regulation of insulin receptor substrate 1 (IRS-1)/AKT kinase-mediated insulin signaling by O-Linked beta-N-acetylglucosamine in 3T3-L1 adipocytes. J. Biol. Chem. *285*, 5204–5211.

Wiedmer, P., Strasser, F., Horvath, T.L., Blum, D., Dimarchi, R., Lutz, T., Schürmann, A., Joost, H.G., Tschöp, M.H., and Tong, J. (2011). Ghrelin-induced hypothermia: a physiological basis but no clinical risk. Physiol. Behav. *105*, 43–51.

Wilkinson, K.D., Lee, K.M., Deshpande, S., Duerksen-Hughes, P., Boss, J.M., and Pohl, J. (1989). The neuron-specific protein PGP 9.5 is a ubiquitin carboxyl-terminal hydrolase. Science *246*, 670–673.

Wu, J., Boström, P., Sparks, L.M., Ye, L., Choi, J.H., Giang, A.H., Khandekar, M., Virtanen, K.A., Nuutila, P., Schaart, G., et al. (2012). Beige adipocytes are a distinct type of thermogenic fat cell in mouse and human. Cell *150*, 366–376.

Wu, J., Cohen, P., and Spiegelman, B.M. (2013). Adaptive thermogenesis in adipocytes: is beige the new brown? Genes Dev. *27*, 234–250.

Xu, A.W., Kaelin, C.B., Takeda, K., Akira, S., Schwartz, M.W., and Barsh, G.S. (2005). PI3K integrates the action of insulin and leptin on hypothalamic neurons. J. Clin. Invest. *115*, 951–958.

Yang, X., Zhang, F., and Kudlow, J.E. (2002). Recruitment of O-GlcNAc transferase to promoters by corepressor mSin3A: coupling protein O-GlcNAcylation to transcriptional repression. Cell *110*, 69–80.

Yang, X., Ongusaha, P.P., Miles, P.D., Havstad, J.C., Zhang, F., So, W.V., Kudlow, J.E., Michell, R.H., Olefsky, J.M., Field, S.J., and Evans, R.M. (2008). Phosphoinositide signalling links O-GlcNAc transferase to insulin resistance. Nature *451*, 964–969.

Yang, Y., Atasoy, D., Su, H.H., and Sternson, S.M. (2011). Hunger states switch a flip-flop memory circuit via a synaptic AMPK-dependent positive feedback loop. Cell *146*, 992–1003.

Yasuda, T., Masaki, T., Kakuma, T., and Yoshimatsu, H. (2004). Hypothalamic melanocortin system regulates sympathetic nerve activity in brown adipose tissue. Exp. Biol. Med. (Maywood) *229*, 235–239.

Annex A-3. Regulation of substrate utilization and adiposity by Agrp neurons

Scientific article published on *Nature Communications*.

nature COMMUNICATIONS

ARTICLE

https://doi.org/10.1038/s41467-018-08239-x OPEN

Regulation of substrate utilization and adiposity by Agrp neurons

João Paulo Cavalcanti-de-Albuquerque[1,2], Jeremy Bober[1], Marcelo R. Zimmer[1,3] & Marcelo O. Dietrich[1,3,4]

The type of nutrient utilized by the organism at any given time—substrate utilization—is a critical component of energy metabolism. The neuronal mechanisms involved in the regulation of substrate utilization in mammals are largely unknown. Here, we found that activation of hypothalamic Agrp neurons rapidly altered whole-body substrate utilization, increasing carbohydrate utilization, while decreasing fat utilization. These metabolic changes occurred even in the absence of caloric ingestion and were coupled to increased lipogenesis. Accordingly, inhibition of fatty acid synthase—a key enzyme that mediates lipogenesis—blunted the effects of Agrp neuron activation on substrate utilization. In pair-fed conditions during positive energy balance, activation of Agrp neurons improved metabolic efficiency, and increased weight gain and adiposity. Conversely, ablation of Agrp neurons impaired fat mass accumulation. These results suggest Agrp neurons regulate substrate utilization, contributing to lipogenesis and fat mass accumulation during positive energy balance.

[1] Department of Comparative Medicine, Yale University School of Medicine, 310 Cedar Street, Brady Memorial Laboratory Room 410, New Haven, CT 06520, USA. [2] Institute of Biophysics Carlos Chagas Filho and of Nutrition Josue de Castro, Universidade Federal do Rio de Janeiro, Rio de Janeiro, RJ 21941, Brazil. [3] Graduate Program in Biochemistry, Universidade Federal do Rio Grande do Sul, Porto Alegre, RS 90035, Brazil. [4] Department of Neuroscience, Yale University School of Medicine, 333 Cedar Street, New Haven, CT 06520, USA. Correspondence and requests for materials should be addressed to M.O.D. (email: marcelo.dietrich@yale.edu)

Obesity is a major health problem that results from altered regulation of energy balance. Energy balance is the relation between energy intake and energy expenditure. When energy balance is positive (intake>expenditure), there is an increase in energy storage and fat accumulation. A chronic state of positive energy balance leads to obesity. However, a less appreciated component in the regulation of energy balance is the selection of the type of substrate—typically carbohydrate versus fat—used in metabolic reactions. This substrate selection (or substrate utilization) is important as different energy substrates yield different amounts of free energy. Impairment in the capacity to shift between different energy substrates is linked to obesity[1]. Thus, it is important to identify how the organism controls substrate utilization for a better understanding of the regulation of energy balance and obesity development.

Energy metabolism is tightly controlled by the hypothalamus. Agouti-related peptide producing neurons (hereafter, Agrp neurons)[2–5] in the hypothalamus regulate energy metabolism by responding to a variety of circulating factors[6–9]. These neurons are active during food deprivation[2,10–12] and are strongly associated to control of food intake[2,5,13–18]. However, recent work suggested that Agrp neurons also regulate other metabolic processes, including white adipose tissue (WAT) browning[19] and brown adipose tissue glucose metabolism[20] and thermogenesis[19,21]. During our previous studies investigating the function of Agrp neurons[14,19,22], we observed rapid changes in whole-body substrate utilization upon activation of Agrp neurons. Based on these unexpected observations, we investigated the involvement of Agrp neurons in the regulation of peripheral substrate utilization and lipogenesis.

Here, we report that Agrp neurons rapidly shift whole-body metabolism towards lipid storage, a mechanism we suggest as being important for fat accumulation during positive energy balance (i.e., a metabolic state coupled to weight gain).

Results

Acute switch in nutrient utilization upon Agrp neuron activation. To gain insight into the acute regulation of metabolism by Agrp neurons, nutrient utilization was measured by indirect calorimetry upon activation of these neurons. *Agrp*^{Trpv1} mice (as previously characterized[14,19]) were used to specifically activate Agrp neurons by selectively expressing the capsaicin-sensitive channel, Trpv1, which is transiently activated by peripheral injection of capsaicin. Activation of Agrp neurons by capsaicin rapidly increased food intake in *Agrp*^{Trpv1} mice (Fig. 1a and Supplementary Figure 1)[14]. We also observed a sharp increase in respiratory exchange ratio (RER)—calculated as the ratio (VCO2/VO2)—in these animals (Fig. 1b), in line with the observed fast kinetics of feeding, suggesting an acute shift in substrate utilization towards carbohydrates relative to fat. Based on gaseous exchange[23], we calculated total rates of fat utilization and carbohydrate utilization for the whole animal. In line with changes in RER, activation of Agrp neurons led to a rapid and prolonged decrease in fat utilization (Fig. 1c) and increase in carbohydrate utilization (Fig. 1d). Because this experiment was performed in the presence of food and the effects on nutrient utilization were prolonged compared to feeding upon Agrp neuron activation (Fig. 1a)[14], these metabolic shifts could be due to changes in postprandial metabolism. Using linear regression analysis between the initial bout of food intake (0–30 min) and the subsequent RER (30–60 min), we could not find a positive correlation between these parameters (Fig. 1e). However, the lack of positive correlation could be explained by a ceiling effect.

We did not observe statistically significant changes in VO_2 (Fig. 1f), VCO_2 (Fig. 1g) or energy expenditure (Fig. 1h). However, non-statistical decreases in VO_2 and increases in VCO_2 accounted for the changes in RER (inserts Fig. 1f, g). We also measured activity levels upon Agrp neuron activation[14] and did not observe statistical changes in ambulatory activity (Fig. 1i). Thus, these results suggest Agrp neurons rapidly control whole-body substrate utilization, an effect that could be the consequence of postprandial metabolic shifts.

Agrp neuron activation control substrate utilization in the absence of ingestion. We further explored the extent to which activation of Agrp neurons and carbohydrate ingestion interact to rapidly shift metabolism (Supplementary Figure 2 and Supplementary Note 1). We infused both control and *Agrp*^{Trpv1} mice with glucose (2 g kg^{-1} body weight, via gavage) and activated Agrp neurons by injecting capsaicin (Fig. 2a). Food was removed from the cage during the experiment to prevent ingestion. Activation of Agrp neurons led to an increased peak and a more sustained elevation of RER (Fig. 2b, c), an effect that was present even in mice that did not receive glucose infusion (Fig. 2b, c). Accordingly, activation of Agrp neurons led to a sustained decrease in fat utilization (Fig. 2d, e) and increase in carbohydrate utilization (Fig. 2f, g), regardless of glucose infusion. These results suggest that activation of Agrp neurons alone is capable of promoting shifts in substrate utilization.

In the previous experiments, even in animals infused with saline via gavage, small amounts of liquid were delivered, raising the possibility that acute gastric distension acts together with Agrp neuron activation to promote changes in substrate utilization. To exclude this possibility, we repeated our experiments in a new cohort of mice in which Agrp neurons were activated in the absence of food (Fig. 3a). In line with our previous findings, activation of Agrp neurons induced an increase in RER (Fig. 3b), a decrease in fat utilization (Fig. 3c) and an increase in carbohydrate utilization (Fig. 3d). In support of these results, activation of Agrp neurons using DREADD (designer receptor exclusively activated by designer drugs) also showed similar shifts in substrate utilization (Supplementary Figure 3 and Supplementary Note 2).

We measured ambulatory activity and found an increase upon activation of Agrp neurons in the absence of food (Fig. 3e), suggestive of foraging behaviors[14,16,24]. Importantly, activity levels between control and *Agrp*^{Trpv1} mice started to diverge around 20–25 min after capsaicin injection, while RER started to diverge around 10–15 min. The fact that RER started to diverge before activity levels suggests that the effect of Agrp neuron activation on RER is independent of an increase in locomotion. To further rule out the effects of activity on RER, we used linear regression analysis (Fig. 3f, g). We found that activity levels and RER were weakly correlated in both control and *Agrp*^{Trpv1} mice (control: $r^2 = 0.244$, $F_{1,63} = 20.12$, $P < 10^{-4}$; *Agrp*^{Trpv1}: $r^2 = 0.155$, $F_{1,63} = 11.21$, $P < 10^{-3}$). However, the slopes were not statistically different from each other (control: slope $= 1.68 \times 10^{-4} \pm 0.37 \times 10^{-4}$; *Agrp*^{Trpv1}: slope $= 1.21 \times 10^{-4} \pm 0.36 \times 10^{-4}$; $F_{1,126} = 0.82$, $P = 0.36$), suggesting the physiological relationship between RER and activity levels is not altered by Agrp neuron activation. Importantly, across different activity levels, activation of Agrp neurons increased RER, as evidenced by the parallel linear regression lines and by statistically different intercepts (control: intercept $= 0.766 \pm 0.005$; *Agrp*^{Trpv1}: intercept $= 0.878 \pm 0.007$, $F_{1,127} = 201.5$, $P < 10^{-4}$) (Fig. 3f, g). Thus, these results demonstrate that activation of Agrp neurons increases RER

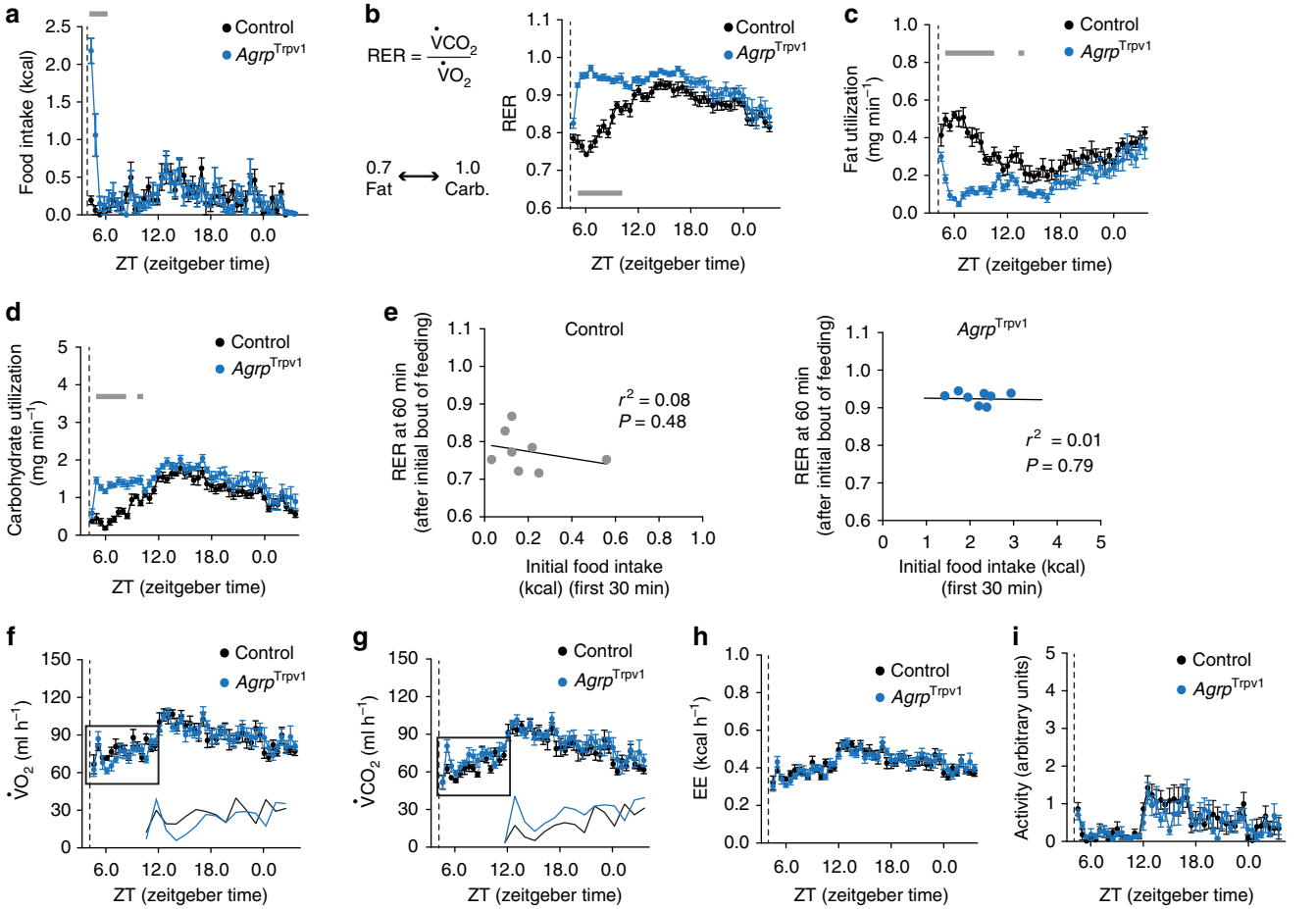

Fig. 1 Rapid shift in substrate utilization upon activation of agouti-related peptide (Agrp) neurons. **a** Food intake. **b** Respiratory exchange ratio (RER) (interaction: $F_{45, 630} = 8.40$, $P < 0.0001$; time: $F_{45, 630} = 13.86$, $P < 0.0001$; group: $F_{1, 14} = 52.59$, $P < 0.0001$). **c** Calculated fat utilization (interaction: $F_{45, 630} = 6.44$, $P < 0.001$; time: $F_{45, 630} = 7.22$, $P < 0.0001$; group: $F_{1, 14} = 33.83$, $P < 0.0001$). **d** Calculated carbohydrate utilization (interaction: $F_{45, 630} = 2.77$, $P < 0.0001$; time: $F_{45, 630} = 18.48$, $P < 0.0001$; group: $F_{1, 14} = 16.73$, $P = 0.001$). **e** Linear regression analysis between the size of the initial bout of food intake (first 30 min) and RER (at the 60 min measurement) in control and *Agrp*^{Trpv1} mice. **f** VO_2 (interaction: $F_{45, 630} = 1.07$, $P = 0.34$; time: $F_{45, 630} = 11.22$, $P < 0.0001$; group: $F_{1, 4} = 0.01$, $P = 0.89$). **g** VCO_2 (interaction: $F_{45, 630} = 0.88$, $P = 0.68$; time: $F_{45, 630} = 15.07$, $P < 0.0001$; group: $F_{1, 14} = 1.58$, $P = 0.22$). In **f** and **g**, inserts show the mean VO_2 and VCO_2. **h** Energy expenditure (interaction: $F_{45, 630} = 0.96$, $P = 0.53$; time: $F_{45, 630} = 12.09$, $P < 0.0001$; group: $F_{1, 14} = 0.02$, $P = 0.87$). **i** Ambulatory activity (interaction: $F_{45, 630} = 0.80$, $P = 0.81$; time: $F_{45, 630} = 6.02$, $P < 0.0001$; group: $F_{1, 14} = 0.31$, $P = 0.58$). Statistical analysis was performed using two-way analysis of variance (ANOVA) with time as a repeated measure followed by Holm–Sidak's multiple comparisons test (MCT). Gray bars indicate time points in which MCTs were statistically significant ($P < 0.05$). From **a**–**i** control (black; $n = 8$) and *Agrp*^{Trpv1} mice (blue; $n = 8$). Dashed line indicates time of capsaicin injection. Symbols indicate mean ± SEM

independently of the ingestion of food, an effect that cannot be fully explained by changes in activity levels.

Participation of lipogenesis in Agrp neuron-mediated shifts in metabolism. We next explored biochemical changes in peripheral tissues that could be mechanistically linked to the observed shifts in metabolism upon activation of Agrp neurons. We found that in the absence of food ingestion, Agrp neuron activation decreased circulating levels of non-esterified fatty acids (NEFAs, Fig. 4a, b) with no changes in basal blood glucose levels (Fig. 4c). The lack of changes in basal blood glucose levels do not exclude the possibility that Agrp neurons control glucose handling during glucose challenge[20]. Because circulating NEFAs decrease upon Agrp neuron activation, these results suggest a decrease in release, and possibly an increase in deposition of fat. To test this hypothesis, we measured expression levels of genes involved in lipid metabolism in the WAT from *Agrp*^{Trpv1} and control mice 60 min after capsaicin injection. We found a decrease in the expression level of *Ppara* (Fig. 4d), a gene involved in the promotion of fat catabolism. We also found a significant increase in expression levels of *hexokinase2* (*hk2*; Fig. 4d), a rate-limiting enzyme involved in glycolysis, a critical metabolic step to provide carbons for de novo lipogenesis. Hormone-sensitive lipase (HSL) is an essential step in the breakdown of triglycerides to release fatty acids in circulation. Activation of hormone-sensitive lipase occurs by phosphorylation of this enzyme in several serine residues. Upon activation of Agrp neurons, we found decreased levels of phosphorylated hormone-sensitive lipase (p-HSL) in WAT compartments (Fig. 4e and Supplementary Figure 6). Together, these experiments indicate activation of Agrp neurons leads to increased lipogenesis and decreased lipolysis in the WAT.

De novo lipogenesis can drive RER above 1.0[23], and could be a potential factor involved in Agrp neuron activation-mediated shifts in RER. To test for the participation of fat synthesis in the rapid effects of Agrp neurons on metabolism, we blocked fatty acid synthase (FAS), a key enzyme involved in fat storage[25]. We treated mice with a pharmacological inhibitor of fatty acid synthase (C75, 10 mg kg^{-1}, i.p.)[26,27] and activated Agrp neurons

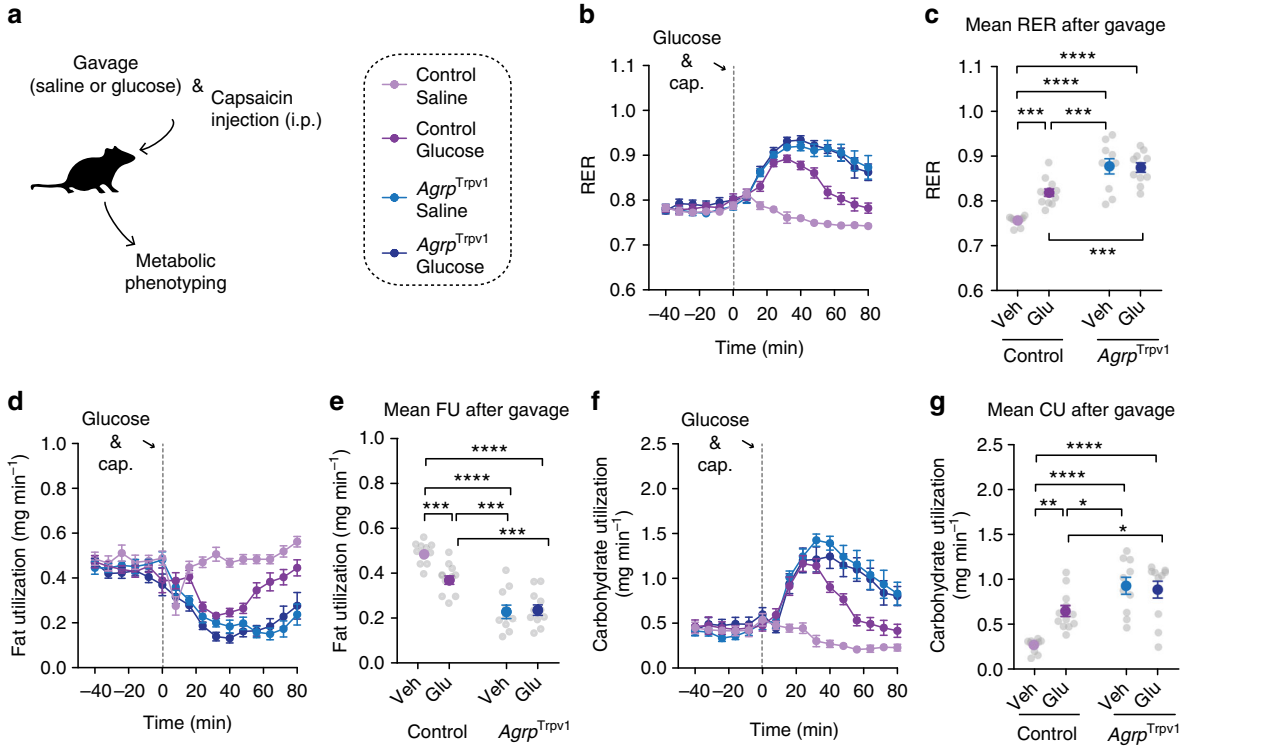

Fig. 2 Glucose ingestion and Agrp neurons control substrate utilization independently. **a** Control and *Agrp*^{Trpv1} mice received a bolus of saline or glucose (2 g kg^{-1}) via gavage followed by peripheral injection of capsaicin (10 mg kg^{-1}, intraperitoneal (i.p.)). **b** Respiratory exchange ratio (RER). **c** Mean RER after gavage (interaction: $F_{1,40} = 9.82$, $P = 0.003$; gavage solution: $F_{1,40} = 8.20$, $P = 0.006$; genotype: $F_{1,40} = 71.31$, $P < 0.0001$). **d** Fat utilization. **e** Mean fat utilization after gavage (interaction: $F_{1,40} = 7.91$, $P = 0.007$; gavage solution: $F_{1,40} = 6.07$, $P = 0.01$; genotype: $F_{1,40} = 79.82$, $P < 0.0001$). **f** Carbohydrate utilization. **g** Mean carbohydrate utilization after gavage (interaction: $F_{1,40} = 8.29$, $P = 0.006$; gavage solution: $F_{1,40} = 5.26$, $P = 0.02$; genotype: $F_{1,40} = 37.44$, $P < 0.0001$). In **c**, **e** and **g** statistical analysis was performed using two-way analysis of variance (ANOVA) on the mean response after gavage and capsaicin injection; genotype (control vs. *Agrp*^{Trpv1}) and gavage infusion (saline vs. glucose) were used as factors for the ANOVA. Holm–Sidak's multiple comparisons test (MCT) was used to find post hoc differences among groups. MCTs are indicated as $^{*}P < 0.05$, $^{**}P < 0.01$, $^{***}P < 0.001$ and $^{****}P < 0.0001$ in figure panels. Control mice + saline gavage ($n = 11$); control mice + glucose gavage ($n = 12$); *Agrp*^{Trpv1} mice + saline gavage ($n = 10$); *Agrp*^{Trpv1} mice + glucose gavage ($n = 11$). Dashed gray line indicates time of oral gavage and capsaicin injection

in indirect calorimetry chambers (Fig. 4f). Treatment of control mice with the fatty acid synthase inhibitor had no effects on RER (Fig. 4g), fat utilization (Fig. 4j) or carbohydrate utilization (Fig. 4m). The lack of effects of fatty acid synthase inhibition on substrate utilization is in line with the low levels of lipogenesis during the light cycle of mice. In contrast to control animals, inhibition of fatty acid synthase blocked the effects of Agrp neuron activation on substrate utilization (Fig. 4h, i, k, l, n, o). These results provide further support for the rapid shift in metabolism towards lipogenesis mediated by Agrp neuron activation in mice.

Sympathetic signaling mediates peripheral effects of Agrp neurons. Norepinephrine release and binding to adrenergic receptors on fat compartments promotes lipolysis, while its inhibition favors lipogenesis. Accordingly, we predicted that Agrp neurons control substrate utilization and lipogenesis by inhibiting sympathetic signaling on fat compartments in anabolic states. Here, we treated mice with a β3-adrenergic receptor agonist (CL 316,243)[28] (Fig. 5a), which are highly selective to fat compartments[29], while activating Agrp neurons (Fig. 5a). Treatment of control mice with CL 316,243 did not alter RER (Figs. 5b and 5d) but prevented the increase in RER upon Agrp neuron activation in *Agrp*^{Trpv1} mice (Fig. 5c-d). When we calculated fat utilization, CL 316,243 completely reverted the inhibition of whole-body fat utilization upon Agrp neuron activation (Fig. 5e, g) but had no effects in control animals (Fig. 5f, g). Concomitantly, CL 316,243 prevented the increase in carbohydrate utilization upon activation of Agrp neurons (Fig. 5h–j). Thus, promotion of β3-adrenergic receptor signaling using a pharmacological agonist reverts the effects of Agrp neuron activation on peripheral fuel metabolism.

Next, we tested whether CL 316,243 could acutely block the effects of Agrp neuron activation on food intake. We first performed a dose response study to detect the range of CL 316,243 doses that could revert the increase in RER upon Agrp neuron activation. We found that doses as low as 0.01 mg kg^{-1} almost completely reverted the effects of Agrp neurons on RER (Fig. 5k). Next, we selected two doses of CL 316,243 (1.00 and 0.01 mg kg^{-1}) to investigate its effects on food intake mediated by Agrp neuron activation. In all conditions tested, CL 316,243 did not revert the effects of Agrp neuron activation on food intake (Fig. 5l, m). Of note, CL 316,243 is highly anorexigenic[29], but its effects are observed after several hours and not as rapid as the effects of Agrp neuron activation on feeding[14–16]. These findings suggest a divergence between the feeding and metabolic mechanisms underlying Agrp neuron function and support the argument that Agrp neuron activation favors the storage of fat (lipogenesis) in situations of energy surfeit by suppressing sympathetic activity.

Agrp neuron activation potentiate adiposity in obesogenic conditions. Since Agrp neuron activity shifts metabolism toward lipogenesis, it is expected that during prolonged neuronal activation mice will accumulate more fat than control counterparts.

XXV

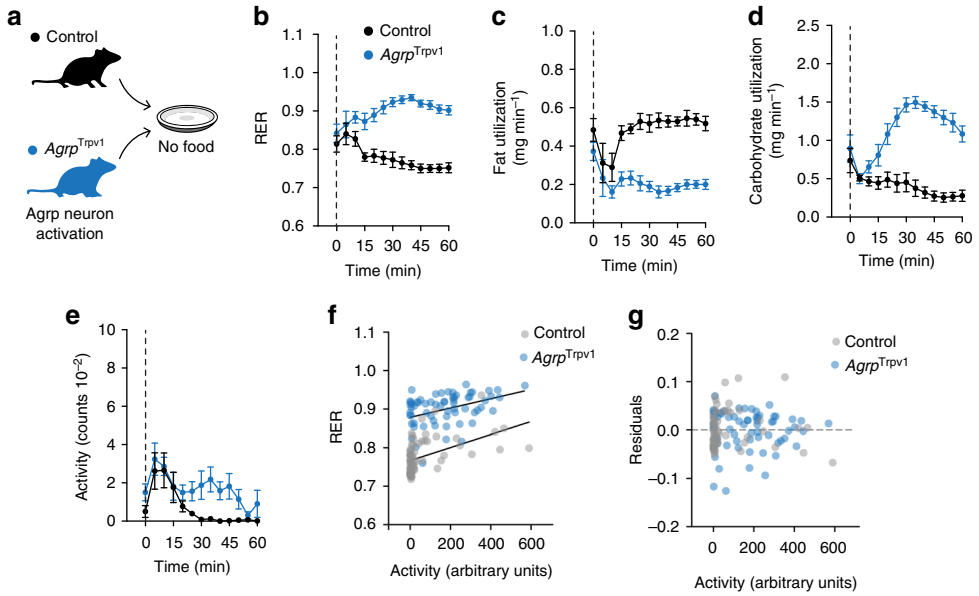

Fig. 3 Agrp neuron activation induces a shift in substrate utilization. **a** Control (black, $n = 5$) and $Agrp^{Trpv1}$ (blue, $n = 5$) mice were tested in indirect calorimetry chambers upon injection of capsaicin without food provided. **b** Respiratory exchange ratio (RER) (interaction: $F_{12, 96} = 8.96$, $P < 0.0001$; time: $F_{12, 96} = 1.31$, $P = 0.22$; genotype: $F_{1, 8} = 54.45$, $P < 0.0001$). **c** Calculated fat utilization (interaction: $F_{12, 96} = 3.52$, $P = 0.0002$; time: $F_{12, 96} = 3.23$, $P = 0.0006$; genotype: $F_{1, 8} = 55.31$, $P < 0.0001$). **d** Calculated carbohydrate utilization (interaction: $F_{12, 96} = 13.52$, $P < 0.0001$; time: $F_{12, 96} = 6.25$, $P < 0.0001$; genotype: $F_{1, 8} = 58.16$, $P < 0.0001$). **e** Ambulatory activity (interaction: $F_{12, 96} = 1.12$, $P = 0.34$; time: $F_{12, 96} = 7.13$, $P < 0.0001$; genotype: $F_{1, 8} = 5.29$, $P = 0.05$). **f** Linear regression models of activity levels (in arbitrary units) and RER in control (gray) and $Agrp^{Trpv1}$ (red) mice. **g** Residuals from the linear regression model. In **b**, **c**, **d** and **e**, statistical analysis was performed using two-way analysis of variance (ANOVA) with time as a repeated measure followed by Holm–Sidak's multiple comparisons test (MCT; not shown). Dashed line indicates time of capsaicin injection. Symbols indicate mean ± SEM

To test this assumption, we daily activated Agrp neurons in $Agrp^{Trpv1}$ mice and measured body weight and fat mass changes over 10 days in ad libitum fed animals. Repeated activation of Agrp neurons led to an increase in food intake, body weight gain, fat mass and metabolic efficiency (Supplementary Figure 4), i.e., the amount of body weight gained related to the amount of energy ingested.

To further dissect the discrete contribution of Agrp neurons to adiposity and weight gain during obesogenic conditions, we set out to selectively activate Agrp neurons under controlled positive energy balance. We took advantage of the physiological hyperphagia that occurs when rodents are switched from a normal chow diet to a high-fat diet in the laboratory[30,31]. In our colony, this acute dietary switch led to an increase of ~86% in the amount of overnight calories consumed (Fig. 6a). Based on these data, we designed a pair-fed study in which control and $Agrp^{Trpv1}$ mice could be fed more calories than they would usually consume under a regular chow diet, thus inducing a state of positive energy balance (Fig. 6b). When control and $Agrp^{Trpv1}$ mice were fed an isocaloric high-fat diet (compared to their ad libitum normal chow intake), activation of Agrp neurons did not lead to changes in body weight gain or metabolic efficiency (Fig. 6c). However, when pair-fed 25% or 50% more calories than their ad libitum food intake under a normal chow diet, activation of Agrp neurons in $Agrp^{Trpv1}$ mice increased body weight gain and metabolic efficiency compared to littermate controls (Fig. 6d, e).

When switched to a high-fat diet, mice displayed hyperphagia lasting 5 days (Fig. 6f)[30,31]. We took advantage of this phenomenon to study mice in positive energy balance in a more prolonged pair-fed experiment (Fig. 6g). Using this approach, we controlled the number of calories ingested by control and Agrp neuron activated mice during 5 days of hyperphagia (Fig. 6h). Despite identical food intake, activation of Agrp neurons increased body weight gain compared to control mice (Fig. 6i). We then measured the metabolic efficiency and changes in fat mass at the end of the study (day 6) compared to day 0—when we introduced the high-fat diet. In this experimental setting, activation of Agrp neurons increased metabolic efficiency (Fig. 6j) and fat mass gain (Fig. 6k) with no changes in lean mass (delta lean mass: control = 0.26 ± 0.39, $n = 8$; $Agrp^{Trpv1}$ = 0.24 ± 0.20, $n = 8$; $t_{14} = 0.04$, $P = 0.96$, t-test). In support of these findings, we found similar results in $Agrp^{hM3Dq}$ mice (Supplementary Figure 5 and Supplementary Note 3).

Ablation of Agrp neurons impairs adiposity. Finally, we tested whether the loss of function of Agrp neurons would impair adiposity in conditions of positive energy balance. We studied control and $Agrp^{DTR}$ mice[17], allowing controlled ablation of these neurons. In adults, ablation of Agrp neurons leads to aphagia and death[17]. To bypass the aphagia after Agrp neuron ablation, we devised an enteral feeding scheme using a gastrostomy tube to deliver controlled amounts of liquid diet into the stomach of mice (Fig. 7a). After tube implantation, mice were allowed to recover from surgery and acclimate to liquid diet for 2 days. We then started to gradually increase the amount of diet infused in the stomach, until reaching positive energy balance (animals started to gain body weight). At post-surgery days 7 and 9, we injected diphtheria toxin (50 µg kg^{-1}, intramuscular) to ablate Agrp neurons. In this feeding regimen, ablation of Agrp neurons did not lead to death and mice continued to increase body weight (Fig. 7b). However, ablation of Agrp neurons led to a significant decrease in fat mass gain (Fig. 7c) but not lean mass (delta lean mass: control = -0.07 ± 0.30, $Agrp^{DTR}$ = 0.13 ± 0.49; $U = 9$, $P = 0.45$, Mann–Whitney test) as measured by repeated magnetic resonance imaging (MRI) scans before the first diphtheria toxin injection and at the end of the study. At 6 days after the first injection of diphtheria toxin, we dissected the fat tissue for

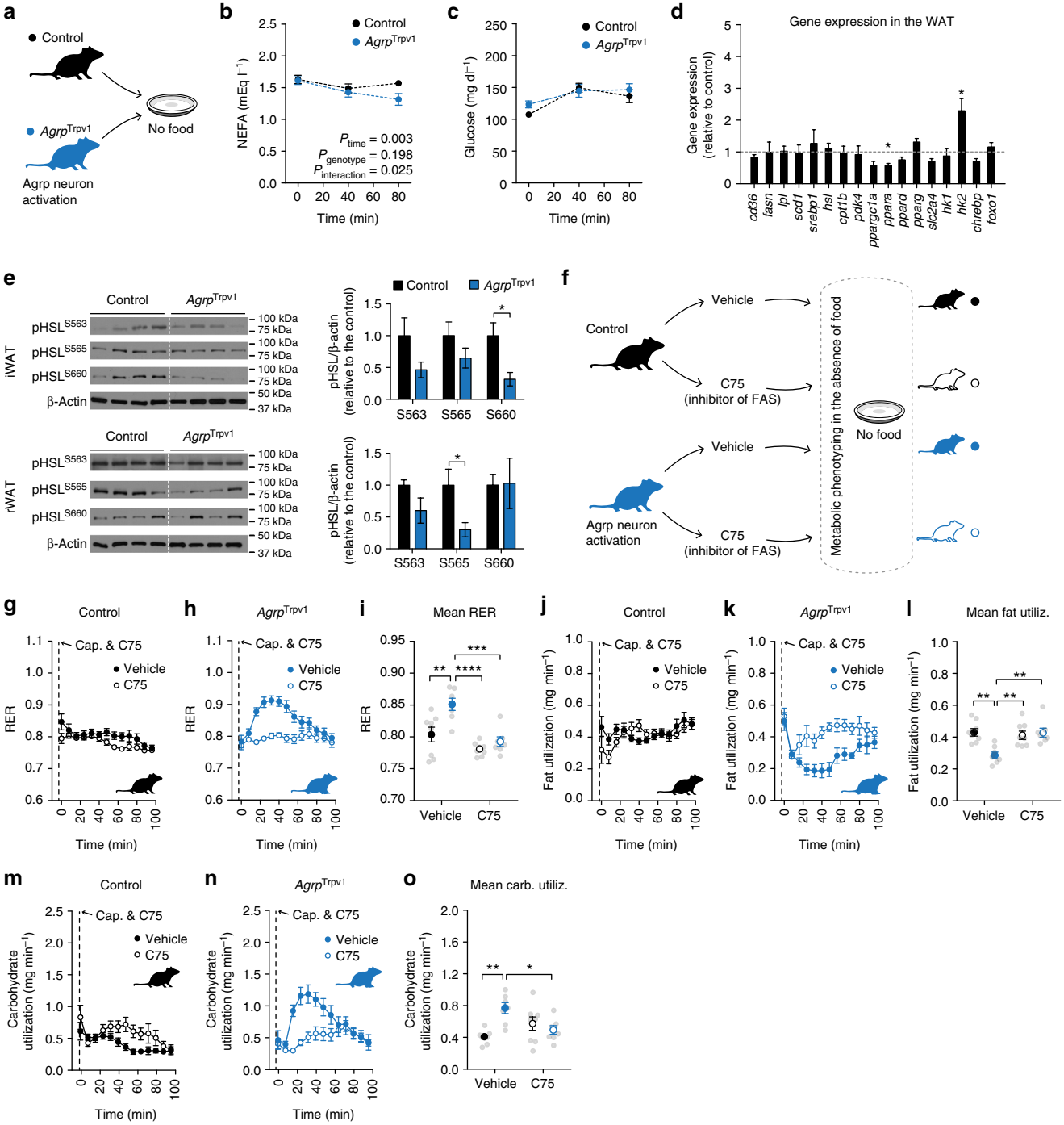

Fig. 4 Agrp neurons promote lipogenesis. **a** Control (black) and *Agrp*^{Trpv1} (blue) mice were injected with capsaicin. **b** NEFA levels (interaction: $F_{2,54} = 3.91$, $P = 0.02$; time: $F_{2,54} = 9.64$, $P = 0.0003$; genotype: $F_{1,27} = 1.74$, $P = 0.19$; MCT: $P_{80\ min} = 0.03$). **c** Blood glucose levels (interaction: $F_{2,54} = 1.47$, $P = 0.23$; time: $F_{2,54} = 14.6$, $P < 0.0001$; genotype: $F_{1,27} = 0.67$, $P = 0.41$; MCT: ns). In **b** and **c**: control ($n = 15$) and *Agrp*^{Trpv1} mice ($n = 14$). Statistics: two-way analysis of variance (ANOVA) with time as a repeated measure followed by Holm–Sidak's multiple comparisons test (MCT). **d** Gene expression in the WAT. Data are normalized to control levels (dashed line). Statistics: Student's *t*-test. $^*P < 0.05$. **e** Western blotting analysis of phosphorylated HSL in inguinal WAT and retroperitoneal WAT ($n = 4$ mice per group). Blots were cropped for clarity. Statistics: Student's *t*-test. $^*P < 0.05$. **f** Control and *Agrp*^{Trpv1} mice randomly received vehicle or the FAS inhibitor (C75, 10 mg kg^{-1}, intraperitoneal (i.p.)) immediately before capsaicin injection. **g–i** Respiratory exchange ratio (RER) (interaction: $F_{1,26} = 4.36$, $P = 0.04$; drug: $F_{1,26} = 22.28$, $P < 0.0001$; genotype: $F_{1,26} = 11.73$, $P = 0.002$). **j–l** Fat utilization (interaction: $F_{1,26} = 9.97$, $P = 0.04$; drug: $F_{1,26} = 6.00$, $P = 0.02$; genotype: $F_{1,26} = 6.56$, $P = 0.01$). **m–o** Carbohydrate utilization: (interaction: $F_{1,26} = 12.18$, $P = 0.001$; drug: $F_{1,26} = 0.76$, $P = 0.38$; genotype: $F_{1,26} = 4.90$, $P = 0.03$). In **g–o**, statistics: two-way ANOVA on the mean response after drug and capsaicin injection; genotype and drug as factors for the ANOVA. Holm–Sidak's multiple comparisons test (MCT) was used and indicated as $^*P < 0.05$, $^{**}P < 0.01$, $^{***}P < 0.001$ and $^{****}P < 0.0001$. Control mice + vehicle ($n = 8$); control mice + C75 ($n = 8$); *Agrp*^{Trpv1} mice + vehicle ($n = 7$); *Agrp*^{Trpv1} mice + C75 ($n = 7$). Dashed line indicates time of injections. Colored symbols indicate mean ± SEM. Gray symbols indicate individual values

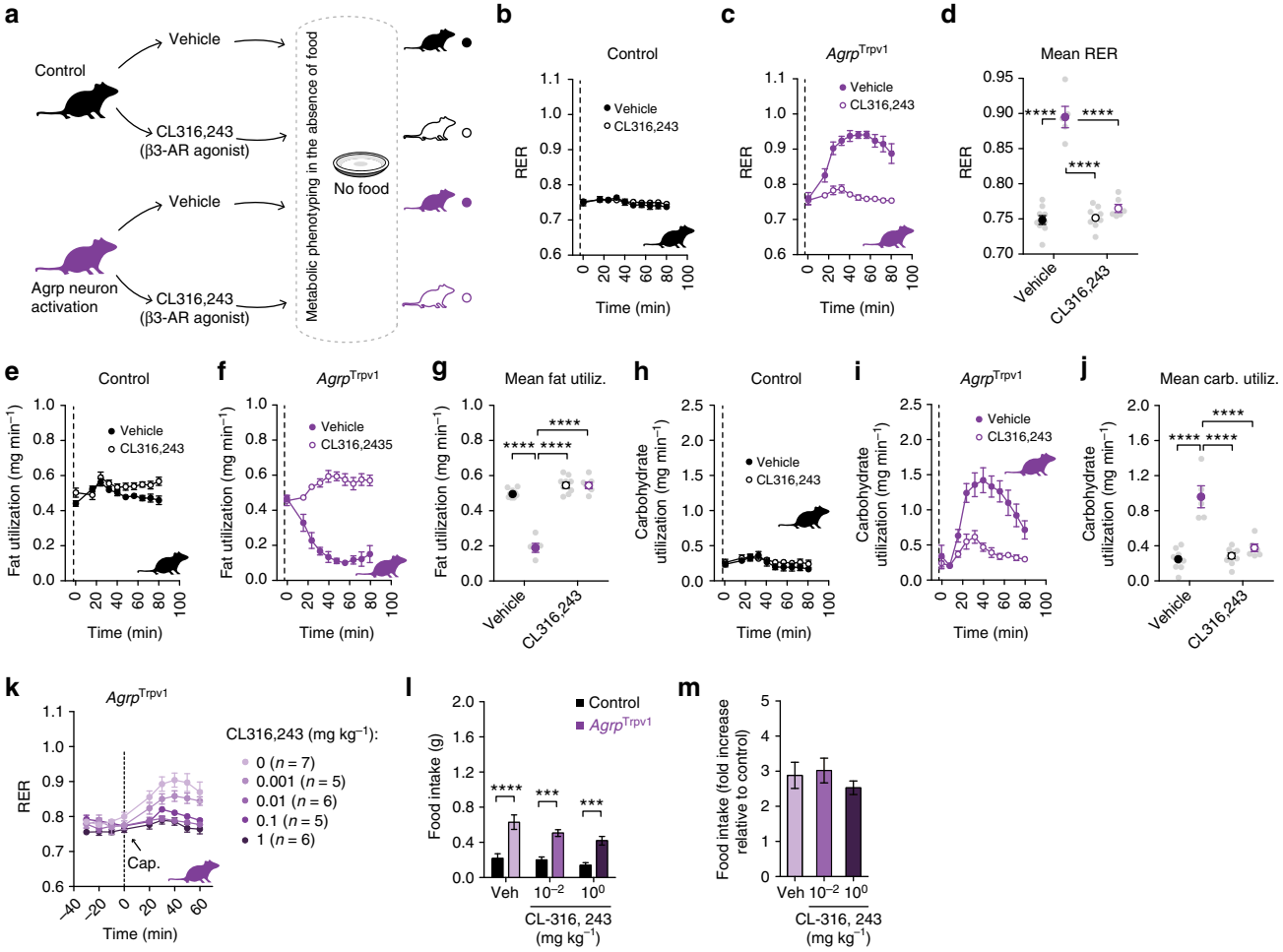

Fig. 5 Sympathetic signaling is involved in peripheral effects of Agrp neurons. **a** Control (black) and *Agrp*^{Trpv1} mice (purple) were randomized to receive vehicle or the β3-adrenergic receptor agonist (CL 316,243, 1 mg kg^{-1}, intraperitoneal (i.p.)); vehicle or CL 316,243 were injected immediately before capsaicin. **b–d** Respiratory exchange ratio (RER) (interaction: $F_{1, 25} = 75.09$, $P < 0.0001$; drug: $F_{1, 25} = 67.96$, $P < 0.0001$; genotype: $F_{1, 25} = 108.4$, $P < 0.0001$). **e–g** Fat utilization (interaction: $F_{1, 25} = 85.56$, $P < 0.0001$; drug: $F_{1, 25} = 150.4$, $P < 0.0001$; genotype: $F_{1, 25} = 86.42$, $P < 0.0001$). **h–j** Carbohydrate utilization (interaction: $F_{1, 25} = 29.74$, $P < 0.0001$; drug: $F_{1, 25} = 22.75$, $P < 0.0001$; genotype: $F_{1, 25} = 50.12$, $P < 0.0001$). In **d**, **g** and **j**, statistics: two-way analysis of variance (ANOVA) on the mean response after drug and capsaicin injection; genotype (control vs. *Agrp*^{Trpv1}) and drug (vehicle vs. CL 316,243) were used as factors for the ANOVA. Holm–Sidak's multiple comparisons test (MCT) was used to find post hoc differences among groups. MCTs are indicated as $^{***}P < 0.001$, and $^{****}P < 0.0001$ in figure panels. Control mice + vehicle ($n = 9$); control mice + CL 316,243 ($n = 9$); *Agrp*^{Trpv1} mice + vehicle ($n = 5$); *Agrp*^{Trpv1} mice + CL 316,243 ($n = 6$). Dashed line indicates time of injections. Colored symbols indicate mean ± SEM. Gray symbols indicate individual values. **k** Dose response of CL 316,243 injected immediately before capsaicin in *Agrp*^{Trpv1} mice (dashed line denotes injection time). Number of animals used per experimental group shown in the panel. **l** Food intake response to activation of Agrp neurons when injected with different doses of CL 316,243 ($n = 7$ for all groups); interaction ($F_{2, 36} = 0.95$, $P = 0.39$); drug ($F_{2, 36} = 4.16$, $P = 0.02$); genotype ($F_{1, 36} = 64.96$, $P < 0.0001$). Statistics: two-way ANOVA with genotype and drug as factors. Holm–Sidak's multiple comparisons test (MCT) was used and indicated as $^{***}P < 0.001$ and $^{****}P < 0.0001$. **m** Related to **l**, but fold change in food intake in *Agrp*^{Trpv1} related to control mice. Bars and symbols indicate mean ± SEM

biochemical analysis and the brain to confirm ablation of Agrp neurons. After diphtheria toxin treatment, only minimal residual Agrp-positive neuronal fibers were visualized in the arcuate nucleus (Fig. 7d), confirming the ablation of Agrp neurons is not affected by enteral feeding. In the WAT, we measure genes involved in lipid metabolism and found decreased expression of several genes involved in lipogenesis (Fig. 7e). Altogether, these results support the idea that Agrp neuron activity mediates weight gain and adiposity in positive energy balance conditions.

Discussion

Here, we reported that Agrp neurons shift metabolism towards lipid storage, a mechanism we suggest being important for fat accumulation during positive energy balance (i.e., a metabolic state coupled to weight gain).

During diet-induced obesity, the activity of Agrp neurons is elevated as recorded using slice electrophysiology[32–35]. This elevated activity of Agrp neurons could be involved in the metabolic shifts towards fat deposition (lipogenesis) reported here. In fact, a recent report showed that activation of Agrp neurons in *Agrp*^{hM3Dq} mice during 2 weeks by providing clozapine-N-oxide (CNO)—the pharmacological agonist of the excitatory receptor hM3Dq—in the drinking water increased food intake only during the first 2 days[36]. However, mice continued to increase body weight during the entire period of study, suggesting a role for Agrp neurons in body weight gain that was not due to increased feeding[36]. Additionally, mice with impaired activity of Agrp

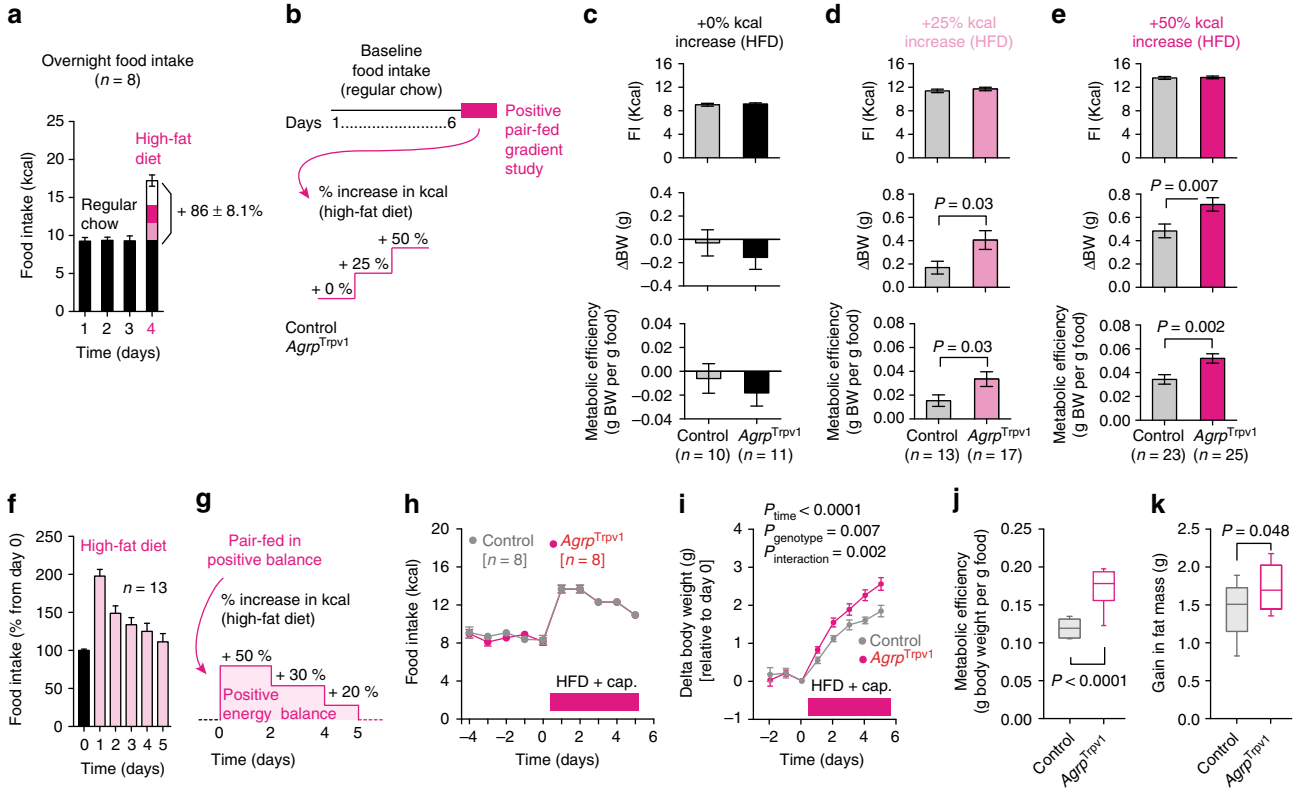

Fig. 6 Agrp neuron activity boosts fat gain in obesogenic conditions. **a** Physiological hyperphagia after acute switch to high-fat diet (45% kcal from fat) in mice. **b** Pair feeding studies: high-fat diet (0, 25 or 50% more calories compared to ad libitum normal chow food intake) was provided after injection of control and *Agrp*^{Trpv1} mice with capsaicin. **c** Top, Mice were fed the same number of calories as they ate during baseline food intake; Middle, delta body weight; Bottom, metabolic efficiency. **d** Similar to **c** but in mice fed 25% more calories when switched to a high-fat diet. **e** Similar to **c** and **d**, but in mice fed 50% more calories. **f** Food intake measured during 5 days after switching mice to a high-fat diet (45% kcal from fat); in pink, period of dietary switch. **g** Control and *Agrp*^{Trpv1} mice were switched to a high-fat diet (shaded pink) after baseline food intake measurements; capsaicin was injected every day before dark cycle. **h** Food intake. **i** Delta changes in body weight relative to the day of diet switch. **j** Metabolic efficiency and **k** gain in fat mass during the period in which mice were fed high-fat diet. Unpaired *t*-test was used in **c**, **d**, **e**, **j** and **k**. Two-way analysis of variance (ANOVA with time as a repeated measure was used in **i**. Number of mice is displayed in the figures. Bars and symbols indicate mean ± SEM. Boxes indicate median ± 25/75 quartiles ± min/max values. Statistically significant *P* values are provided in the figures

neurons during high-fat feeding were resistant to diet-induced obesity with only minor or no effects on food intake[32]. Thus, previous reports and our current findings strongly suggest that persistent elevation of Agrp neuron activity during positive energy balance propagate adiposity.

In the WAT, activation of the sympathetic nervous system leads to lipolysis[37–39], whereas its inhibition favors lipogenesis[40]. Our results suggest a model in which Agrp neuron activity during obesogenic conditions suppresses sympathetic tone in the WAT to promote adiposity. In support of this model, activation of Agrp neurons decreased the sympathetic nervous system activity in peripheral tissues[19,20,41]. Direct recordings of sympathetic nerve electrical activity showed that activation of Agrp neurons decreased in approximately 30% the firing rate of sympathetic nerves[20,41]. Conversely, inhibition of Agrp neurons increased sympathetic nerve activity in up to 60%[41]. These effects were mediated by projections of Agrp neurons to paraventricular nucleus (PVH) and dorsomedial hypothalamic nucleus[41]. Together with our studies using a pharmacological agonist of β3-adrenergic receptors (Fig. 4), these findings support that Agrp neurons control sympathetic nerve activity in the WAT to control lipogenesis and adiposity. As we will discuss below, we speculate that in addition to diet-induced obesity this function of Agrp neurons is important in the daily anticipatory responses to food ingestion[42].

Agrp neurons release gamma-aminobutyric acid (GABA)[43,44] and neuropeptide-Y (NPY)[2,43], in addition to AGRP[2,4]. In our experiments, we did not identify which of these transmitters is involved in the effects of Agrp neurons on peripheral substrate utilization. However, previous reports showed that infusion of NPY in the rat brain increases RER[45–47]. The effect of NPY on substrate utilization was prominent in the PVH[47], an area in which NPY treatment also induces hyperphagia[48,49]. Because Agrp neurons project to the PVH to promote feeding[50,51], it is possible that NPY released from Agrp neurons in the PVH also promotes the observed changes in substrate utilization. In addition to NPY, Agrp neurons also likely regulate lipogenesis via release of the neuropeptide AGRP, which is an endogenous antagonist of melanocortin receptors[3,4,52–54]. Pharmacological inhibition of melanocortin receptors in the brain—by delivery of SHU9119—increased adiposity and RER[55], similar to our results. The pharmacological agonist of melanocortin receptors, MTII, when infused in the rat brain increased the sympathetic nervous system activity in the WAT, an effect blocked by SHU9119[55]. Thus, it is plausible that Agrp neurons regulate substrate utilization and lipogenesis via release of both NPY and AGRP.

Contrary to adult ablation of Agrp neurons which leads to aphagia[17,18,56], neonatal ablation of these neurons is compatible with life[17]. In a previous study[57], Agrp neurons were ablated during the first postnatal week. The authors found that adult mice

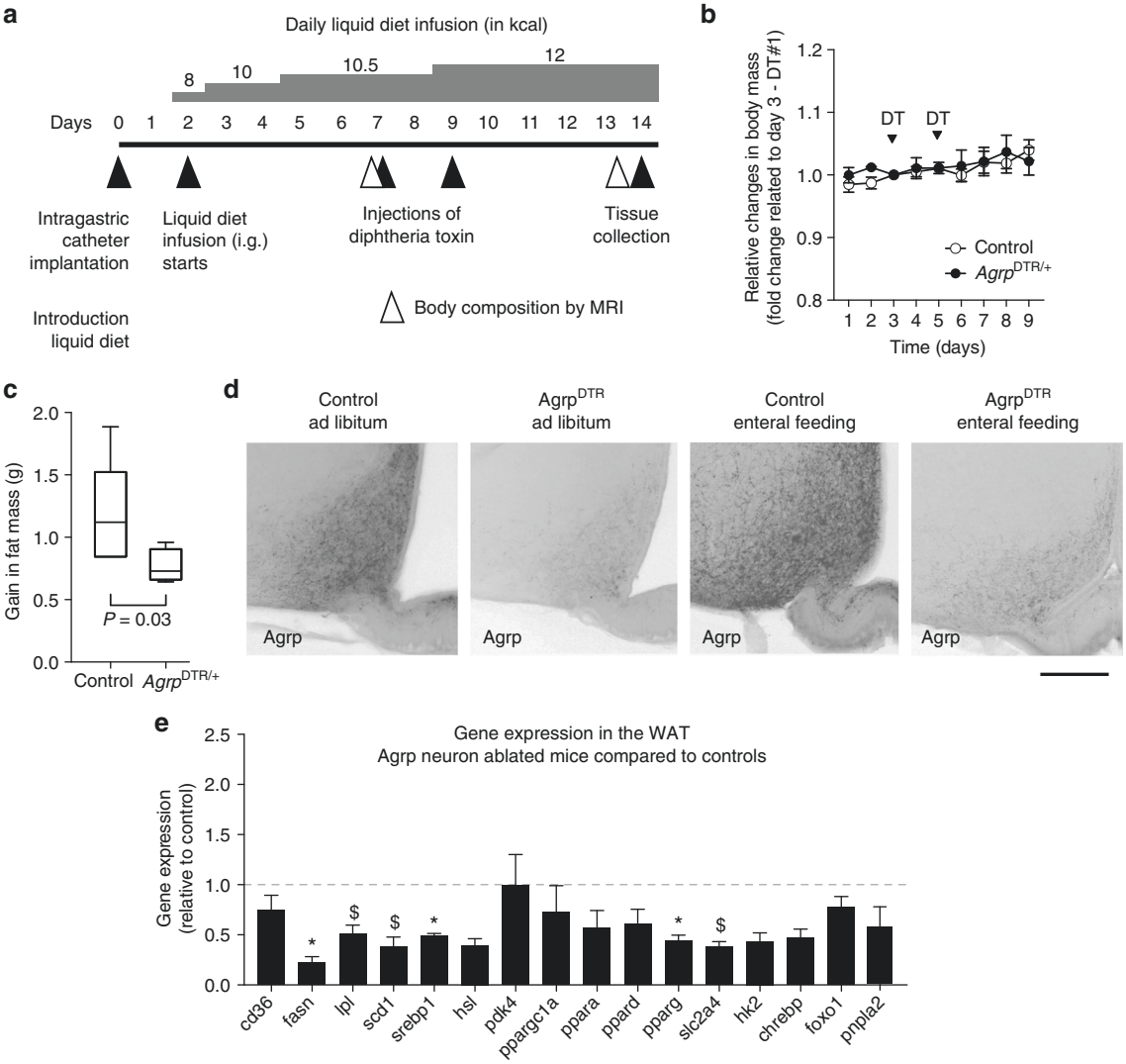

Fig. 7 Agrp neuron ablation impairs fat gain during positive energy balance. **a** Model of positive energy balance by intragastric delivery of liquid diet in mice concomitant with ablation of Agrp neurons. **b** Relative changes in body weight represented by fold-changes related to day 3 of the protocol—when animals received the first injection of diphtheria toxin. **c** Gain in fat mass. **d** Immunohistochemistry for AGRP. **e** Gene expression in the WAT. Data are normalized to control levels (dashed line). Statistical analysis was performed using Student's *t*-test. $^{*}P < 0.05$, $^{\$}P < 0.10$ (non-significant). Bars and symbols indicate mean ± SEM. $N = 4$ animals per group. Boxes indicate median ± 25/75 quartiles ± min/max values. *P* values are provided in the figures. Scale bar = 50 µm

without Agrp neurons showed decreased RER at the beginning of the dark cycle[57], a time when Agrp neuron activity is high[11]. These results suggested that Agrp neurons are important for the increase in RER that occurs at the onset of the dark phase when lipogenesis is turned on and animals enter an anabolic state, in anticipation to food ingestion. In support of this argument, animals trained in a scheduled feeding regimen showed an elevation of NPY levels in anticipation to a meal[58,59] and NPY signaling promotes lipogenesis[60]. Additionally, when fed a scheduled feeding regimen, mice with partial ablation of Agrp neurons showed impaired anticipatory activity before food presentation[61]. Thus, these findings support a function for Agrp neurons in coordinating the daily anticipatory responses to food intake (see also ref. [42]), including anticipatory substrate utilization switches.

More recently, two additional reports highlighted the involvement of Agrp neurons in peripheral substrate metabolism[62,63]. These studies reported on the role of carnitine acetyltransferase (Crat) as a critical enzyme in Agrp neurons to control the switch in peripheral energy metabolism during different metabolic states. Mice knockout for Crat selectively in Agrp neurons had impaired metabolic flexibility—the capacity to shift between energy substrates—and were more predisposed to fat accumulation during positive energy balance[62,63]. However, the authors did not directly assess the activity of Agrp neurons. Based on the experiments reported here, an increase in Agrp neuron activity in Cart knockout Agrp neurons is expected during positive energy balance. Collectively, these recent reports support the importance of Agrp neurons in regulating peripheral substrate utilization and fat accumulation.

In summary, we showed that Agrp neurons in the hypothalamus rapidly control whole-body nutrient utilization by shifting metabolism towards lipogenesis. These findings have implications for our understanding of how neuronal circuits control energy metabolism and, consequently, to our understanding of severe disordered conditions such as obesity.

Methods

Animals. Mice used in the experiments were 3 to 8 months old from both genders. *Agrp*^{Trpv1} mice were generated by crossing *Agrp*^{Cre} to *Rosa26*$^{LSL\text{-}Trpv1}$ mice backcrossed to a *Trpv1*^{KO} background to prevent capsaicin action on other cell

XXX

types[64,65]. As a result, *Agrp*^{Trpv1} mice selectively expressed the capsaicin-sensitive channel, Trpv1, in Agrp neurons. Because capsaicin is a highly specific ligand of Trpv1[66], peripheral injection of capsaicin allowed for a rapid, reliable and transient chemogenetic activation of Agrp neurons in *Agrp*^{Trpv1} mice[14,19]. Using *Agrp*^{Trpv1} mice allowed us to rapidly activate Agrp neurons without the necessity of tethers (as for example, using optogenetics), facilitating the study of animals in indirect calorimetry chambers to measure gas (O_2 and CO_2) exchange. Importantly, Trpv1-mediated activation of Agrp neurons was both rapid (latency to start is ~2 min) and short lived (last <1 h)[65], unlike the effects of activating Agrp neurons via the designer receptor hM3Dq[16].

More specifically, *Agrp*^{Trpv1} mice were: *Agrp*$^{Cre/+}$::*Trpv1*$^{KO/KO}$::*R26-LSL-Trpv1*$^{Gt/+}$; control animals were either *Agrp*^{Trpv1} mice injected with vehicle (3.3% Tween-80 in saline) or *Trpv1*$^{KO/KO}$:*R26-LSL-Trpv1*$^{Gt/+}$ mice injected with capsaicin. In the experiments reported, all mice were littermates (Agrp neuron activated and controls). We did not observe any differences between the two control groups (in feeding behavior and calorimetry measurements[14,19]). Therefore, throughout the study we referred to both groups as "controls". We have carefully characterized this animal model elsewhere[14,19]. Briefly, to control for ectopic expression of *Cre* outside Agrp neurons, we have genotyped all our animals to the excised conditional allele[14] and found only rare (<1%) occurrence of ectopic excision of *Rosa26*$^{LSL\text{-}Trpv1}$. Mice with ectopic excision of the conditional allele were excluded from our studies.

We have performed dose–response curves for capsaicin and identified the dose of 10 mg kg^{-1} (intraperitoneal (i.p.)) as optimal to induce feeding behavior in *Agrp*^{Trpv1} mice. We have also performed a dose response of capsaicin and measured changes in RER (1, 3, 10 and 30 mg kg^{-1}, i.p.; experiments not reported). We found that 10 mg kg^{-1} was also the optimal dose to promote changes in RER. Thus, we selected this dose of capsaicin for our studies. The following mouse lines were used in this study: *Agrp*$^{tm1(cre)Lowl/J}$ (stock number 012899, Jax); *Gt(ROSA)26*$^{Sortm1(Trpv1,ECFP)Mde/J}$ (stock number 008513, Jax); *Trpv1*$^{tm1Jul/J}$ (stock number 003770, Jax); and *Agrp*^{DTR} (donated by Richard Palmiter). All animals were kept in temperature- and humidity-controlled rooms, in a 12/12 h light/dark cycle, with lights on from 7:00 AM to 7:00 PM. Food and water were provided ad libitum, unless otherwise stated. All procedures were approved by Institutional Animal Care and Use Committee (Yale University).

Drugs. The following compounds were used in the reported studies: CL 316,241 (in saline; from Tocris); C75 (RPMI medium 1640; from Tocris);[67,68] capsaicin (3.3% Tween-80 in saline; from Sigma)[14], CNO (in saline; from Enzo Life Science)[14], and diphtheria toxin (in saline; List Biological, cat. no. 150). All drugs were injected in a volume of 10 ml kg^{-1} of body weight i.p. except for diphtheria toxin, which was injected at the dose of 50 µg kg^{-1} and the volume was 2.66 µl g^{-1} of body weight. When multiple injections were performed in the same experiment, the volume of each injection was adjusted to a total volume of 10 ml kg^{-1} per animal.

Viral vector and stereotaxic surgery. The 3–5-month-old homozygous Agrp-IRES-Cre mice (*Agrp*$^{tm1(cre)Lowl/J}$) were used for stereotaxic viral injections. At 30 min prior to the first incision, animals were administered a subcutaneous injection of the analgesic buprenorphine (0.1 mg kg^{-1}). Animals were anesthetized with a ketamine/xylazine cocktail (100 and 10 mg kg^{-1}, respectively) and placed upon a heated stage to await a sufficient plane of anesthesia. Next, a small amount of ophthalmic ointment was applied to the eyes to protect from drying. The stage was then situated within a stereotaxic instrument with digital display (Kopf model #942) and the animal was head-fixed with ear bars. After exposure of the skull via a small incision, the bregma and lambda points were identified and the head was leveled in an anterior–posterior fashion by adjusting these two points to the same *z*-depth. Lateral leveling was performed by choosing a point at a fixed lateral distance from bregma and the head was adjusted to match the *z*-depth on each side. Two small holes were drilled in the skull above the points of injection using a 0.9 mm diameter carbon steel burr attached to a high speed stereotaxic drill (Kopf Model #1474). The arcuate nucleus of the hypothalamus was targeted utilizing the following coordinates with bregma as the reference point: anterior/posterior: −1.4 mm, lateral: ± 0.3 mm, dorsal/ventral: −5.9 mm. The virus rAAV5-hSyn-DIO-hM3D(Gq)-mCherry (University of North Carolina Vector Core, titer 6.0 × 10^{12} viral genomes per ml) was then loaded into a blunt tip Neuros syringe (1 µl, Hamilton, cat. no. 7001KH) and the needle was slowly lowered into place. Then, 500 nL bilateral injections of the virus were administered at a rate of 100 nL min^{-1}. The needle was left in place for 6 min post injection to allow for spread of the virus, then was slowly withdrawn to prevent backflow of the virus up the needle track. Skin above the skull was closed with two Michel suture clips and the animal was administered a subcutaneous injection of sterile saline and allowed to recover on a heated pad. As a post-operative analgesic, buprenorphine (0.1 mg kg^{-1}) was administered every 6–12 h after surgery for a total of 48 h. Mice were allowed to recover within their homecage and testing commenced at a minimum of 3 weeks after injection to allow for sufficient infection and viral gene expression.

Food intake assay. Mice injected with rAAV5-Ef1a-DIO-hM3D(Gq)-mCherry were singly housed 1 week prior to food intake studies. Animals were administered saline (i.p.) every other day for a total of 3 injections to acclimate to handling and injection. At 48 h prior to the test, mice were placed in a fresh cage to minimize any food that might be in the bedding. On the day of the test, mice were injected with either saline or CNO and food intake was manually assessed after injection.

Intragastric surgery. The 8–10-week-old singly housed *Agrp*$^{DTR/+}$ and *Agrp*$^{+/+}$ mice were used. At 30 min prior to the first incision, animals were administered a subcutaneous injection of the analgesic buprenorphine (0.1 mg kg^{-1}). Inhalation anesthesia was initiated in an induction chamber via an isofluorane vaporizer. After being deeply anesthetized, animals were immediately laid on a heated mat and a nosecone delivering 2 % isofluorane was placed over the nose of the animal to provide continuous plane of anesthesia throughout the procedure. The dorsal neck and abdomen were shaved and then cleaned with alternating scrubs of 70% ethanol and betadine. A dorsal midline skin incision was made on the neck of the animal and the skin immediately surrounding the incision was separated from the muscle with scissors. Also, a subcutaneous tunnel was opened by extending this separation toward the right flank. Following this, an approximately 2 cm vertical midline abdominal incision was made in the skin and scissors were used to separate the skin from the muscle surrounding the incision and to the right side of the animal. A 1.5 cm incision was then made in the linea alba to allow access to the abdominal cavity. The stomach was gently maneuvered, with sterile cotton swabs saturated with saline, to give specific access to the forestomach. A small triangular pattern of 3 stitches was made with 4-0 silk sutures in the forestomach leaving loose ends of the suture to allow for cinching after insertion of the infusion tube. A 13 cm piece of Micro-Renethane tubing (Braintree Scientific, MRE065, 0.065" OD × 0.030" ID) was previously prepared by quickly exposing the tip to a flame to round the edge and provide a subtle flange. The non-flanged end was connected to a 1 mL syringe containing sterile saline. Using a 20 G sterile needle, the stomach was carefully punctured in the center of the triangular stitch and the flanged end of the tube was inserted. The silk suture was then cinched closed and tied. The tubing was gently pulled to verify secure attachment to the stomach and 0.1 mL of saline was infused to confirm flow and a leak free connection. Prior to any subsequent removal of the syringe attached side of the tubing, the tubing was clamped with a soft hemostat to prevent any leakage from the stomach. To route the tube through the peritoneum, a sharp forceps was used to puncture the right exterior side of the peritoneum and the tube was inserted over the tip and pulled through the hole. Then, allowing ample slack between the peritoneum and the stomach, the tube was sutured to the abdominal wall using 4-0 silk. This prevents slippage of the tubing during normal movement. The abdominal wall was then closed with 4-0 absorbable Vicryl sutures in a continuous pattern. The animal was laid on its side and a trochar was inserted through the skin on the neck and routed dorsally and then laterally until it could be visualized close to the site of the tube. The tube was then inserted into the trochar and pulled through the incision on the back of the neck. The abdominal skin was closed with 5-0 Monofilament sutures. A sterile polyester felt button, 0.563 in. (14 mm) diameter (Instech, cat. no. DF65BS) was moistened with saline and inserted over the tubing and placed under the skin on the interscapular region of the animal. This procedure allows for secure externalization of the tubing while preventing stress to the skin. The skin was then closed over the button with 5-0 monofilament sutures and a small droplet of tissue adhesive was used to secure the tube to the plastic exit hole on the felt button. The tubing was cut 12 mm above the button and a 5 mm blunted and crimped section of an 18 G needle was inserted into the tube to keep the line clean and to prevent any leakage of gastric liquid up the tube. Animals were then given a subcutaneous injection of sterile saline and allowed to recover from anesthesia on a heated pad, then returned to their homecage. As a post-operative analgesic, buprenorphine (0.1 mg kg^{-1}) was administered every 6–12 h after surgery for a total of 48 h.

Intragastric diet infusion. Immediately after returning to the homecage, mice were provided with ad libitum access to water, normal chow (Envigo, Teklad 2018S), and a nutritionally assayed AIN-76 liquid diet (Bio-Serv, cat. no. F1268; composition: protein, 180 kcal L^{-1}; fat, 125 kcal L^{-1}; carbohydrate, 695 kcal L^{-1}—total of 1 kcal mL^{-1}). Liquid diet, supplied as a powder, was mixed fresh daily according to the manufacturer's specifications. After passing through a mesh filter, liquid diet was provided to mice in 50 mL glass feeding tubes (Bio-Serv cat. no. 9019) mounted to the side of the homecage. At 2 days post surgery, normal chow was removed, and mice were connected to a 1.5 m length of Micro-Renethane tubing attached to syringes containing liquid diet. Syringes were mounted in a syringe pump (Harvard Apparatus, model PHD2000) and diet was infused at the following volumes: day 2: 8 mL at 0.4 mL h^{-1}; days 3–4: 10 mL at 0.46 mL h^{-1}; days 5–8: 10.5 mL at 0.48 mL h^{-1}; days 9–14: 12 mL at 1.84 mL h^{-1}. Every 24 h, the 1.5 m tube was detached, and animals were administered 0.1 mL of saline through the catheter in order to flush the line and keep it clean. On post-operative days 7 and 9, mice were administered a 50 µg kg^{-1} intramuscular injection of diphtheria toxin. On days 7 and 13 postoperatively, mice were assessed for body composition in an Echo-MRI 100H analyzer. Animals were killed on day 14 for tissue collection.

Metabolic assays and biochemical analysis. Blood samples were collected from the tail in order to measure glucose and free fatty acids (NEFA) levels. Glucose was measured using a One Touch Ultra 2 glucometer. After blood centrifugation,

XXX1

serum was collected and used to measure NEFA as indicated by the manufacturer (WAKO, Japan). Body composition was assessed using an Echo-MRI system. Fat gain was measured by the delta between the last and the first MRI scan.

Gene expression and western blotting. Animals were deeply anesthetized with ketamine and xylazine and killed by decapitation. Tissues were collected and frozen in liquid nitrogen. Tissues were lysed in buffer containing 1% Nonidet P-40, 50 mM Tris 3 HCl, 0.1 mM EDTA, 150 mM NaCl, proteinase inhibitors and protein phosphatase inhibitors. Equal amounts of protein lysate were electrophoresed on sodium dodecyl sulfate–polyacrylamide gel electrophoresis and transferred to polyvinylidene difluoride membranes. Primary antibodies (Lipolysis Activation Antibody Sampler Kit #8334, Cell Signaling) were incubated at 4 °C overnight at a 1:1000 dilution. Membranes were washed and incubated with secondary antibodies conjugated to horseradish peroxidase. Protein levels were visualized using ECL chemiluminescent substrate and quantified using ImageJ.

Total RNA was extracted from mouse tissues using RNeasy® lipid mini kit (Qiagen). Complementary DNA was reverse transcribed (Bio-Rad) and amplified with SYBR Green Supermix (Bio-Rad) using a Light Cycler 480 real-time PCR system (Roche). Data were normalized to the expression of *Actin*, *Gusb* and *Arbp*. The following primers were used: *cd36* (F-GCGACATGATTAATGGCACA; R-CCTGCAAATGTCAGAGGAAA); *fasn* (F-GTCGTCTGCCTCCAGAGC; R-GTTGGCCCAGAACTCCTGTA); *lpl* (F-TTCACTTTTCTGGGACTGAGAATG; R-GCCACTGTGCCGTACAGAGA); *scd1* (F-CCGGAGACCCCTTAGATCGA; R-TAGCCTGTAAAAGATTTCTGCAAACC); *srebp1* (F-GGCTCTGGAACAGACACTGG; R-TGGTTGTTGATGAGCTGGAG); *hsl* (F-CCTGCAAGAGTATGTCACGC; R-GGAGAGAGTCTGCAGGAACG); *cpt1b* (F-TGTCTACCTCCGAAGCAGGA; R-GCTGCTTGCACATTTGTGTT); *pdk4* (F-TGACAGGGCTTTCTGGTCTT; R-AGTGAACACTCCTTCGGTGC); *ppargc1a* (F-TGTAGCGACCAATCGGAAAT; R-TGAGGACCGCTAGCAAGTTT); *ppara* (F-AGTTCGGGAACAAGACGTTG; R-CAGTGGGGAGAGAGGACAGA); *ppard* (F- ACTCAGAGGCTCCTGCTCAC; R-GGTCATAGCTCTGCCACCAT); *pparg* (F-GATGCACTGCCTATGAGCAC; R-TCTTCCATCACGGAGAGGTC); *slc2a4* (F- CAGTGTTCCAGTCACTCGCT; R-TTTTAAAACAAGATGCCGTCG); *hk1* (F-GCGAGGACAGGCTGTAGATG; R-GAATTTCATCAGAGAGCCGC); *hk2* (F- GGAGCTCAACCAAAACCAAG; R-GGAACCGCCTAGAAATCTCC); *chrebp* (F-CTGGGGACCTAAACAGGAGC; R-GAAGCCACCCTATAGCTCCC); *foxo1* (F- GCGCATAGCACCAAGTCTTCA; R-AGCGTGACACAGGGCATCA); *actb* (F-GGCTGTATTCCCCTCCATCG; R-CCAGTTGGTAACAATGCCATGT); *gusb* (F- CCGACCTCTCGAACAACCG; R- GCTTCCCGTTCATACCACACC); *arbp* (F-CGACCTGGAAGTCCAACTAC; R-ATCTGCTGCATCTGCTTG). Additionally, the TaqMan probe for *pnpla2* was used (Mm00503040_m1).

Immunohistochemistry. Mice were deeply anesthetized by isoflurane inhalation and killed by decapitation. Brains were immersion fixed in 4% paraformaldehyde for 48 h at 4 °C. Next, coronal brain sections of the arcuate nucleus were cut at thickness of 50 µm on a vibrating blade microtome (Leica VT1000S) and free-floating tissue sections were washed in phosphate-buffer saline (PBS, pH 7.4). Sections were incubated in 0.3% Triton X-100 in PBS for 30 min at room temperature for permeabilization. For blocking, sections were incubated in PBS containing 5% normal donkey serum and 0.3% Triton X-100 for 60 min at room temperature. Tissue was then treated with the primary antibody, Rabbit-anti-AgRP (Pheonix Pharmaceuticals, cat. H-003-57, 1:1000), in blocking solution overnight at room temperature. Tissue sections were next washed 5 times for 5 min in PBS and subsequently incubated in PBS containing the secondary antibody, Donkey-anti-Rabbit Alexa Fluor 594 (Invitrogen, A21207), for 2 h at room temperature. Finally, sections of the arcuate nucleus were washed in PBS, mounted and coverslipped with ProLong Gold Antifade Reagent (Invitrogen) for fluorescent microscopic analysis.

Indirect calorimetry and nutrient utilization. Nutrient utilization can be measured by indirect calorimetry, where the measurements of VCO_2 production and VO_2 consumption are used to calculate the RER[23]. Under normal conditions, a RER approaching 0.7 indicates predominant fat oxidation, while a RER approaching 1.0 indicates predominant carbohydrate oxidation[23]. Oxygen consumption (VO_2) and CO_2 production (VCO_2) were measured in four to eight mice simultaneously in indirect calorimetry chambers (TSE Systems, Germany). Measurements were recorded every 8–12 min over the entire course of the experiment (except for the experiment reported in Fig. 1 and Supplementary Figure 1, in which measurements were recorded every 30 min). RER was calculated as the ratio between VCO_2 and VO_2. Whole-body fat utilization was calculated using the follow equation: $1.67 \times (VO_2 - VCO_2)$. Whole-body carbohydrate utilization was calculate using the follow equation: $4.55 \times VCO_2 - 3.21 \times VO_2$[23]. In these equations, VO_2 and VCO_2 were in L min^{-1} and constants are in L g^{-1} (representing the amount of gas production or consumption in liters per gram of substrate oxidized. The calculate substrate utilization rate (in g min^{-1}) was converted to mg min^{-1} for better visualization. All animals were single housed during the experiments in calorimetry chambers. Mice were acclimated to the chambers for several days until they displayed normal circadian variance in metabolic measurements (as reported in Supplementary Figure 1). Typically, this acclimation period lasts ~5–7 days in our laboratory. We also acclimated animals to mock injections to minimize stress response. In all experiments, animals were injected 3–4 times with vehicle in consecutive days (Supplementary Figure 1).

For the glucose response study, mice were provided with glucose (D-Glucose, G8270, Sigma, USA) via gavage. We used saline as vehicle and three doses of glucose (1, 2 and 3 g kg^{-1} body weight, via gavage feeding). Food was removed 2 h before the experiment during the light cycle of the animals. Indirect calorimetry was recorded for 60 min prior injection of capsaicin and diet switch. For the experiments where no food was provided, food was removed from the cages 2 h before injecting mice with capsaicin/vehicle. Baseline indirect calorimetry was recorded for 60 min, and then the effects of Agrp neuron activation were recorded for additional 60–120 min. Similar procedures were used in the experiments using hM3Dq to activate Agrp neurons and in the experiments in which compounds were given to mice prior the experiment. Glucose (2 g kg^{-1}, via gavage), C75 (10 mg kg^{-1}, i.p.) or CL 316,243 (0.01-1.00 mg kg^{-1}, i.p.) were given together with capsaicin. In all cases, the drugs were injected immediately before capsaicin using two different syringes.

Statistical considerations. Matlab R2016a, PASW Statistics 18.0, Prism 7.0 and Adobe Illustrator CS6/CC were used to analyze data and plot figures. Student's *t*-test was used to compare two groups. Analysis of variance (ANOVA) was used to compare multiple groups. When necessary, multiple comparisons post hoc test (MCT) was used (Holm–Sidak's test). When homogeneity was not assumed, the Kruskal–Wallis non-parametric ANOVA was selected for multiple statistical comparisons. The Mann–Whitney *U* test was used to determine significance between groups. Statistical data are provided in the figures. $P < 0.05$ was considered statistically significant.

Reporting summary. Further information on experimental design is available in the Nature Research Reporting Summary linked to this article.

Data availability

The data that support the findings of this study are available from the corresponding author upon reasonable request.

Received: 28 June 2017 Accepted: 20 December 2018
Published online: 18 January 2019

References

1. Goodpaster, B. H. & Sparks, L. M. Metabolic flexibility in health and disease. *Cell Metab.* **25**, 1027–1036 (2017).
2. Hahn, T. M., Breininger, J. F., Baskin, D. G. & Schwartz, M. W. Coexpression of Agrp and NPY in fasting-activated hypothalamic neurons. *Nat. Neurosci.* **1**, 271–272 (1998).
3. Rossi, M. et al. A C-terminal fragment of Agouti-related protein increases feeding and antagonizes the effect of alpha-melanocyte stimulating hormone in vivo. *Endocrinology* **139**, 4428–4431 (1998).
4. Ollmann, M. M. et al. Antagonism of central melanocortin receptors in vitro and in vivo by agouti-related protein. *Science* **278**, 135–138 (1997).
5. Broberger, C., Johansen, J., Johansson, C., Schalling, M. & Hökfelt, T. The neuropeptide Y/agouti gene-related protein (AGRP) brain circuitry in normal, anorectic, and monosodium glutamate-treated mice. *Proc. Natl. Acad. Sci. USA* **95**, 15043–15048 (1998).
6. Steculorum, S. M. et al. Hypothalamic UDP increases in obesity and promotes feeding via P2Y6-dependent activation of AgRP neurons. *Cell* **162**, 1404–1417 (2015).
7. van den Top, M., Lee, K., Whyment, A. D., Blanks, A. M. & Spanswick, D. Orexigen-sensitive NPY/AgRP pacemaker neurons in the hypothalamic arcuate nucleus. *Nat. Neurosci.* **7**, 493–494 (2004).
8. Pinto, S. et al. Rapid rewiring of arcuate nucleus feeding circuits by leptin. *Science* **304**, 110–115 (2004).
9. Könner, A. et al. Insulin action in AgRP-expressing neurons is required for suppression of hepatic glucose production. *Cell Metab.* **5**, 438–449 (2007).
10. Takahashi, K. A. & Cone, R. D. Fasting induces a large, leptin-dependent increase in the intrinsic action potential frequency of orexigenic arcuate nucleus neuropeptide Y/Agouti-related protein neurons. *Endocrinology* **146**, 1043–1047 (2005).
11. Mandelblat-Cerf, Y. et al. Arcuate hypothalamic AgRP and putative POMC neurons show opposite changes in spiking across multiple timescales. *Elife* **4**, e07122 (2015).
12. Grove, K. L. et al. Fasting activates neuropeptide Y neurons in the arcuate nucleus and the paraventricular nucleus in the rhesus macaque. *Brain Res. Mol. Brain Res.* **113**, 133–138 (2003).

13. Clark, J. T., Kalra, P. S., Crowley, W. R. & Kalra, S. P. Neuropeptide Y and human pancreatic polypeptide stimulate feeding behavior in rats. *Endocrinology* **115**, 427–429 (1984).
14. Dietrich, M. O., Zimmer, M. R., Bober, J. & Horvath, T. L. Hypothalamic Agrp neurons drive stereotypic behaviors beyond feeding. *Cell* **160**, 1222–1232 (2015).
15. Aponte, Y., Atasoy, D. & Sternson, S. M. AGRP neurons are sufficient to orchestrate feeding behavior rapidly and without training. *Nat. Neurosci.* **14**, 351–355 (2011).
16. Krashes, M. J. et al. Rapid, reversible activation of AgRP neurons drives feeding behavior in mice. *J. Clin. Invest.* **121**, 1424–1428 (2011).
17. Luquet, S., Perez, F., Hnasko, T. & Palmiter, R. NPY/AgRP neurons are essential for feeding in adult mice but can be ablated in neonates. *Science* **310**, 683–685 (2005).
18. Gropp, E. et al. Agouti-related peptide-expressing neurons are mandatory for feeding. *Nat. Neurosci.* **8**, 1289–1291 (2005).
19. Ruan, H. B. et al. O-GlcNAc transferase enables AgRP neurons to suppress browning of white fat. *Cell* **159**, 306–317 (2014).
20. Steculorum, S. M. et al. AgRP neurons control systemic insulin sensitivity via myostatin expression in brown adipose tissue. *Cell* **165**, 125–138 (2016).
21. Burke, L. K. et al. mTORC1 in AGRP neurons integrates exteroceptive and interoceptive food-related cues in the modulation of adaptive energy expenditure in mice. *eLife* **6**, pii: e22848 (2017).
22. Cavalcanti-de-Albuquerque, J. P., Zimmer, M. R., Bober J. & Dietrich M. O. Rapid shift in substrate utilization driven by hypothalamic Agrp neurons. Preprint at https://doi.org/10.1101/086348 (2016).
23. Frayn, K. N. Calculation of substrate oxidation rates in vivo from gaseous exchange. *J. Appl. Physiol.* **55**, 628–634 (1983).
24. Burnett, C. J. et al. Hunger-driven motivational state competition. *Neuron* **92**, 187–201 (2016).
25. Lodhi, I. J. et al. Inhibiting adipose tissue lipogenesis reprograms thermogenesis and PPARgamma activation to decrease diet-induced obesity. *Cell Metab.* **16**, 189–201 (2012).
26. Loftus, T. M. et al. Reduced food intake and body weight in mice treated with fatty acid synthase inhibitors. *Science* **288**, 2379–2381 (2000).
27. Kuhajda, F. P. et al. Synthesis and antitumor activity of an inhibitor of fatty acid synthase. *Proc. Natl. Acad. Sci. USA* **97**, 3450–3454 (2000).
28. Bloom, J. D. et al. Disodium (R,R)-5-[2-[[2-(3-chlorophenyl)-2-hydroxyethyl]-amino] propyl]-1,3-benzodioxole-2,2-dicarboxylate (CL 316,243). A potent beta-adrenergic agonist virtually specific for beta 3 receptors. A promising antidiabetic and antiobesity agent. *J. Med. Chem.* **35**, 3081–3084 (1992).
29. Grujic, D. et al. Beta3-adrenergic receptors on white and brown adipocytes mediate beta3-selective agonist-induced effects on energy expenditure, insulin secretion, and food intake. A study using transgenic and gene knockout mice. *J. Biol. Chem.* **272**, 17686–17693 (1997).
30. Thaler, J. P. et al. Obesity is associated with hypothalamic injury in rodents and humans. *J. Clin. Investig.* **122**, 153–162 (2012).
31. Srisai, D. et al. Characterization of the hyperphagic response to dietary fat in the MC4R knockout mouse. *Endocrinology* **152**, 890–902 (2011).
32. Dietrich, M. O., Liu, Z. W. & Horvath, T. L. Mitochondrial dynamics controlled by mitofusins regulate agrp neuronal activity and diet-induced obesity. *Cell* **155**, 188–199 (2013).
33. Wei, W. et al. Diet composition, not calorie intake, rapidly alters intrinsic excitability of hypothalamic AgRP/NPY neurons in mice. *Sci. Rep.* **5**, 16810 (2015).
34. Baver, S. B. et al. Leptin modulates the intrinsic excitability of AgRP/NPY neurons in the arcuate nucleus of the hypothalamus. *J. Neurosci.* **34**, 5486–5496 (2014).
35. Diano, S. et al. Peroxisome proliferation-associated control of reactive oxygen species sets melanocortin tone and feeding in diet-induced obesity. *Nat. Med.* **17**, 1121–U1130 (2011).
36. Padilla, S. L. et al. AgRP to Kiss1 neuron signaling links nutritional state and fertility. *Proc. Natl. Acad. Sci. USA* **114**, 2413–2418 (2017).
37. Zeng, W. et al. Sympathetic neuro-adipose connections mediate leptin-driven lipolysis. *Cell* **163**, 84–94 (2015).
38. Correll, J. W. Adipose tissue: ability to respond to nerve stimulation in vitro. *Science* **140**, 387–388 (1963).
39. Bartness, T. J., Liu, Y., Shrestha, Y. B. & Ryu, V. Neural innervation of white adipose tissue and the control of lipolysis. *Front. Neuroendocrinol.* **35**, 473–493 (2014).
40. Rutkowski, J. M., Stern, J. H. & Scherer, P. E. The cell biology of fat expansion. *J. Cell. Biol.* **208**, 501–512 (2015).
41. Shi, Z., Madden, C. J. & Brooks, V. L. Arcuate neuropeptide Y inhibits sympathetic nerve activity via multiple neuropathways. *J. Clin. Invest.* **127**, 2868–2880 (2017).
42. Woods, S. C. The eating paradox: how we tolerate food. *Psychol. Rev.* **98**, 488–505 (1991).
43. Horvath, T. L., Bechmann, I., Naftolin, F., Kalra, S. P. & Leranth, C. Heterogeneity in the neuropeptide Y-containing neurons of the rat arcuate nucleus: GABAergic and non-GABAergic subpopulations. *Brain Res.* **756**, 283–286 (1997).
44. Tong, Q., Ye, C. P., Jones, J. E., Elmquist, J. K. & Lowell, B. B. Synaptic release of GABA by AgRP neurons is required for normal regulation of energy balance. *Nat. Neurosci.* **11**, 998–1000 (2008).
45. McGregor, I. S., Menendez, J. A. & Atrens, D. M. Metabolic effects of neuropeptide Y injected into the sulcal prefrontal cortex. *Brain Res. Bull.* **24**, 363–367 (1990).
46. Menendez, J. A., McGregor, I. S., Healey, P. A., Atrens, D. M. & Leibowitz, S. F. Metabolic effects of neuropeptide Y injections into the paraventricular nucleus of the hypothalamus. *Brain Res.* **516**, 8–14 (1990).
47. Currie, P. J. & Coscina, D. V. Regional hypothalamic differences in neuropeptide Y-induced feeding and energy substrate utilization. *Brain Res.* **737**, 238–242 (1996).
48. Stanley, B. G., Leibowitz, S. F. & Neuropeptide, Y. stimulation of feeding and drinking by injection into the paraventricular nucleus. *Life Sci.* **35**, 2635–2642 (1984).
49. Levine, A. S. & Morley, J. E. Neuropeptide Y: a potent inducer of consummatory behavior in rats. *Peptides* **5**, 1025–1029 (1984).
50. Atasoy, D., Betley, J. N., Su, H. H. & Sternson, S. M. Deconstruction of a neural circuit for hunger. *Nature* **488**, 172–177 (2012).
51. Garfield, A. S. et al. A neural basis for melanocortin-4 receptor-regulated appetite. *Nat. Neurosci.* **18**, 863–871 (2015).
52. Lu, D. et al. Agouti protein is an antagonist of the melanocyte-stimulating-hormone receptor. *Nature* **371**, 799–802 (1994).
53. Shutter, J. R. et al. Hypothalamic expression of ART, a novel gene related to agouti, is up-regulated in obese and diabetic mutant mice. *Genes* **11**, 593–602 (1997).
54. Fong, T. M. et al. ART (protein product of agouti-related transcript) as an antagonist of MC-3 and MC-4 receptors. *Biochem. Biophys. Res. Commun.* **237**, 629–631 (1997).
55. Nogueiras, R. et al. The central melanocortin system directly controls peripheral lipid metabolism. *J. Clin. Invest.* **117**, 3475–3488 (2007).
56. Wu, Q. & Palmiter, R. D. GABAergic signaling by AgRP neurons prevents anorexia via a melanocortin-independent mechanism. *Eur. J. Pharmacol.* **660**, 21–27 (2011).
57. Joly-Amado, A. et al. Hypothalamic AgRP-neurons control peripheral substrate utilization and nutrient partitioning. *EMBO J.* **31**, 4276–4288 (2012).
58. Yoshihara, T., Honma, S. & Honma, K. Effects of restricted daily feeding on neuropeptide Y release in the rat paraventricular nucleus. *Am. J. Physiol.* **270**, E589–E595 (1996).
59. Kalra, S. P., Dube, M. G., Sahu, A., Phelps, C. P. & Kalra, P. S. Neuropeptide Y secretion increases in the paraventricular nucleus in association with increased appetite for food. *Proc. Natl. Acad. Sci. USA* **88**, 10931–10935 (1991).
60. Zarjevski, N., Cusin, I., Vettor, R., Rohner-Jeanrenaud, F. & Jeanrenaud, B. Chronic intracerebroventricular neuropeptide-Y administration to normal rats mimics hormonal and metabolic changes of obesity. *Endocrinology* **133**, 1753–1758 (1993).
61. Tan, K., Knight, Z. A. & Friedman, J. M. Ablation of AgRP neurons impairs adaption to restricted feeding. *Mol. Metab.* **3**, 694–704 (2014).
62. Reichenbach, A. et al. Carnitine acetyltransferase (Crat) in hunger-sensing AgRP neurons permits adaptation to calorie restriction. *FASEB J.* **32**, 6923–6933 (2018).
63. Reichenbach, A. et al. AgRP neurons require carnitine acetyltransferase to regulate metabolic flexibility and peripheral nutrient partitioning. *Cell Rep.* **22**, 1745–1759 (2018).
64. Arenkiel, B. R., Klein, M. E., Davison, I. G., Katz, L. C. & Ehlers, M. D. Genetic control of neuronal activity in mice conditionally expressing TRPV1. *Nat. Methods* **5**, 299–302 (2008).
65. Guler, A. D. et al. Transient activation of specific neurons in mice by selective expression of the capsaicin receptor. *Nat. Commun.* **3**, 746 (2012).
66. Caterina, M. J. et al. The capsaicin receptor: a heat-activated ion channel in the pain pathway. *Nature* **389**, 816–824 (1997).
67. Kim, E. K. et al. C75, a fatty acid synthase inhibitor, reduces food intake via hypothalamic AMP-activated protein kinase. *J. Biol. Chem.* **279**, 19970–19976 (2004).
68. Landree, L. E. et al. C75, a fatty acid synthase inhibitor, modulates AMP-activated protein kinase to alter neuronal energy metabolism. *J. Biol. Chem.* **279**, 3817–3827 (2004).

Acknowledgements

We thank Serge Luquet, Matthew Rodeheffer, Ivan de Araujo, Hai-bin Ruan and Xiaoyong Yang for comments on this project and manuscript. Serge Luquet raised the

important point that Agrp neurons mediate the physiological increase in RER in anticipation to ingestion. M.O.D. received support from Brain and Behavior Research Foundation (NARSAD Young Investigator Award), Yale Center for Clinical Investigation Scholars Award (NCATS, UL1 TR000142), National Institute of Diabetes and Digestive and Kidney Diseases (1R01DK10791601), DRC (P30 DK045735), Whitehall Foundation, Charles H. Hood Foundation, CNPq (487096/2013-4 and 401476/2012-0, Brazil) and CAPES (88881.068059/2014-01, Brazil). J.P.C.-d.-A. and M.R.Z. were partially supported by a fellowship from the Science Without Borders program (Brazil).

Author contributions

J.B. performed experiments and analyzed data. M.R.Z. generated critical animal models and performed initial experiments. J.P.C.-d.-A. designed and performed experiments and analyzed data. M.O.D. designed and performed the experiments, analyzed the data, and wrote the manuscript.

Additional information

Supplementary Information accompanies this paper at https://doi.org/10.1038/s41467-018-08239-x.

Competing interests: The authors declare no competing interests.

Reprints and permission information is available online at http://npg.nature.com/reprintsandpermissions/

Journal peer review information: *Nature Communications* thanks the anonymous reviewers for their contribution to the peer review of this work. Peer reviewer reports are available.

Publisher's note: Springer Nature remains neutral with regard to jurisdictional claims in published maps and institutional affiliations.